

# Influence of *trans*-polyoctylene rubber content on styrene-butadiene rubber properties

Patrik Macúrik<sup>a</sup>, Rafal Anyszka<sup>b,c</sup>, Ivan Hudec<sup>a</sup>,  
Terézia Malčeková<sup>a</sup>, Ján Kruželák<sup>a</sup>

<sup>a</sup>*Department of Plastics, Rubber and Fibres, Slovak University of Technology in Bratislava, Radlinského 9, 812 37 Bratislava, Slovakia*

<sup>b</sup>*Chair of Elastomer Technology and Engineering, University of Twente, De Horst 2, 7522 LW Enschede, The Netherlands*

<sup>c</sup>*Institute of Polymer and Dye Technology, Lodz University of Technology, Stefanowskiego 12/16, 90-924 Łódź, Poland*  
*patrik.macurik@stuba.sk*

**Abstract:** The study was focused on the investigation of *trans*-polyoctylene (TOR) influence on cross-linking as well as mechanical and rheological properties of rubber compounds based on styrene-butadiene rubber (SBR). SBR was compounded with different proportions of TOR in the concentration range from 0 to 30 phr. Integration of TOR into rubber leads to the prolongation of the optimum curing time and scorch time and thus the decrease of the curing rate. Higher content of TOR led to less viscous rubber due to the plasticizing effect. Cross-link density of vulcanizates was reduced, which correlates with higher elongation at break. Tensile strength and hardness of vulcanizates increased with the increasing TOR content, probably due to the increasing amount of the crystalline phase.

**Keywords:** *trans*-polyoctylene rubber, styrene-butadiene rubber

## Introduction

Styrene-butadiene rubber is the most widely used and very important synthetic rubber worldwide. It has entered the market due to its low cost, use in automotive industry (good abrasion resistance) and high level of product uniformity (Niyogi, 2007). SBR is nonpolar rubber with good mechanical characteristics. In comparison with natural rubber, it has better oxygen and ozone resistance and good abrasion resistance (Noriman et al., 2010). SBR is used in a wide range of applications such as automotive tire sidewalls, cover strips, wires, cables, footwear, roofing barriers and sporting goods (Zhou et al., 2010). Vestenamer is produced by ring-opening metathesis polymerization (ROMP) from cyclooctene and it is known as *trans*-polyoctene rubber (TOR) consisting of unbranched linear and cyclic macromolecules which contain one double bond for every eighth carbon atom with prevalently *trans* isomeric double bonds. TOR is a semicrystalline rubber known as a compatibilizer for incompatible blends as well as a processing aid. It can provide good processability in the temperature range of rubber processing (100–150 °C) as well as good collapse resistance below the melting temperature (54 °C) due to recrystallization (Awang et al., 2007; Evonik website, 2019). It is a high-performance polymer with dual character. During rubber processing, blends play the role of plasticizers and in process of vulcanization they react as unsaturated

rubber. Due to this dual character, processing of natural rubber/styrene-butadiene rubber blend is improved in terms of energy savings and handling of intermediary compounds and the vulcanization profile is changed. TOR as unsaturated rubber can enable cross-linking with sulfur, sulfur donors, peroxides or cure resins (Pana et al., 2008; Nah, 2002; Noriman et al., 2012; Chang et al., 1999).

## Material and methods

As the rubber matrix, a solution of polymerized styrene-butadiene rubber containing 25 % of styrene (Arlanxeo, Germany) was used. *Trans*-polyoctylene rubber (TOR), trademark Vestenamer 8012 (Evonik, Germany), was dosed to the rubber matrix as an additive in the concentration range from 0 phr to 30 phr (weight parts of TOR per hundred weight parts of rubber). Compounds contained standard semi EV sulfur curing system consisting of zinc oxide – 3 phr (Slovzink, Košeca, Slovakia) and stearic acid – 2 phr (Setuza, Ústí nad Labem, Czech republic) as activators, N-cyclohexyl-2-benzothiazole sulfonamide CBS – 1.5 phr (Duslo, Šafa, Slovakia) as accelerator, and sulfur – 1.5 phr (Siarkopol, Tarnobrzeg, Poland) as curing agent.

## Preparation and curing of rubber compounds

The two-step mixing of rubber compounds was carried out in a laboratory mixer Brabender. Rubber, zinc oxide and stearic acid were compounded in the

first step (9 minutes, 90 °C), whereas the curing system (CBS and sulfur) was introduced in the second step (4 minutes, 90 °C). After that, the blends were homogenized in a two roll mill. One reference and six samples with different content of TOR additive (5; 10; 15; 20; 25; 30 phr) were prepared. Curing characteristics of the rubber compounds were investigated from the corresponding curing isotherms measured by a MDR rheometer at 160 °C. The curing process was performed at 160 °C for the optimum curing time calculated from the curing isotherms under the pressure of 15 MPa using a hydraulic press (Fontijne, N.V. Machinefabriek, Vlaardingen, The Netherlands). Finally, thin sheets (150 × 150 mm, thickness of 2 mm) of cured rubber were obtained.

#### Determination of cross-link density of rubber blends

Cross-link density,  $\nu$ , was determined based on equilibrium swelling of the samples in *o*-xylene. First, the samples were swelled in *o*-xylene until equilibrium swelling was reached. The cross-link density was then calculated based on the equilibrium swelling degree by applying the Flory-Rehner equation (1) (Noriman et al., 2012):

$$\nu = -\frac{\ln(1-V_r) + V_r + \chi V_r^2}{V_s(V_r^{1/3} - 0,5V_r)} \quad (1)$$

where  $\nu$  – is the cross-link density (mol/cm<sup>3</sup>),  $V_r$  – volume fraction of rubber in equilibrium swelling sample of a vulcanizate,  $V_s$  – molar volume of solvent (123.45 cm<sup>3</sup>/mol for *o*-xylene),  $\chi$  – Huggins interaction parameter (0.4106 in this case).

#### Evaluation of physical-mechanical properties

Tensile properties of the tested cured rubber compounds were measured using a Zwick Roell/Z 2.5, (Ulm, Germany) tester operating at the crosshead speed of 500 mm/min and room temperature in accordance with the valid technical standards. Testing was performed with dumbbell-shaped test specimens (width of 6.4 mm, length of 80 mm, and thickness of 2 mm). Hardness was measured using a durometer (HW WALLACE and CO LTD CROYDON CR9 2HR) and the unit was expressed in IRHD (International Rubber Hardness Degree).

#### Determination of rheological properties – complex viscosity

Rheological properties of the samples were determined by an oscillating rheometer RPA 2000 in accordance with ISO 13145 standard for rubber mixtures. Torque was measured over time at constant oscillation deflection and the oscillation frequency of the oscillating cone at 80 °C. The sam-

ples were placed between thick polymer film layers. The measurements were performed in shear mode in a closed chamber and the results are in form of flow curves characterized by shear rate,  $\dot{\gamma}$  [s<sup>-1</sup>], and complex viscosity,  $\eta^*$  [Pa s].

#### Differential scanning calorimetry

Differential scanning calorimetry measurements were performed under nitrogen atmosphere at the heating/cooling rate of 10 °C/min using a Mettler-Toledo Inc apparatus and the “SW STARE” software. The samples were placed in standard aluminum pans with pierced lids. Heating and cooling programs were performed as follows: the sample was heated from 25 °C to 200 °C, cooled from 200 °C to -65 °C and again heated to 200 °C.

## Results and discussion

#### Influence of TOR on curing process and cross-link density

Fig. 1 shows the curing characteristics of SBR/TOR rubber compounds. As it is shown, optimum curing time,  $t_{90}$ , and scorch time,  $t_{s1}$ , were prolonged with the increasing content of TOR, which suggests that TOR influences the cross-linking process of rubber compounds. TOR contains a double bond at every eighth carbon atom, which is why the curing rate was lower in comparison with unmodified SBR blends.

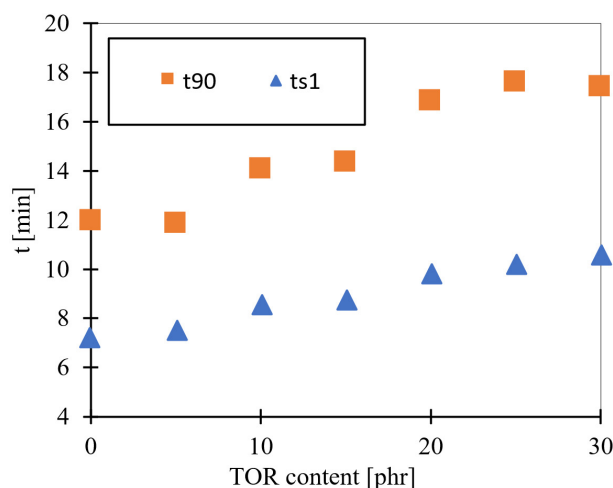


**Fig. 1.** Influence of TOR content on optimum curing time,  $t_{90}$ , and scorch time,  $t_{s1}$ , of rubber compounds.

Minimum torque,  $M_L$ , and maximum torque,  $M_H$ , values are listed in Table 1; they decrease with the increasing TOR content. This can be attributed to the decrease in the cross-linking density of vulcanizates (Fig. 2) and of the viscosity of rubber compounds

with the increasing amount of TOR. Usually, a correlation between the torque difference (difference between the maximum and the minimum torque) and the cross-linking density is observed. This means that with the decreasing cross-linking density, the torque difference also decreases. Similarly, lower viscosity of rubber compounds shifts the torque difference to lower values. The results obtained from the determination of cross-linking density (Fig. 2) and complex viscosity (Fig. 3) confirmed the presumption of both parameters decrease proportional to the amount of TOR. A possible explanation of the cross-linking density decrease can be the curable character of TOR added without increasing the sulfur and CBS content. Therefore, each sample containing a higher amount of TOR contained relatively lower amounts of sulfur and CBS for curing. Higher number of curable macromolecules decreased the cross-linking density.

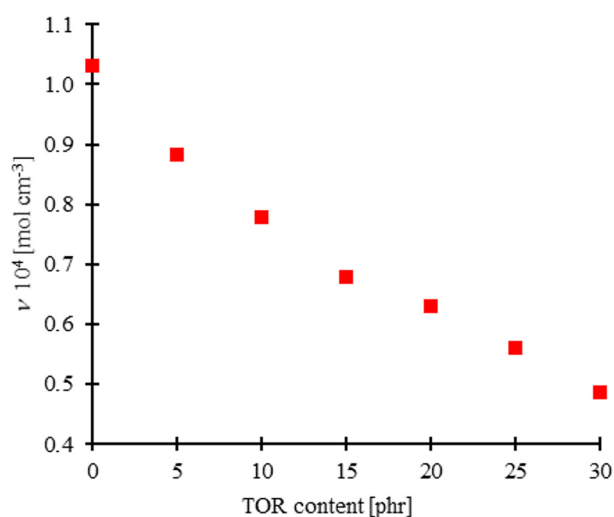


**Fig. 2.** Influence of TOR content on cross-linking density,  $\nu$ , of vulcanizates.

#### ***Influence of TOR on complex viscosity of rubber compounds***

In Fig. 3, the pseudoplastic behavior of tested rubber compounds was confirmed. When higher shear rate was applied, lower complex viscosity was

reached. Plasticizer effect of TOR is acknowledged because lower viscosity of rubber compounds was achieved with the increasing content of TOR. When comparing individual complex viscosities (Fig. 4) for one shear rate (10 Pa s), it can be clearly seen that a higher amount of TOR can improve the processability of rubber compounds by reducing the complex viscosity (Fig. 4).

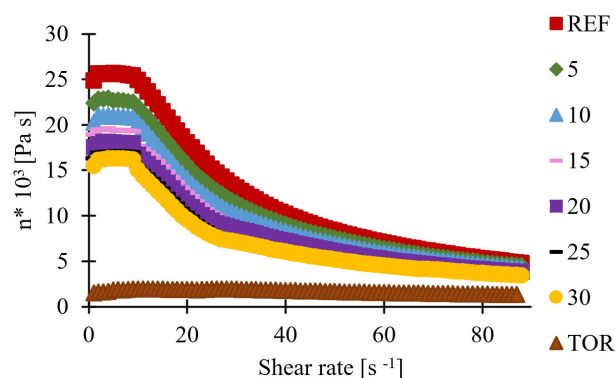


**Fig. 3.** Dependence of complex viscosity,  $\eta^*$ , on shear rate,  $\dot{\gamma}$ , of rubber compounds with different content of TOR [phr].

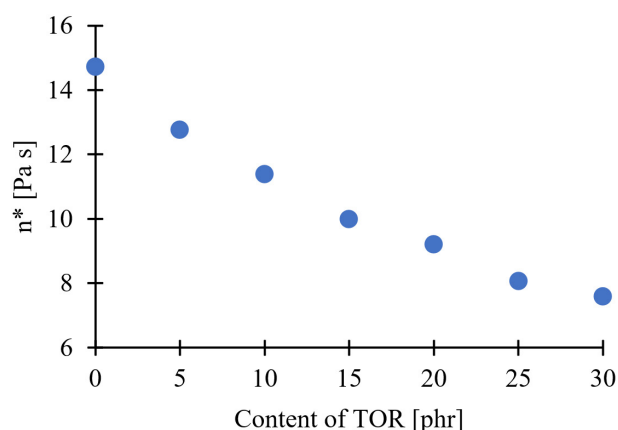


**Fig. 4.** Dependence of complex viscosity on TOR content at the shear rate of 10 s<sup>-1</sup>.

***Influence of TOR on physical-mechanical properties***  
Mechanical properties of vulcanizates are illustrated in Figs. 5 and 6. It becomes obvious that

**Tab. 1.**  $M_L$  (minimum torque) and  $M_H$  (maximum torque) of SBR/TOR blends.

TOR content [phr]	0	5	10	15	20	25	30
$M_L$ [dN m]	0.63	0.60	0.57	0.54	0.51	0.48	0.46
$M_H$ [dN m]	10.89	10.54	10.70	9.96	9.75	9.36	9.21
$\Delta M$ [dN m]	10.26	9.94	10.13	9.42	9.24	8.88	8.75

increasing the TOR content has positive influence on the tensile strength and hardness (Fig. 5). In the vulcanized compounds, crystalline *trans*-polyoctylenes, such as TOR, are supposed to have a certain reinforcing effect on the vulcanizates. As a result, the hardness and the tensile properties of the vulcanizates increased (Kraus, 1963). The increase of elongation at break was also recorded, which can be attributed to the decrease of cross-link density of vulcanizates with the increasing amount of TOR (Fig. 6). Higher cross-link density leads to higher rubber chains mobility and lower elasticity. Also, mechanical properties of vulcanizates are positively influenced by TOR addition contributing thus, together with the improved processability, to the preparation of vulcanizates with higher tensile strength and elongation at break.

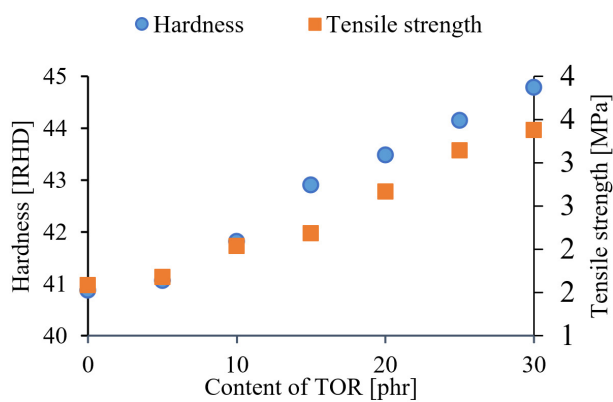


**Fig. 5.** Influence of TOR content on tensile strength and hardness of SBR/TOR vulcanizates.

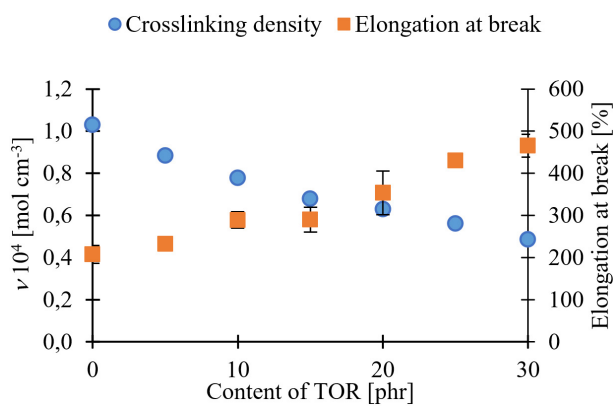


**Fig. 6.** Correlation between cross-linking density,  $\nu$ , and elongation at break of vulcanizates.

#### Differential scanning calorimetry

SBR is an amorphous type of rubber while TOR is a semicrystalline polymer with a 35 % crystallinity. High proportion of the crystalline phase influences the properties of vulcanizates due to its reinforcing effect (Figs. 7, 8). In general, increasing the amount

of the crystalline phase increases the reinforcing effect of vulcanizates (Bhowmick, 2001).

**Tab. 2.** Thermal properties (change of crystallization enthalpy,  $\Delta H$ , melting temperature,  $T_m$ , and crystallization temperature,  $T_c$ ) of SBR compounds with different content of TOR [phr].

Blend	TOR	SBR TOR 30	SBR TOR 20	SBR TOR 10
$\Delta H$ [J/g] melting	53.7	7.7	4.0	2.2
$T_m$ [°C] (onset)	50.0	34.3	39.6	37.3
$T_m$ [°C] (peak)	65.2	50.6	50.2	48.9
$\Delta H$ [J/g] cooling	-33.7	-2.7	-0.4	-0.2
$T_c$ [°C] (onset)	34.8	28.1	27.4	25.8
$T_c$ [°C] (peak)	29.4	23.4	22.2	22.0

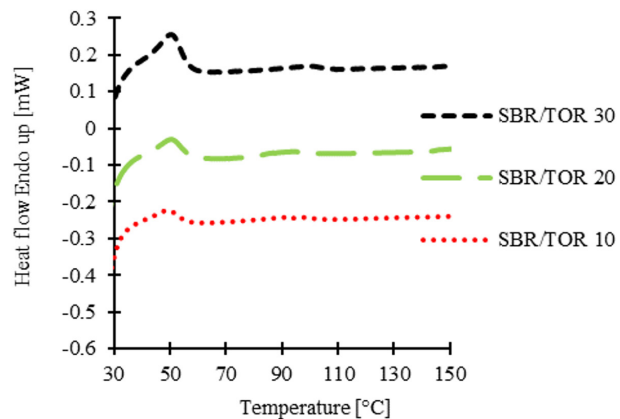


**Fig. 7.** DSC curve for SBR/TOR rubber compounds with different TOR content (heating).

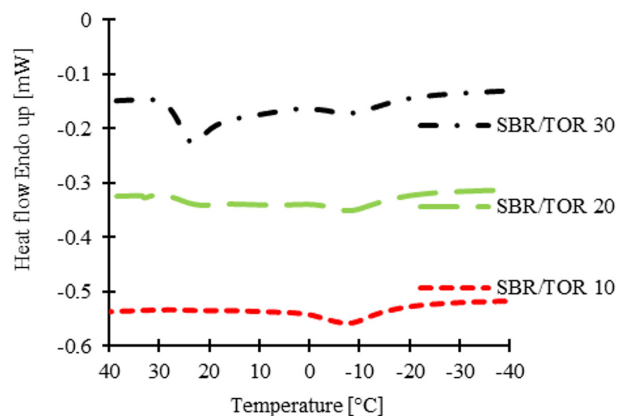


**Fig. 8.** DSC curve for SBR/TOR rubber compounds with different TOR content (cooling).

## Conclusion

The goal of this work was to investigate the influence of TOR on the properties of prepared SBR/TOR rubber. The presence of TOR caused a decrease in the vulcanization rate and thus an increase in the optimal curing time and scorch time. The modified rubber had a pseudoplastic character. Increasing content of TOR reduced the complex viscosity. The tensile strength and hardness increased with the TOR addition as the increasing amount of TOR leads to the increasing amount of the crystalline phase in vulcanizates. The elongation at break of vulcanizates also increased with the increasing amount of TOR as a result of the decrease in the cross-link density. TOR increased also the melting point and crystallization temperature of SBR blends. Residual crystalline phase was presented proportionally with the increasing amount of TOR.

### *Acknowledgement*

This work was supported by the Slovak Research and Development Agency under the contract No. APVV-0694-12.

## References

- Awang M, Ismail H, Hazizan MA (2007) Polypropylene-based blends containing waste tire dust: Effects of *trans*-polyoctylene rubber (TOR) and dynamic vulcanization. *Polymer testing*, 26: 779–787.
- Bhowmick AK, Stephens HL (2001) In: Handbook of elastomers, second edition (p 710), CRC press, New York.
- Evonik official website (2020) <https://www.vestenamer.com/product/vestenamer/en/Pages/vestenamer.aspx>.
- Chang YW, Shin YS, Chun H, Nah C (1999) Effects of *trans*-polyoctylene rubber (TOR) on the properties of NR/EPDM blends, *J Appl Polym Sci*, 73, 5: 749–756.
- Kraus G (1963) *J. Appl. Polym. Sci.* 7: 861–871.
- Nah C (2002) Effects of *trans*-polyoctylene rubber on rheological and green tensile properties of natural rubber/acrylonitrile-butadiene rubber blends, *Polym Int* 51: 245.
- Niyogi KU (2007) In: Introduction to fibre science and rubber technology (p. 11–14), Shri Ram institute for industrial research, Delhi.
- Noriman NZ, Ismail H, Rashid AA (2010) Characterization of styrene butadiene rubber/recycled acrylonitrile-butadiene rubber (SBR/NBRr) blends: The effects of epoxidized natural rubber (ENR-50) as a compatibilizer.
- Noriman NZ, Ismail H, Rashid AA (2012) Properties of styrene butadiene rubber/recycled acrylonitrile-butadiene rubber (SBR/NBRr) blends: Effect of the addition of *trans*-polyoctylene rubber, *J Appl Polym Sci*, 126, S2, E56–E63.
- Pena BCM, DemarquetteNR, Effect of the processing conditions and the addition of *trans*-polyoctylene rubber on the properties of natural rubber/styrene-butadiene rubber blends, *J Appl Polym Sci* 109: 445–451.
- Zhou XW, Zhu YF, Liang J, Yu SY (2010) New fabrication and mechanical properties of styrene butadiene rubber/carbon nanotubes nanocomposite, *J. Mater. Sci. Technol.*, 26(12): 1127–1132.

# Determination of carotenoids in flowers and food supplements by HPLC-DAD

Petra Pavelková, Aleš Krmela, Věra Schulzová

Department of Food Analysis and Nutrition, University of Chemistry and Technology, Prague, Technická 3, 166 28, Prague, Czech Republic  
pavelkova.petra@seznam.cz

**Abstract:** Marigold flowers (*Tagetes patula* and *Calendula officinalis*) were chosen for analysis because they are the most often used source of lutein and its isomer zeaxanthin for the production of food supplements on the Czech market. Direct extraction and extraction with alkaline hydrolysis were compared to detect free or bound carotenoids. For carotenoid separation, C18 and C30 columns were used. A new method for determination of carotenoid content in food supplements in form of capsules has been developed and validated. All matrices were analysed by high-performance liquid chromatography with diode array detection (HPLC-DAD). It has been found that alkaline hydrolysis is required for both Marigold flowers and food supplements to release lutein from ester bonds to fatty acids. In *Calendula officinalis* lutein in the concentration of 807–1472 mg·kg<sup>-1</sup> of dry matter was detected. *Tagetes patula* has been identified as a better lutein source with the content of 5906–8677 mg·kg<sup>-1</sup> of dry matter. It has been found that the content of lutein and zeaxanthin in commercial food supplements (*Lutein Complex Premium* and *Occutein Brilliant*) is consistent with the declared quantity. Linearity of the HPLC-DAD method ranged from 0.1–20 µg·mL<sup>-1</sup> with the limit of quantification (LOQ) of 1.7 mg·kg<sup>-1</sup> for lutein in Marigold flowers and 200 mg·kg<sup>-1</sup> in food supplements. Repeatability was 2.3 % for lutein in all tested matrices.

**Keywords:** food supplements, HPLC-DAD, lutein, Marigold flowers, zeaxanthin

## Introduction

Carotenoids are ubiquitous organic compounds, mainly of yellow, orange and red colour, soluble in fats and organic solvents (Watkins and Pogson, 2020). Currently, more than 1100 carotenoids are known (Yabuzaki, 2017). Several of these pigments are retinoids because of their vitamin A activity (Becerra et al., 2020; Watkins and Pogson, 2020).

From the chemical point of view, these compounds are predominantly tetraterpenes composed of eight isoprene units. In their chain, they have a conjugated double bond system representing a light-absorbing chromophore that gives carotenoids their characteristic colour (Rodriguez-Amaya, 2019). Carotenoids are identified from their visible absorption spectrum (Saini et al., 2015).

Carotenoids are divided into two basic groups – carotenes and xanthophylls. Carotenes are formed by a hydrocarbon chain (lycopene, α-carotene, β-carotene) while xanthophylls are oxidized derivatives of carotenes (β-cryptoxanthin, lutein, zeaxanthin) (Becerra et al., 2020).

Lutein (Fig. 1) and its isomer zeaxanthin (Fig. 2) are natural pigments of yellow colour.

These substances are labile and they easily isomerize and degrade in the presence of light, heat and oxygen; thus, preventive procedures have to be taken to adapt both storage and processing conditions (Saini et al., 2015; Becerra et al., 2020). Human bodies are not able to synthesize carotenoids themselves, so they have to take them in food or food supplements (Woodside et al., 2015). The most important sources of xanthophylls include fruits, vegetables,

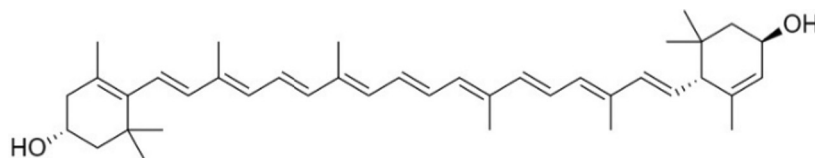


Fig. 1. Structural formula of lutein.

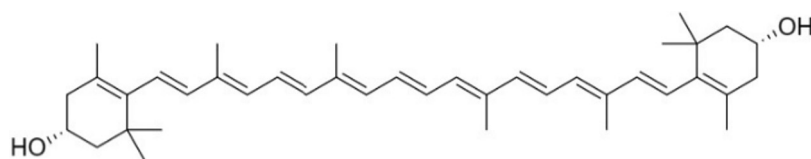


Fig. 2. Structural formula of zeaxanthin.

and some plant species such as Marigold flowers (Lin et al., 2015; Watkins and Pogson, 2020). *Tagetes erecta* is the most often used source of lutein and zeaxanthin for food supplements production on the Czech market. A typical example is Lutein PLUS (Walmark), Lutein Premium (Generica), Lutein-z (Jamieson) or ProVision (Vitaland). Lutein is present in free form or bound to fatty acids via an ester bond (Abdel-Aal and Rabalski, 2015). It is used as a food colourant (E 161b) but also as an additive in fodder for hens or in the food industry as a food supplement mainly for its antioxidant properties (Ree, 2006; Marounek and Pebriansyah, 2018). A link between lutein intake and its positive effect on vision has been shown many times. The central part of retina, called *macula lutea* (yellow spot), is responsible for high visual acuity and it is composed of lutein, zeaxanthin and meso-zeaxanthin, in common called macular pigment (Bernstein et al., 2016), which plays an important role in protecting the eye from UV and phototoxic blue light (Peng et al., 2016). Scientists conducted an experiment in the eyes of monkeys proving that those lacking xanthophylls in the diet do not have these pigments detectable in serum. However, when lutein and zeaxanthin were incorporated in their diet despite lifetime deficiency, the macular pigment quickly returned to normal levels (Tsao et al., 2007). Lutein has a preventive effect against diseases such as cataract or age-related macular degradation (AMD) (Bernstein et al., 2016; Nwachukwu et al., 2016). The major risk factor affecting AMD is oxidative stress. Taiwanese scientists have found that if people with early stage AMD receive 12 mg of lutein and 2 mg of zeaxanthin daily for five months, antioxidant activity improves. This study also claims that long-term consumption can suppress oxidative stress and thereby avoid AMD (Peng et al., 2016). Lutein is also involved in the skin protection from UV radiation, positively affects cognitive functions, helps reducing the risk of cardiovascular disease and also strengthens immunity (Mares-Perlman et al., 2002; Nwachukwu et al., 2016; Buscemi et al., 2018). Despite their many beneficial effects, the European Food Safety Authority (EFSA) has not approved any health claims concerning lutein and zeaxanthin. There is not enough evidence to prove a cause and effect relationship between the consumption of lutein and subsequent normal vision (EFSA Panel on Dietetic Products, Nutrition and Allergies, 2010). The recommended daily dose is not specified.

For the determination of carotenoids in plant matrices and food supplements, the most frequently used method is HPLC-DAD (or UV/VIS) (Aman et al., 2004; Abdel-Aal and Rabalski, 2015; Bernstein

et al., 2016). In the past, mainly normal phase HPLC was used, while nowadays reverse phase HPLC with analytical columns C18 and C30 are used for their separation (Amorim-Carrilho et al., 2014; Fratianni et al., 2015). C18 column is not capable to separate structural and geometrical isomers so it cannot be used for the separation of lutein and zeaxanthin due to their co-elution. Column C30 is the best choice for efficient separation of isomers even though their retention times are similar (Amorim-Carrilho et al., 2014). Carotenoid identification is also possible using tandem mass spectrometry (de Rosso and Mercadante, 2007; Tsiaka et al., 2018; Zhang et al., 2019) or thin layer chromatography (TLC) combined with UV/VIS visualization and densitometry (Altemimi et al., 2015).

## Materials and Methods

### Chemicals and standards

Standard of lutein (purity 95 %) was purchased from Labicom (Czech Republic) and  $\beta$ -carotene (purity  $\geq 99$  %) from Sigma-Aldrich (Germany). Sodium hydroxide and sodium sulphate were obtained from Lach-Ner s.r.o. (Czech Republic), ethanol, methanol, n-hexane and methyl tert-butyl ether (MTBE) from Merck KGaA (Germany), acetonitrile, tert-butyl-hydroxytoluene (t-BHT) from Sigma-Aldrich (Germany) and acetone from Penta Chrudim (Czech Republic). Water was purified using a Milli-Q Ultrapure water purification system from Millipore (Germany).

### Sample preparation

The first group of analysed samples consisted of Marigold flowers used commonly as carotenoid source for food supplement preparation. *Calendula officinalis* and *Tagetes patula*, specifically their blooms from the Institute of Botany in Prague, were stored in a freezer ( $-20$  °C) before the analysis and *Calendula officinalis* tea from blooms manufactured by Mediate, s.r.o. was also analysed. The samples were thoroughly homogenized in a mortar without using a solvent. Half a gram of each sample was weighed into a 15 ml plastic cuvette wrapped in aluminium foil.

Food supplements, more specifically capsules (*Lutein Complex Premium*, *Ocutein Brilliant*), available on the Czech market were analysed for carotenoid content, weighed – first the whole capsule and then just the dried shell purified with hexane, cut with a sharp scalpel and 3–5 mg of the sample was transferred into a 50 ml cuvette wrapped in aluminium foil.

### Standard preparation

The stock solution of lutein for carotenoid analysis was prepared at the concentration of  $100 \mu\text{g} \cdot \text{mL}^{-1}$ ,

concentrations of the working solution in ethanol (0.2 % t-BHT)/acetone (6:4; v/v) solvent mixture ranged from 0.1 to 20  $\mu\text{g}\cdot\text{mL}^{-1}$ . The working solution was always prepared fresh using the stock solution stored in a freezer ( $-20\text{ }^{\circ}\text{C}$ ).

#### **Determination of dry matter**

Homogenised flower samples were dried to a constant weight at  $105\text{ }^{\circ}\text{C}$ .

#### **Extraction of lutein, zeaxanthin and $\beta$ -carotene**

The first method used was direct extraction for blooms of *Calendula officinalis* and *Tagetes patula*. First, 2 ml of the mixture of ethanol (0.2 % t-BHT)/n-hexane – 4:4 (v/v) were added to the weighed sample. The cuvette was capped, coated with parafilm and shaken for 30 minutes on a shaker. Then, 2 ml of deionised water were used to separate the layers and the mixture was centrifuged (6000 RPM,  $5\text{ }^{\circ}\text{C}$ , 5 min). Subsequently, the upper hexane layer was removed into a 50 ml heart flask and re-extraction of the ethanol portion was repeated with another 4 ml of n-hexane (followed by shaking, centrifugation and removal of the upper hexane layer). The re-extraction was carried out until the upper hexane layer was colourless. All hexane extracts were combined and evaporated on the evaporator at  $30\text{ }^{\circ}\text{C}$ , followed by slow evaporation to dryness in a stream of nitrogen gas. The residue was reconstituted in a 10 ml mixture of ethanol (0.2 % t-BHT)/acetone – 6:4 (v/v) and filtered through a microfilter on a centrifuge (10000 RPM,  $5\text{ }^{\circ}\text{C}$ , 3 min) to obtain approximately 1 ml of solution which was transferred to an amber vial and prepared for HPLC analysis.

The second extraction method for blooms of *Calendula officinalis* and *Tagetes patula* involved alkaline hydrolysis. First, 2 ml of the mixture of ethanol (0.2 % t-BHT)/acetone – 6:4 (v/v) and 2 ml of n-hexane were added to the weighed sample followed by vortexing for 5 min. Then, 6 ml of n-hexane and then 5 ml of the mixture of ethanol (0.2 % t-BHT)/acetone – 6:4 (v/v) were added and vortexing was repeated for another 5 min. Afterward, 5 ml of methanolic potassium hydroxide (conc.  $20\text{ g}\cdot\text{l}^{-1}$ ) were added to saponify the whole suspension. Cuvettes covered in aluminium foil and filled with nitrogen gas (to maintain inert atmosphere in the cuvette) were kept at room temperature (approx.  $23\text{ }^{\circ}\text{C}$ ) overnight. The next day, 10 ml of n-hexane and 10 ml of a solution of  $\text{Na}_2\text{SO}_4$  in deionized water (conc.  $100\text{ g}\cdot\text{l}^{-1}$ ) were added to the mixture. The cuvette covered with parafilm was intensively hand-shaken for 2 min and then centrifuged (10000 RPM,  $5\text{ }^{\circ}\text{C}$ , 5 min). The upper hexane layer was removed into a 50 ml heart

flask and then the procedure was exactly same as in direct extraction.

Direct extraction and alkaline hydrolysis extraction were used also for the analysis of food supplements. The procedures were almost identical to the extraction methods for Marigold flowers, the only difference was the use of hexane/acetone – 1:1 (v/v) with the addition of t-BHT (0.2 g per 100 ml solution) as an extracting agent.

#### **HPLC-DAD determination**

High-performance liquid chromatography coupled with a diode array detector (HPLC-DAD) was used for chromatographic separation and sample analysis (Agilent Technologies 1200 series, Santa Clara, CA, USA). The separation of carotenoids was carried out using analytical column Poroshell 120 EC-C18 ( $2.1 \times 100\text{ mm}$ ;  $2.7\text{ }\mu\text{m}$ ) at the column temperature of  $30\text{ }^{\circ}\text{C}$  and the flow rate of  $0.5\text{ ml}\cdot\text{min}^{-1}$ . The mobile phase was composed of 100% acetonitrile (A) and 90 % acetonitrile in deionized water (B). Gradient elution was used (0–2 min for 100 % B, 5–28 min for 0 % B, 28.5–30 min for 100 % B). The injection volume was  $3\text{ }\mu\text{L}$ . As lutein and zeaxanthin are not separated in the C18 column, the C30 column ( $3.0 \times 100\text{ mm}$ ;  $3\text{ }\mu\text{m}$ , YMC, Japan) was also used to determine the ratio of lutein and zeaxanthin in all matrices. Column temperature was  $35\text{ }^{\circ}\text{C}$ , flow rate was  $0.4\text{ ml}\cdot\text{min}^{-1}$ , injection volume was  $3\text{ }\mu\text{l}$  and mobile phase consisted of MeOH/MTBE/ $\text{H}_2\text{O}$  in the ratio of 81:15:4, v/v/v (A) and MeOH/MTBE/ $\text{H}_2\text{O}$ , 7:90:3, v/v/v (B). Gradient elution was also used (0–10 min for 0 % B, 45 min for 56 % B, 50 min for 100 % B, 55–60 min for 0 % B). Carotenoids were detected at the wavelengths of 444 nm – lutein and zeaxanthin, and 450 nm –  $\beta$ -carotene. The identification was performed by comparing the retention times of chromatograms and spectra of the measured samples with the standards of lutein and  $\beta$ -carotene. The external calibration method was used for quantification. Zeaxanthin was quantified on the lutein standard.

#### **Methods performance characteristics**

Response of the detector in the used calibration range of  $0.1\text{--}20\text{ }\mu\text{g}\cdot\text{ml}^{-1}$  was linear. Detection limit (LOD) for lutein and  $\beta$ -carotene in Marigold flowers and food supplements was  $0.1\text{ }\mu\text{g}\cdot\text{ml}^{-1}$ , determined as the lowest point on the calibration line. Repeatability was expressed as a relative standard deviation (RSD). For the finally used method with alkaline hydrolysis, RSD values were 2.3 % for lutein and 5.1 % for  $\beta$ -carotene in Marigold flowers and 2.3 % for lutein in food supplements. Limit of quantification (LOQ) was recalculated per kilogram of the

sample according to the weight and performed extraction procedure to be  $1.7 \text{ mg} \cdot \text{kg}^{-1}$  for lutein and  $7.3 \text{ mg} \cdot \text{kg}^{-1}$  for  $\beta$ -carotene in Marigold flowers. In case of food supplements, LOQ was quite high, specifically  $200 \text{ mg} \cdot \text{kg}^{-1}$  for lutein, which corresponds to 0.25 mg per one Lutein Complex Premium capsule weighing approximately 1.27 g.

## Results and discussion

The performed experiments aimed to determine the content of free and bound lutein/zeaxanthin in matrices used for the production of food supplements (*Calendula officinalis*, *Tagetes patula*) and the content of these xanthophylls in food supplements as well as to compare the determined levels with the producer's declaration. Supplements Lutein Complex Premium and Ocuttein Brillant were chosen for the analysis. These food supplements are very popular and often used by the Czech population, which is the main reason why the analysis was focused on them.

The first analysed matrices were dried and frozen blooms of *Calendula officinalis*. In both cases, satisfactory extraction yields were achieved using minimum three repeated extractions, both for direct extraction and for the alkaline hydrolysis process. Dried blooms of *Calendula officinalis* purchased as tea had very low water content of approximately 7 %. The water content of frozen flowers varied between 81–86 %. To compare results obtained in different matrices, the carotenoid content was expressed on the dry matter of the sample. C18 column was sufficient for the determination of total lutein and zeaxanthin content as the time needed for separation is significantly shorter, approximately twice, compared to the C30 column separation. It has been found that in case of *Calendula officinalis*, the inclusion of an alkaline hydrolysis step is necessary. In dried flowers used for tea preparation, lutein content was determined to be  $11.9 \text{ mg} \cdot \text{kg}^{-1}$  of dry matter by direct extraction. After alkaline hydrolysis, the content increased approximately three times compared to the direct extraction method, to  $46.0 \text{ mg} \cdot \text{kg}^{-1}$  of dry matter. The overall relatively low detected content of this xanthophyll was probably due to its degradation during flower drying. Based on the determined content it can be claimed that *Calendula officinalis* tea is not a very good source of xanthophylls. Lutein content in frozen flowers ranged from 807 to  $1472 \text{ mg} \cdot \text{kg}^{-1}$  of dry matter. In comparison with literature data, the content was also expressed on fresh matter ranging from 122 to  $253 \text{ mg} \cdot \text{kg}^{-1}$ . Lower, but also similar xanthophyll contents were determined by Romanian scientists who analysed four different varieties of *Calendula officinalis*. The lutein

content ranged from 40 to  $256 \text{ mg} \cdot \text{kg}^{-1}$  (Pintea et al., 2003). On the other hand, Brazilian scientists have determined in *Calendula officinalis* lutein content of  $298 \text{ mg} \cdot \text{kg}^{-1}$  (Manke Natchigal et al., 2010). In literature, a significant difference between the lowest and highest concentration of lutein can be observed, which is probably due to various varieties, different geographical and climatic growth conditions or different way of storage. During our experiment, *Calendula officinalis* extracts were also analysed on a C30 column and the approximate lutein to zeaxanthin ratio was found to be 14:3. After the inclusion of the alkaline hydrolysis step, there was no significant increase in the  $\beta$ -carotene content. However, the used method included alkaline hydrolysis for all determined carotenoids. In *Calendula officinalis* dried blooms, the content of  $\beta$ -carotene was determined to be  $13.8 \text{ mg} \cdot \text{kg}^{-1}$  of dry matter, in frozen flowers it ranged from 220– $904 \text{ mg} \cdot \text{kg}^{-1}$  of dry matter, expressed on fresh matter it was 32– $155 \text{ mg} \cdot \text{kg}^{-1}$ . The measured data were compared with the available literature. The content determined by Romanian scientists ranged from 23– $460 \text{ mg} \cdot \text{kg}^{-1}$  (Pintea et al., 2003). It was found that the concentration range is wide, in Romanian varieties bought in specialized stores in France it is even wider than that determined in this study.

Another plant matrix analysed was frozen flowers of *Tagetes patula* with the water content of approximately 84–86 %. In this case, three extractions were also needed for the two tested extraction procedures. The inclusion of alkaline hydrolysis for extraction has been proven to be essential for this analysis. Fig. 3 shows chromatograms documenting the increase in the xanthophyll content after the inclusion of the alkaline hydrolysis step including the separation of isomers. Figure 4 shows the UV/VIS spectra of lutein and zeaxanthin.

The combined content of lutein and zeaxanthin ranged from 5906 to  $8677 \text{ mg} \cdot \text{kg}^{-1}$  of dry matter. Literature data for a *Tagetes erecta* cultivar harvested on Bali and called Mega Orange show lutein and zeaxanthin range from 8950 to  $14550 \text{ mg} \cdot \text{kg}^{-1}$  of dry matter. The content we determined was lower as well as that of another cultivar called Mega Gold also from Bali ( $2560$ – $3730 \text{ mg} \cdot \text{kg}^{-1}$  of dry matter) (Kurniawan et al., 2019). The determined xanthophyll content was also expressed on fresh matter for comparison with the published literature data. Brazilian scientists determined lutein content in brown flowers of *Tagetes patula* to be  $12306 \text{ mg} \cdot \text{kg}^{-1}$  and in yellow flowers it was  $597 \text{ mg} \cdot \text{kg}^{-1}$  (Manke Natchigal et al., 2010). We determined higher lutein concentrations in comparison with the cited levels in yellow flowers, but lower than published for brown flowers. Lutein content in our samples ranged from

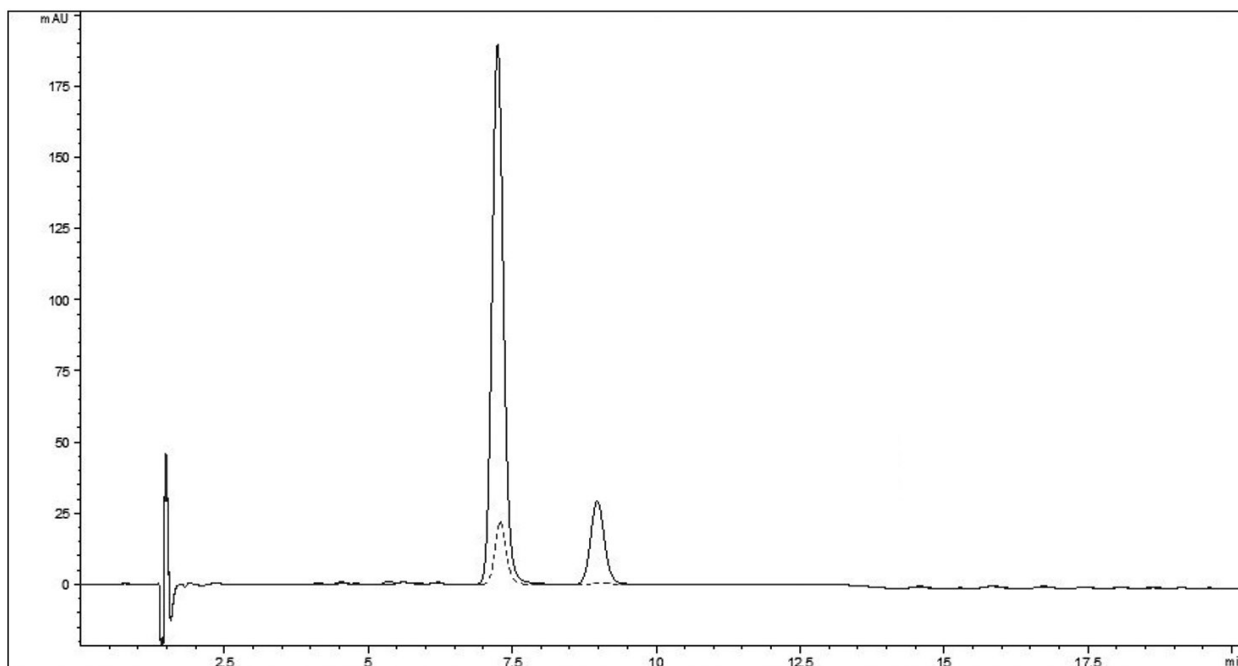


**Fig. 3.** Chromatograms of the *Tagetes patula* sample, comparison of direct extraction method (dashed line) and extraction with alkaline hydrolysis (solid line); C30 column,  $\lambda = 444$  nm.

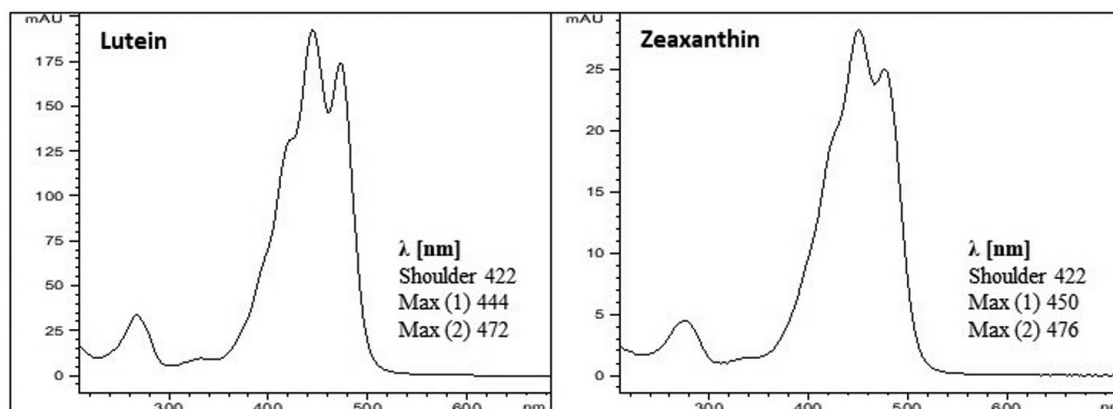


**Fig. 4.** UV/VIS spectra of lutein and zeaxanthin in *Tagetes patula*.

850–1362 mg · kg<sup>-1</sup> of fresh matter. When separated on the C30 column, the lutein:zeaxanthin ratio of 24:1 was determined for *Tagetes patula* flowers. The average content of  $\beta$ -carotene was 467.5 mg · kg<sup>-1</sup> of dry matter in frozen flowers of *Tagetes patula*.

Due to its high lutein content, approximately six times higher than in *Calendula officinalis*, *Tagetes patula* is widely used for the production of food supplements. The advantage of this raw material is its good availability, low price and also high yields in cultivation.

Food supplements in form of capsules were also analysed within the experiments and an analytical method for their extraction has been developed and validated. The alkaline hydrolysis extraction procedure for plant matrices has been found to be unsuitable for food supplements in form of capsules

since it results in lower yields than the extraction procedure based on the published article (Aman et al., 2004). In our case, the vortex was replaced by a shaker (1800 RPM) mentioned in the article, a mixture of BHA and BHT was recommended as an antioxidant but only BHT was used. Due to the lack of accurate information in the experimental part, the procedure was linked to the alkaline hydrolysis extraction procedure for plant matrices mentioned in the experimental part. The resulting modified and subsequently validated method for food supplements is described in details in the experimental part.

In order to optimize the extraction procedure with alkaline hydrolysis, a sample of 50 mg was initially selected but the carotenoid content was too high and no decolourisation of the extracted sample was achieved even after nine re-extractions. At

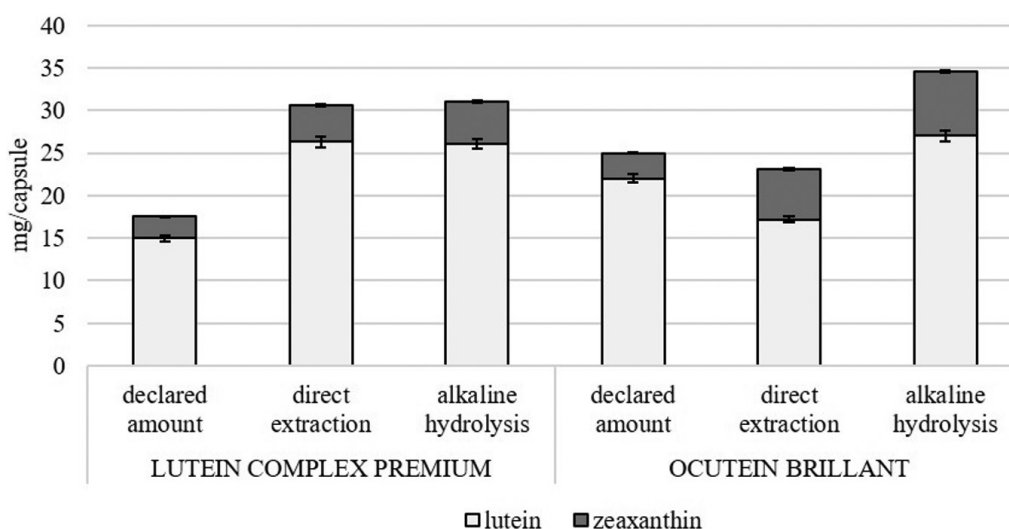


**Fig. 5.** Comparison of declared amounts of lutein and zeaxanthin with the values determined in the food supplements by direct extraction and extraction with alkaline hydrolysis.

the sample weight of 13 mg and, seven repeated extractions provided the amount of lutein and zeaxanthin of  $15.9 \text{ mg} \cdot \text{capsule}^{-1}$  (declared amount  $17.5 \text{ mg} \cdot \text{capsule}^{-1}$ ) on the C18 column and the sample had to be diluted ten times prior to the analysis because the concentration was out of the linear range of the method. Reduced sample weight was used in other experiments and 3–5 mg proved to be an ideal weighed-in portion. Because of the homogeneous consistency of the sample, it can be easily weighed on an analytical balance, and it is sufficient to repeat the extraction step three to four times for the quantitative extraction of analytes. For the Lutein Complex Premium samples, the repeatability of the method, calculated as Relative Standard Deviation (RSD), was determined based on six parallel measurements performed.

Lutein content of  $26.1 \text{ mg} \cdot \text{capsule}^{-1}$  (declared value  $15 \text{ mg} \cdot \text{capsule}^{-1}$ ), zeaxanthin content of  $4.9 \text{ mg} \cdot \text{capsule}^{-1}$  (declared value  $2.5 \text{ mg} \cdot \text{capsule}^{-1}$ ) and  $\beta$ -carotene content of  $6.6 \text{ mg} \cdot \text{capsule}^{-1}$  (declared  $2 \text{ mg} \cdot \text{capsule}^{-1}$ ) were detected using the C30 column for separation. Application of an extraction method without the alkaline hydrolysis step yielded approximately the same amount of lutein ( $26.3 \text{ mg} \cdot \text{capsule}^{-1}$ ) and zeaxanthin ( $4.3 \text{ mg} \cdot \text{capsule}^{-1}$ ) but the extraction procedure was more difficult and the sample had to be extracted more times to achieve its discolouration. For this reason, alkaline hydrolysis was also included in the analysis of the capsules. Carotenoid levels were analysed in food supplements with an expiration date of more than two years. It is likely that the manufacturer tries to ensure sufficient carotenoid content in the capsules at the end of the expiration date. The Lutein Complex Premium declaration states that lutein is present in the capsule in form of

20 % marigold extract.

The Ocutein Brilliant food supplement analysed was also gel-like but with harder coating. In this sample, the extraction method without hydrolysis was not sufficiently effective as the matrix is very concentrated and despite the low sample weight it was not possible to extract carotenoids (until the sample was discoloured) even by multiple extractions. Therefore, a validated alkaline hydrolysis method described in the experimental part was used for both food supplements analysed with three to four extraction steps required to completely decolour the upper hexane layer. Experimentally,  $27 \text{ mg} \cdot \text{capsule}^{-1}$  of lutein (declared amount of  $22 \text{ mg} \cdot \text{capsule}^{-1}$ ) and  $7.6 \text{ mg} \cdot \text{capsule}^{-1}$  of zeaxanthin (declared  $3 \text{ mg} \cdot \text{capsule}^{-1}$ ) were determined. The expiration date for Ocutein Brilliant capsules was more than two years after purchase at the store. The source of xanthophylls has not been reported for this food supplement.

A comparison of the declared and experimentally determined xanthophyll content of food supplements is summarized in Fig. 5.

## Conclusion

For the determination of carotenoids in Marigold flowers (*Tagetes patula* and *Calendula officinalis*) as well as in food supplements, an analytical method including an alkaline hydrolysis step to release bound carotenoids from the matrix has been developed and validated. Lutein content determined by this method for *Calendula officinalis* was  $807\text{--}1472 \text{ mg} \cdot \text{kg}^{-1}$  of dry matter and that for *Tagetes patula* was  $5906\text{--}8677 \text{ mg} \cdot \text{kg}^{-1}$ . For the separation of lutein and zeaxanthin, C30 analytical columns were used.

Marigold flowers, especially *Tagetes patula*, are considered to be a good source of carotenoids for the production of food supplements for eye health but also as a suitable addition to feed for laying hens. The amount of xanthophylls was determined in food supplements, specifically capsules, and the levels were compared with the manufacturer's declaration. Food supplement manufacturers maintain the declared amounts and ensure that the product contains enough carotenoids throughout the expiration period.

#### Acknowledgements

*This work was supported by METROFOOD-CZ research infrastructure project (MEYS Grant No: LM2018100) including access to its facilities; the Operational Programme Prague – Competitiveness (CZ.2.16/3.1.00/21537 and CZ.2.16/3.1.00/24503) and by the “National Program of Sustainability I” – NPU I (LO1601 – No.: MSMT-43760/2015).*

#### References

- Abdel-Aal SM, Rabalski I (2015) *Journal of Agricultural and Food Chemistry* 63(44): 9740–9746.
- Altemimi A, Lightfoot DA, Kinsel M, Watson DG (2015) *Molecules* 20(4): 6611–6625.
- Aman R, Bayha S, Carle R, Schieber A (2004) *Journal of Agricultural and Food Chemistry* 52(20): 6086–6090.
- Amorim-Carrilho KT, Cepeda A, Fente C, Regal P (2014) *TrAC Trends in Analytical Chemistry* 56: 49–73.
- Becerra MO, Contreras LM, Lo MH, Díaz JM, Herrera GC (2020) *Journal of Functional Foods* 66: 103771.
- Bernstein PS, Li B, Vachali PP, Gorusupudi A, Shyam R, Henriksen BS, Nolan JM (2016) *Progress in Retinal and Eye Research* 50: 34–66.
- Buscemi S, Corleo D, Di Pace F, Petroni ML, Satriano A, Marchesini G (2018) *Nutrients* 10(9): 1321.
- de Rosso VV, Mercadante AZ (2007) *Journal of Agricultural and Food Chemistry* 55(13): 5062–5072.
- EFSA Panel on Dietetic Products, Nutrition and Allergies (2010) *EFSA Journal* 8(2): 1492.
- Fратиanni A, Mignogna R, Niro S, Panfili G (2015) *Journal of Food Science* 80(12): C2686–C2691.
- Kurniawan JM, Yusuf MM, Azmi SS, Salim KP, Prihastyanti MNU, Indrawati R, Shioi Y, Limantara L, Brotosudarmo THP (2019) *IOP Conference Series: Materials Science and Engineering* 509: 012060.
- Lin JH, Lee DJ, Chang JS (2015) *Journal of the Taiwan Institute of Chemical Engineers* 49: 90–94.
- Manke Natchigal A, Oliveira Stringheta AC, Corrêa Bertoldi M, Stringheta PC (2010) *ISHS Acta Horticulturae* 939: 309–314.
- Mares-Perlman JA, Millen AE, Ficek TL, Hankinson SE (2002) *The Journal of Nutrition* 132(3): 518S–524S.
- Marounek M, Pebriansyah A (2018) *Agricultura Tropica et Subtropica* 51: 107–111.
- Nwachukwu ID, Udenigwe CC, Aluko RE (2016) *Trends in Food Science & Technology* 49: 74–84.
- Peng ML, Chiu HF, Chou H, Liao HJ, Chen ST, Wong YC, Shen YC, Venkatakrishnan K, Wang CK (2016) *Journal of Functional Foods* 24: 122–130.
- Pintea A, Bele C, Andrei S, Socaciu C (2003) *Acta Biologica Szegediensis* 47(1–4): 37–40.
- Ree E (2006) *The EFSA Journal* 315(1): 1–12.
- Rodriguez-Amaya DB (2019) *Food Research International* 124: 200–205.
- Saini RK, Nile SH, Park SW (2015) *Food Research International* 76: 735–750.
- Tsao R, Wang M, Deng Z (2007) *American Chemical Society* 956: 352–372.
- Tsiaka T, Lantzouraki DZ, Siapi E, Sinanoglou VJ, Heropoulos GA, Calokerinos AC, Zoumpoulakis P (2018) *Journal of Chromatography B* 1096: 160–171.
- Watkins JL, Pogson BJ (2020) *Trends in Plant Science* (19)30346-2: 1360–1385.
- Woodside JV, McGrath AJ, Lyner N, McKinley MC (2015) *Maturitas* 80(1): 63–68.
- Yabuzaki J (2017) *The Journal of Biological Databases and Curation* 2017(1): bax004.
- Zhang L, Wang S, Yang R, Mao J, Jiang J, Wang X, Zhang W, Zhang Q, Li P (2019) *Food Chemistry* 289: 313–319.

# Absorption removal of hydrogen sulfide from recirculated biogas

Nikolas Gróf, Jana Barbušová, Kristína Hencelová, Miroslav Hutňan

*Department of Environmental Engineering, Faculty of Chemical and Food Technology, Slovak University of Technology, Radlinského 9, 812 37 Bratislava, Slovak Republic  
nikolas.grof@stuba.sk*

**Abstract:** This study is focused on the effect of biogas recirculation with hydrogen sulfide removal on anaerobic treatment of sulfur-enriched synthetic wastewater in a UASB reactor. The presence of hydrogen sulfide in biogas causes problems in its further energy recovery while sulfides inhibit the anaerobic process. The reactor was gradually loaded with sulfates and their effect on the reactor operation was monitored. At the same time, external absorption of hydrogen sulfide from biogas with absorbent regeneration was operated. The results show that low concentrations of added sulfates support biogas production. At the sulfate concentration of 125 mgL<sup>-1</sup>, biogas production increased by approximately 2 ld<sup>-1</sup>. However, further increasing of the amount of sulfates in the substrate led to the opposite effect. At twice the amount of sulfates, the biogas production decrease by 1 ld<sup>-1</sup> and its adverse effects on the removal of N-NH<sub>4</sub>, N<sub>C</sub> and P-PO<sub>4</sub> were observed. Biogas recirculation through the absorption column ensured a decrease in the hydrogen sulfide concentration from 19 960 ppm to 4 030 ppm and an increase in the methane content from 59.2 % to 83 % and also a decrease in the sulfides concentration in the reactor. From the measured data it can be concluded that this method reduces sulfides inhibition.

**Keywords:** absorption, anaerobic digestion, hydrogen sulfide, UASB reactor

## Introduction

Anaerobic digestion is the decomposition of biomass by microorganisms under anaerobic condition, i.e. without oxygen. In the process, four sets of biochemical reactions can be recognized: hydrolysis, acidogenesis, acetogenesis and methanogenesis (Kadam and Panwar, 2017). During the process of anaerobic digestion (AD) of solid waste and wastewater, biogas, a renewable energy source, is produced (Watsuntorn et al., 2019). Biogas consists of 50–70 % of methane (CH<sub>4</sub>) and 30–50 % of carbon dioxide (CO<sub>2</sub>) and of a small portion of other compounds, such as 0–3 % of nitrogen (N<sub>2</sub>), 5–10 % of water vapor (H<sub>2</sub>O), 0–1 % of oxygen (O<sub>2</sub>), 0–20 000 % of hydrogen sulfide (H<sub>2</sub>S) depending on the feedstock origin (Angelidaki et al., 2018).

Industries, such as paper, textile and pharmaceutical, produce sulfate-rich wastewater which is reduced to sulfides, including gaseous hydrogen sulfide (H<sub>2</sub>S), during anaerobic treatment and causes process inhibition due to toxicity to methanogens (Pokorna-Krayzelova et al., 2017). H<sub>2</sub>S is one of the most common biogas pollutants causing corrosion to internal combustion devices and industrial pipes (Maizonnasse et al., 2013). It is deadly for humans at the concentration of 300 ppm (Aita et al., 2016). The upper limit of H<sub>2</sub>S concentration permissible for the combined heat and power engines is in the range of 100–500 ppm. Therefore, hydrogen sulfide has to be removed from the biogas (San-Valero et al., 2019). Hydrogen sulfide

can be removed from contaminated streams (liquid or gaseous) by physico-chemical (adsorption, precipitation, etc.) or biological methods. Physico-chemical methods are energy-intensive and expensive because they are carried out under high temperatures and pressures and also additional chemicals are needed. In contrast, biological methods employ biochemical oxidation of sulfides to sulfates, thiosulfates or elemental sulfur and thus they have lower operating cost with lower or no addition of chemicals (Krayzelova et al., 2014).

Hydrogen sulfide has an inhibitory or toxic effect on methanogenic organisms, especially in its undissociated form. The free H<sub>2</sub>S molecule penetrates the cell wall directly into the cell and its inhibitory effects are manifested immediately after the cytoplasm is overcome. H<sub>2</sub>S inhibits protein production, deactivates various coenzymes in the cell and interferes with the assimilative metabolism of sulfur. To reduce this impact, in situ methods as microaeration and precipitation, dilution with water and a co-fermentation with a low sulfur content substrate to increase the C:N ratio can be used (Hutňan et al., 2016; Krayzelova et al., 2015). Hutňan et al. (2016) used precipitation to control sulfide inhibition in anaerobic treatment of waste biomass from the production of cystine with high sulfur content – about 6% of total dry matter. Chávez Fuentes J.J. et al. (2015) also investigated the possibility of using dilution of waste biomass from cystine production to reduce sulfide inhibition.

Biogas recirculation to reduce sulfide toxicity in the anaerobic system was used by Olivier et al. (2020) who investigated the use of four different wood-derived biochar types (softwood and hardwood-derived biochar produced at 550 °C and 800 °C) to alleviate sulfide toxicity to methane producing archaea (MPA) and sulfate-reducing bacteria (SRB) during anaerobic treatment of sulfate rich wastewater.

Wang et al. (2003) investigated dosing of oxygen for the oxidation of sulfides into recycled biogas. Oxygen dosing was controlled by oxidation–reduction potential (ORP).

The aim of this work was to study the impact of hydrogen sulfide removal technology in recirculated biogas on reducing sulfide inhibition of anaerobic processes.

## Materials and Methods

The experiment was performed in a upflow anaerobic sludge blanked (UASB) reactor (Fig. 1) with the operating volume of 3.9 l. This reactor was inoculated with anaerobic sludge from the wastewater treatment plant (WWTP) Devínska Nová Ves, with the initial total solid concentration of 19.48 g·l<sup>-1</sup> and the volatile solids concentration of 8.24 g·l<sup>-1</sup> (57.7 %). The reactor was operated at mesophilic condition (37 °C) and pH of the sludge was 7.82. Volume flow rate of the substrate during the process increased gradually to 6.5 l·d<sup>-1</sup>, which represents the hydraulic retention time of 14 hours. A synthetic substrate consisting of glucose, sodium

acetate, macro- and micronutrients was fed to the bottom of the reactor using a peristaltic pump. The substrate advanced up through a sludge bed formed by a layer of biomass. At the top of the reactor, biomass and biogas were separated from the treated water using a gas-liquid-solids separator (G-L-S separator). The amount of biogas was measured using a drum gas meter. Upon completion of the reactor start-up phase, sulfur was added to the system as sodium sulfate. At the same time, external absorption of hydrogen sulfide was started with absorbent regeneration. At the top of the reactor, a separating element was introduced to ensure biogas recirculation and simultaneous measurement of the produced biogas. Recirculation was provided by a peristaltic pump that pumped biogas through a counter-current absorption column packed with plastic tubes to increase the surface for the phase transfer of hydrogen sulfide from biogas to water, which was used as the absorption agent. Purified biogas was fed back through the partition element to the top of the reactor (fig. 1).

Water enriched with hydrogen sulfide was drained gravitationally to an aerated regeneration column providing oxidation. It was passed through a settling tank and accumulated in a beaker from where it was pumped back to the absorption column.

During the long-term operation of the laboratory model, parameters such as pH, chemical oxygen demand (COD), ammonia nitrogen (N-NH<sub>4</sub>), orthophosphate-phosphorus (P-PO<sub>4</sub>), volatile fatty acids (VFA), sulfides (S<sup>2-</sup>) and sulfates (SO<sub>4</sub><sup>2-</sup>) concentrations were monitored in the anaerobic reactor

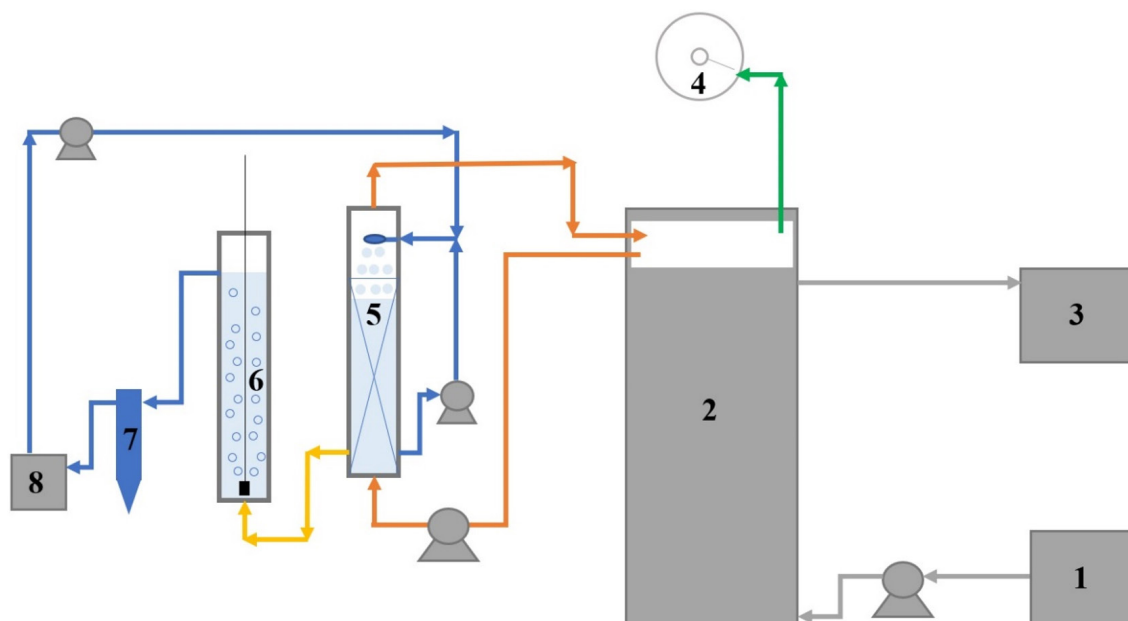


**Fig. 1.** Laboratory UASB reactor with external removal of hydrogen sulfide from recirculated biogas: 1 – tank for substrate, 2 – UASB reactor, 3 – tank for effluent, 4 – drum gas meter, 5 – counter-current absorption column, 6 – regeneration column, 7 – settling tank, 8 – tank for regenerated water.

(filtered sample) according to APHA, AWWA, WEF (2017). In addition, the amount of biogas (drum gas meter type AMS Spectrum TCM 143/10 – 4726) produced at laboratory temperature and its composition were measured using a gas analyzer GA 2000 Plus (Geotechnical Instruments, UK).

## Results and Discussion

Start-up of UASB reactor was initiated at the organic load rate (ORL) of  $0.5 \text{ kg (COD)} \cdot \text{m}^{-3} \cdot \text{d}^{-1}$ . Successful granulation was reached within 218 day, subsequently, 2 l of sludge were withdrawn from the reactor for the maximum specific methanogenic activity test (MSMA), which was performed according to Hussain and Dubey (2014). From the experimental values, the value of MSMA was calculated to be  $0.589 \text{ kg} \cdot \text{kg}^{-1} \cdot \text{d}^{-1}$ , which represents five times higher methanogenic activity of anaerobic biomass compared to suspended anaerobically stabilized biomass. The mean values of methanogenic activity for stabilized sludge are up to  $0.1 \text{ kg} \cdot \text{kg}^{-1} \cdot \text{d}^{-1}$ . After completion of the MSMA tests and stabilization of biogas production, the reactor was operated in three phases.

The first phase began on the 224<sup>th</sup> day when sulfur was added to the reactor. This phase lasted for 20 days, during which synthetic substrate with the sulfate concentration of  $125 \text{ mg} \cdot \text{l}^{-1}$  was continuously dosed. Biogas production and composition was measured and qualitative analyzes of the sludge water leaving the reactor were done. Fig. 2 shows that low sulfate concentration has a positive effect on biogas production. Production was in the range of  $16\text{--}17 \text{ l} \cdot \text{d}^{-1}$ , which is approximately  $1 \text{ l} \cdot \text{d}^{-1}$  higher than before the sulfate addition to the reactor ( $15\text{--}16 \text{ l} \cdot \text{d}^{-1}$ ). These results were confirmed by the tests of biochemical methane potential (BMP). In Fig. 3, concentrations of the quality parameters at the reactor outlet are presented, which indicate that this concentration does not affect the removal of ammonia nitrogen ( $\text{N-NH}_4$ ), total nitrogen ( $\text{N}_\text{C}$ )

or orthophosphate-phosphorus ( $\text{P-PO}_4$ ):  $\text{N-NH}_4$  concentration ranged from  $10\text{--}25 \text{ mg} \cdot \text{l}^{-1}$ ,  $\text{N}_\text{C}$  concentration was  $40 \text{ mg} \cdot \text{l}^{-1}$ , and  $\text{P-PO}_4$  concentration was approximately  $9 \text{ mg} \cdot \text{l}^{-1}$ .

The second phase of the process began on day 245 when the sulfate concentration was increased to  $250 \text{ mg} \cdot \text{l}^{-1}$ . Fig. 2 shows that this concentration already affects the process. Biogas production decreased to its original value ( $15\text{--}16 \text{ l} \cdot \text{d}^{-1}$ ). The presence of sulfates in the wastewater causes a change in the metabolic pathways in the anaerobic reactor due to competition for substrate between sulfate-reducing bacteria (SRB) and fermentative, acetogenic and methanogenic microorganisms. The degree of this competition is mainly related to the pH and the  $\text{COD}/\text{SO}_4^{2-}$  ratio in the wastewater. Preferably, SRBs oxidize methanogenic substrates thereby reducing biogas production. From Fig. 3 it can be concluded that increasing the concentration of sulfates has an adverse effect on the removal of  $\text{N-NH}_4$  and  $\text{N}_\text{C}$ . The concentration of  $\text{N-NH}_4$  at the reactor outlet ranged from  $30$  to  $45 \text{ mg} \cdot \text{l}^{-1}$ , which is approximately double compared with the first phase ( $10\text{--}25 \text{ mg} \cdot \text{l}^{-1}$ ). The same trend was observed for  $\text{N}_\text{C}$  with the concentration ranging from  $50$  to  $70 \text{ mg} \cdot \text{l}^{-1}$ . The  $\text{P-PO}_4$  concentration increased only slightly, from  $9 \text{ mg} \cdot \text{l}^{-1}$  to  $13 \text{ mg} \cdot \text{l}^{-1}$ . From the beginning of the second phase, the outlet concentration of sulfates was also monitored and it was approximately  $40 \text{ mg} \cdot \text{l}^{-1}$ .

On day 265, the sulfate concentration was increased to  $700 \text{ mg} \cdot \text{l}^{-1}$  to initiate the third phase of the UASB reactor operation. This concentration already slightly inhibited the whole process, as it can be seen in Fig. 2. Biogas production decreased, which was also expected based on the BMP tests performed. The decrease in biogas production was about  $2\text{--}4 \text{ l} \cdot \text{d}^{-1}$ . The outlet parameters (Fig. 3) indicate deterioration of the quality of the outlet sludge water. The concentration of  $\text{N-NH}_4$  ranged from  $50$  to  $90 \text{ mg} \cdot \text{l}^{-1}$  while that of  $\text{N}_\text{C}$  ranged from  $60$  to  $100 \text{ mg} \cdot \text{l}^{-1}$ . The adverse effect of high

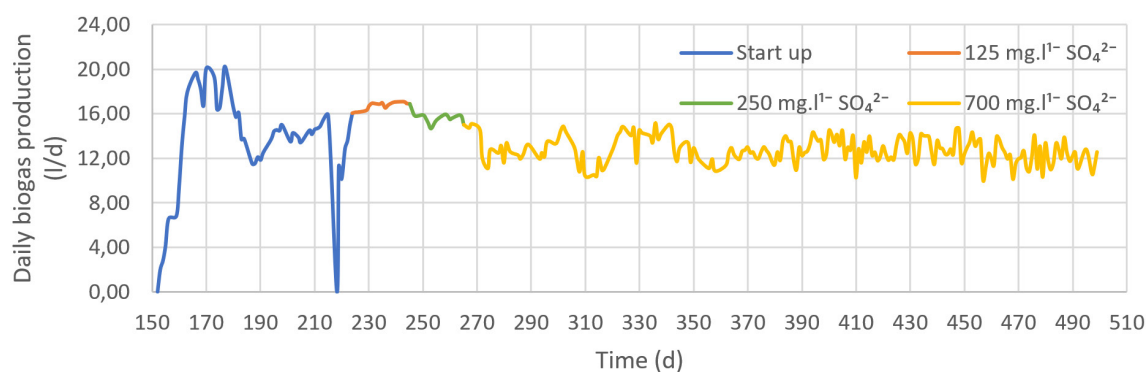


**Fig. 2.** Daily biogas production at various sulfate concentrations.

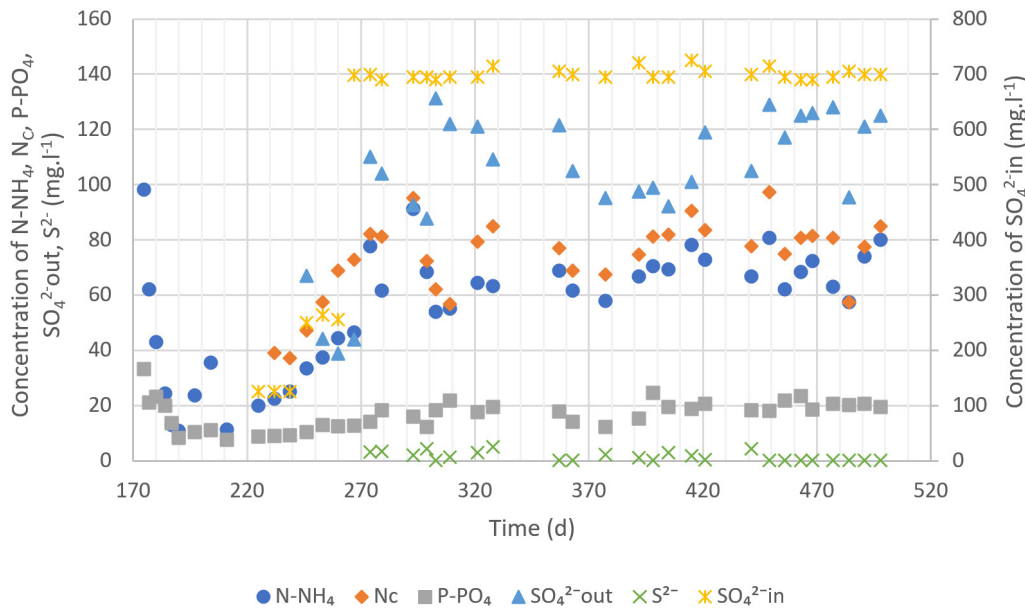


**Fig. 3.** Qualitative parameters of UASB reactor.

sulfate concentration was also observed through the removal of P-PO<sub>4</sub>. The concentration of P-PO<sub>4</sub> at the reactor outlet ranged from 12 to 25 mg·l<sup>-1</sup>. When comparing the second and third phases, the outlet concentration of all monitored parameters (N-NH<sub>4</sub>, N<sub>C</sub>, P-PO<sub>4</sub>, SO<sub>4</sub><sup>2-</sup>) were approximately doubled. In the third phase, sulfides concentration at the reactor outlet was monitored. During operation, the sulfide concentration in the sludge water did not exceed 5 mg·l<sup>-1</sup>.

In Fig. 4 shows the pH value of around 7.5 during the whole operation, only at the beginning of the start-up (187<sup>th</sup> day), the value dropped to 6.5 probably due to the reactor overload. The reac-

tor overload also indicates a significant increase in the concentrations of VFA (1 000–1 200 mg·l<sup>-1</sup>) and COD (2 000–2 500 mg·l<sup>-1</sup>) at the outlet. After stabilization of the system, the VFA concentration decreased below 250 mg·l<sup>-1</sup> and the COD removal efficiency was above 90 %.

During the reactor operation, the effect of hydrogen sulfide absorption in the recirculated biogas stream on the anaerobic process was assessed. The set values of biogas composition are given in Tab. 1. In the first biogas composition analysis, carried out on the 223<sup>rd</sup> measurement day, no recirculation occurred and sulfur was not added to the system but biogas contained 780 ppm of hydrogen sulfide.

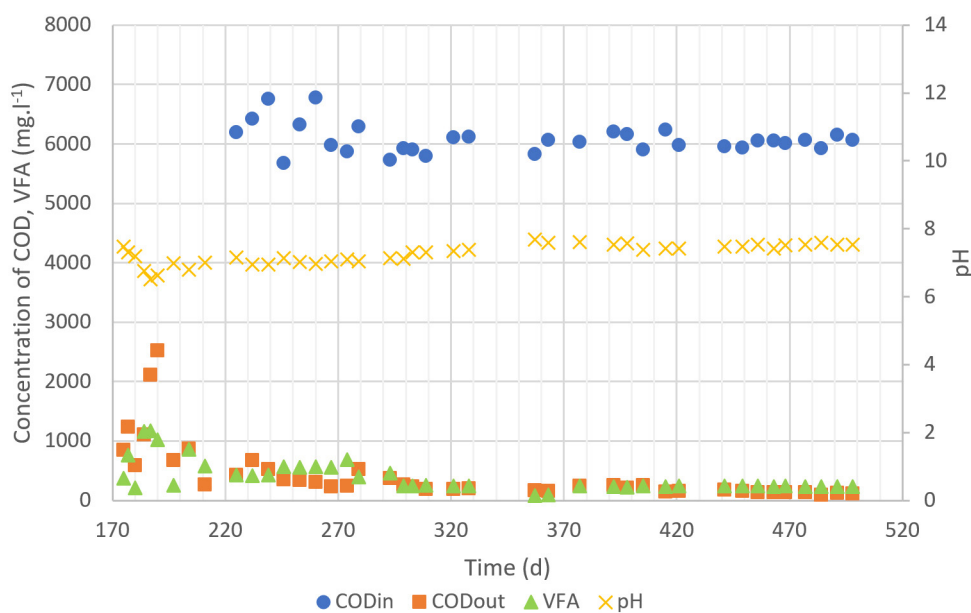


**Fig. 4.** Inlet concentration of COD, outlet concentration of COD and VFA from reactor, and pH.

The presence of hydrogen sulfide in the biogas was probably caused by sulfates contained in tap water used to make the synthetic substrate. Subsequent increase in the sulfate concentration to 125 mg·l<sup>-1</sup> (first phase) caused an increase in the amount of hydrogen sulfide in the biogas to 3 940 ppm. Introduction of hydrogen sulfide absorption from recirculated biogas led to a decrease in the hydrogen sulfide concentration by more than a half.

On the next day (day 245), sulfate concentration was increased to 250 mg·l<sup>-1</sup> (second phase). After recirculation was interrupted, the quality of biogas further deteriorated. Methane levels dropped below 60 % on day 251. Later that day, recirculation was reintroduced. On day 258, biogas composition was determined. After eight days of hydrogen sulfide absorption in the recirculated biogas stream, the hydrogen sulfide concentration decreased to 3175 ppm. Also, the amount of H<sub>2</sub> was reduced to 370 ppm. However, the amount of methane decreased to 67.3 %. On day 260, recirculation was disconnected and biogas composition was determined four days later. Since the removal of hydrogen sulfide did no longer occur, the amount of hydrogen sulfide increased to 13 970 ppm. The methane content was approximately the same (67.2 %) but the amount of hydrogen in biogas increased to 7 006 ppm.

On day 265, the third phase of reactor operation began when the sulfate concentration was increased to 700 mg·l<sup>-1</sup>. Biogas was recirculated for nine days and the biogas composition was determined. The amount of hydrogen sulfide increased to 16518 ppm, which could be due to low flow rate of recirculated biogas (10 l·d<sup>-1</sup>). The next day, the recirculated biogas flow rate was increased to around 30 l·d<sup>-1</sup>. The absorption column was

operated for 20 days followed by re-determination of the biogas composition (day 295). From the measured values (Tab. 1) it can be argued that the increase in the flow rate had a positive effect on the biogas quality. The methane content increased to 78.1 % while the amount of hydrogen sulfide in the biogas decreased to 12 890 ppm. However, the detected amount of hydrogen sulfide is still high, so the flow rate of recirculated biogas was increased to approximately 65 l·d<sup>-1</sup>. After 33 days of the absorption column operation, biogas composition was again determined. Increasing the flow rate ensured the decrease of hydrogen sulfide content in the biogas to 7 970 ppm. Control pH measurement in the recovery column was done. Optimum pH for sulfates precipitation to elemental sulfur is about 7. However, from the control measurement pH decrease to 4 was observed. To ensure the required pH value, sodium hydrogen carbonate was added to the storage tank.

The next biogas composition measurement was performed on day 376. The methane content increased to 83 % and the amount of hydrogen sulfide in the biogas decreased to 4030 ppm. The amount of hydrogen in biogas was also reduced to 715 ppm. The increased methane concentration in biogas is also caused not only by hydrogen sulfide but also by carbon dioxide absorbed in water. On day 393, biogas recirculation was interrupted and the biogas composition was determined after four days. The methane content decreased to 66.2 %, and the amount of hydrogen sulfide increased to 19960 ppm. Immediately after the measurement, biogas recirculation was switched back on and on the following day (398<sup>th</sup> day), biogas composition was measured again. From the results it can be seen that the amount of hydrogen sulfide decreased to

**Tab. 1.** Biogas composition and sulfide concentration in the reactor.

Recirculation	Day	CH <sub>4</sub> (%)	CO <sub>2</sub> (%)	O <sub>2</sub> (%)	H <sub>2</sub> (ppm)	H <sub>2</sub> S (ppm)	S <sup>2-</sup> (mg l <sup>-1</sup> )
Off	223	68,4	32,1	0,7	<1 000	780	-
Off	230	67,6	30,2	0,7	<1 000	3 940	-
On	244	73,1	23,1	0,8	<1 000	1 860	-
Off	251	59,2	24,6	2,7	<1 000	<5 000	-
On	258	67,3	22,4	1,7	370	3 180	-
Off	264	67,2	31,4	0,5	7 010	13 970	3,17
On	274	68,1	26,6	0,7	6 300	16 520	0,00
On	295	78,1	16,4	0,4	9 070	12 890	0,00
On	329	78,7	16,2	0,5	4 480	7 970	0,00
On	376	83,0	10,6	0,5	715	4 030	0,00
Off	397	66,2	17,5	1,6	27 430	19 960	4,18
On	398	73,7	14,3	1,5	7 960	8 400	0,00
On	468	77,9	16,2	0,5	9 010	8 760	0,00

8400 ppm, which also improved the biogas quality. The methane content increased to 73.7 %. The last measurement was made on day 468, when a slight increase in the methane content (77.9 %) in biogas was observed. The amount of hydrogen sulfide in the biogas remained the same.

## Conclusion

Dosing of sulfates together with synthetic substrate into an UASB reactor was found to affect biogas production. In case of low levels of sulfates, a slight increase in biogas production was observed, which confirms the results of biogas potential tests. Before the addition of sulfates, biogas production was 15  $\text{ld}^{-1}$ . During dosing of the synthetic substrate with the sulfate concentration of 125  $\text{mg l}^{-1}$ , production increased to approximately 17  $\text{ld}^{-1}$ . However, further increase in the sulfates concentration caused the biogas production to decrease again. When 700  $\text{mg l}^{-1}$  of sulfates were added, the production reached 13  $\text{ld}^{-1}$ . Also a negative effect on the removal of  $\text{N-NH}_4$ ,  $\text{P-PO}_4$  and other nitrogen compounds was found. The decrease in the removal efficiency of these qualitative indicators was most evident when 250  $\text{mg l}^{-1}$  of sulfates were added.

Biogas recirculation with hydrogen sulfide absorption has proven to be an effective method of reducing hydrogen sulfide content in biogas. During the recirculation, concentrations of hydrogen sulfide was reduced and also the biogas quality improved. The highest methane content was 78.7 % and 83 %, respectively. Considering hydrogen sulfide content, long-term operation of recirculation led to high efficiency of its removal from biogas. After recirculation was disconnected, the hydrogen sulfide concentration in biogas increased to 19 960 ppm.

Our aim was to determine the effect biogas recirculation with hydrogen sulfide removal on sulfide inhibition of the anaerobic process. When biogas recirculation was switched off, sulfide concentration in the reactor increased up to 4.18  $\text{mg l}^{-1}$ . When the recirculation was restarted, a decrease in the sulfide concentration (0  $\text{mg l}^{-1}$ ) was observed, which suggests that the inhibitory effect of sulfides is partially suppressed.

## Acknowledgement

*This work was supported by the Slovak Grant Agency for Science VEGA (grant 1/0772/16).*

## References

- Aita BC, Mayer FD, Muratt DT, Brondani M, Pujol ST, Denardi LB, Hoffmann R, Dias da Silveira D (2016) *Clean Technologies and Environmental Policy*, 18, 689–703.
- Angelidaki I, Treu L, Tsapekos P, Luo G, Campanaro S, Wenzel H, Kougias PG (2018) *Biotechnology Advances* 36, 452–466.
- APHA/AWWA/WEF (2017) *Standard Methods for the Examination of Water and Wastewater*. American Public Health Association, USA.
- Hussain A, Dubey SK (2014) *Desalination and Water Treatment* 52, 7015–7025.
- Hutňan M, Chávez Fuentes JJ, Czölderová M (2016) *Applied Mechanics and Materials* 832, 122–127.
- Chávez Fuentes JJ, Hutňan M, Bodík I, Zakhar R, Czölderová M (2015) *Water Science and Technology* 72, 585–592.
- Kadam R, Panwar NL (2017) *Renewable and Sustainable Energy Reviews* 73, 892–903.
- Khanal SK, Huang JC (2003) *Water research* 37, 2053–2062.
- Krayzelova L, Bartacek J, Kolesarova N, Jenicek P (2014) *Bioresource Technology* 172, 297–302.
- Krayzelova L, Bartacek J, Díaz I, Jeison D, Volcke EIP, Jenicek P (2015) *Reviews in Environmental Science and Bio/Technology* 14, 703–725.
- Maizonnasse M, Plante JS, Oh D, Laflamme CB (2013) *Renewable Energy* 55, 501–513.
- Oliviera FR, Surendra KC, Jaisi DP, Lu H, Unal-Tosun G, Sung S, Khanal SK (2020) *Bioresource Technology* 301, 122711.
- Pokorna-Krayzelova L, Mampaey KE, Vennecke TPW, Bartacek J, Jenicek P, Volcke EIP (2017) *Biochemical Engineering Journal*, 125, 171–179.
- San-Valero P, Penya-roja JM, Álvarez-Hornos J, Buitrón G, Gabaldón C, Quijano G (2019) Fully aerobic bioscrubber for the desulfurization of  $\text{H}_2\text{S}$ -rich biogas, *Fuel* 241, 884–891.
- Watsuntorn W, Khanongnuch R, Chulalaksananukul W, Rene ER, Lens PNL (2019) *Journal of Cleaner Production* 249, 119351.

# Sample matrix influence on microdrop hold-up in single drop microextraction

Nikola Kubasová, Silvia Zichová, Adriána Brisudová, Svetlana Hrouzková

*Slovak University of Technology in Bratislava, Faculty of Chemical and Food Technology,  
Institute of Analytical Chemistry, Radlinského 9, 812 37 Bratislava, Slovak Republic  
svetlana.hrouzkova@stuba.sk*

**Abstract:** Single drop microextraction has become a widespread liquid/liquid microextraction technique owing to its simplicity, high preconcentration factor and low consumption of organic solvents in the extraction due to direct introduction of the very low volume of extract into the analytical system. Crucial features ensuring excellent repeatability of single drop microextraction include: solvent volume, solvent type, sample agitation, salts addition, and pH. The influence of sample quality on the microdrop volume and agitation type was studied. Effect of the sample matrix, such as water, acid content samples (orange juice), sample containing alcohol (plum brandy) and protein content sample (milk), on the microdrop hold-up was also investigated. For water analysis, several organic solvents such as chloroform, dichloromethane, tetrachloromethane, tetrachloroethane and chlorobenzene were tested; last three mentioned were suitable for SDME experiments. For milk samples analysis, chlorobenzene microdrop was found to be optimal; advantage of salt addition has been reported. For orange samples, 1:10 dilution was suggested with stable microdrop volumes (toluene) of up to 6  $\mu\text{L}$  for lower stirring rates (100 rpm and 250 rpm). For alcohol-content samples, the change of alcohol percentage of real-life samples had to be considered. A strong influence of the matrix quality on the microdrop stability has been proven.

**Keywords:** matrix influence, microdrop hold-up, microdrop stability, single drop microextraction

## Introduction

Actual trends in analytes extraction from various food or environmental samples follow green chemistry philosophy taking into account simplification and miniaturisation, especially minimisation of the volume of necessary organic solvents which are potentially harmful and unwanted in large scale in analytical procedures (Hrouzková, 2017). For the liquid-liquid extraction, a set of techniques called liquid-phase microextraction (LPME) has undergone a dramatic increase in a variety of approaches (Andraščíková et al., 2015) using only microliters of solvent to preconcentrate analytes from various samples rather than hundreds of millilitres needed in traditional LLE (Sarafraz-Yazdi and Amiri, 2010). One of these techniques, single-drop microextraction (SDME) (Liu and Dasgupta, 1995) has drawn much interest. Recently, several review papers have addressed this emerging technique as an efficient approach to the pretreatment in a wide variety of analytes and matrices (Jain and Verma, 2020, Jeannot et al., 2010; Kumar Kailasa and Wu, 2013; Tang et al., 2018; Tegladza et al., 2020, Zichová et al., 2018a) highlighting the green approach of the technique in minimisation of the hazards associated with the use of toxic organic solvents.

The principle of SDME is the separation of compounds between a few microlitres volume drop of organic solvent, named microdrop, at the tip of a microsyringe needle or in the headspace above the

sample and a liquid sample containing the desired analytes. The syringe needle is immersed into the sample and the microdrop of solvent is exposed to the sample for limited time at specified conditions. SDME is often used to represent the acceptor phase where only a small microdroplet (0.5–2.0  $\mu\text{L}$ ) is suspended on the tip of a microsyringe. After sampling/extraction of analytes, the microdrop is drawn into the syringe and all its volume is analysed by an instrumental analytical technique such as gas chromatography with the appropriate detection.

Development of an analytical method using SDME requires optimisation of a high number of variables and parameters affecting the extraction step. It has been shown in our previously published review (Zichová et al., 2018b) that parameters such as the type of investigated analytes, quality of the extraction solvent, type of microsyringe, sample volume, physical properties such as temperature, ion strength and pH of the sample affect the efficiency of the extraction procedure. It was stated that in SDME development, it is important to find extraction conditions ensuring drop stability. The ease of dislodgment of the microdrop hanging from the tip of the microsyringe needle during the extraction process limits the use of extended extraction times, high stirring rates, sample temperature and the type of sample matrix (Jain and Verma, 2011).

Only a few comprehensive information on the influence of the liquid sample matrix on the stability

and hold-up of the microdrop hanging from the tip of the microsyringe needle during the extraction process are available. Therefore, the aim of this paper was to investigate the microdrop hold-up in SDME for four various liquid samples, namely orange juice, alcohol-containing sample, deionised water and milk. The influence of SDME parameters on the food analysis application area was studied.

## Materials and Methods

### Chemicals

Several organic solvents were used for microdrop stability evaluation. Chloroform and acetone were purchased from Centralchem, s.r.o. (Bratislava, Slovakia). Dichloromethane, *n*-hexane, tetrachloromethane, and toluene were purchased from Merck KGaA (Darmstadt, Germany). Chlorobenzene was obtained from Lachema, n.p. (Brno, Czech Rep.) and tetrachloroethane from Alfa Aesar (Havehill, USA). Ion strength of the sample was altered by NaCl obtained from laboratory sources.

### Samples

Orange juice (100 %), plum distillate (40 % alc.), and milk (0.5 % of fat) were purchased from local shops. These samples were diluted with deionised water and used for the extraction as follows: Orange juice was diluted in the ratio 1:2 (v/v) and 1:10 (v/v), alcohol samples were each diluted to 20 % alc., and milk was diluted in the ratio 1:10 (v/v). The sample volume of 2 mL for each sample was used in the experiments. Grape distillate (62 % alc.) was obtained from a private producer.

### Equipment

For the extraction procedure, a 10  $\mu$ L Agilent Technologies microsyringe was used to maintain the microdrop during the extraction and to determine

the microdrop volume. A glass vial containing the sample solution, magnetic stir bar and silicone septum was used as the sample reservoir.

Magnetic stirrer IKA RTC basic safety control (IKA®) with adjustable speed range from 50 to 1500 rpm, digital display and aluminium heating plate was used to stir the sample solution. A scheme of SDME is shown in Fig. 1.

## Results and Discussion

Stability and hold-up of the microdrop at the tip of the microsyringe needle in SDME is affected by many parameters. The primary concern of the study was to investigate the matrix influence on the stability of the microdrop on the tip of the microsyringe needle for direct immersion (DI) and headspace (HS) mode of SDME. Several matrices were investigated to cover a large scale of water-based matrices with various organic solvents and stirring conditions. Specifically, microdrop stability for acids-containing matrix (orange juice), alcohol-containing matrix (plum distillate, grape distillate), water matrix and protein-containing matrix (milk) was studied.

### Single drop microextraction procedure

Microsyringe was rinsed six times with acetone, then six times with *n*-hexane and three times with the tested extraction solvent. The plunger was placed in position 0 and the tested extraction solvent (volumes in the range of 1–6  $\mu$ L) was drawn into the syringe. Subsequently, the microsyringe needle was inserted through the silicon septum and immersed in the sample solution (volume of the sample was 2 mL) under stirring (in the range of 100–1000 rpm). After the extraction time (tested range: 5–20 min) passed, the microdrop was drawn back into the microsyringe and the needle was removed from the glass vial. The volume after the extraction was registered. Each ex-

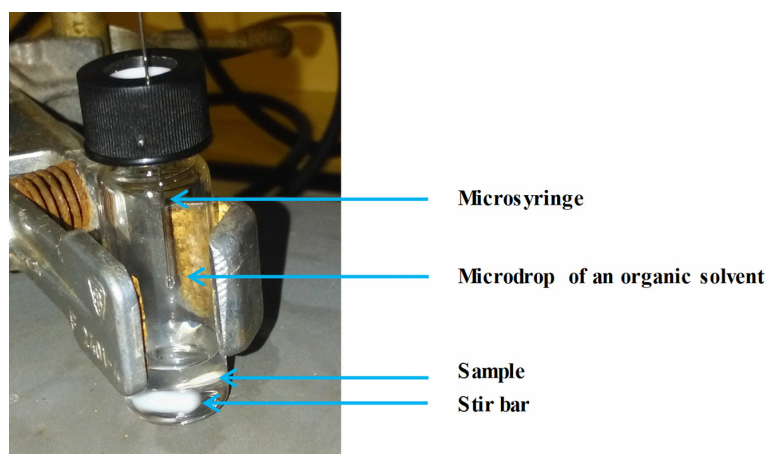


Fig. 1. Scheme of SDME.

periment was repeated three times. Figs. 1–4 show the average volume of the extraction solvent after the extraction.

#### ***Microdrop behaviour in water***

Stability of the microdrop was investigated in a simple matrix – deionised water, assuming no matrix components affecting the microdrop stability. The selection of organic solvent is a crucial step in ensuring good performance of SDME. The selected solvent has to preserve the integrity of the microdrop during the extraction. For microdrop extraction in an aqueous-based solution by DI, immiscibility of the organic solvent in the sample has to be ensured. Also viscosity, which should be adequate for the formation and retention of the microdrop on the tip of the microsyringe needle during the extraction of the SDME process, has to be considered in the extractant solvent selection. Several chlorinated solvents such as tetrachloromethane (TCM), chloroform (CHF), dichloromethane (DCM), tetrachloroethane (TCE) and chlorobenzene (CHB) meet these requirements and they were used for microdrop formation. A volume of 2 mL of deionised water was stirred for 2 min at 100 rpm and 250 rpm, and the volume of 2  $\mu$ L of the studied solvent was exposed to the stirred sample. After the selected period of time, the volume of the withdrawn extraction solvent was recorded. All of the studied extraction solvent microdrops were stable in the water sample, except for the DCM microdrop, which fell off the syringe needle after half a minute at 100 rpm. Volumes above 1.8  $\mu$ L at both 100 rpm and 250 rpm were withdrawn using solvents CHB, TCE and TCM, whereas CHF microdrop could not be withdrawn back into the microsyringe without air bubbles, which complicated the determination of the withdrawn volume. The decrease of the CHF microdrop volume of more than 25 % was observed at higher stirring speed.

#### ***Microdrop behaviour in orange juice***

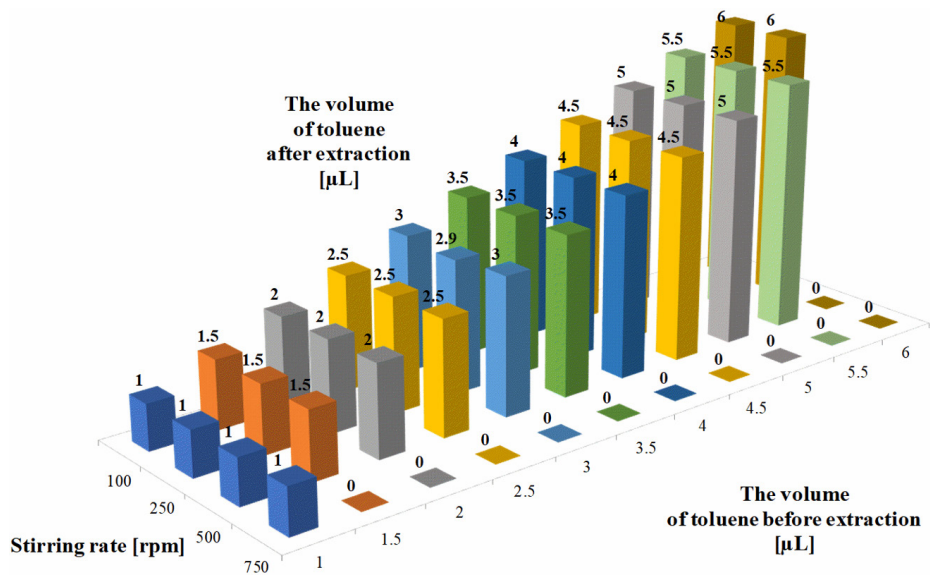
Orange juice is a complex matrix which contains, apart from acids and sugars, also pigments. Organic acids can alter the sample pH and its initial check is thus necessary. Pigments can easily transfer into the microdrop and result in its dislocation from the tip needle. Also, high content of fibres is a problem and therefore dilution or preconcentration of the sample were tested. Considering these requirements based on our previously published literature review (Zichová et al., 2018 b), toluene is the first choice as solvent for these samples. Therefore, toluene was tested as the extractive solvent, showing immiscibility with the sample with non-colour microdrop after extraction. Stability of the toluene microdrop for HS and DI depends on the stirring

rate as well as on the volume of microdrop drawn back to the microsyringe after its extraction and dislocation were evaluated. The stirring rate has to be investigated considering the microdrop integrity. Higher agitation rates increase the occurrence of microdrop displacement from the microsyringe tip and decrease the volume of the extractant after the extraction due to the dissolution of the solvent microdrop in the sample.

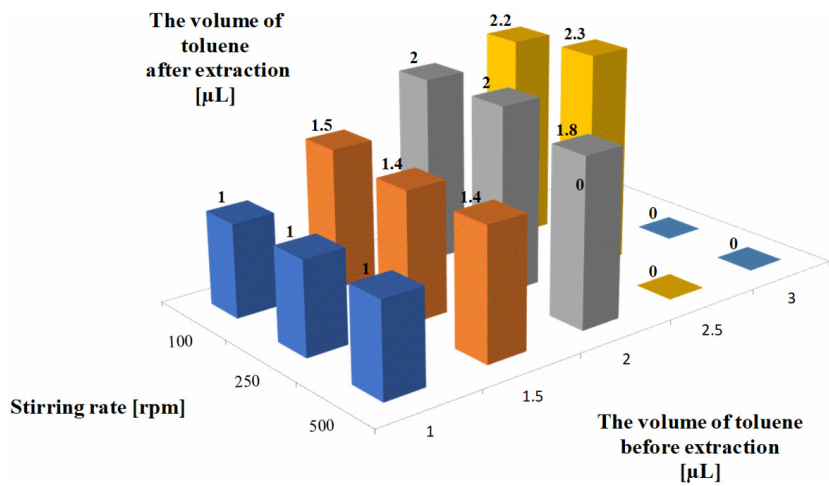
Experimental assays were performed using concentrated original orange juice, orange juice diluted with water in the ratio of 1:10 (v/v) and in that of 1:2 (v/v). Influence of the sample dilution on the microdrop stability was also studied. The results were recorded and compared. All sets of measurements were performed at various stirring rates; the maximum stirring rate depended on the microdrop hold-up at the microsyringe tip. Data showing stability of the toluene microdrop in DI mode for all tested samples: diluted juice sample in the ratio of 1:10, diluted sample in the ratio of 1:2 and concentrated original sample, and in dependence on the stirring rate are depicted in Figs. 2A, 2B and 2C, respectively. The column bars represent the volume of extractant originally taken for the extraction and the number at the top of the column bar represents the volume of toluene measured after the extraction. The toluene volume after the extraction equal to 0 means that the microdrop was dislocated during the experiment and therefore no toluene was drawn back to the microsyringe.

As it can be seen in Fig. 2A, the widest range of toluene volume (1–6  $\mu$ L) was determined in orange juice sample diluted in the ratio of 1:10. The microdrop was easily visible despite the sample colouring and the stability was notable in the whole range of the studied volumes for lower stirring rates in all experiments (100 rpm and 250 rpm). Higher stirring rates (> 500 rpm) caused instability of microdrop with the volume higher than 5.5  $\mu$ L at the stirring rate of 500 rpm and that with the volume higher than 1  $\mu$ L at the stirring rate of 600 rpm.

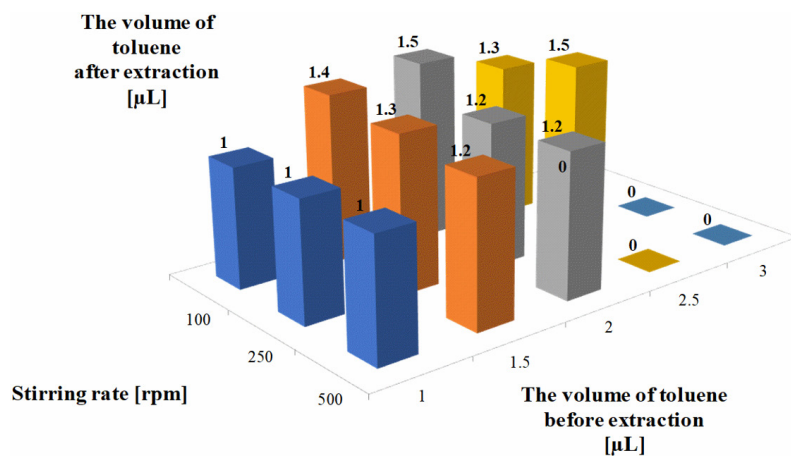
Further experiments with sample diluted in the ratio of 1:2 and the un-diluted sample showed differences in the maximum microdrop volume as well as conditions at which the microdrop was stable. Stirring rate of 750 rpm was excluded from the experiments due to the microdrop instability; the microdrop up to the volume of 2.5  $\mu$ L was stable at stirring rates up to 500 rpm. However, in both cases, visibility of the microdrop in the sample was low, and an effort to white-out the samples was made in un-diluted sample. Nevertheless, the microdrop was invisible even when a lightening compound was applied. Thus, withdrawal of the microdrop after extraction is complicated.



A



B



C

**Fig. 2.** Stability of toluene microdrop (DI-SDME) at various stirring rates in: A – orange juice sample diluted with water in the ratio of 1:10; B – orange juice sample diluted with water in the ratio of 1:2; C – original orange juice sample (undiluted).

The stability of toluene microdrop was investigated in the HS mode in the range of 1–4  $\mu\text{L}$ , stable microdrop was observed up to 3  $\mu\text{L}$  for all sample types and at stirring rates between 500 rpm and 1400 rpm. It is important to emphasize that the difference in the volume before and after extraction was higher for the DI mode than for HS mode. In addition, the decrement of the microdrop volume in the DI mode increased in the order: diluted sample in the ratio of 1:10 < diluted sample in the ratio of 1:2 < un-diluted sample.

#### *Microdrop behaviour in alcohol-containing samples*

Stability of toluene microdrop in the sample with alcohol content of above 40 % was studied. Plum distillate with the alcohol content of 40 % and grape

distillate with the alcohol content of 62 % were used in these experiments. These samples were diluted with deionised water in order to obtain a 20 % alcohol content of each distillate and results from experiments using samples with higher alcohol content were compared with those with lower alcohol content. Detailed results showing the stability of toluene microdrop in the DI mode for plum distillate with the alcohol content of 40 % and 20 % are depicted in Figs. 3A and 3B, respectively.

Microdrop volumes ranging from 1  $\mu\text{L}$  to 4  $\mu\text{L}$  were examined in case of the 40 % plum distillate and in the range of 1–6  $\mu\text{L}$  for the 20 % plum distillate. Observations showed that higher alcohol content limited the microdrop volume (limit was 3  $\mu\text{L}$ ) and stirring rates (limit was 750 rpm). A 3  $\mu\text{L}$  toluene mi-

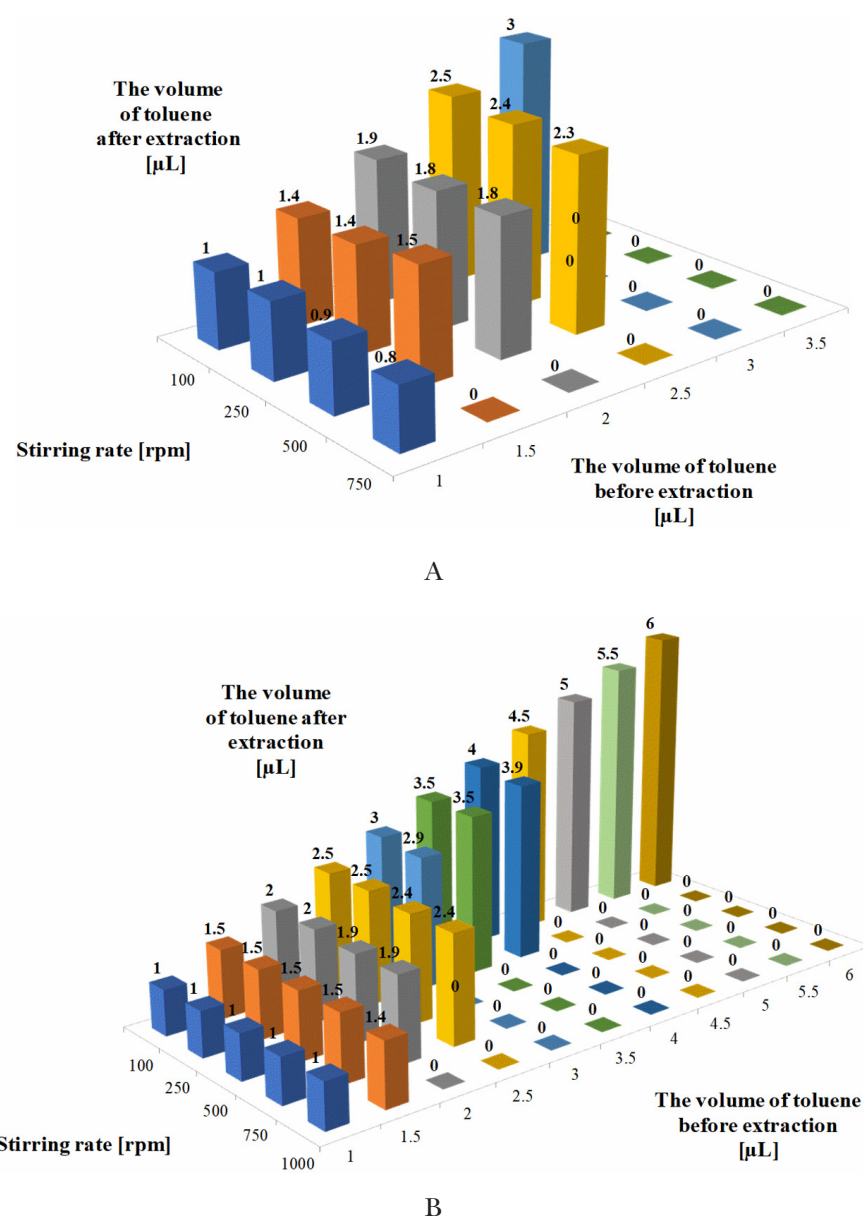


**Fig. 3.** Stability of toluene microdrop (DI-SDME) at various stirring rates in: A – plum distillate 40 %; B – plum distillate 20 %.

crodrop was stable using the lowest studied stirring speed of 100 rpm and no notable decrement of the extractive solvent was observed. At higher stirring speeds, a 3  $\mu\text{L}$  microdrop was unstable at the tip of the needle and dropped off after a couple of seconds of stirring. Dilution of the plum distillate sample to half the alcohol content with deionised water enabled using considerably higher toluene microdrops (up to 6  $\mu\text{L}$ ) and higher stirring rates (up to 1000 rpm). The microdrops of all tested volumes were stable at the lowest stirring rate of 100 rpm, whereas those with the volume of up to 2.5  $\mu\text{L}$  were stable up to the stirring rate of 750 rpm. Lower microdrop volumes of up to 1.5  $\mu\text{L}$  led to microdrop instability at the highest stirring rate (1000 rpm).

Similar results were obtained in experiments using the 62 % grape distillate, when the toluene microdrop showed stability difficulties even at low stirring rates (100 rpm, 200 rpm). The maximal stable microdrop volume was about 1.5  $\mu\text{L}$  at 100 rpm. Presumably, high alcohol content caused a significant decrement of the toluene microdrop after the extraction probably due to the toluene solubility in ethanol (dos Anjos et al. 2015). Dilution of the grape sample to 20 %, significantly improved the microdrop stability similarly as in case of the plum distillate, while the toluene microdrop was stable up to the volume of 6  $\mu\text{L}$ .

It is necessary to consider the change of alcohol content in real-life samples and to make the respective correction or fix the alcohol content to constant value.

#### ***Microdrop behaviour in milk samples***

Due to high content of proteins and lipids in milk and their solubility in non-polar solvents such as

toluene, an appropriate extraction solvent with the lowest possible solubility in milk ensuring stable microdrop during the extraction has first to be identified. The stability of toluene microdrop in the milk sample (DI mode) was studied at the stirring rates of 100 rpm and 250 rpm, and the extraction time varied from 5 min to 25 min (with a 5-minute increment for consecutive experiments). The milk sample was diluted with deionised water in the ratio of 1:10 (v/v) and the aliquot volume of 2 mL was used in the experiments. Results showed stability problems of the toluene microdrop at the stirring rate of 250 rpm. The main limitation of toluene application was the loss of the microdrop volume after the extraction exceeding 25 % of the original microdrop volume. At high extraction times (e. g. 20 min), microdrop volume after the extraction was below 1.7  $\mu\text{L}$  (original volume was 2  $\mu\text{L}$ ). Based on the results, satisfactory microdrop stability was obtained under the following extraction conditions: extraction time of 5 min and sample stirring rate of 100 rpm. However, due to the short extraction time of 5 min, several different extractive solvents were studied.

A set of experimental assays using TCM, CHF, DCM, TCE and CHB as extractive solvents were performed with a milk sample diluted with deionised water in the ratio of 1:10 (v/v). The sample volume was set to 2 mL. Significant difference in the stability of the above-mentioned chlorinated solvents was observed and only the CHB microdrop was stable in the diluted milk sample. Microdrops of other solvents fell down immediately after the microdrop exposure to the sample. Thus, subsequent experiments were devoted to the CHB microdrop stability. Extraction parameters were as follows: stir-

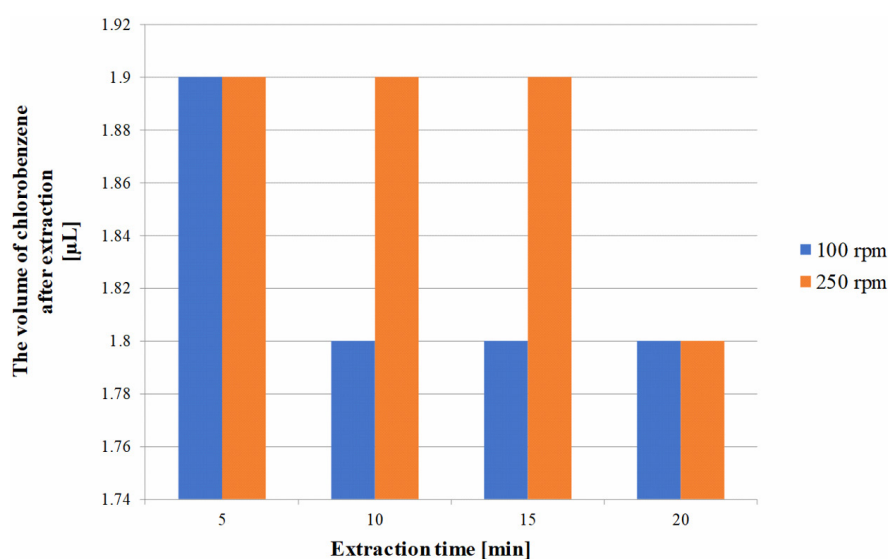


**Fig. 4.** Dependence of CHB microdrop volume after DI-SDME at the stirring speed of 100 rpm and 200 rpm on the extraction time.

ring rates of 100 rpm and 250 rpm, extraction time in the range of 5 min to 25 min (with a 5-min step). The disadvantage of the DI mode is the impossible visual control of the microdrop in the sample which could lead to a delay in sample treatment if the microdrop fell down from the needle tip. Moreover, differences in the microdrop volumes withdrawn after the extraction in the three samples were notable due to the worse visibility of the microdrop. The maximum CHB microdrop volume withdrawn in the dependence on extraction time is shown in Fig. 4. Relative standard deviation (RSD) for different combinations of stirring rate and extraction time was in the range of 3.1–6.9 %. Based on these observations, sample centrifugation and the addition of salt to the sample were tested to increase the possibility of visual control in the sample.

The diluted milk sample was centrifuged at 4000 rpm for 5 min. CHB microdrop exhibited lower stability at both stirring rates and the centrifugation did not improve the microdrop visibility. In the next step, the addition of NaCl to the diluted milk sample after centrifugation was studied. The NaCl addition was carried out successively in the range of 0.1–0.4 g (with a step of 0.1 g). The sample was clarified by the salt addition and the drop was easily observed. Furthermore, salt addition improved the stability of microdrop directly immersed in the sample. Increasing the amount of NaCl consecutively improved the stability of the CHB microdrop at both stirring rates and at all tested extraction times. The most satisfactory microdrop stability was obtained at the salt addition of 0.4 g. Lower NaCl addition led to the instability of the microdrop after 15 min as well as a decrement of the extracted volume (withdrawn volume was 1.7  $\mu$ L).

## Conclusions

SDME is a sample preparation technique for various instrumental detection analyses employing simple equipment and leading to low environmental impact. The essential condition of SDME is maintaining a microdrop of an organic solvent suspended at the tip of a microsyringe needle, which is then immersed in a sample under agitation. Drop instability and its dislocation are the main disadvantages of this technique. The microdrop has to be retracted back into the microsyringe and transferred to the subsequent system for analyses system and thus detailed optimisation of conditions such as solvent

type, solvent volume, agitation type and time etc. is crucial. The change of matrix composition (content of acid compounds, content of alcohol, protein content) has been proven to affect the stability of the solvent microdrop. Concentration of fibres and organic acids also affects the microdrop solubility and stability. For alcohol content samples, the content of alcohol has to be considered in solvent selection because of the solubility either of microdrop in water or in alcohol; the alcohol content should be determined before the analysis. For milk samples, careful optimisation of extraction parameters has to be done in dependence on protein and fat content, or the removed matrix has to be tested.

## Acknowledgement

*This work was supported by the Scientific Grant Agency of the Slovak Republic VEGA project No. 1/0412/20 and the Program for support of excellent teams of young researchers STU. NK would like to thank for the kind support of AXA Foundation and the foundation of Pontis in the frame of the “Young innovator” program.*

## References

- Andraščíková M, Matisová E, Hrouzková S (2015) Sep. Purif. Revs. 44: 1–18.
- dos Anjos JP, de Andrade JB (2015) Microchem J. 120: 69–76.
- Hrouzková S (2017) In: “Food analysis: Innovative analytical tools for safety and quality assessment”, Umile Gianfranco Spizzirri, Giuseppe Cirillo (Ed), John Wiley & Sons, Hoboken, New Jersey and Scrivener Publishing, Beverly, MA, p. 221.
- Jain A, Verma KK (2011) Anal. Chim. Acta 706: 37–65.
- Jain A, Verma KK (2020) In “Liquid-Phase Extraction”. Poole CF (Ed), Elsevier, London UK, pp. 439–472.
- Jeannot MA, Przyjazny A, Kokosa JM (2010) J. Chromatogr. A 1217: 2326–2336.
- Kumar Kailasa S, Wu H-F (2013) Bioanalysis 5 (21): 2593–2596.
- Liu S, Dasgupta PK (1995) Anal. Chem. 67: 2042–2049.
- Sarafraz-Yazdi A, Amiri A (2010) Trends in Anal. Chem. 29: 1–14.
- Tang S, Qi T, Ansah PD, Nalouzebi Fouemina JCh, Shen W, Basheer Ch, Lee HK (2018) Trends in Anal. Chem. 108: 306–313.
- Tegladza ID, Qi T, Chen T, Alorku K, Tang S, Shen W, Kong D, Yuan A, Liu J, Lee HK (2020) J. Hazard. Mat. 393 No 122403.
- Zichová S, Brisudová A, Hrouzková S (2018a) Nova Biotechnol Chim 17(1): 1–15.
- Zichová S, Brisudová A, Hrouzková S (2018b) Acta Chimica Slovaca 11: 60–67.

# Low-temperature plasma applications in chemical fungicide treatment reduction

Lucia Hoppanová<sup>a</sup>, Veronika Medvecká<sup>b</sup>, Juliana Dylíková<sup>a</sup>, Daniela Hudcová<sup>a</sup>,  
Barbora Kaliňáková<sup>a</sup>, Svetlana Kryštofová<sup>a</sup>, Anna Zahoranová<sup>b</sup>

<sup>a</sup>*Institute of Biochemistry and Microbiology, Faculty of Chemical and Food Technology, Slovak University of Technology, Radlinského 9, 812 37 Bratislava, Slovak Republic*

<sup>b</sup>*Department of Experimental Physics, Faculty of Mathematics, Physics and Informatics, Comenius University, Mlynská dolina F2, 842 48 Bratislava, Slovak Republic  
lucka.hopp@gmail.com*

**Abstract:** In order to reduce the environmental burden of chemicals, various new alternatives to seed protection are being sought. Our aim was to find an environmentally acceptable solution leading to the inactivation of seed-borne phytopathogenic fungi *Fusarium culmorum* on the surface of wheat and barley seeds with a positive effect on their germination. As a low-temperature plasma (LTP) source, a Diffuse Coplanar Surface Barrier Discharge (DCSBD) was used. Plasma generated by DCSBD is non-equilibrium, cold, diffuse, macroscopically homogeneous even in ambient air at atmospheric pressure. Experimental results showed that LTP treatment in the range of 120–300 s significantly inhibits the growth of *F. culmorum* on the surface of the seeds. The efficiency of LTP treatment was compared with traditional seed protection processes using chemical fungicide and also with combined seed pretreatment by plasma and subsequent application of chemical fungicide. No growth of *F. culmorum* was observed after the combination of Vitavax 2000 fungicide application in the dose of 10 % and 60 s of LTP treatment even on the 5th day of incubation. Better wettability of seeds with the chemical fungicide was related to the change on seed surface, which becomes hydrophilic after 10 s of LTP application. Short LTP exposure times did not affect germination and improved the growth parameter of cereal seeds. By combining physical (LTP) and chemical (Vitavax 2000) treatments of cereal seeds, it is possible to effectively reduce the required amount of chemical fungicide and to stimulate germination and early growth seed parameters.

**Keywords:** Cereal seeds; Chemical fungicide Vitavax 2000; Decontamination; *Fusarium culmorum*; Germination; Low-temperature plasma

## Introduction

Cereals represent the main part of human and animal nutrition. Wheat, barley and maize are grown on more land area than any other food crop. In 2017, European production of wheat was 270 million tons, making it the second most-produced cereal after maize. European production of barley was 89 million tons (FAOSTAT, 2019). Cereal contamination by microscopic fungi is one of the main causes of stored seeds depletion since microscopic mycelial fungi reduce seed germination and seed nutritional quality (Ramos et al., 1998). Cereals are particularly susceptible to microbial deterioration during growth, ripening, storage and processing. Mycotic contamination of cereals is the highest at the time of harvest when it can reach 10<sup>6</sup> CFU (Colony Forming Units) of microscopic fungi in one gram of seed (Tančínová et al., 2001).

Microscopic mycelial fungi can grow on cereal surface in form of mycelium and spores (Laca et al., 2006). Genera *Alternaria*, *Fusarium* and *Cladosporium* are primarily responsible for the contamination of cereal seeds in the field (Montville and Matthews, 2005). Stored seeds are contaminated mainly by

*Penicillium* and *Aspergillus* species (Magan et al., 2003). The development of fungal contamination is affected by storage conditions such as temperature, relative humidity, pH, and aqueous activity. During optimal storage conditions, the number of CFU of fungi decreases (Tančínová et al., 2001). The greatest risk for food safety and quality at pre- and post-harvest stages is associated with the production of mycotoxins, which are species and strain specific (Montville and Matthews, 2005). *Fusarium* spp. (a model organism in this study) are well-known pathogens of cereals that produce mycotoxins, e.g. trichothecenes, fumonisins, zearalenone, deoxynivalenol, with carcinogenic, mutagenic and genotoxic effects. They cause acute or chronic human and animal health problems (Pereira et al., 2014). This fungal genus causes a crop disease – fusariose, which reduces germination and seed quality and causes crop losses (McMullen et al., 2012).

For more than 200 years, fungicides have been used to protect plants from fungal infections in order to increase crop yield and reduce economic losses. There are currently around 150 different fungicidal compounds used in global agriculture (Ishii and Holloman, 2015; Lucas et al., 2015). Protection

of seeds by chemical agents leads to contamination of the environment and accumulation of hazardous chemicals in soil and water. However, excessive use of chemicals is now being abandoned and new alternatives for crop protection with minimal environmental impact are implemented.

In recent years, the research and application of low-temperature plasma (LTP) has received great attention. Plasma finds its application in various spheres of interest in biological sciences (Šimončicová et al., 2019). A lot of significant data were obtained by the application of plasma treatment to plant seeds, indicating positive effects on seed germination, quality of plants grown from the plasma treated seeds, early growth parameters such as root and shoot length and increase of dry weight (Mitra et al. 2014; Šerá et al., 2010; Jiafeng et al., 2014). Plasma treatment resulted in a change of seed surface wettability, improved hydrophilic properties of the seed surface, and led to better water imbibition and faster start of the germination process (Stolárik et al., 2015; Zahoranová et al., 2016). Plasma technology has the potential to play an important role in addressing the challenges in food production and security, as reviewed in many articles (Moreau et al., 2008; Cullen et al., 2018; Randeniya and de Groot, 2015; Muhammad et al., 2018; Zahoranová et al., 2018; Chen et al., 2019).

In this study, a hypothesis that additional application of LTP in decontamination treatment of seeds reduces the chemical load on the environment without negative changes in seed morphology and physiology has been proposed and evaluated. Plasma interaction with wheat and barley seeds was studied and plasma treatment and application of chemical fungicide Vitavax 2000 on *Fusarium culmorum* on the surface of wheat and barley seeds were compared. The effect of a combination of plasma and fungicide treatments was also determined.

## Materials and methods

### Cereal seeds and microbial strains

Wheat seeds (*Triticum vulgare* L.; cv. “Forhand”) and barley seeds (*Hordeum vulgare* L.; cv. “Maltz”) were

purchased from the Central Control and Testing Agriculture Institute (Bratislava, Slovak Republic). The seeds were stored at 10 °C in the dark. *Fusarium culmorum* (CCM F-163) was obtained from the Czech Collection of Microorganisms (Masaryk University, Brno, Czech Republic) and was cultivated on slants of Malt Extract Agar (Biolife, Milano, Italy; 21 days, 25 °C) and then stored at 5 °C.

### Low-temperature plasma reactor

The experiments were carried out at atmospheric pressure in ambient air. Plasma was generated by Diffuse Coplanar Surface Barrier Discharge (DCSBD). The experimental set-up is depicted in Fig. 1. DCSBD was powered by 14 kHz sinusoidal high voltage with an amplitude of up to 20 kV peak-to-peak, supplied by an HV generator VF 700 (Lifetech Ltd., Brno, Czech Republic). DCSBD generates a thin layer of plasma (~ 0.3 mm) on a ceramic plate with the dimensions of 20 cm × 8 cm. DCSBD was described in detail in previous studies (Černák et al., 2009).

Seeds/sterilized seeds (10 g) were placed in the plasma generated on the ceramic plate. To ensure their uniform surface treatment, mechanically stirring was applied. The experiments were performed at the input power of 400 W while the whole DCSBD electrode was covered by macroscopically homogeneous plasma layer. From the electric measurement and determination of plasma source efficiency, and the size of the plasma area (160 cm<sup>2</sup>), the corresponding plasma volume power density was determined to be approximately 70 W cm<sup>-3</sup> (Černák et al., 2009).

### Cereal seeds surface decontamination from *Fusarium culmorum*

Ten grams of wheat and barley sterile (autoclaving – 120 kPa, 120 °C, 20 min) seeds were artificially infected with 1 mL of spore suspension of seed-borne phytopathogen *F. culmorum* (1 × 10<sup>5</sup> spores g<sub>seed</sub><sup>-1</sup>). The spore suspension was prepared from 21-day-old cultures grown on Malt Extract Agar medium (Biolife, Milano, Italy). The spores were harvested in 0.1 % Tween 80 (Biolife, Milano,

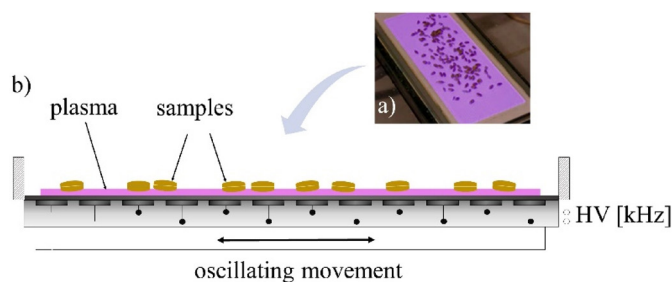


**Fig. 1.** LTP treatment of seeds (a) and scheme of the DCSBD electrode system (b)

Italy). The spore suspension was filtered through three layers of sterile gauze and centrifuged at 12 000×g for 5 min. The number of spores was counted using a Burkner chamber. Concentration of spores was adjusted by sterile water. The infected seeds were treated by LTP at the treatment time of 15, 30, 60, 120, 180, 240 and 300 s. Chemical fungicide Vitavax 2000 (200 g a.i. thiram and carboxin L<sup>-1</sup>; Chemtura Co., Bratislava, Slovakia) was used in different doses (100 % – application dose used in agricultural practice and 75 %, 50 %, 25 %, 10 % of the dose used). After 15, 30 and 60 s of LTP treatment and subsequent application of Vitavax 2000 at a 10 %, 25 % and 50 % dose were combined for seed treatment. Twenty hours later (time required to air dry the seeds treated by fungicide), individual samples of wheat and barley seeds, as well as of untreated control, were placed on the Malt Extract Agar medium (Biolife, Milano, Italy; 50 seeds per Petri dish with diameter of 185 mm). After five days of incubation at 25 °C, each individual cereal seed was visually classified on a scale of 0–5 according to the intensity of fungal attack on the surface of each cereal seed. Score equal to 0 indicated an absence of fungal attack; the score of 5 – fungal attack of more than 60 % of the infected seed surface. The infection degree (ID) was calculated using the Townsend-Heuberger's formula (1) (Rekanovic et al., 2010):

$$ID = \frac{\sum(nv) \times 100}{NV} \quad (1)$$

$n$  – degree of infection rate (scale 0–5),  $v$  – number of seeds in each category,  $N$  – highest degree of infection rate,  $V$  – total number of seeds screened. Efficacy of seed surface treatment using fungicide, plasma, and plasma + fungicide combination was compared.

### Seed surface diagnostics

#### A. Water contact angle

Wettability changes were identified by measuring the water contact angle (WCA) on the seed surface after plasma treatment using a DSA30 device (Krüss GmbH, Hamburg, Germany). The volume of water droplets was 2 µL and the average value of WCA for each sample was calculated from 12 droplets recorded by a CCD camera and processed using additional software for Drop Shape Analysis DSA1 allowing analysis of a curved surface.

#### B. Scanning electron microscopy (SEM)

SEM measurements were performed using a Scanning Electron Microscope Vega II SBH (Tescan, Czech Republic) at the acceleration voltage of

30 kV and magnification of 150×. The samples were plated with gold by SEM Coating System (BIO-RAD E52-5199) at the pressure of 8 Pa in argon. Thickness of the gold layer was 20 nm.

### Seed germination

Cereal seeds were treated by LTP for 15–300 s. Fifty pieces of LTP treated and untreated wheat and barley seeds were placed on a continuously wetted filter paper (Whatman 1) in sterile Petri dishes (diameter of 185 mm) and incubated for five days at 25 °C. Germination ( $G$ ) was calculated by the following equation (2):

$$G = \frac{SG}{ST} \times 100 \% \quad (2)$$

where  $G$  – germination,  $SG$  – number of germinated seeds,  $ST$  – total number of seeds.

Vigor of the seedlings was evaluated by measuring the root length and shoot length of the seedlings. Seedling vigor index was calculated according to Eq. (3) (Abdul-Baki and Anderson, 1973):

$$SV = \frac{(LR + LS) \times G(\text{treated seeds})}{(LR + LS) \times G(\text{untreated seeds})} \times 100 \% \quad (3)$$

where  $SV$  – seedling vigor,  $LR$  – length of roots in mm,  $LS$  – length of shoots in mm,  $G$  – germination.

### Statistical analysis

Significant differences between the samples were determined using the one-way analysis of variance (ANOVA) with post hoc tests with the Bonferroni correction. Differences were considered significant for \* $P < 0.05$ ; \*\* $P < 0.01$ ; \*\*\* $P < 0.001$ . Values are expressed as the mean ± standard deviation (SD) of at least five measurements.

## Results

### Cereal seed surface decontamination from *Fusarium culmorum*

Two methods were used to reduce the growth of *F. culmorum* on the surface of cereal seeds: a chemical method using the fungicidal effect of Vitavax 2000 and a physical method using the effect of LTP. For the chemical treatment of cereal seeds, Vitavax 2000 was used in doses from 10 % to 100 % of standard recommended agricultural application. In Fig. 2, significantly different results of the fungicide protective effect were obtained for wheat and barley seeds. In wheat, a significant decrease in the ID to 60 % was observed after using a 10% dose of the fungicide. With the increase of the fungicide dose, the ID dropped significantly. However, even after applying a 100 % fungicide dose, complete elimination of *F. culmorum* on the surface of wheat

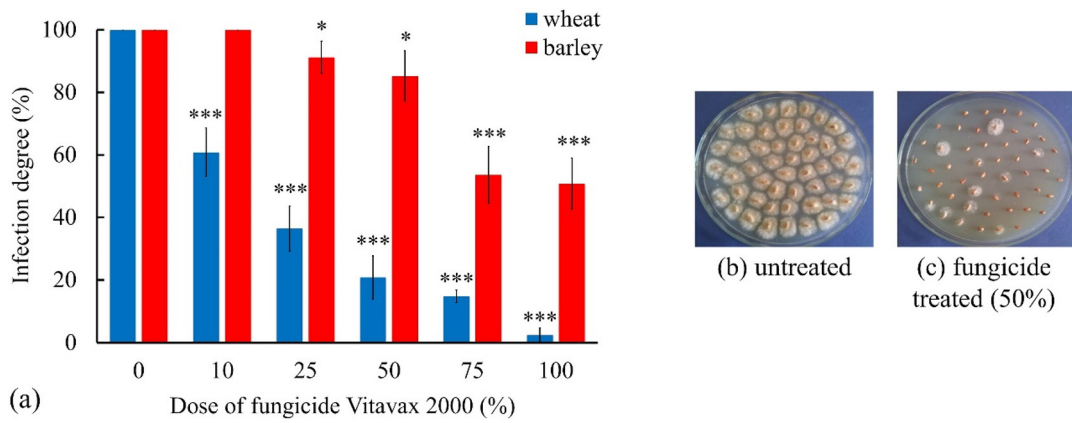


**Fig. 2.** Decontamination of cereal seed surface from seed-borne phytopathogen *F. culmorum* after Vitavax 2000 application (a). Results were significant at \* $P < 0.05$ ; \*\*\* $P < 0.001$  compared to control (0% dose of Vitavax 2000). Growth of *F. culmorum* on the surface of untreated wheat seeds (b) and after the application of a 50 % dose of Vitavax 2000 (c).

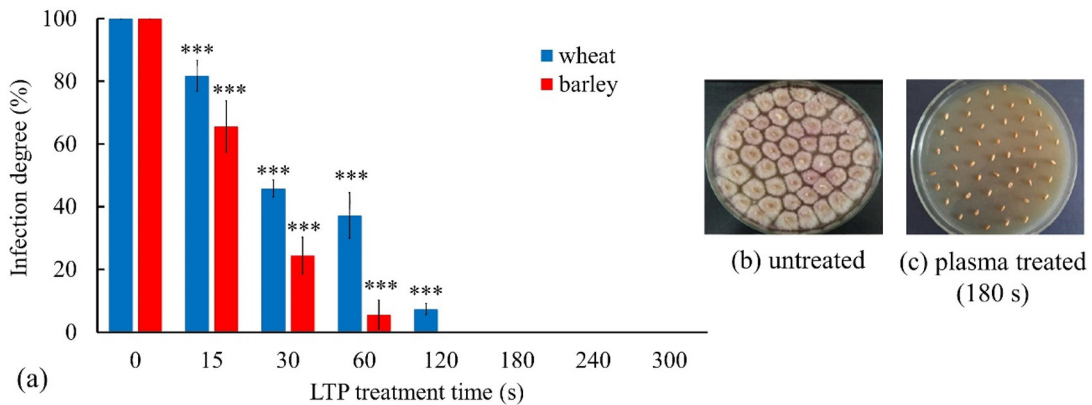


**Fig. 3.** Decontamination of cereal seed surface from seed-borne phytopathogen *F. culmorum* after plasma treatment (a). Results were significant at \*\*\* $P < 0.001$  compared to control (0 s LTP). Growth of *F. culmorum* on the surface of untreated wheat seeds (b) and after the application of 180 s of LTP treatment (c).

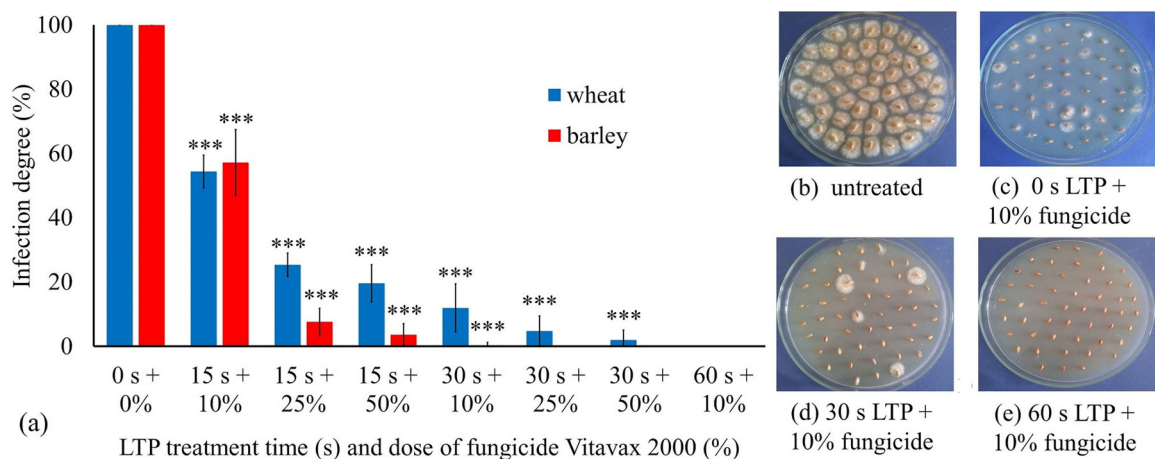


**Fig. 4.** Decontamination of cereal seed surface from seed born phytopathogen *F. culmorum* after combined treatment (LTP + fungicide) (a). Results were significant at \*\*\* $P < 0.001$  compared to control (0 s LTP + 0 % fungicide). Growth of *F. culmorum* on the surface of untreated wheat seeds (b) and after the application of combined treatment (0 s + 10 % (c); 30 s + 10 % (d); 60 s + 10 % (e)).

seeds was not reached – ID was below 5 %. A 10 % dose of fungicide on barley seeds had no effect on the ID. The reduction of ID after the application of a 50 % fungicide dose was only about 20 % and a 100 % dose led to a 50 % reduction in *F. culmorum* on the barley seed surface.

In physical treatment, the seeds were exposed to LTP for 15–300 s (Fig. 3). After 15 s of LTP treatment, a significant decrease of 20 % in wheat seed ID was observed and of more than 30 % in barley seeds. After 30 s of plasma treatment, ID of the seeds was below 50 % for both kinds of cereals. Complete devitalization of *F. culmorum* on the wheat seed surface was observed after 180 s of plasma exposure and after 120 s in barley seeds.

The effect of the combined treatment (LTP + Vitavax 2000) on the reduction of *F. culmorum* is presented in Fig. 4. A significant decrease of the ID in both cereal seeds to about 60 % was achieved after 15 s of LTP combined with a 10 % fungicide

dose. With the increasing LTP exposure time and fungicide dose, the cereal seeds infection degree decreased significantly. Complete reduction of *F. culmorum* on the surface of cereal seeds was observed after the combined treatment applying 60 s LTP + 10 % dose of fungicide.

#### Seed surface diagnostics – WCA and SEM

LTP treatment caused changes in the surface properties of cereal seeds. Wettability of wheat and barley seed surface was determined by measuring the WCA of a distilled water drop. WCA of the cereal seed reference samples was  $106.4 \pm 9.4^\circ$  (wheat) and  $95.2 \pm 2.4^\circ$  (barley). The surface of a sample with WCA above  $90^\circ$  is considered as hydrophobic. After a 10 s exposure of seeds to LTP, a decrease of WCA to  $56.9 \pm 8.6^\circ$  for wheat and to  $61.8 \pm 5.21^\circ$  for barley was observed and the samples became hydrophilic; contact angles of the cereal seeds were less than  $5^\circ$  – maximum

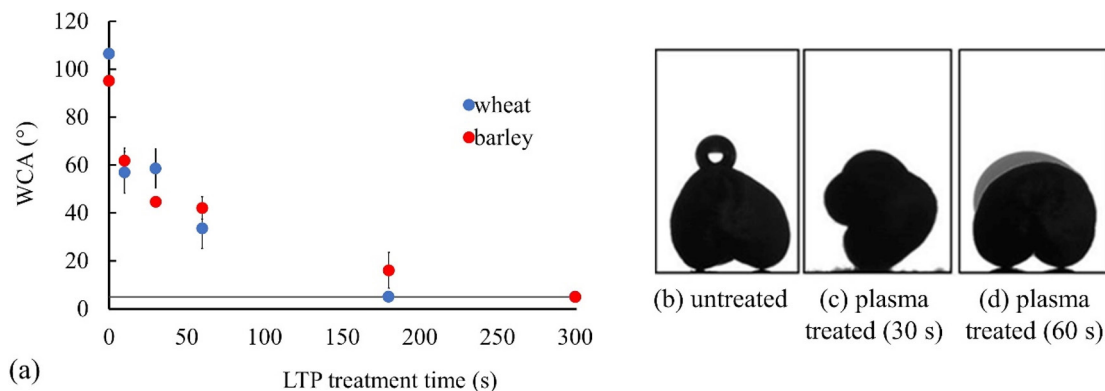


**Fig. 5.** Effect of treatment time on the water contact angle measured on cereal seed samples treated by LTP (a). A drop of water on the surface of untreated (b) and LTP treated barley seeds (c, d).

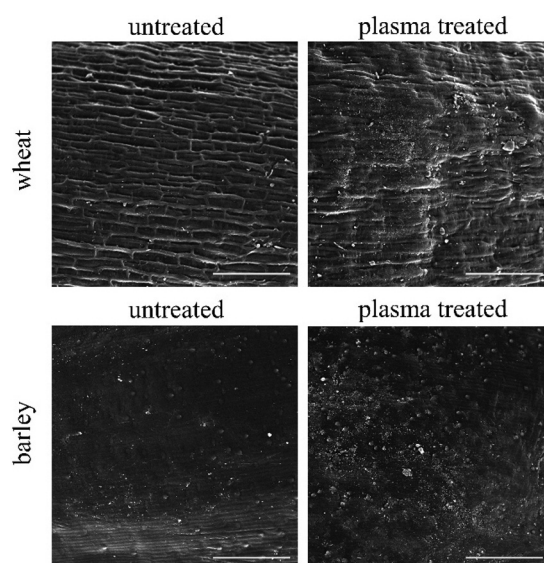


**Fig. 6.** Scanning electron microscopy (SEM) of untreated and plasma treated (120 s) wheat and barley seeds. Total magnification was 150 $\times$ ; SEM HV 30 kV; scale bars represent 200  $\mu$ m.

**Tab. 1.** Germination (G) and seedling vigor (SV) of cereal seeds after LTP treatment compared to untreated control.

LTP treatment (s)	wheat		barley	
	G (%)	SV (%)	G (%)	SV (%)
0	100 ± 0	100 ± 0	100 ± 0	100 ± 0
15	100 ± 0	117 ± 4**	100 ± 0	115 ± 7**
30	98 ± 4	99 ± 13	98 ± 4	101 ± 5
60	96 ± 8	74 ± 18	94 ± 8	74 ± 10**
120	80 ± 10*	23 ± 12***	72 ± 15*	20 ± 5***
180	74 ± 10**	14 ± 5***	54 ± 14***	10 ± 3***
240	52 ± 11***	4 ± 5***	48 ± 4***	4 ± 0.8***
300	46 ± 10***	3 ± 3***	32 ± 7***	2 ± 0.6***

Results were significant at \* $P < 0.05$ ; \*\* $P < 0.01$ ; \*\*\* $P < 0.001$  compared to control.

hydrophilic surface ( $WCA < 5^\circ$ ), after a 180 s LTP treatment of wheat seeds and after a 300 s LTP treatment of barley seeds (Fig. 5).

Seed surface morphology before and after the plasma treatment was compared by SEM. As it can be seen in Fig. 6, not even a 120 s plasma treatment caused significant changes in the cereal seed surface. In case of wheat seeds, slight surface smoothing was observed while no visible surface changes were observed in barley seeds.

#### *Seed germination and seedling vigor*

The effect of plasma treatment on germination and seedling vigor of cereal seeds is summarized in Tab. 1. Cereal germination was not adversely affected after a 15 s plasma exposure. On the contrary, slight stimulation of growth parameters (seedling vigor) in both cereals was achieved. The 30 s and 60 s plasma treatment resulted in a minor decrease of germination. A 60 s treatment by LTP inhibited the growth parameters of wheat and barley seeds by almost 30 %. Effect of a 120 s plasma treatment caused inhibition of the seed growth parameters by almost 80 %. After 300 s of treatment, the germination of both cereal seeds decreased below 50 % and the seedling vigor was less than 5 %. Seeds with germination below 80 % are not suitable for planting.

#### **Discussion**

Vitavax 2000 is a combined fungicide which acts as a systemic and contact fungicide inhibiting spore germination and blocks the growth of some fungal pathogens. Vitavax 2000 in various doses was used to decontaminate wheat and barley seeds' surface from *F. culmorum*. While almost complete devitalization of *F. culmorum* was achieved with a 100 % fungicide dose used in agriculture for pre-sowing seed treatment of wheat, in case of barley it was only about 50 % (Fig. 2). This difference

is probably due to the morphological difference (size and surface) between wheat and barley seeds. Fungicides are designed to protect emerging plants (wheat, barley, maize). A positive effect of fungicides on germination and root growth has also been observed in chickpea, maize, peanuts (Dhanamanjuri et al., 2013; El-Deeb et al., 2002). The effect of fungicides on the quality of lentil seeds during storage was also investigated previously (Khatun et al., 2016). Fungicide treated seeds demonstrate higher germination and seedling vigor than untreated seeds. However, the yield of seeds is not affected only by fungicides but also by other factors (temperature, drought) (Jalakas et al., 2018; Stetkiewicz et al., 2019). The efficacy of some long-term used fungicides has been influenced by the development of antifungal resistance in target fungal pathogens (Ishii and Holloman, 2015; Lucas et al., 2015). Although the use of fungicides in agriculture cannot be completely excluded, ways to reduce their levels are researched, which could ultimately slow down the spread and development of resistance to fungicides and reduce the chemical burden of the environment.

LTP was used as a possible alternative method to chemical seed protection. A significant decrease of fungal contamination after 15 s of plasma treatment was observed. Complete decontamination of the seed surface of both cereals was achieved after a 180 s LTP exposure (Fig. 3). The effect of plasma was also investigated on maize seeds (Zahoranová et al., 2018). *F. culmorum* was completely devitalized after 120 s. This result is comparable with the results presented in this study.

Improvement of seed germination is also caused by the decontamination of the seed surface (Yvin and Coste, 1997; Guang-Liang et al., 2005; Dobrin et al., 2015), which could be significant because phytopathogenic microorganisms negatively influence the

seed quality and subsequent production of any agriculture commodity. In comparison, physical treatment does not protect the seeds after their placement in soil. In this study, physical plasma treatment and chemical fungicide application were combined in synergistic treatments to protect seeds from fungal contamination. The results showed a beneficial effect of LTP on *F. culmorum* decontamination as well as the reduction of fungicide doses needed. A significant decrease of cereal seed contamination was already observed after combined treatment applying 15 s LTP and 10 % Vitavax 2000. Combination of 60 s of plasma and 10 % Vitavax 2000 was sufficient for complete *F. culmorum* decontamination, which represents a 90 % reduction in the fungicide dose (Fig. 4). The combination of LTP + Vitavax 2000 seems to be the most appropriate method.

LTP also changes the surface properties of the seeds. The surface of wheat and barley seeds changed from hydrophobic to hydrophilic after 10 s of plasma treatment (Fig. 5). Prolongation of the LTP exposure led to a drop in the contact angle of distilled water below 5°, making the seed surface perfectly hydrophilic as opposed to the hydrophobic surface of untreated seeds. LTP can modify the seed surface and thus increase its wettability and absorbability. This feature is of interest in agriculture because better water absorption reduces the seed requirements for water content in the environment during the germination period. Plasma treated seeds are more wettable which improves the adhesion of the fungicide to their surface and thus, a smaller dose of fungicide is required to cover the seed surface in comparison to untreated seeds. SEM confirmed that plasma does not cause visible morphological changes in the surface of barley seeds and only very slight morphological changes in the surface of wheat seeds (Fig. 6). Stolárik et al. (2015) detected significant surface structural modifications in pea seeds after 120 s of plasma treatment using electron microscopy. Disruptions, abrasions and loosening of the original structures were observed. Such significant changes were not observed in maize, which is probably due to different seed hardness (Zahoranová et al., 2018). Based on the results obtained from WCA and SEM, the surface changes of the seeds after plasma application were caused by a change in the chemical structure of seed surface and not by morphological changes.

In this study, the effect of plasma on seed germination was investigated. To improve seed absorption, plasma treatment is expected to have positive effect on germination. This would correlate with the published results (Bafail et al., 2018; Štěpánová et al., 2018; Magureanu et al., 2018; Guo et al., 2018;

Los et al., 2018). A 15 s plasma treatment did not affect germination but stimulated the growth parameter of the seeds of both cereals. After 30 s and 60 s of plasma application, germination inhibition was minor. A 60 s plasma treatment caused a 26 % inhibition of growth parameters (Tab. 1). It was concluded that a 60 s LTP treatment is the most potent in combined seed treatment reducing the fungicide dose. Vitavax 2000 fungicide itself had positive effect on growth parameters (unpublished results), which could compensate for the inhibition of growth parameters caused by plasma. Positive effects of plasma (shorter exposure times) on growth parameters have also been found in maize, wheat, soybeans, peas (Zahoranová et al., 2016; Henselová et al., 2012; Roy et al., 2018; Pizá et al., 2018). LTP treatment of the seeds for more than 60 s resulted in germination and growth parameters inhibition.

## Conclusion

Experimental results presented in this study indicate that low-temperature atmospheric pressure plasma generated by a plasma source based on DCSD in ambient air can be successfully used for the treatment of cereal seeds. LTP treatment of wheat and barley seeds led to increased surface wettability and therefore better germination and chemical fungicide penetration. The synergistic effect of fungicide and LTP treatment used against seed-borne phytopathogens present on the surface of wheat and barley seeds was more effective than when each of them is used individually. An optimal combination of plasma treatment time and chemical fungicide dose can significantly reduce the use of harmful chemicals in practice but at the same time stimulate germination via plasma treatment. Our data demonstrate that 30 s of LTP treatment is the optimal dose to reduce of *F. culmorum* by more than 80 % and the amount of fungicides by 50–90 % without impairment of seed physiology. Furthermore, the combinatory approach to seed treatment can also be used for other phytopathogenic fungi, but optimization is required. The data presented in this study provide a good basis for further experiments that have to be performed directly in soil.

## Acknowledgement

*This study was supported by the Slovak Research and Development Agency under the contract No. APVV-16-0216.*

## Declarations of interest

None.

## References

- Abdul-Baki AA, Anderson JD (1973) *Crop Science* 13: 630–633.
- Bafoif M, Jemmat A, Martinez Y, Merbahi N, Eichwald O, Dunand C, Yousfi, M (2018) *PLOS One* 13: 1–16.
- Černák M, Černáková E, Hudec I, Kováčik D, Zahoranová A (2009) *The European Physical Journal Applied Physics* 47.
- Chen D, Peng P, Zhou N, Cheng Y, Min M, Ma Y, Mao Q, Chen P, Chen C, Ruan R (2019) *Food chemistry* 290: 270–276.
- Cullen PJ, Lalor J, Scally L, Boehm D, Milosavljević V, Bourke P, Keener K (2018) *Plasma Processes and Polymers* 15: 1–11.
- Dhanamanjuri W, Thoudam R, Dutta BK (2013) *Middle-East Journal of Scientific Research* 17: 627–632.
- Dobrin D, Magureanu M, Mandache NB, Ionita MD (2015) *Innovative Food Science and Emerging Technologies* 29: 255–260.
- El-Deeb AA, Abdel-Momen SM, Hanafi AA (2002) *Egyptian Journal of Agricultural Research* 80: 71–82.
- Guang-Liang C, Song-Hua F, Chun-Ling L, Wei-Chao G, Wen-Ran F, Gu-Ling Z, Jiu-Li W, Latif K, Shu-Gen Z, Zhen-Quan W, Er-Li H, Ya-Bo F, Si-Ze Y (2005) *Chinese Physics Letters* 22: 1980.
- Guo Q, Meng Y, Qu G, Wang T, Yang F, Liang D, Hu S (2018) *Bioelectromagnetics* 39: 120–131.
- Henselová M, Slovákova L, Martinka M, Zahoranová A (2012) *Biologia* 67: 490–497.
- Ishii H, Holloman DW (2015) *Fungicide resistance in plant pathogens*. Springer, Tokyo.
- Jalakas P, Tulva I, Kangor T, Sooväli P, Rasulov B, Tamm Ü, Koppel M, Kollist H, Merilo E (2018) *European Journal of Agronomy* 99: 129–137.
- Jiafeng J, Xin H, Ling LI, Jiangang L, Hanliang S, Qilai X, Renhong Y, Yuanhua D (2014) *Plasma Science and Technol.* 16: 54.
- Khatun A, Bhuiyan MAH, Tahmid A (2016) *Jahangirnagar University Journal of Biological Sciences* 5: 51–56.
- Laca A, Mousia Z, Díaz M, Webb C, Pandiella SS (2006) *Journal of Food Engineering* 72: 332–338.
- Los A, Ziuzina D, Akkermans S, Boehm D, Cullen PJ, Van Impe J, Bourke P (2018) *Food Research International* 106: 509–521.
- Lucas JA, Hawkins NJ, Fraaije BA (2015) *Advances in Applied Microbiology* 90: 29–92.
- Magan N, Hope R, Cairns V, Aldred D (2003) In: Xu X., Bailey JA, Cooke BM (Eds.), *Epidemiology of Mycotoxin Producing Fungi*. Springer, Dordrecht, pp. 723–730.
- Magureanu M, Sirbu R, Dobrin D, Gidea M (2018) *Plasma Chemistry and Plasma Processing* 38: 989–1001.
- McMullen M, Bergstrom G, DeWolf E, Dill-Macky R, Hershman D, Shaner G, Sanford DV (2012) *Plant Disease* 96: 1712–1728.
- Mitra A, Li YF, Klämpfl TG, Shimizu T, Jeon J, Morfill GE, Zimmermann JL (2014) *Food and Bioprocess Technology* 7: 645–653.
- Montville TJ, Matthews KR (2005) *Food microbiology*. ASM Press, Washington.
- Moreau M, Orange N, Feuilloley MGJ (2008) *Biotechnology Advances* 26: 610–617.
- Muhammad AI, Liao X, Cullen PJ, Liu D, Xiang Q, Wang J, Chen S, Ye X (2018) *Comprehensive Reviews in Food Science and Food Safety* 17: 1379–1394.
- Pereira VL, Fernandes JO, Cunha SC (2014) *Trends in Food Science & Technology* 36: 96–136.
- Pizá MCP, Prevosto L, Zilli C, Cejas E, Kelly H, Balestrasse K (2018) *Innovative Food Science and Emerging Technologies* 49: 82–91.
- Ramos AJ, Labernia N, Marín S, Sanchis V, Magan N (1998) *International Journal of Food Microbiology* 44:133–140.
- Randeniya LK, de Groot GJJ (2015) *Plasma Processes and Polymers* 12: 608–623.
- Rekanovic E, Potocnik I, Milijasevic-Marcic S, Stepanovic M, Todorovic B, Mihajlovic M (2010) *Pesticides and phytomedicine* 25: 319–324.
- Roy NC, Hasan MM, Talukder MR, Hossain MD, Chowdhury AN (2018) *Plasma Chemistry and Plasma Processing* 38: 13.
- Šerá B, Špatenka P, Šerý M, Vrchotová N, Hrušková I (2010) *IEEE Transactions on Plasma Science* 38: 2963–2968.
- Šimončicová J, Kryštofová S, Medvecká V, Ďurišová K, Kaliňáková B (2019) *Applied Microbiology and Biotechnology* 103: 5117–5129.
- Štěpánová V, Slavíček P, Kelar J, Prášil J, Smékal M, Stupavská M, Jurmanová J, Černák M (2018) *Plasma Processes and Polymers* 15: 1–9.
- Stetkiewicz S, Burnett FJ, Ennos RA, Topp CF (2019) *European Journal of Agronomy* 105: 111–118.
- Stolárik T, Henselová M, Martinka M, Novák O, Zahoranová A, Černák M (2015) *Plasma Chemistry and Plasma Processing* 35: 659–676.
- Tančínová D, Kačániová M, Javorekova S (2001) *Biologia* 56: 247–250.
- United Nations, Food and Agriculture Organization, Statistics Division (FAOSTAT) (2019) <http://www.fao.org/faostat/en/#data/QC> (accessed 7 October 2019).
- Yvin JC, Coste C (1997) U.S. Patent No. 5,703,009. Washington, DC: U.S. Patent and Trademark Office.
- Zahoranová A, Henselová M, Hudecová D, Kaliňáková B, Kováčik D, Medvecká V, Černák M (2016) *Plasma Chemistry and Plasma Processing* 36: 397–414.
- Zahoranová A, Hoppanová L, Šimončicová J, Tučeková Z, Medvecká V, Hudecová D, Kaliňáková B, Kováčik D, Černák M (2018) *Plasma Chemistry and Plasma Processing* 38: 969–988.

# Determination of biological markers of organic substances in sediment and soil samples by gas chromatography

Nemanja Koljančić<sup>a</sup>, Olga Vyviurska<sup>a</sup>, Milica Balaban<sup>b</sup>, Ivan Špánik<sup>a</sup>

<sup>a</sup>*Institute of Analytical Chemistry, Faculty of Chemical and Food Technology,  
Slovak University of Technology in Bratislava, Radlinského 9, Bratislava, 812 37 Slovakia*

<sup>b</sup>*Faculty of Natural Sciences and Mathematics, University of Banja Luka,  
Mladena Stojanovića 2, Banja Luka, 78000 Bosnia and Herzegovina  
ivan.spanik@stuba.sk*

**Abstract:** Once they reach the environment, petroleum hydrocarbons undergo various chemical, physico-chemical and biochemical transformation processes. Organic compounds which are not or are very poorly subject to these processes are thermodynamically the most stable isomers and they are called biological markers (biomarkers). This paper presents the results of the determination of organic substances in twelve samples taken in the area of the city of Banja Luka (Bosnia and Herzegovina). Two soil samples were taken in the Banja Luka city heating plant area and ten river sediment and soil samples were taken in the upper and lower basin of the Vrbas river in the Banja Luka city area. The aim of this study was to determine the biomarkers of oil-type pollutants in contaminated samples as well as the type of organic substances in samples taken near the contaminated area. Assisted solvent extraction was used to isolate the total petroleum hydrocarbons (TPH) from all twelve samples. Fractionation of the extracts into saturated and aromatic hydrocarbon fractions was performed by column chromatography. The fractions were analyzed by gas chromatography-mass spectrometry (GC-MS). On basis of the obtained chromatograms, biomarkers of petroleum pollutants and specific correlation parameters of organic substances in the samples were determined. The dominance of *n*-alkanes with odd C atoms as well as the presence of an unresolved complex mixture (UCM) on chromatograms of saturated and aromatic hydrocarbons showed the presence of anthropogenic organic substances of petroleum origin in the analyzed samples. Based on the obtained chromatograms, it can be concluded that microbial degradation of hydrocarbons in all samples occurred.

**Keywords:** organic substances, hydrocarbon composition, biomarkers, GC-MS analysis, correlation parameters, assisted solvent extraction

## Introduction

Hydrocarbons found in soil and sediments reflect both natural and anthropogenic inputs as well as diagenetic processes taking place in the water column and during transport and sedimentation (Shirneshan et al., 2016). Crude oil consists mainly of a complex mixture of hydrocarbon compounds (aliphatic and aromatic) and non-hydrocarbon compounds (resins and asphaltenes). Environmental contamination occurs frequently and it is associated with production processes, refining, transportation and storage of oil and petroleum products. Oil undergoes various transformation processes in the environment conditions, depending on the physico-chemical and biological factors such as evaporation, dissolution, microbial degradation, photooxidation and interaction between oils and sediments (Faboya et al., 2016). Lower molecular weight hydrocarbons normally evaporate, while heavier compounds, such as asphaltenes and resins, partially undergo deposition in sediments (Kakhki et al., 2018; Yogaswara et al., 2020). Therefore, these compounds

are frequently found in petroleum, coal, sedimentary rocks, recent sediments, and soils. Molecular structures of stable geochemical products can be attributed to biogenic precursor molecules. At the same time, conversion from biogenic and thermodynamically less stable compounds to more stable ones is especially interesting in isomers and stereoisomers (Hazra et al., 2019). From the chemical point of view, a majority of biomarker molecules belong to aliphatic or aromatic hydrocarbons (Walters et al., 2018; He et al., 2018; Kao et al., 2018). Thus, hydrocarbon composition of petroleum has been extensively used for the determination of hydrocarbon sources in coastal sediments and soils. A heating plant in the Banja Luka city still uses heavy oil fractions like mazut as a heating medium. Thus, the objectives of the present study are: (i) to determine the occurrence, distribution and source of saturated and aromatic hydrocarbons, (ii) to examine the distribution, composition, and relative maturity levels of saturated and aromatic hydrocarbons in sediments and soils, and (iii) to evaluate the degree of microbial degradation of organic sub-

stances in analyzed samples. Twelve sediment and soil samples were taken for analysis in the area of the city of Banja Luka within the heating plant and in the lower and upper basin of the Vrbas river. The fractions of saturated and aromatic hydrocarbons were analyzed by the GC-MS method to determine the specific correlation parameters, e.g. the degree of maturation and origin of the organic substances.

## Material and Methods

### Chemicals

Dichloromethane, *n*-hexane, elemental copper and sodium sulfate were purchased from Merck (Darmstadt, Germany). Florisil® was obtained from Fluka AG (Buchs, Switzerland) and acetone was obtained from Mikrochem (Pezinok, Slovakia).

### Sampling

Exact sampling locations are shown in Fig. 1. Totally twelve samples were studied in this work, while two were taken in the Banja Luka city heating plant area – samples 1 and 2. Other ten samples represent river sediment samples and soil samples taken in the upper and the lower basin of the Vrbas river in the Banja Luka city area. All samples were air-dried for 24 hours and sieved through 0.063 mm sieves.

### Total petroleum hydrocarbons extraction

Extraction of total petroleum hydrocarbons (TPH) from sediment and soil samples was performed by assisted solvent extraction using the Dionex ASE 150 apparatus. Extraction cells were filled with 28 g of previously air-dried and sieved samples and the extraction was accomplished according to a previously established method (Thermo Fisher

Scientific Inc., 2011). Dichloromethane/acetone (1:1) mixture was used as an extraction solvent, and the following conditions were set: extraction temperature of 175 °C, static time of 5 min, flush volume of 60 %, gas purging time of 100 s, 1 static cycle. The obtained extract volume was reduced to 5 mL using a rotary evaporator. Activated copper powder was added to the extract and it was sonicated for 3 min in order to remove elemental sulfur from the sample extracts.

### Fractionation of total petroleum hydrocarbons extracts

Column chromatography was used to separate the TPH extract into the saturated and aromatic hydrocarbons fractions using 2.5 g of Florisil® and 0.2 g of sodium sulfate, both activated at 130 °C for 24 h, as adsorbents. The column was loaded with 1 mL of the extract which was previously conditioned with 10 mL of *n*-hexane. The saturated hydrocarbon fraction was eluted with 5 mL of *n*-hexane while the aromatic hydrocarbon fraction was eluted with 3 mL of dichloromethane.

### GC-MS analysis

The fractions of saturated and aromatic hydrocarbons were analyzed using gas-chromatography/mass-spectrometry (GC-MS). For this purpose, an Agilent 7890A gas chromatograph with an Agilent 5975C Mass Selective Detector (MSD) was used. Large volume of aliquots was injected in a programmed temperature vaporizer (PTV) in 5 µL portions with a repetition of ten times (total aliquot volume was 50 µL) onto a HP-1ms capillary column (30 m × 0.250 mm i.d. × 0.250 µm film thickness). The inlet temperature program was set as follows:

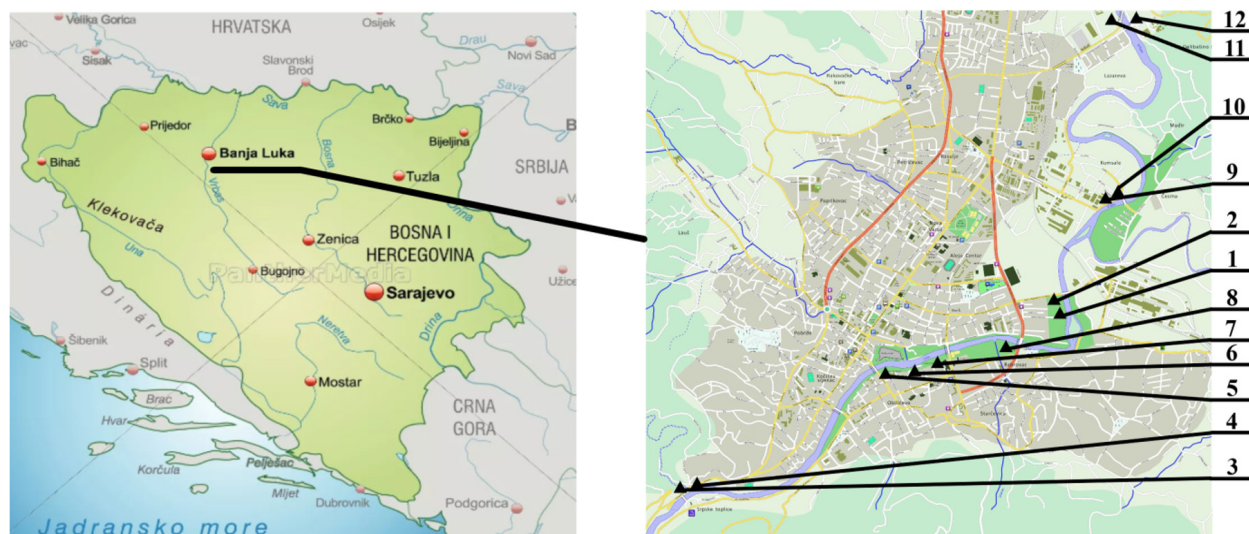


**Fig. 1.** A map of Bosnia and Herzegovina (left) and a map of the sampling locations in the area of the city of Banja Luka (right).

40 °C (2 min) up to 300 °C (5 min) at 600 °C min<sup>-1</sup>. Helium (99.999 % purity) was used as a carrier gas at the flow rate of 1 mL min<sup>-1</sup>. The oven temperature program was set as follows: 40 °C up to 50 °C (7 min) at 100 °C min<sup>-1</sup>, and to the final temperature of 300 °C (15 min) at 10 °C min<sup>-1</sup>. Duration of the measurement was 47.1 min. The transfer line temperature was set to 300 °C, MS source temperature and MS quadrupole temperature were 230 °C and 130 °C, respectively. Mass spectra were analyzed using the MSD ChemStation software with NIST14, MPW2007 and W9N11 databases.

## Results and Discussion

### Total petroleum hydrocarbons content

Results of assisted solvent extraction are shown in Tab. 1. Concentration of TPH extracts ranged from 0.1786 mg g<sup>-1</sup> to 25.8214 mg g<sup>-1</sup>. An increase in the TPH concentration in samples 1 and 2 was expected because both sample places are located in the area of the city heating plant. Similar concentration of TPH was observed for samples 3, 4, 5, 6, 7 and 8, from the upper basin of the Vrbas river (before the heating plant). In samples 9 and 10 from the lower river basin (after the city heating plant), a decrease of TPH concentration was observed. This effect is probably due to the dilution with the tributary effluents. A contribution of anthropogenic contamination to the total TPH concentration is clearly visible for sample 11 collected at a site located in the industrial zone.

**Tab. 1.** TPH concentration in samples.

Sample	TPH concentration (mg g <sup>-1</sup> )
1	25.8214
2	19.2857
3	0.2500
4	0.2500
5	1.7143
6	1.1786
7	0.8214
8	0.6786
9	0.1786
10	0.2143
11	2.6071
12	0.7143

### Saturated hydrocarbons

Chromatograms obtained for specific *m/z* 71 ratio characteristic for *n*-alkanes of the most contaminated samples (no. 1 and 11) are shown in Fig. 2. Specific correlation parameters of saturated hydro-

carbons are shown in Tab. 2. *n*-Alkane compounds in all samples ranged from C<sub>12</sub> to C<sub>35</sub>. Carbon preference index (CPI) values, representing the ratio of odd to even *n*-alkanes, was found to be in the range from 1.3881 to 2.6383. CPI values close to 1 indicate petroleum and other anthropogenic substances e.g. from the combustion of fossil fuels, wood and agricultural debris (Faboya et al., 2016). The dominance of hydrocarbons with an odd carbon number also indicates the presence of organic substances of anthropogenic origin. Furthermore, organic substances in the sediment and soil samples could originate from native organic substances and oil-type anthropogenic organic substances (Samelak et al., 2018). The presence of unresolved complex mixture (UCM) on *n*-alkane chromatograms is associated with the presence of aromatic heterocyclic compounds formed by the biological degradation of hydrocarbons (*n*-alkanes, steranes and terpanes) (Romero, et al., 2015; Di Gregorio et al., 2016; Catania et al., 2018; Wang et al., 2018). This group of compounds is typical for samples that have undergone microbial degradation of organic substances (Romero, et al., 2015; Di Gregorio et al., 2016; Catania et al., 2018; Wang et al., 2018). Separation of UCM is commonly a challenge for the 1D gas chromatographic method. Pristane and phytane are isoprenoid alkanes usually derived from phytol side-chains in chlorophyll (Tissot and Welte, 1984; Vitorović and Jovančićević, 2016). Due to their high resistance to microbial and thermal degradation, these compounds can serve as biomarkers for fossil fuels. Pristane and phytane can be used to assess the degradation level of petroleum residues (Samelak et al., 2020). Low values of Pristane/Phytane (Pr/Ph) ratios (0.9601–1.2771) were found in all samples; Pr/Ph values below or near 1 indicate the presence of anthropogenic organic substances of petroleum origin (Rushdi et al., 2017; Zhu et al., 2018; Gdara et al., 2020). Furthermore, based the UCM profile and the Pr/Ph ratios, it can be concluded that the samples are contaminated with fresh and partially biodegraded hydrocarbons (Cabrerizo et al., 2016; Iheonye et al., 2019; Zhu et al., 2018). Values of *n*-alkanes/isoprenoid homologs ratios, *n*-C<sub>17</sub>/Pr and *n*-C<sub>18</sub>/Ph ranged from 1.1449 to 3.3875 and from 1.1695 to 4.3249, respectively, which indicates the dominance of *n*-alkanes over isoprenoid alkanes in all samples. Although the microbial degradation of *n*-alkanes proceeds much faster than that of isoprenoid alkanes of pristane and phytane type, the results indicate increased concentration of petroleum hydrocarbons contributing to the total *n*-alkane concentration. At the same time, degradation of both *n*-alkanes and isoprenoid occurred in the samples.

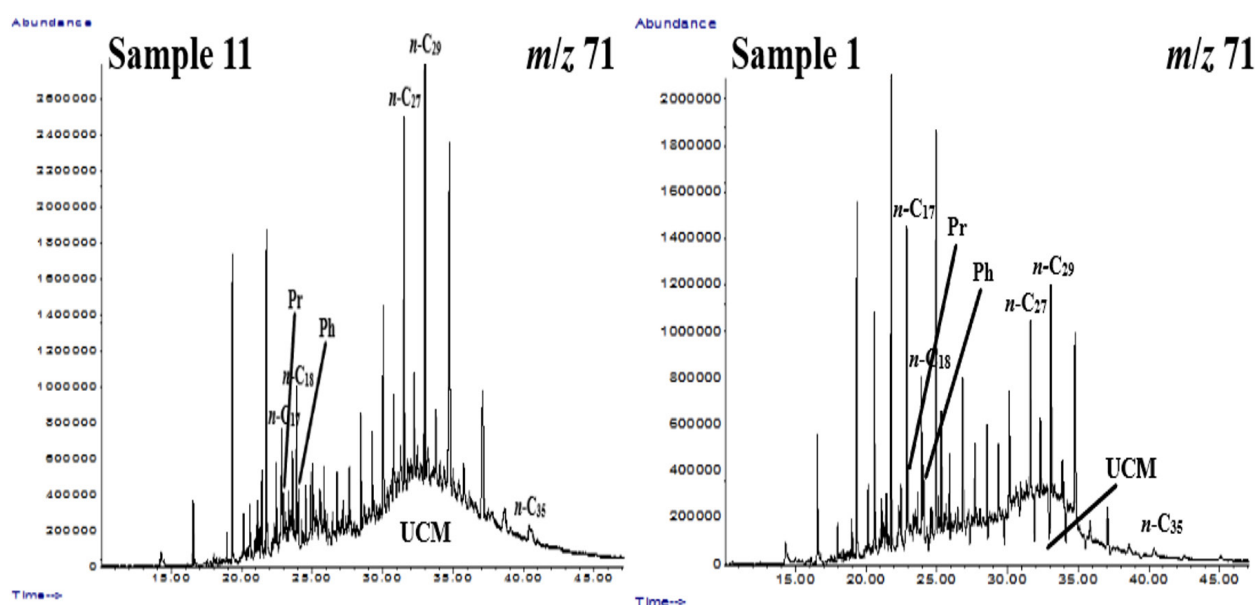


**Fig. 2.** Chromatograms of selected  $m/z$  ratios 71 characteristic for  $n$ -alkanes in samples 11 and 1.

**Tab. 2.** Characteristic correlation parameters of saturated hydrocarbons in sediment and soil samples.

Sample	CPI <sup>a</sup>	Pr/Ph	$n$ -C <sub>17</sub> /Pr	$n$ -C <sub>18</sub> /Ph	$n$ -Alkanes range	Most abundant $n$ -alkanes
1	2.2491	0.9884	3.3875	1.8715	C <sub>12</sub> –C <sub>35</sub>	C <sub>16</sub> ; C <sub>19</sub>
2	1.5767	0.9993	2.8479	1.7826	C <sub>12</sub> –C <sub>35</sub>	C <sub>19</sub> ; C <sub>22</sub>
3	2.6383	1.1242	1.5224	2.2195	C <sub>12</sub> –C <sub>35</sub>	C <sub>27</sub> ; C <sub>29</sub>
4	1.9284	1.2290	1.5272	1.9709	C <sub>12</sub> –C <sub>35</sub>	C <sub>14</sub> ; C <sub>16</sub>
5	1.3981	0.9868	1.7802	1.6554	C <sub>12</sub> –C <sub>35</sub>	C <sub>13</sub> ; C <sub>16</sub>
6	2.5811	1.0730	1.2290	1.2427	C <sub>12</sub> –C <sub>35</sub>	C <sub>27</sub> ; C <sub>29</sub>
7	1.6120	0.9796	1.3851	1.4975	C <sub>12</sub> –C <sub>35</sub>	C <sub>27</sub> ; C <sub>29</sub>
8	2.1728	1.0863	1.2418	1.2712	C <sub>12</sub> –C <sub>35</sub>	C <sub>16</sub> ; C <sub>29</sub>
9	2.0567	0.9495	1.1449	1.1695	C <sub>12</sub> –C <sub>35</sub>	C <sub>27</sub> ; C <sub>29</sub>
10	1.4164	1.2134	2.0405	4.3249	C <sub>12</sub> –C <sub>35</sub>	C <sub>14</sub> ; C <sub>16</sub>
11	1.9956	1.2771	3.8451	1.9327	C <sub>12</sub> –C <sub>35</sub>	C <sub>17</sub> ; C <sub>29</sub>
12	2.5324	0.9601	1.8459	2.2834	C <sub>12</sub> –C <sub>35</sub>	C <sub>27</sub> ; C <sub>29</sub>

$$^a \text{CPI} = \frac{1}{2} \times \left( \frac{\text{C}_{25} + \text{C}_{27} + \text{C}_{29} + \text{C}_{31} + \text{C}_{33}}{\text{C}_{24} + \text{C}_{26} + \text{C}_{28} + \text{C}_{30} + \text{C}_{32}} + \frac{\text{C}_{25} + \text{C}_{27} + \text{C}_{29} + \text{C}_{31} + \text{C}_{33}}{\text{C}_{26} + \text{C}_{28} + \text{C}_{30} + \text{C}_{32} + \text{C}_{34}} \right)$$

Chromatograms showing the presence of steranes ( $m/z$  217) and terpanes ( $m/z$  191) in representative samples are shown in Figs. 3. and 4., respectively. The presence of steranes and terpanes in recent sediments and soil samples indicates the presence of oil-type anthropogenic organic substances. Detector response for UCM is visible on the chromatograms of selected  $m/z$  ratio 217 characteristic for steranes. Partial degradation of steranes and terpanes contributes to the total UCM content in all samples. As it can be seen from Fig. 3, distribution of terpanes in samples 11 and 1 does not differ significantly. Samples collected near the heating plant showed higher UCM content. Basic group of molecular fossils used in petroleum geochemistry

is called polycyclic terpenoids (Belin et al., 2018). These alicyclic compounds originate dominantly from cell membranes of bacteria, microorganisms and algae, which are ubiquitous in sediments. The group includes several homologous series of tri-, tetra-, and pentacyclic triterpanes (Shirneshan et al., 2016; Paul and Dutta, 2016; Belin et al., 2018). The most commonly used alicyclic biomarkers are hopanes, which provide information on oil-source-rock correlations (Grigoriadou et al., 2008). The most definitive indicators of petroleum contamination are probably  $17\alpha(\text{H})$ ,  $21\beta(\text{H})$ -hopanes (Rushdi et al., 2017; Hazra et al., 2019). Biological origin of  $17\alpha(\text{H})$ ,  $21\beta(\text{H})$ -hopanes has not been confirmed. However,  $17\alpha(\text{H})$ ,  $21\beta(\text{H})$ -hopanes are found in

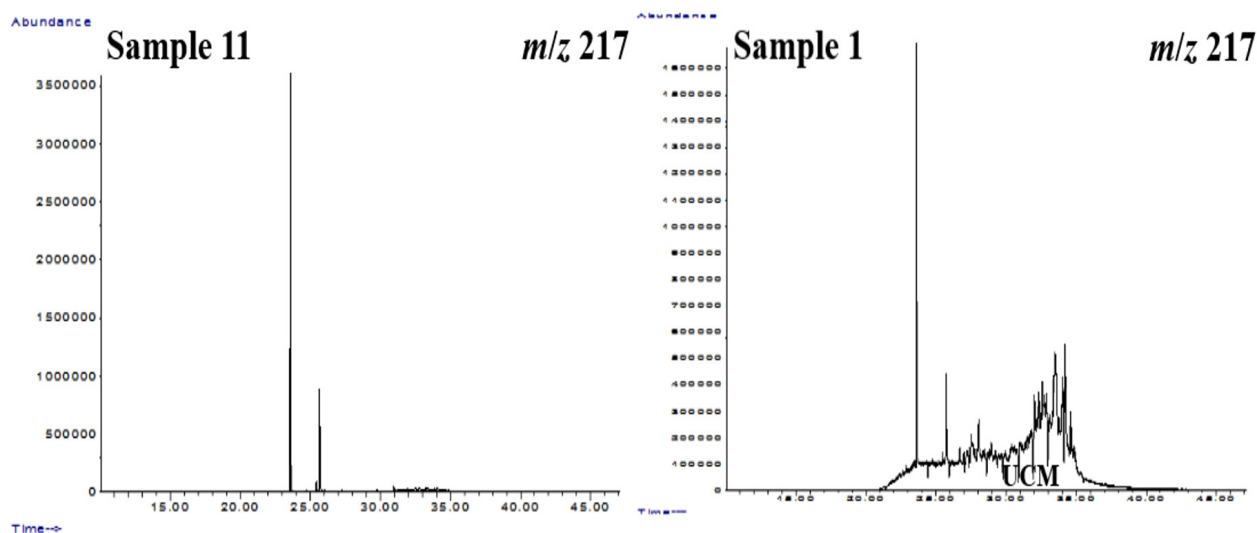


Fig. 3. Chromatograms of selected  $m/z$  ratios 217 characteristic for steranes in samples 11 and 1.

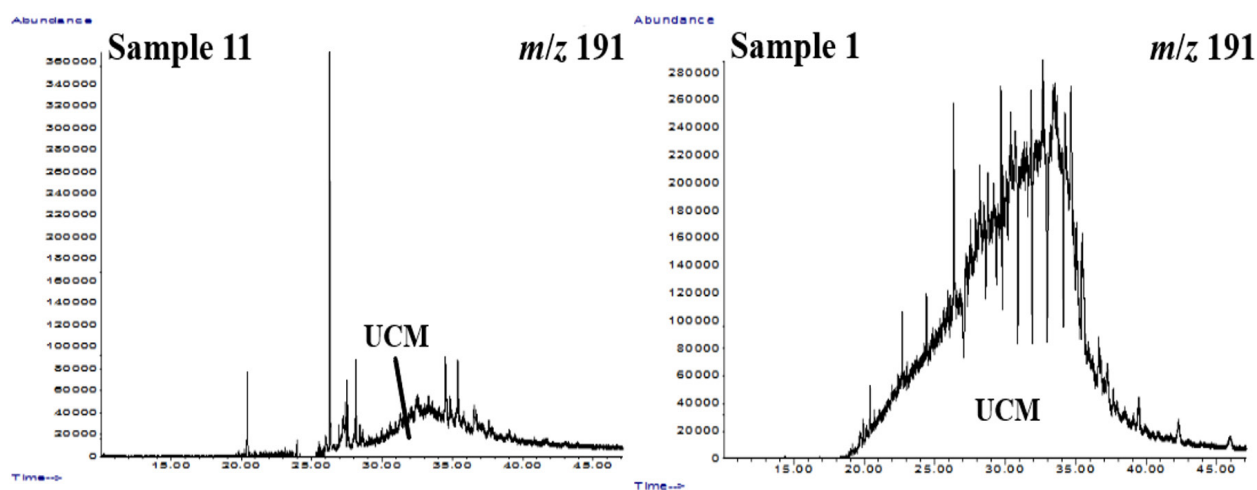


Fig. 4. Chromatograms of selected  $m/z$  ratios 191 characteristic for terpanes in samples 11 and 1.

petroleum and related sediments where they result from the isomerization of  $17\beta(H)$ -hopanes (Inglis et al., 2018). In this case, the degradation pathway leads to relative depletion of  $\alpha\alpha$  over  $\beta\beta$  isomers, R over S, and the removal trend  $C_{27} > C_{28} > C_{29}$  (Díez et al., 2005). Compared to terpanes, a slightly lower concentration of steranes was observed in all samples. The increase in sterane concentrations occurred only in samples 1 and 2 collected in the area of the city heating plant.

#### **Aromatic hydrocarbons**

Due to their environmental impact and toxicity, aromatic compounds have proven to be very useful as indicators of the fate of petroleum pollutants in the environment and as specific source markers of petroleum pollutants in sediments, tissue samples of living organisms and water (Jafarabadi et al., 2017 and 2019; Ghribi et al.,

2019; Han et al., 2018). Aromatic compounds identified in the samples belong to a group of bicyclic and tricyclic aromatic hydrocarbons. Bicyclic aromatic hydrocarbons include alkylated naphthalene derivatives: methyl-naphthalenes ( $m/z$  142), dimethyl- and ethyl-naphthalenes ( $m/z$  156) and trimethyl-naphthalenes ( $m/z$  170). The presence of alkylated phenanthrene ( $m/z$  178) and anthracene ( $m/z$  178) derivatives like methyl-phenanthrene and methyl-anthracene ( $m/z$  192), dimethyl- and ethyl-phenanthrene and dimethyl- and ethyl anthracene ( $m/z$  206) has also been reported. Individual chromatograms of bicyclic and tricyclic aromatic hydrocarbon compounds in samples 11 and 1 are shown in Figs. 5 and 6, respectively. Chromatograms of selected  $m/z$  ratios characteristic for aromatic hydrocarbons and for saturated hydrocarbons are characterized by the presence of UCM.

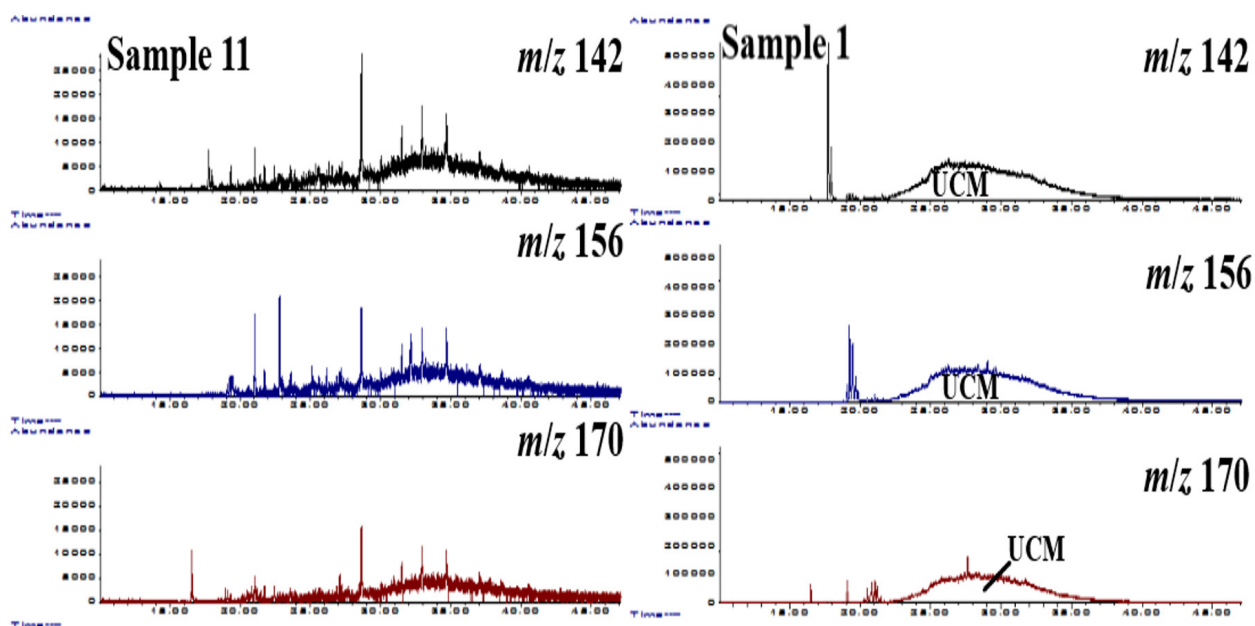


Fig. 5. Chromatograms of selected  $m/z$  ratios characteristic for bicyclic aromatic hydrocarbons in samples 11 and 1.

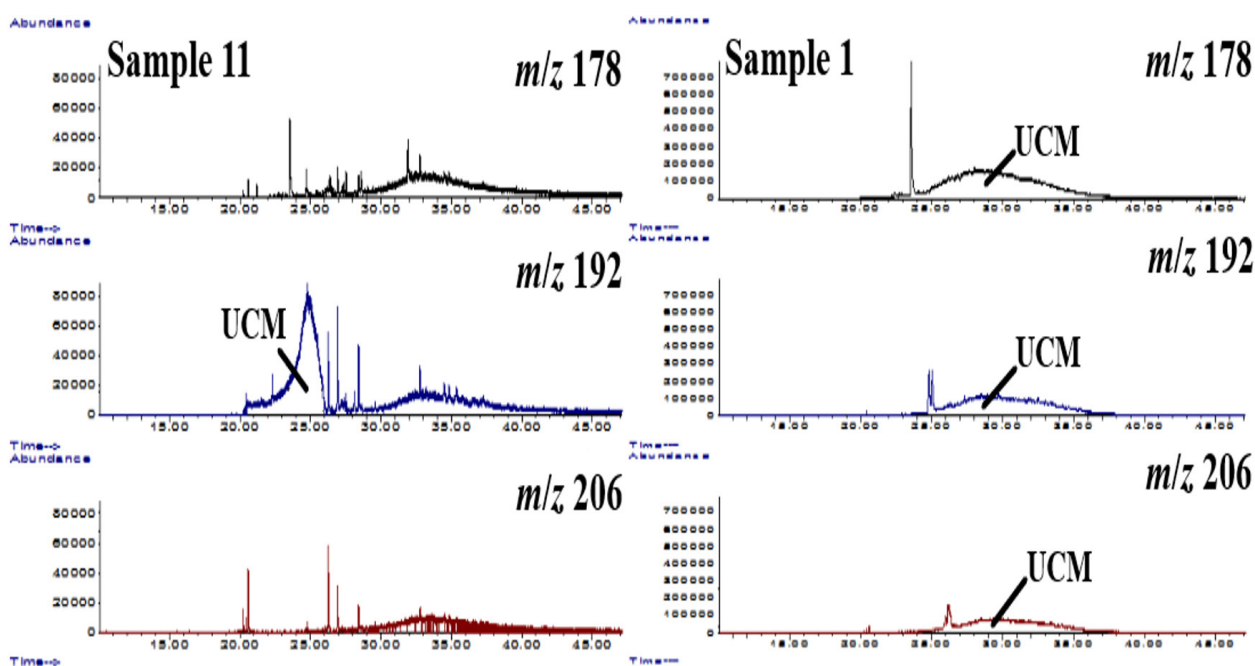


Fig. 6. Chromatograms of selected  $m/z$  ratios characteristic for tricyclic aromatic hydrocarbons in samples 11 and 1.

## Conclusions

This paper investigates the origin and type of organic substances in sediment and soil samples taken in the area of the heating plant and the basin of the Vrbas river in the city of Banja Luka. The results confirmed very efficient TPH extraction by assisted solvent extraction. Characteristic correlation parameters were calculated by examining the  $n$ -alkane, sterane and terpane profiles in the sam-

ples. CPI values were characterized by increased  $n$ -alkane content and the dominance of hydrocarbons with an odd number of C atoms. It has been shown that the obtained ratio of  $n$ -alkanes to isoprenoid alkanes indicates the presence of anthropogenic organic substances. This result indicates terrestrial organic contamination of anthropogenic origin. At the same time, microbial degradation of hydrocarbons was confirmed by the presence of UCM on chromatograms of saturated and aromatic

hydrocarbons. Identification of steranes and terpanes in the samples also supports the assumption of the presence of oil-type anthropogenic organic substances in all samples. Polycyclic aromatic compounds from the group of bicyclic and tricyclic aromatic hydrocarbons were detected based on their characteristic *m/z* ratios. PAHs also contribute to the UCM observed on the saturated and aromatic hydrocarbon chromatograms.

#### Acknowledgement

*Nemanja Koljančić would like to thank the Visegrad fellowship program for contract number 51810301 allowing his ten months staying at the Slovak University of Technology in Bratislava.*

#### References

- Belin BJ, Busset N, Giraud E, Molinaro A, Silipo A, Newman DK (2018) *Nat. Rev. Microbiol.* 16(5): 304–315.
- Cabrerizo A, Tejedo P, Dachs J, Benayas J (2016) *Sci. Total Environ.* 569–570: 1500–1509.
- Catania V, Cappello S, Di Giorgi V, Santisi S, Di Maria R, Mazzola A, Vizzini S, Quatrini P (2018) *Mar. Pollut. Bull.* 131: 396–406.
- Di Gregorio S, Siracusa G, Becarelli S, Mariotti L, Gentini A, Lorenzi R (2016) *Environ. Sci. Pollut. Res.* 23: 10587–10594.
- Diez S, Sabatté J, Viñas M, Bayona JM, Solanas AM, Albaigés J (2005) *Environ. Toxicol. Chem.* 24(9): 2203–2217.
- Faboya OL, Sojnu SO, Sonibare OO, Falodun OT, Liao Z (2016) *Environ. Forensics* 17: 27–35.
- Gdara I, Zrafi I, Balducci C, Cecinato A, Ghrabi A (2020) *Arch. Environ. Contam. Toxicol.* 78: 1–19.
- Ghribi R, Correia AT, Elleuch B, Nunes B (2019) *Arch. Environ. Contam. Toxicol.* 76: 678–691.
- Grigoriadou A, Schwarzbauer J, Georgakopoulos A (2008) *J. Soils Sediments* 8: 253–262.
- Han Y, Nambib IM, Clementa TP (2018) *Sci. Total Environ.* 626: 795–806.
- Hazra B, Wood DA, Mani D, Singh PK, Singh AK (2019) *Sedimentary Biomarkers and Their Stable Isotope Proxies in Evaluation of Shale Source and Reservoir Rocks*. In: *Evaluation of Shale Source Rocks and Reservoirs*. Petroleum Engineering. Springer, Cham.
- He M, Moldowan MJ, Peters KE (2018) *Biomarkers: Petroleum*. In: White W. (eds) *Encyclopedia of Geochemistry*. Encyclopedia of Earth Sciences Series. Springer, Cham.
- Iheonye C, Osuji LC, Onyema MO (2019) *J. Appl. Sci. Environ. Manage.* 23(4): 805–809.
- Inglis GN, Naafs BDA, Zheng Y, McClymont EL, Evershed RP, Pancost RD, the ‘T-GRES Peat Database collaborators’ (2018) *Geochim. Cosmochim. Acta* 224: 249–261.
- Jafarabadi AR, Bakhtiari AR, Aliabadian M, Toosi AS (2017) *Environ. Pollut.* 224: 195–223.
- Jafarabadi AR, Dashtbozorg M, Mitra S, Bakhtiari AR, Dehkordi M, Cappello T (2019) *Sci. Total Environ.* 696: 133969.
- Kakhki FV, Zakaria MP, Mohammadi M, Aris AZ, Tajik H (2018) *Polycycl Aromat Compd* (0): 1–17.
- Kao NH, Su MC, Yen CC, Huang YJ (2018) *J. Soils Sediments* 19: 241–254.
- Paul S, Dutta S (2016) *Int. J. Coal Geol.* 167: 65–74.
- Romero IC, Schwing PT, Brooks GR, Larson RA, Hastings DW, Ellis G, Goddard EA, Hollander DJ (2015) *PLoS One* 10(5): e0128371.
- Rushdi AI, Al-Shaikh I, El-Mubarak AH, Alnaimi HAJA, Al-Shamary N, Hassan HM, Assali MA (2017) *Mar. Pollut. Bull.* 124: 56–66.
- Samelak I, Balaban M, Antić M, Šolević-Knudsen T, Jovančićević B. (2020) *Environ. Chem. Lett.* 18: 459–466.
- Samelak I, Balaban M, Vidović N, Koljančić N, Antić M, Šolević-Knudsen T, Jovančićević B (2018) *J. Serb. Chem. Soc.* 83(10): 1167–1175.
- Shirneshan G, Bakhtiari AR, Memariani M (2016) *Environ Sci Pollut Res* 23: 17484–17495.
- Thermo Fisher Scientific Inc. (2011) *Dionex ASE 150 Accelerated Solvent Extractor Operator’s Manual*. Thermo Fisher Scientific Inc., USA.
- Tissot BP, Welte DH (1984) *Petroleum Formation and Occurrence*. Springer-Verlag, Berlin, Heidelberg, New York, Tokyo.
- Vitorović D, Jovančićević B (2016) *Fundamentals of Organic Geochemistry for students of the Faculty of Chemistry, University of Belgrade*. Faculty of Chemistry, University of Belgrade.
- Walters CC, Wang FC, Higgins MB, Madince ME (2018) *Org. Geochem.* 124: 205–214.
- Wang G, Simoneit BRT, Shi S, Wang T, Zhong N, Wang P (2018) *Acta Geol Sin-Engl* 92(5): 1959–1972.
- Yogaswara ED, Wulandari KI, Falahudin D (2020) *The 3<sup>rd</sup> International Symposium on Marine and Fisheries Research (3rd ISMFR)* 147, 02002.
- Zhu X, Mao S, Sun Y, Jia G, Wu N, Wu D, Guan H, Yan W (2018) *J. Asian Earth Sci.* 168: 155–162.

# Control of heat exchangers in series using neural network predictive controllers

Anna Vasičkaninová, Monika Bakošová, Alajos Mészáros

*Slovak University of Technology in Bratislava, Faculty of Chemical and Food Technology,  
Institute of Information Engineering, Automation and Mathematics,  
Radlinského 9, 812 37 Bratislava, Slovak Republic  
anna.vasickaninova@stuba.sk*

**Abstract:** The paper reveals three applications of neural network predictive control (NNPC) to a system of four heat exchangers (HEs) in series with counterflow configuration to save energy expressed by cooling water in the system of HEs cooling the distillation product. Neural networks (NNs) are used at first in conventional NNPC and subsequently, neural network predictive controllers (NNPCLs) are employed as a master controller in a cascade control, and as a feedback controller in the control system with disturbance measurement. Neural-network-predictive-control-based (NNPC-based) feedback control systems are compared with PI controller based feedback control loop. Series of simulation experiments were done and the results showed that using NNPC-based cascade control reduced cooling water consumption. This control system also significantly reduced the settling time and overshoots in the control responses and provided the best assessed integral quality criteria compared to other control systems. NNPC-based cascade control can also be interesting for industrial use. Generally, simulation results proved that NNPC-based control systems are promising means for the improvement of HEs control and achievement of energy saving.

**Keywords:** heat exchanger; neural network predictive control; neural-network-predictive-control-based cascade control; neural-network-predictive-control-based control system with disturbance measurement

## Introduction

In contemporary industrial and technological world characterized by increasing energy demands and energy prices, energy consumption and clean energy utilization belong to the most important global challenges. Sustainability requirements on all production processes and especially on energy intensive processes are also intensified to save our planet for future generations. Industrial production cannot do without HEs, which are used to exchange heat between media. Efficient heat recovery in an industrial plant is also a challenging task and one possibility is to combine HEs optimally in heat exchanger networks (HENs). Pashchenko (2020) published the calculation method for recovery rate as the main measure of heat recovery efficiency in a thermochemical waste-heat recuperation plant. Advanced control systems represent the other technical solution for efficient heat recovery. Markowski and Trzcinski (2019) introduced the HEN mathematical model and on-line control algorithm to maximize heat recovery.

From the viewpoint of heat, cold, vapor or electricity production continuous improvement, HEs and HENs have become the midpoint of research and development. Saranya et al. (2017) modeled various types of heat exchangers, i.e., plate type HE, spiral type HE and shell and tube type HE. They also compared different model-based and

non-model-based control systems and stated that NNs can act as controllers. Nemet et al. (2017) designed HEN with improved safety during its whole lifetime. Secure HEN was obtained considering the risk in the early phase of the synthesis by including the changing failure frequency. Sun et al. (2018) investigated two different enhanced ejector heat exchangers and presented a configuration that optimizes exergy efficiency. Baruque et al. (2019) designed a heat exchanger as a part of a geothermal system and helped to regulate temperature by means of the developed prediction system. Thermally integrated preheater and heat exchanger network configurations were used by Yang et al. (2019) to save energy. The proposed method can be extended to other industrial processes that diminish energy spending and CO<sub>2</sub> emissions. Elsis (2019) proposed a new predictive control system for energy conversion in a wind system. Controller parameters were tuned by a new intelligence technique called the crow search algorithm. Controller efficiency was confirmed in various situations with changes in the load requirements, wind speed, and the presence of system parameter uncertainties. Kim et al. (2009) presented an effective strategy to minimize the total annual cost of designing HE and wastewater networks. Cost estimates for optimized HE and wastewater networks in the oil refining process were assessed to illustrate the efficiency of the proposed strategy. Yang et al. (2016) introduced a systematic

and comprehensive comparative methodology that can be used to assess energy efficiency and energy saving potential of an energy-intensive chemical production system. The proposed approach was implemented to reduce energy consumption and to identify the most advanced energy use system.

Intensive research has been done in advanced control of various types and configurations of heat exchangers. Vasičkaninová and Bakošová (2015) successfully applied neural network and fuzzy system in a control system with the NNPC-based main and a fuzzy auxiliary controller to control a tubular HE. NNPC of tubular HEs in series with counter current configuration was introduced by Vasičkaninová et al. (2017), ensuring energy savings compared to PID control. Bakošová et al. (2017) compared NNPC, robust model-based predictive control (RMPC) and PID control in tubular HEs control, examined in set-point tracking. Simulation results proved better closed-loop control performance and energy savings measured by hot water consumption for NNPC and RMPC over conventional PID control. Oravec et al. (2018) designed RMPC with integral action and implemented this control strategy for shell-and-tube HEs with fouling and proving considerable improvement in control performance and energy savings in contrast to conventional PID control.

This paper exceeds the paper by Vasičkaninová et al. (2019). The aim of the research represented by results in this paper is to show that NNPC-based control systems are very attractive for HEs operation improvement as they provide higher energy efficiency, lower carbon footprint and cooling water savings. Especially water savings are very important for sustainable management of natural freshwater resources, for the protection of the aquatic environment and for meeting the current and future human needs.

## Controlled process description

Optimal operation of HEs and HENs is one of the tools of energy saving in the process industry ensuring the integration of heat between hot and cold process streams to reduce heat and cold consumption during the heat exchange process.

Based on the previous work (Vasičkaninová et al., 2017), four identical shell-and-tube HEs in series

with counter current flow configuration create the controlled process (Fig. 1). Two main objectives of control are to decrease the temperature of kerosene in the outlet stream from the 4<sup>th</sup> HE to the reference temperature and to minimize the cooling water consumption.

A simplified nonlinear dynamic mathematical model of the HEs can take the form of eight first-order differential equations (Oravec et al., 2016). Values of the parameters and steady-state inputs of HEs are given in Vasičkaninová et al. (2017).

Water is used as a coolant and flows in the shell of each HE, kerosene flows in the inner tubes. Tubes as well as shell are constructed of steel.

The first-principle nonlinear dynamic mathematical model of HEs (Fig. 1) reflecting the energy balances and heat transfer relations was derived in a simplified form and it contains eight first-order ordinary differential equations (Oravec et al., 2016). Four differential equations (1) describe the dynamics of cold fluid and the other four differential equations (2) represent the dynamics of hot fluid.

$$\begin{aligned} \frac{dT_1^j(t)}{dt} &= \\ &= k_1((T_2^j(t) - T_1^{j+1}(t)) + (T_2^{j-1}(t) - T_1^j(t))) + \\ &\quad + k_2(T_2^j(t) - T_1^{j+1}(t)), T_1^j(0) = T_{1,0}^j \end{aligned} \quad (1)$$

$$\begin{aligned} \frac{dT_2^j(t)}{dt} &= \\ &= k_3((T_2^j(t) - T_1^{j+1}(t)) + (T_2^{j-1}(t) - T_1^j(t))) + \\ &\quad + k_4(T_2^j(t) - T_1^{j+1}(t)), T_2^j(0) = T_{2,0}^j \end{aligned} \quad (2)$$

where

$$k_1 = \frac{AU}{2V_1\rho_1c_{p1}}, k_2 = \frac{q_1}{V_1}, k_3 = \frac{AU}{2V_2\rho_2c_{p2}}, k_4 = \frac{q_2}{V_2} \quad (3)$$

In (1)–(3), subscripts 1 and 2 indicate the heated and the heating stream, respectively. Superscript  $j = 1, \dots, 4$  denotes the heat exchanger. Temperatures  $T_1^j(0) = T_{1,0}^j$ ,  $T_2^j(0) = T_{2,0}^j$  are the initial conditions, i.e. temperatures in a steady-state operation regime of the HEs and they can be calculated using the steady-state model of HEs represented by (1)–(3) with zero derivatives at the left-hand sides. Further,  $t$  is time,  $T$  is temperature,  $A$  is the heat transfer area,  $U$  is the overall heat transfer coefficient,  $V$  is

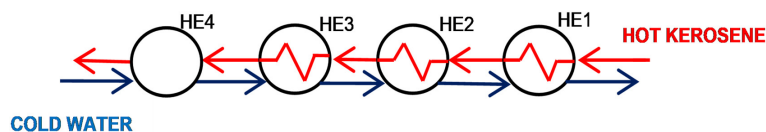


Fig. 1. Shell-and-tube heat exchangers in series with counter current flow configuration.

the volume of fluid in the HE,  $\rho$  is the density,  $c_p$  is the specific heat capacity and  $q$  is the volumetric flow rate of the fluid (Vasičkaninová et al., 2017).

## Basic concepts of NNPC

The scheme in Fig. 2 illustrates the predictive control based on the NN model. The neural network predictive controller contains an NN model and an optimization block. The controller predicts process output variables based on the values of NN model output variables while the optimization block calculates control inputs.

The controlled process can be nonlinear and affected by various uncertainties. In NNPC, it is important to obtain a process model based on NN which is trained based on a prediction error representing the difference between the measured process output and the predicted neural network output (Soloway and Haley, 1996).

The quadratic performance function (4) is minimized to provide the optimum sequence of control inputs and only the first control input of the sequence is applied on the controlled nonlinear plant.

$$E(k) = \sum_{j=N_1}^{N_2} (r(k+j) - y_m(k+j))^2 + \lambda \sum_{j=1}^{N_u} (\Delta u(k+j-1))^2 \quad (4)$$

Performance function parameters are:  $N_1$  – minimum prediction horizon,  $N_2$  – maximum prediction horizon and  $N_u$  – control horizon. Prediction horizons  $N_1$ ,  $N_2$  indicate the future time interval in which it is desirable to track the reference trajectory  $r$ ,  $k$  denotes discrete time,  $i$  is the order of the predictor, positive number  $\lambda$  represents weight factor expressing the contribution of the control increments to the cost function,  $y_m$  is the NN model output, and  $\Delta u$  is the sequence of future control increments (Beale et al., 2015).

The above described NN predictive control structure uses a two-layer NN process model with sigmoid hidden-layer transfer functions and linear output-layer transfer functions. The network is usually trained off-line in batch mode using data gathered by measuring of the controlled process outputs. The Levenberg-Marquardt (LM) training algorithm for the NN model is commonly used (Lera and Pinzolas, 2002). Due to the convergence properties, the LM algorithm has become a widely adopted standard technique for nonlinear least-squares problems. It iteratively searches a minimum of the sum of nonlinear function squares according to Eq. (5):

$$x(k) = x(k+1) + (J^T J + \mu I)^{-1} J^T e(k) \quad (5)$$

where  $I$  is the identity matrix,  $J$  denotes the Jacobian matrix from the difference of error to the weight value,  $e$  denotes the control error and  $\mu$  is a damping parameter representing an adaptive balance between two steps. Both the success and the efficiency of the LM algorithm depend on the choice of parameter  $\mu$ .

## Conventional control of heat exchangers in series with counter current flow arrangement

### Conventional PI control

Four heat exchangers in series with counter current flow configuration described in the previous section represent the controlled process. Kerosene temperature in the outlet stream from the 4<sup>th</sup> heat exchanger is the controlled output, and volumetric flow rate of cold water in the inlet stream into the 4<sup>th</sup> heat exchanger is the manipulated variable. The feedback control system is presented in Fig. 3, where TC is the temperature PI controller. HEN has nonlinear and asymmetric dynamics and it is influenced by load disturbances. These distur-

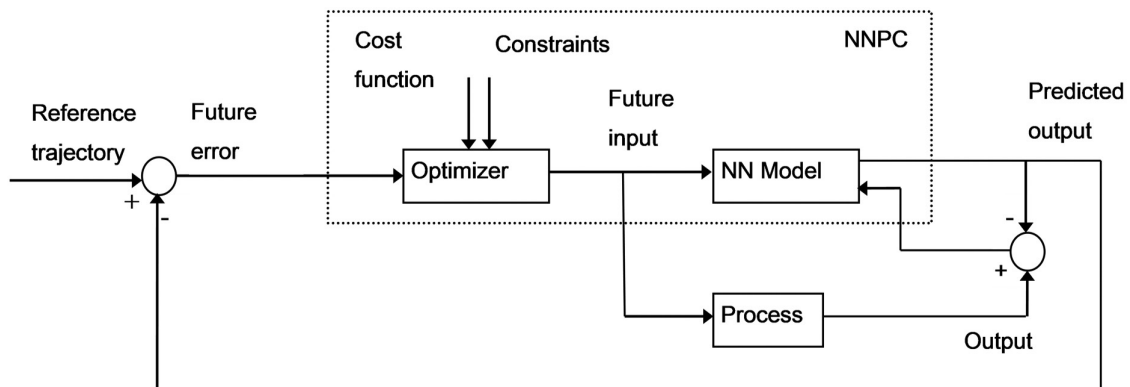
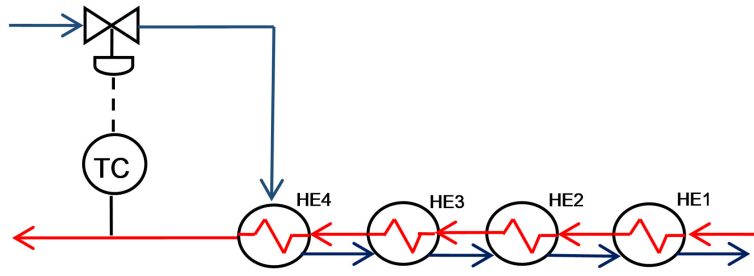


Fig. 2. Feedback control system with a neural-network-based predictive controller.



**Fig. 3.** Feedback control system with temperature PI controller.

bances were represented by the coolant temperature changes in the inlet stream into the first HE in the simulation experiments and they were as follows: temperature decreased by 3 °C at  $t = 30$  min, then increased by 4 °C at  $t = 90$  min and finally decreased by 2 °C at  $t = 150$  min.

The conventional PI controller is represented by the transfer function (6)

$$C(s) = k_p \left( 1 + \frac{1}{t_i s} \right) = k_p + \frac{k_i}{s} = -0.1274 - \frac{0.0337}{s} \quad (6)$$

The controller parameters are:  $k_p$  – proportional gain,  $t_i$  – integral time.

For PI controller tuning, HEN was identified using the step-response-based method. The resulting model took the form of the  $n$ -th order plus time delay transfer function (7) with the transfer function parameters: order  $n = 2$ , gain

$K = -69.25 \text{ } ^\circ\text{C min m}^{-3}$ , time constant  $\tau = 3.15$  min and time delay  $D = 0.125$  min (Mikleš and Fikar, 2007). The Chien-Hrones-Reswick method was used for controller tuning (Corriou, 2004). The PI controller parameters are:  $k_p = -0.1274 \text{ } ^\circ\text{C}^{-1} \text{ min}^{-1} \text{ m}^3$ ,  $k_i = -0.0337 \text{ } ^\circ\text{C}^{-1} \text{ min}^{-2} \text{ m}^3$ . Negative values of controller parameters reflect the fact that an increase of cooling fluid flow rate decreases the temperature of hot fluid.

$$P(s) = \frac{K}{(\tau s + 1)^n} e^{-Ds} = \frac{-69.25}{(3.15s + 1)^2} e^{-0.125s} \quad (7)$$

#### Conventional neural network predictive control of HEs

As mentioned above, the NN process model has first to be trained (Vasičkaninová et al., 2017) to design NNPC. The neural network had four delayed

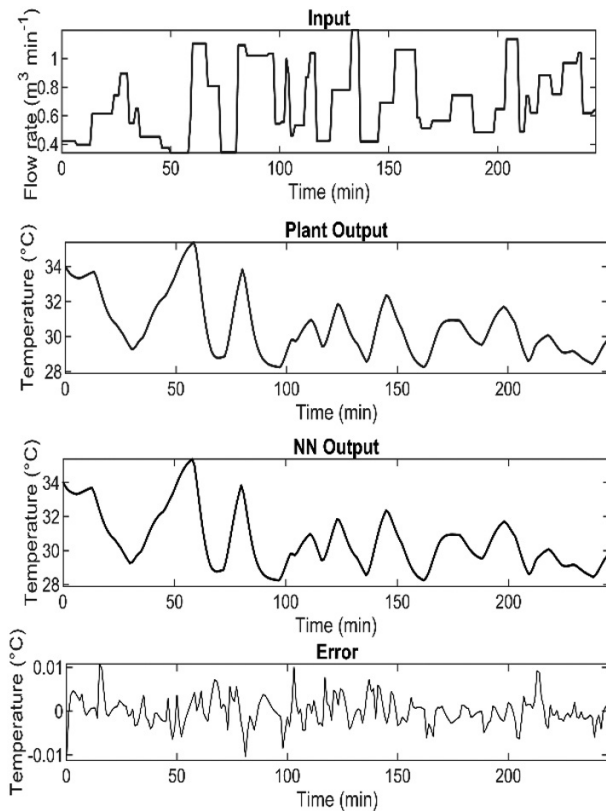


**Fig. 4.** Training data for NN model.

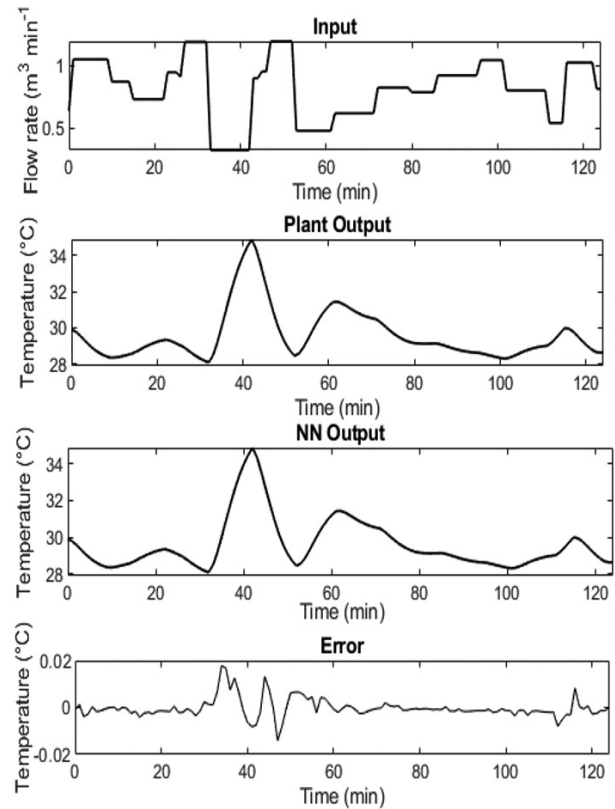


**Fig. 5.** Validation data for NN model.

process inputs, three delayed process outputs, and one hidden layer with six neurons and 1,500 training samples were used for training, validation, and testing. Training and validation results are shown in Figs. 4 and 5. A small prediction error confirms the success of the training.

The parameters' values in the performance criterion (4) used for the NNPC design were: horizons values:  $N_1 = 1$ ,  $N_2 = 7$ ,  $N_u = 2$ , weight parameter:  $\lambda = 0.1$ . The control input constraints were selected as follows: minimum control input:  $q_{1min} = 0.01 \text{ m}^3 \text{ min}^{-1}$ , maximum control input:  $q_{1max} = 1 \text{ m}^3 \text{ min}^{-1}$ .

## Neural-network-predictive-control-based control systems

### NNPC-based cascade control

Cascade control, which represents a multi-loop control structure with an auxiliary controlled variable, is often used in the process industry to improve the quality of feedback control when certain types of disturbances and uncertainties occur (Bequette, 2003).

This setting shows one manipulated variable and more than one measured variables. The inner and outer control loops contain separate feedback controllers. The main advantage of using cascade control is that the disturbances occurring in the secondary loop are corrected by the secondary controller before they affect the primary controlled output value. The primary controller is usually tuned as a controller with integral action because it is responsible for the control objective achievement and steady-state error removal. The secondary controller has to compensate the load disturbance as fast as possible; usually, high gain P controller is used for very fast action. The secondary controller is tuned first and the primary controller is tuned with the inner loop in action. Because the behavior of the controlled process is often non-linear and asymmetric, and since the internal loop dynamics

has to be taken into account, tuning the primary controller is not simple (Ogunnaike and Ray, 1994). Thus, the neural network model of the controlled process can be used to improve the tuning of the primary controller (Fig. 6). Primary controlled output was the temperature of the cooled fluid in the outlet stream of the 4<sup>th</sup> HE. The primary NN predictive controller settings were as follows: four delayed process inputs, three delayed process outputs and one hidden layer with six neurons, and 1,000 training samples were used for training, validation, and testing. Parameters' values in the performance criterion (4) were: horizons:  $N_1 = 1$ ,  $N_2 = 7$ ,  $N_u = 4$ , weight parameter:  $\lambda = 0.01$ , minimum controlled output:  $T_{cmin} = 25 \text{ }^\circ\text{C}$ , maximum controlled output:  $T_{cmax} = 180 \text{ }^\circ\text{C}$ . The conventional P controller was used as a secondary controller to compensate load disturbance as quickly as possible. The secondary controlled output was the cold water flow rate in the inlet stream into the 4<sup>th</sup> HE. The gain of the secondary P controller was  $-0.04 \text{ }^\circ\text{C}^{-1} \text{ min}^{-1} \text{ m}^3$ .

### NNPC-based control system with disturbance measurement

Feedback control is usually used with feedforward control to combine the advantages and avoid the disadvantages of both control structures (Bequette, 2003). The feedforward controller, also called a compensator, compensates for the effect of disturbances on the controlled variable if both an accurate model of the controlled process and an accurate model of the disturbance process for measurable disturbance are used. The control loop with feedforward compensation of the disturbance is forced to eliminate the influence of the disturbance to its full extent. By introducing a compensator in the feedforward loop, the disturbances are partially eliminated before they enter the feedback loop, and thus the feedback controller does not have to generate large control actions as in case of a simple feedback control loop.

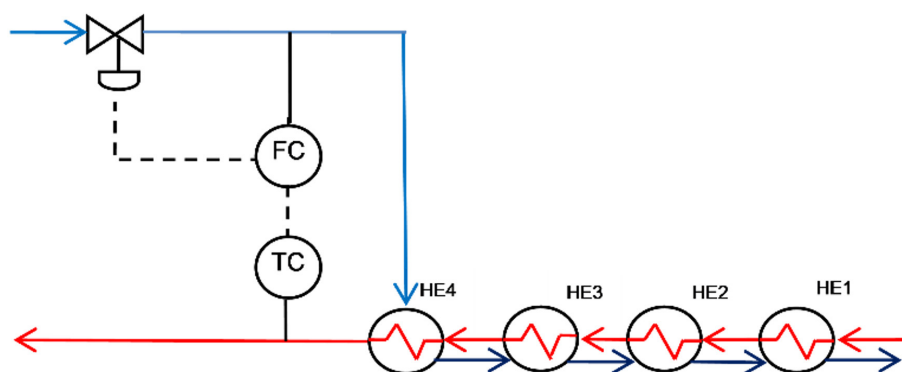


**Fig. 6.** NNPC-based cascade control for HEs, TC – primary NN predictive controller, FC – secondary conventional P controller.

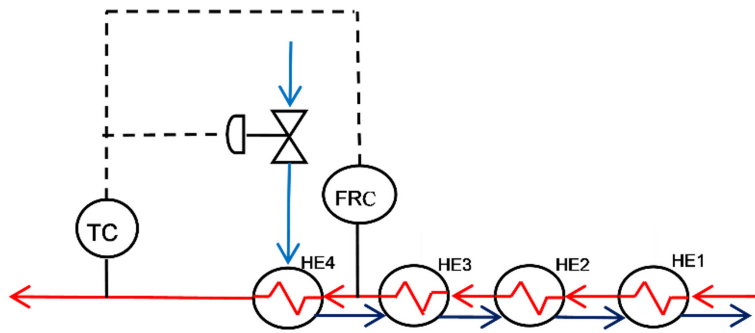


**Fig. 7.** NNPC-based control system with disturbance measurement for HEs, TC – NN predictive feedback controller, FRC – feedforward compensator.

In the designed NNPC-based control system with disturbance measurement (Fig. 7), feedforward control is used in combination with the NNPC-based feedback control. The NN predictive controller described in section *Conventional neural network predictive control of HEs* was used as the feedback controller. The transfer function of the feedforward compensator was calculated from the transfer functions of the controlled system and the disturbance process and it was simplified to the conventional P controller with the gain of  $0.001 \text{ } ^\circ\text{C}^{-1} \text{ min}^{-1} \text{ m}^3$ .

### Simulation results

Simulation results obtained using the designed control systems without and with measurement noise are presented in Figs. 8 and 9, respectively. The simulation results were compared according to the total cooling agent consumption,  $V_{total}$  consumed

during control, and the integral IAE (integrated absolute error) and ISE (integrated squared error) quality criteria defined e.g. in Ogunnaike and Ray (1994) as follows:

$$\text{IAE} = \int_0^\infty |e(t)| dt \quad (8)$$

$$\text{ISE} = \int_0^\infty e(t)^2 dt \quad (9)$$

Reference temperature  $r = 34 \text{ } ^\circ\text{C}$  changed to  $32 \text{ } ^\circ\text{C}$  at 60 min and then to  $31 \text{ } ^\circ\text{C}$  at 120 min.

The simulation results in reference tracking and disturbance rejection without measurement noise are presented in Fig. 8. Table 1 summarizes the obtained numerical results. Consumption of the cooling agent expressed by the total consumed volume,  $V_{total}$  and the values of IAE and ISE was the lowest with the NNPC-based cascade control.

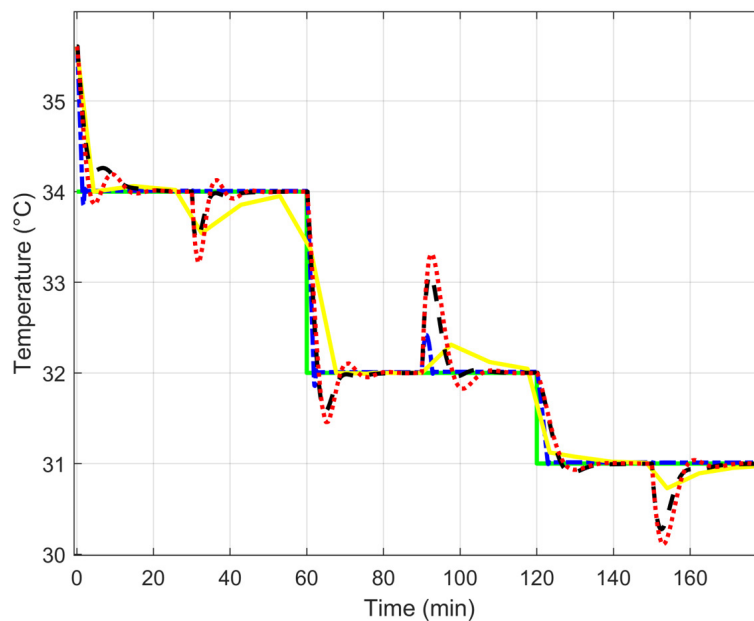


**Fig. 8.** Controlled temperature without measurement noise.

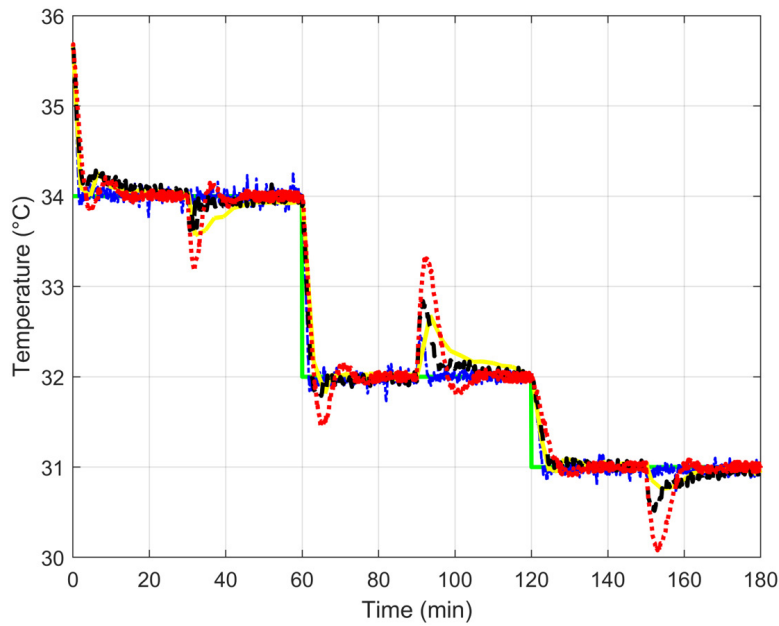


**Fig. 9.** Controlled temperature with measurement noise.

**Tab. 1.** Values of IAE, ISE, and  $V_{total}$  in simulation experiments without measurement noise.

Control system	IAE ( $^{\circ}\text{C min}$ )	ISE ( $^{\circ}\text{C}^2 \text{ min}$ )	$V_{total}$ ( $\text{m}^3$ )
PI control	27.86	21.18	84.02
NNPC	24.73	17.16	83.94
NNPC-based cascade control	7.38	5.69	83.12
NNPC-based control system with disturbance measurement	22.27	12.02	84.26

**Tab. 2.** Values of IAE, ISE, and  $V_{total}$  in simulation experiments with measurement noise.

Control system	IAE ( $^{\circ}\text{C min}$ )	ISE ( $^{\circ}\text{C}^2 \text{ min}$ )	$V_{total}$ ( $\text{m}^3$ )
PI control	28.13	21.69	84.56
NNPC	23.80	11.83	84.30
NNPC-based cascade control	12.36	5.81	83.62
NNPC-based control system with disturbance measurement	22.47	12.45	84.95

In Figs. 8 and 9, the reference is represented by the green solid line and the controlled output is indicated as follows: red dotted line – PI control, black dashed line – NNPC, blue dashed-dotted line – NNPC-based cascade control, yellow line – NNPC-based control system with disturbance measurement.

The simulation results in reference tracking and disturbance rejection with measurement noise are presented in Fig. 9. Table 2 summarizes the obtained numerical results. Consumption of cooling agent,  $V_{total}$  and the values of IAE and ISE were the lowest when using the NNPC-based cascade control.

## Conclusions

Conventional PI controller designed using the Chien-Hrones-Reswick method and NNPC were

compared to a complex two-controller control structure, namely NNPC-based cascade control, and NNPC-based control system with disturbance measurement. These advanced control strategies were used to control four heat exchangers in series with counter current configuration. Simulation results in reference tracking and disturbance rejection without noise and with measurement noise were compared. According to the IAE and ISE criteria, all control structures with NNPC have overcome conventional PI control. Results of the simulation experiments showed that the NNPC-based cascade control reduced both, the settling time and overshoots. The best results were achieved when using the NNPC-based cascade control, as confirmed by the IAE and ISE criteria, as well as to the minimum volume of consumed cooling water. Cascade control is often used to eliminate unmeasurable

disturbances and accelerate process response. From this perspective, the NNPC-based cascade control strategy is suitable to be implemented in practice with promising control performance.

#### *Acknowledgment*

*The authors gratefully acknowledge the contribution of the Scientific Grant Agency of the Slovak Republic under the grant 1/0545/20.*

#### **References**

- Bakošová M, Oravec J, Vasičkaninová A, Mészáros A (2017) Neural-network-based and robust model-based predictive control of a tubular heat exchanger. *Chemical Engineering Transactions*. 61: 301–306.
- Baruque B, Porrás S, Jove E, Calvo-Rolle JL (2019) Geothermal heat exchanger energy prediction based on time series and monitoring sensors optimization. *Energy*. 171: 49–60.
- Beale MH, Hagan MT, Demuth HB (2015) *Neural Network Toolbox™, User's Guide, MATLAB® R2015a*, The MathWorks, Inc., Natick, MA, USA, 410 ps. ISBN: 0-9717321-0-8.
- Bequette WB (2003) *Process Control: Modeling, Design, and Simulation*, Prentice-Hall of India, New Delhi, India, 800 ps. ISBN-10: 0133536408, ISBN-13: 978-0133536409.
- Corriou JP (2004) *Process Control – Theory and Applications*, Springer, London, UK, 860 ps. Print ISBN 978-3-319-61142-6, Online ISBN 978-3-319-61143-3.
- Lera G, Pinzolas M (2002) Neighborhood based Levenberg Marquardt algorithm for neural network training, *IEEE Trans. Neural Networks* 13(5): 1200–1203.
- Elsisi M (2019) New design of adaptive model predictive control for energy conversion system with wind torque effect. *Journal of Cleaner Production* 240: 118265.
- Kim J, Kim J, Kim J, Yoo CK, Moon I (2009) A simultaneous optimization approach for the design of wastewater and heat exchange networks based on cost estimation. *Journal of Cleaner Production* 17(2): 162–171.
- Markowski M, Trzcinski P (2019) On-line control of the heat exchanger network under fouling constraints. *Energy* 185: 521–526.
- Mikleš J, Fikar M (2007) *Process Modeling, Identification, and Control*, Springer, Berlin/Heidelberg, Germany. 480 ps. ISBN: 978-3-540-71969-4.
- Nemet A, Klemeš JJ, Kravanja Z (2017) Heat exchanger network synthesis considering risk assessment for entire network lifetime. *Chemical Engineering Transactions* 57: 307–312.
- Ogunnaike BA, Ray WH (1994) *Process Dynamics, Modelling, and Control*, Oxford University Press, New York, USA, 1260 ps. ISBN: 978-0195091199.
- Oravec J, Bakošová M, Mészáros A (2016) Robust model predictive control of heat exchangers in series, *Chemical Engineering Transactions* 52: 253–258.
- Oravec J, Bakošová M, Trafczynski M, Vasičkaninová A, Mészáros A, Markowski M (2018) Robust model predictive control and PID control of shell-and-tube heat exchangers. *Energy* 159: 1–10.
- Pashchenko D (2020) A heat recovery rate of the thermochemical waste-heat recuperation systems based on experimental prediction. *Energy*. 198: 117395.
- Saranya SN, Thirumarumurugan M, Sivakumar VM, Sowparnika GC (2017) An Optimal Analysis of Controller Strategies for Different Heat Exchangers – A Review. *Middle-East Journal of Scientific Research*. 25(4): 761–775. ISSN 1990-9233.
- Soloway D, Haley PJ (1996) Neural generalized predictive control, *Proceedings of the 1996 IEEE International Symposium on Intelligent Control*, Dearborn, MI, USA, 277–281.
- Sun F, Chen X, Fu L, Zhang S (2018) Configuration optimization of an enhanced ejector heat exchanger based on an ejector refrigerator and a plate heat exchanger. *Energy* 164: 408–417.
- Vasičkaninová A, Bakošová M (2015) Control of a heat exchanger using neural network predictive controller combined with an auxiliary fuzzy controller, *Applied Thermal Engineering* 89: 1046–1053.
- Vasičkaninová A, Bakošová M, Oravec J, Mészáros A (2017) Neural network predictive controller design for counter-current tubular heat exchangers in series, *Chemical Engineering Transactions* 61: 121–126.
- Vasičkaninová A, Bakošová M, Oravec J, Mészáros A (2019) Control of Heat Exchangers Using Complex Control Structures with Neural Network Predictive Controllers, *Chemical Engineering Transactions* 76: 361–366.
- Yang A, Jin S, Shen W, Cui P, Chien IL, Ren J (2019) Investigation of energy-saving azeotropic dividing wall column to achieve cleaner production via heat exchanger network and heat pump technique. *Journal of Cleaner Production*. 234: 410–422.
- Yang F, Liu Y, Liu G (2016) A process simulation based benchmarking approach for evaluating energy consumption of a chemical process system, *Journal of Cleaner Production*. 112(4): 2730–2743.

# Influence of catecholic ring torsion on hydroxyflavones

Martin Michalík, Monika Biela, Denisa Cagardová, Vladimír Lukeš

*Institute of Physical Chemistry and Chemical Physics, Slovak University of Technology in Bratislava, Radlinského 9, SK-812 37 Bratislava, Slovakia  
martin.michalik@stuba.sk*

**Abstract:** Systematic quantum chemical investigation of quercetin and selected eight mono- and bi-hydroxyflavonols is presented. Structural analysis based on the Density Functional Theory showed that the energetically preferred conformation of flavonols substituted at the C5 and C3 atoms by a hydroxyl group is stabilised via intramolecular hydrogen bonds occurring between the (C4)O...HO(3 or 5) atomic pairs. Depending on the hydroxyl group positions, energetically preferred torsional orientation of the phenyl ring with respect to the planar benzo- $\gamma$ -pyrone moiety changed from 0 to 180 degrees. Gas-phase electron transitions were investigated using the time-dependent DFT treatment. The dependence of maximal wavelengths on the torsional deformation of the phenyl ring is of a similar shape, i.e. minima observed for the perpendicular orientation and maxima for the planar one. Shape and energies of the Highest Occupied (HOMO) and Lowest Unoccupied (LUMO) Molecular Orbitals were compared. The obtained theoretical results were compared with available experimental data.

**Keywords:** BDE, hydroxyflavones, torsion

## Introduction

Polyphenols are aromatic compounds with large systems of  $\pi$ -electron configurations. Thanks to this configuration they absorb visible light which makes them colourful. Their name derives from the Ancient Greek word πολὺς (polus, meaning “many, much”) and the word phenol which refers to a chemical structure formed by attaching of a hydroxyl (—OH) group to an aromatic benzenoid (phenyl) ring as it is found in alcohols (hence the -ol suffix, Quideau et al., 2011). The term polyphenol has been in use at least since 1894 (Merriam-webster). The number and characteristics of these phenol structures underlie the unique physical, chemical, toxic, metabolic or pharmaceutical properties of the class members (Williams et al., 2004). These compounds are not polymers of phenol. Although phenol can be polymerised by electrochemical oxidation, the formed products are not referred to as “polyphenols” (Mengoli et al., 1987). Polyphenols also possess significant binding affinity for proteins, which can lead to the formation of soluble and insoluble protein-polyphenol complexes (Papadopoulou et al., 2004).

Flavonoids are a specific group of naturally occurring polyphenolic compounds ubiquitously found in fruits and vegetables (Hollman et al., 2000). Physicochemical properties of flavonoids are generally associated with three chemical features: (i) ortho-dihydroxy structure in the B-ring, (ii) presence of a 2,3 double bond in the C-ring, and/or (iii) presence of a 4-oxo function in the C-ring (Figure 1). The

various classes of flavonoids differ in the level of oxidation of the ‘C’ ring of the basic benzo- $\gamma$ -pyrone structure. Common family members of flavonoids include flavones, flavanes, flavonols, catechins and anthocyanidins. Flavonols are flavonoids of particular importance because they have been found to possess antioxidant and free radical scavenging activity in foods (Shahidi et al., 1992). Some polyphenols are traditionally used as dyes. For example, 5-hydroxyflavonol and 3-hydroxyflavonol and their derivatives usually exhibit two strongly separated bands in their fluorescence spectrum due to the excited state intramolecular proton transfer, leading to two excited forms: normal N\*, and tautomer T\*. Fluorescence maxima positions and relative intensities depend on the solvent environment (Sengupta et al., 1979). This phenomenon is used in the construction of effective probes used in bio-structures’ analysis (Klymchenko et al., 2002).

Excited states of flavonoids were experimentally studied as well as predicted by means of semiempirical, *ab initio*, and density functional theory (DFT) quantum mechanical methods (Tošović et al., 2017). The semiempirical ZINDO method combined with the configuration interaction, where singlet excitations are included, showed unpredictable accuracy (Kotzian et al., 1992). The more computing-demanding *ab initio* methods, e.g. complete active space self-consistent field (CASSCF) method (Andresson and Roos, 1995) or multi-reference configuration interaction (MRCI, Sherrill et al., 1999), are usually successful, but the quality of the obtained results is highly dependent on the selec-

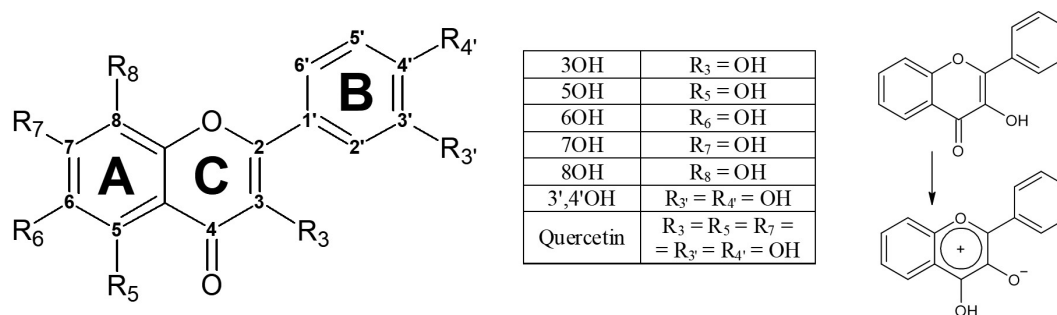


**Fig. 1.** General structure and numbering scheme of hydroxyflavones ( $R_x = \text{H}$  unless stated otherwise) and the reaction scheme of 3-hydroxyflavone **3OH** tautomerisation into **t3OH**.

tion of the created active space. In the last decade, the time-dependent density functional theory (TD-DFT) has been successfully applied to examine the excited states of some polyphenolic compounds (Gierschner et al., 2012).

Although many published works reported experimental and theoretical studies on the electronic structure and spectroscopic properties of a large variety of flavone and flavonol derivatives (Valle, 2006; Ash et al., 2010; Ahmed et al., 2017), systematic comparative studies on electron structure changes upon torsional deformation of the B ring are lacking. Therefore, a systematic theoretical analysis of selected flavonols is here presented (Fig. 1). Partial aims of this quantum chemical study are: (1) finding optimal structures of ground electron states and corresponding radicals formed after homolytic O—H group cleavage; (2) investigating the shape of gas-phase torsional potentials belonging to the B ring with respect to the hydroxyl group positions; (3) analyzing the torsional dependence of experimentally relevant vertical optical transitions and bond dissociation energies. Finally, the shapes and energies of the Highest Occupied (HOMO) and Lowest Unoccupied (LUMO) Molecular Orbitals were compared. Theoretical results were compared with available experimental data.

## Methods

Gaussian program package at current revision 16 (Frisch et al., 2016) was used for all calculation done at the DFT level of theory. The B3LYP (Becke, 1988; Lee et al., 1988) hybrid functional and 6-31G\* basis sets were employed for all atoms (Rassolov et al., 2001). To study the flexibility of neutral molecules in their singlet or doublet (for radicals after  $\text{H}^\bullet$  abstraction) electron ground state, a relaxed scan was done by optimizing the geometry with fixed C3—C2—C1'—C2' dihedral angle. Total of ten steps by 18 degrees were considered. First 3- excited states were calculated at each step by the TD-DFT method with the B3LYP functional.

Molecular orbitals were depicted using the Jsmol HTML5 web applet (Jmol 2019).

Based on the optimised structures, cleavage of the hydroxyl O—H bonds in terms of bond dissociation energies (BDE) was calculated following the equation

$$\text{BDE} = E(\text{Ph—O}^\bullet) + E(\text{H}^\bullet) - E(\text{Ph—OH}) \quad (1)$$

where  $E(\text{Ph—OH})$  represents the DFT energy of hydroxyflavone and  $E(\text{Ph—O}^\bullet)$  is the DFT energy of its radical. Hydrogen atom energy  $E(\text{H}^\bullet)$  in the gas phase is  $-0.500272784186$  hartree.

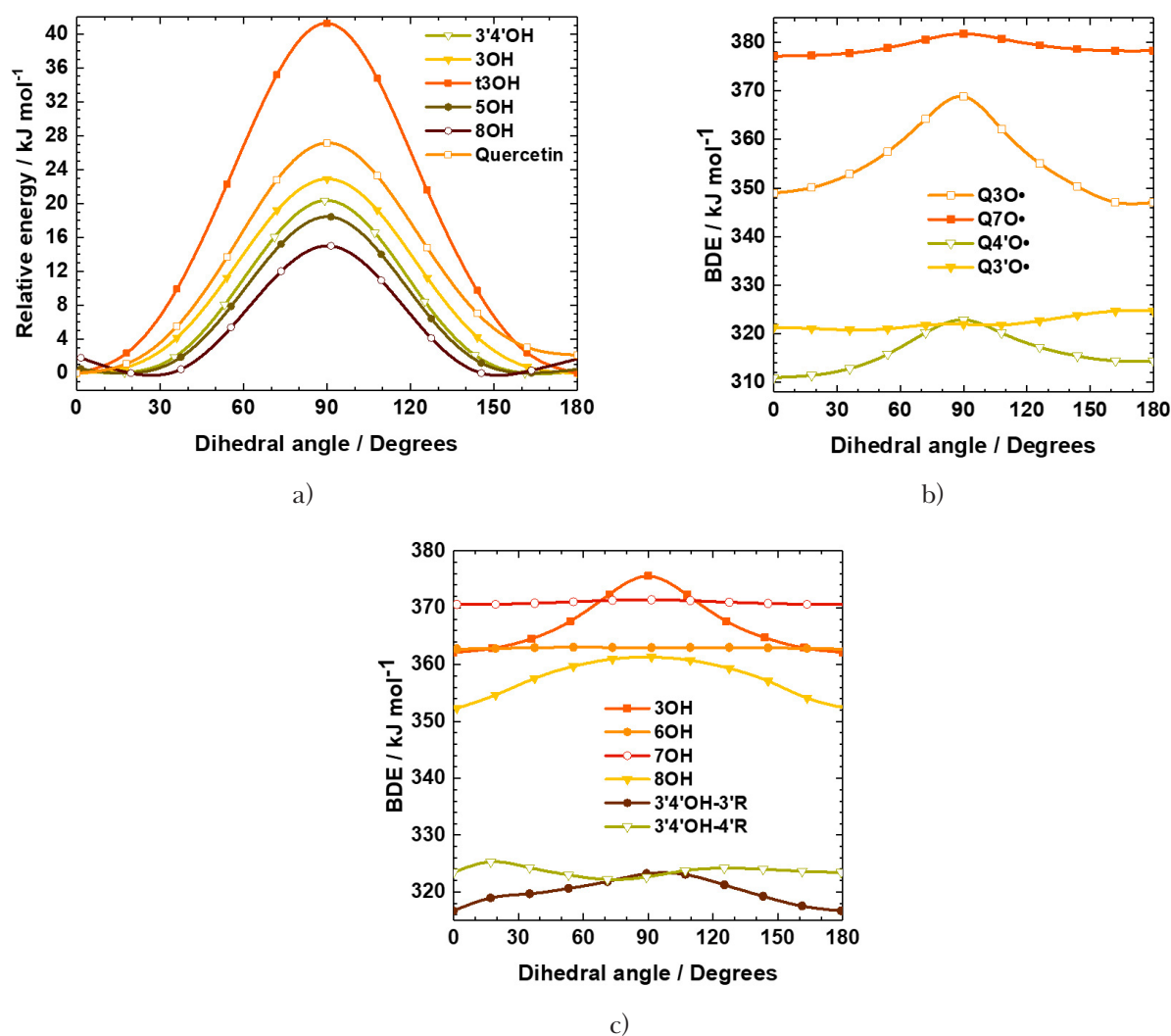
## Results

Within the selected theoretical method, most of the optimised structures are not planar with the exception of 3-hydroxyflavone (**3OH**). As a reference, predicted dihedral angles between rings AC and B (see Fig. 1) are compared in Tab. 1 with the experimental ones determined from crystal structures. Notable discrepancies can be found at first sight, but they can be argued quite easily. To begin with, the dihedral angle varies wildly even within the crystal structures of the same molecule (see e.g. quercetin), which is caused by solvent and crystal packing effects. Moreover, Fig. 2a indicates the barrier of less than  $2 \text{ kJ mol}^{-1}$  for significant torsion for most of the moieties. In the solvent environment, this barrier is probably even lower; therefore, free rotations of at least  $\pm 20^\circ$  are definitely enabled. From the symmetry point of view, quercetin and 3',4'-hydroxyflavone (**3',4'OH**) conformations with dihedral angles of  $0^\circ$  and  $180^\circ$  are not identical. While for the latter one, they are virtually the same from the energy point of view, in case of quercetin there is a small energy preference of around  $2 \text{ kJ mol}^{-1}$  for the  $0^\circ$  angle (Fig. 2a). Given this negligible difference, only  $180^\circ$  torsion starting with the most stable conformations was considered in the following discussion.

Falantin et al. (2017) also found **3OH** with  $C_s$  symmetry with the strong intramolecular H-bond

**Tab. 1.** Theoretical angles and BDEs, angles from X-ray structures are in parenthesis.

	Dihedral angle C3—C2—C1'—C2'	BDE/kJ mol <sup>-1</sup>
<b>3OH</b>	0 ° (5.5 ° – Etter, 1986) (4.7 ° – Schutte-Smith, 2019)	362
<b>5OH</b>	37 ° (5.8 ° – Shoja, 1990)	430
<b>6OH</b>	19 ° (9.8 ° – Seetharaman, 1992) (13 ° – Shoja, 1998)	363
<b>7OH</b>	19 ° (18.6 ° – Kumar, 1998)	371
<b>8OH</b>	19 °	352
<b>3',4'OH</b>	35 °	317(4'O•), 322(3'O•)
<b>Quercetin</b>	18 ° (1.0 ° – Domagała, 2011)	321(3'O•)
	(7 ° – Rossi, 1986)	314(4'O•)
	(6.7 ° – Jin, 1990)	346(3O•)
	(32 ° – Vasisht, 2016)	415(5O•)
		377(7O•)

**Fig. 2.** Scan of catecholic ring torsion: a) neutral state energy (optimised geometry as reference), b) bond dissociation energy of quercetin, c) BDEs of other hydroxyflavones.

between the H3 atom of the hydroxyl group and the O4 atom. This H-bond also supports proton transfer, creating a tautomer (denoted by prefix **t**).

Multiple experimental results confirm the significance of the tautomeric form of 3-hydroxyflavone (**t3OH**, shown in Fig. 1) and 5-hydroxyflavone

(**t5OH**). Incidentally, the highest rotational barrier shows **t3OH**, which can be explained by the conjugation of AC rings extended to the B ring. This is not the case in the **t5OH** tautomer, which was found to be very similar to **3'4'OH** in terms of torsion energy demands (not shown in Fig. 2). For other molecules, the findings are consistent with the single bond character of the C2—C1' bond. Position of the hydroxyl group in case of **5OH**, **6OH** and **7OH** seems to play a little to no role as almost identical curves were found in these cases; therefore, only one of them is shown in Fig. 2. The catecholic ring is the least restrained from the rotation in 8-hydroxyflavone. Apart from tautomers, quercetin has the most restrained B ring rotation.

Since flavonoids are often studied for their antioxidant properties, investigations of the change in dihedral angle on the energetics of the homolytic O—H bond cleavage should be considered essential. Despite employing somewhat small basis sets, our BDEs are in very good agreement with the very precise G4 BDEs (Alvareda 2016). Correlation coefficient between the data reached the value of 0.991 (not presented). Calculated BDEs of our studied hydroxyflavones have mostly the lowest values for ca. 0° and 180° angles and the highest values for 90°. An exception is the 3'R radical formed from **3'4'OH** with a different type of dependence as seen in Fig. 2c: two maxima at 18° and at 126°. Interestingly, when the quercetin

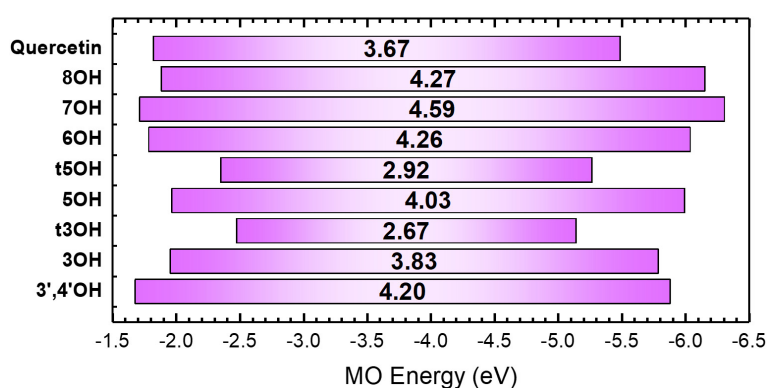


**Fig. 3.** Frontier MOs energy diagram. HOMO-LUMO energy gap is indicated by numbers.

**Tab. 2.** Electron transitions to the first 3- excited state of studied molecules with oscillator strengths  $f$ . Experimental absorption maxima are in parentheses (Wolfbeis et al., 1984; Dangleterre et al., 2008). H stands for HOMO and L for LUMO.

	$\lambda_{\text{abs}}$ nm	$E$ eV	$f$ a.u.	Assignment		$\lambda_{\text{abs}}$ nm	$E$ eV	$f$ a.u.	Assignment			
<b>3',4'OH</b>	348(342)	3.56	0.0055	H-1 $\rightarrow$ L	44 %	<b>6OH</b>	353	3.51	0.0006	H-2 $\rightarrow$ L	12 %	
				H-1 $\rightarrow$ L+1	15 %					H-1 $\rightarrow$ L	35 %	
	311(308)	3.99	0.3752	H $\rightarrow$ L	45 %		324(308)	3.83	0.0781	H $\rightarrow$ L	47 %	
<b>3OH</b>	283	4.38	0.0504	H-2 $\rightarrow$ L	42 %		285(266)	4.35	0.3869	H-2 $\rightarrow$ L	31 %	
	346(342)	3.58	0.3578	H $\rightarrow$ L	48 %				H-1 $\rightarrow$ L	11 %		
	306	4.05	0.0000	H-3 $\rightarrow$ L	49 %	<b>7OH</b>	354(335)	3.51	0.0006	H-2 $\rightarrow$ L	18 %	
291	4.27	0.1051	H-1 $\rightarrow$ L	45 %					H-1 $\rightarrow$ L	25 %		
483	2.57	0.3398	H $\rightarrow$ L	50 %	298(309)		4.16	0.2627	H-2 $\rightarrow$ L	29 %		
<b>t3OH</b>	377	3.29	0.0000	H-1 $\rightarrow$ L	50 %				H-1 $\rightarrow$ L	13 %		
	331	3.75	0.0043	H-2 $\rightarrow$ L	47 %		290	4.27	0.0829	H $\rightarrow$ L	33 %	
	351(332)	3.53	0.0438	H $\rightarrow$ L	49 %	<b>8OH</b>	356	3.48	0.0005	H-1 $\rightarrow$ L	45 %	
316(298)	3.92	0.0030	H-3 $\rightarrow$ L	24 %			334(302)	3.72	0.0211	H $\rightarrow$ L	48 %	
			H-2 $\rightarrow$ L	17 %			277(264)	4.48	0.0683	H-3 $\rightarrow$ L	38 %	
<b>5OH</b>	277(266)	4.47	0.0060	H $\rightarrow$ L+1	28 %	<b>Quercetin</b>	371(370)	3.34	0.4787	H $\rightarrow$ L	47 %	
	522	2.37	0.0584	H $\rightarrow$ L	49 %			324	3.83	0.0722	H-1 $\rightarrow$ L	47 %
	386	3.21	0.0000	H-1 $\rightarrow$ L	48 %			293	4.23	0.0302	H-2 $\rightarrow$ L	43 %
<b>t5OH</b>	331	3.74	0.0880	H $\rightarrow$ L+1	48 %							

catecholic ring is rotated by 90 ° with respect to the plane defined by AC rings, difference in the energy demand for the cleavage of 4'O—H and 3'O—H bond becomes almost the same. In terms of O—H bond cleavage, monohydroxyflavone resembles quercetin. For example, Figs. 2b, 2c show BDE of 3-hydroxy group largely affected both in quercetin and in 3-hydroxyflavone in contrast to the very mildly changed quercetin BDEs of 7- and 5-hydroxy group or to those of **7OH** and **5OH** (not shown). BDE of **6OH** is also almost unaffected by the torsion.

Energy difference between the ground states of 3-hydroxyflavone and its tautomer is almost of 50 kJ mol<sup>-1</sup> but ultrafast spectroscopy experiments confirmed that the first excited state of **3OH** spontaneously forms excited state tautomer followed by the decay to the tautomer ground state (Dzuga et al., 1986). Significant difference in energy of HOMO, LUMO as well as their energy gap can

be seen comparing the ground state of **3OH** with **t3OH** (Fig. 3, also see Fig. 1 for chemical structure of **t3OH**). For the most hydroxyflavones, the first visible absorption band corresponds to the HOMO to LUMO  $\pi \rightarrow \pi^*$  absorption, which is confirmed by the theoretical electron transitions to excited states compiled in Tab. 2.

Lower energy gap of the tautomers is projected in redshifted electron transition (e.g. 346 nm for **3OH** compared to 483 nm for **t3OH**). Flavonoids experimental absorption bands maxima often exhibit high sensitivity to solvent properties such as polarity, pH and temperature. Also, the UV-vis spectra are highly dependent on the number and position of substituents. Despite the calculations being done only in the gas phase, the predicted electron transitions, except for **7OH**, are in fair agreement with the experimental ones ( $R = 0.966$ ). The typical  $\pi$  character of ground state HOMO and LUMO is illustrated in Fig. 4.

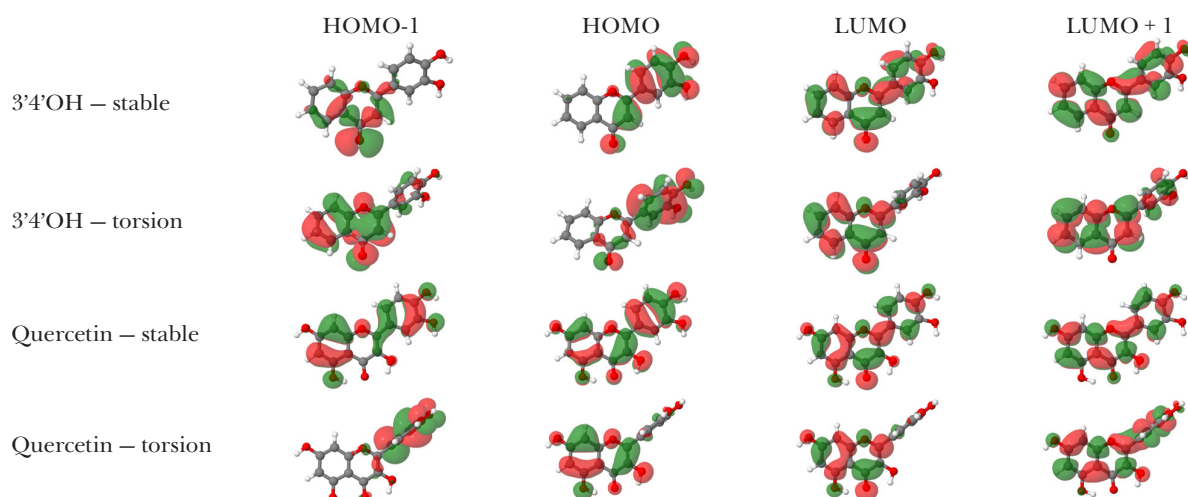


**Fig. 4.** Relevant molecular orbitals of stable geometries and after catecholic ring torsion (isosurface of 0.025 a.u.).

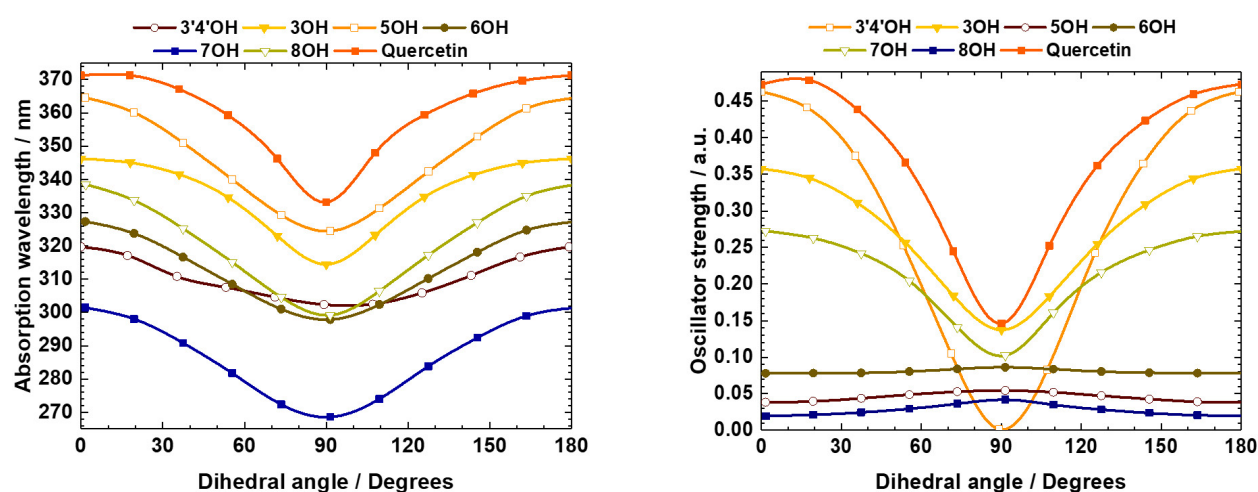


**Fig. 5.** Effect of dihedral C3—C2—C1'—C2' angle change on experimentally relevant excited state parameters.

On the other hand, HOMO-1 is of a non-bonding character yielding HOMO-1→LUMO transitions forbidden with almost zero predicted oscillator strength. Frontier molecular orbital shapes exhibit exceptional changes due to the torsional defects. In case of **3'4'OH**, visible transformation of  $\pi$ -type HOMO into non-bonding type orbital occurred while the opposite was observed for HOMO-1. Quercetin in particular has HOMO-1 of  $\pi$  character but the torsion shifts the electron delocalisation to the above catecholic ring only. In experimental spectra, these HOMO-1→LUMO transitions are slightly visible. Also, any change in dihedral C3—C2—C1'—C2' angles causes a blueshift in the excited states transitions. The largest blueshift accompanied by the largest drop in the oscillator strength was observed for the quercetin HOMO→LUMO transition (Fig. 5). Despite this, **5OH**, **6OH** and **8OH** showed an increase in the oscillator strengths.

## Conclusion

Knowledge of the rotation energy barrier around the C2—C1' bond is essential for the description of the dynamic behaviour of hydroxyflavones. Theoretical calculations based on density functional theory predict a small energy barrier permitting at least  $\pm 20^\circ$  torsion of the catecholic ring with respect to the AC rings plane for most studied free molecules. Therefore, most hydroxyflavones are very far from a rigid molecule. For neutral molecules, the potential function is of a single-barrier type. The dihedral angle dependence of BDEs provided another useful information; 3-hydroxyflavonol showed the biggest difference between the highest and the lowest BDE values among mono-hydroxyflavones. Any deviation in dihedral C3—C2—C1'—C2' from the optimised geometry angle resulted in a blueshift of the excited states electron transitions. Since the effect of solvent and solid phase matrices is expected to be even more significant, application of molecular dynamics methods with multiple explicit molecules are planned for the future work.

### Acknowledgement

*The authors are grateful to the HPC center at the Slovak University of Technology in Bratislava, which is a part of the Slovak Infrastructure of High Performance Computing (SIVVP project, ITMS code 26230120002, funded by the European Region Development Funds, ERDF) for the computational time and resources made available. V. L. thanks the Ministry of Education, Science, Research and Sport of the Slovak Republic for funding within the scheme "Excellent research teams".*

## References

- Ahmed SA, Maity B, Seth S, Seth D (2017) J. Photoch. Photobio. B 168: 132–141.
- Alvareda E, Denis PA, Iribarne F, Paulino M (2016) Comp. Theo. Chem. 1091: 18–23.
- Andersson K, Roos BO (1995) Modern electronic structure theory. Part I, World Scientific, Singapore.
- Ash S, De SP, Pyne S, Misra A (2010) J. Mol. Model. 16(5): 831–839.
- Awad WL, El-Newehy MF, Selim SF (1960) J. Org. Chem. 25(8): 1333–1336.
- Becke AD (1988) Phys Rev A 38: 3098–3100.
- Cornard JP, Boudet AC, Merlin JC (2001) Spectrochim. Acta A 57(3): 591–602.
- Dangleterre L, Cornard JP, Lapouge C (2008) Polyhedron 27(6): 1581–1590.
- Domagała S, Munshi P, Ahmed M, Guillot B, Jelsch C (2011) Acta Crystallogr B 67(1): 63–78.
- Dzuga TP, Schmidt J, Aartsma TJ (1986) Chem. Phys. Lett. 127(4): 336–342.
- Etter MC, Urbańczyk-Lipkowska Z, Baer S, Barbara PF (1986) J. Mol. Struct. 144(1-2): 155–167.
- Falantin C, Moncomble A, Le Person A, Cornard JP (2017) Spectrochim Acta A 187: 49–60.
- Frisch MJ, Trucks GW, Schlegel HB, Scuseria GE, Robb MA, Cheeseman JR, Scalmani G, Barone V, Petersson GA, Nakatsuji H, Li X, Caricato M, Marenich AV, Bloino J, Janesko BG, Gomperts R, Mennucci B, Hratchian HP, Ortiz JV, Izmaylov AF, Sonnenberg JL, Williams-Young D, Ding F, Lipparini F, Egidi F, Goings J, Peng B, Petrone A, Henderson T, Ranasinghe D, Zakrzewski VG, Gao J, Rega N, Zheng G, Liang W, Hada M, Ehara M, Toyota K, Fukuda R, Hasegawa J, Ishida M, Nakajima T, Honda Y, Kitao O, Nakai H, Vreven T, Throssell K, Montgomery JA Jr., Peralta JE, Ogliaro F, Bearpark MJ, Heyd JJ, Brothers EN, Kudin KN, Staroverov VN, Keith TA, Kobayashi R, Normand J, Raghavachari K, Rendell AP, Burant JC, Iyengar SS, Tomasi J, Cossi M, Millam JM, Klene M, Adamo C, Cammi R, Ochterski JW, Martin RL, Morokuma K, Farkas O, Foresman JB and Fox DJ (2016) Gaussian 16, Revision B.01, Gaussian, Inc. Wallingford CT.
- Gierschner J, Duroux JL, Trouillas P (2012) Food Chem. 131(1): 79–89.
- Hollman PCH, Arts ICW (2000) J. Sci. Food Agricult. 80(7): 1081–1093.
- Jin GZ, Yamagata Y, Tomita K (1990) Acta Crystallogr C 46(2): 310–313.
- Jmol: an open-source Java viewer for chemical structures in 3D. <http://www.jmol.org/>.
- Kotzian M, Rösch N, Zerner MC (1992) Theo. Chim. Acta 81(4-5): 201–222.
- Klymchenko AS, Demchenko AP (2002) Langmuir 18(15): 5637–5639.
- Kumar S, Ramanathan T, Subramanian K, Steiner T (1998) J. Chem. Crystallogr. 28(12): 931–933.
- Lee C, Yang W, Parr RG (1988) Phys Rev B 37: 785–789.
- Mengoli G, Musiani MM (1987) J. Electrochem. Soc. 134(12): 643C.
- Merriam-webster dictionary <https://www.merriam-webster.com/dictionary/polyphenol>.
- Quideau S, Deffieux D, Douat-Casassus C, Pouységu L (2011) Angew. Chem. Int. Edit. 50: 586–621.

- Rassolov VA, Ratner MA, Pople JA, Redfern PC, Curtiss LA (2001) *J. Comp. Chem.* 22: 976–984.
- Rossi M, Rickles LF, Halpin WA (1986) *Bioorg. Chem.* 14(1): 55–69.
- Seetharaman J, Rajan SS (1992) *Acta Crystallogr. C* 48(9): 1714–1715.
- Schutte-Smith M, Roodt A, Alberto R, Twigge L, Visser HG, Kirsten L, Koen R (2019) *Acta Crystallogr. C* 75(4): 378–387.
- Shahidi F, Janitha PK, Wanasundara PD (1992) *Crit. Rev. Food Sci. & Nutri.* 32(1): 67–103.
- Sherrill CD, Schaefer IIIHF (1999) *Adv. Quant. Chem.* 34: 143–269.
- Shoja M (1990) *Acta Crystallogr. C* 46(3): 517–519.
- Shoja M, Yen MW, Peterson L (1998) *Z. Krist.-New Cryst. St.* 213(1-4): 769–770.
- Tošović J, Marković S (2017) *Chemical Papers* 71(3): 543–552.
- Valle JC (2006) *J. Chem. Phys.* 124(10): 104506.
- Vasisht K, Chadha K, Karan M, Bhalla Y, Jena AK, Chadha R (2016) *CrystEngComm* 18(8): 1403–1415.
- Williams RJ, Spencer JP, Rice-Evans C (2004) *Free Radical Bio. Med.* 36: 838–849.
- Wolfbeis OS, Leiner M, Hochmuth P, Geiger H (1984) *Berich. Bunsen. Gesell.* 88(8): 759–767.

# Application of selective polymeric sorbents for simple coumarins extraction from deodorant samples

Katarína Hroboňová, Andrea Špačková

Slovak University of Technology in Bratislava, Faculty of Chemical and Food Technology, Institute of Analytical Chemistry, Radlinského 9, SK-812 37 Bratislava, Slovak Republic  
katarina.hrobonova@stuba.sk

**Abstract:** Coumarins (2H-1-benzopyran-2-coumarin derivatives) are derivatives of cinnamic acid naturally occurring in many plants, fungi, and fruits. They are used as ingredients in cosmetics to enhance the aroma and other biological effects. In this work, cosmetic samples (deodorants) were treated by solid phase extraction prior to high performance liquid chromatography determination of coumarins. Traditional sorbent (C18) and selective polymer-based sorbents (laboratory prepared and commercial) were used for solid phase extraction. Recovery values were above 85 % (RSDs below 6 %) except for esculin, where the recovery was lower. Core-shell column of C18 type and gradient of mobile phase methanol–1 % acetic acid were used for high performance liquid chromatography analysis of extracts. Limits of quantitation were 0.5 µg mL<sup>-1</sup> for coumarin (ultraviolet detection) and below 12 ng mL<sup>-1</sup> for esculin, umbelliferonene, scoparone, 4-methylumbelliferone, herniarin (fluorescence detection). In the tested samples, no coumarins were detected.

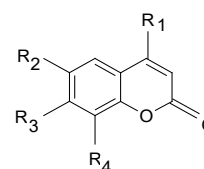
**Keywords:** simple coumarins, deodorants, high performance liquid chromatography, selective sorbent, solid phase extraction

## Introduction

Coumarins (Fig. 1) are substances naturally occurring in plants (e.g. tonka bean, yellow sweet clover, lavender), and other natural sources. They exhibit several biological effects with a wide range of applications, e.g. UV protection, antibacterial, nematocidal, phytotoxic, antifungal activity, etc. (Pan et al., 2014). Coumarin, as the main group representative, is characterized by its smell which is sweet, from herbal-spicy to slightly balsamic with coconut variations; in dilution it smells like freshly cut hay.

Fragrances are used extensively in cosmetics, perfumes and personal care products (aftershave lotions, bath products, bubble baths, cleansing products, moisturizers, skin care products and suntan products). Among coumarins, synthetic coumarin is the main compound utilized as fragrance ingredient in cosmetic products at concentrations from 0.08 % to 5.8 % (Quantitative Risk Assessment aggregate exposure adjusted upper concentration levels; Guidance for the use of IFRA standards, 2019). Some natural coumarins may be present in cosmetic preparations from plant extracts (Murray, 2002). In the EU, seven coumarins (herniarin, dicoumarol, 7-ethoxy-4-methylcoumarin, dihydrocoumarin, 7-methylcoumarin, acenocoumarol, and pyranocoumarin) are forbidden in cosmetic products (Regulation (EC) No 1223/2009). Coumarins not only improve the aroma of the products, but from a technological

point of view they serve mainly as a modifier and fixator of the final fragrant composition. However, they can also cause allergic reactions (Srikrishna et al., 2018). A quantitative human health risk assessment integrating both cancer and non-cancer effects confirmed the safety of coumarin exposure from natural dietary sources as well as from its use as perfume in personal care products (Felter et al., 2006).



	R <sub>1</sub>	R <sub>2</sub>	R <sub>3</sub>	R <sub>4</sub>
Coumarin	H	H	H	H
Esculin	H	Glucose	OH	H
Umbelliferone	H	H	OH	H
4-Methylumbelliferone	CH <sub>3</sub>	H	OH	H
Scoparone	H	CH <sub>3</sub> O	CH <sub>3</sub> O	H
Herniarin	H	H	CH <sub>3</sub> O	H

**Fig. 1.** Chemical structure of selected natural coumarins.

According to EU Council Directive, if fragrances concentration exceeds 100 ppm in “wash-off” products such as shampoos and body wash, or 10 ppm in “leave-on” products such as creams and perfumes, they need to be enumerated in the ingredients list

of the product (EU Council Directive No 76/768/EEC). Analytical methods that screen for these fragrance compounds in complex matrices have to be developed. HPLC is most commonly used method for separation and determination of coumarins, while GC and TLC are rarely used for separation of some coumarins (Waksmundzka-Hajnos et al., 2006; Rahim et al., 2011). The most common HPLC stationary phase is the C18, C8, phenyl or phenyl-hexyl type. A mixture of an organic solvent and aqueous acid solution with gradient elution is often chosen as the mobile phase. A spectrophotometric detector, fluorescent detector (Hroboňová et al., 2013) or a mass spectrometric detector (Ma et al., 2015) are used to detect coumarins. An important part of chemical analysis is the preparation of samples to remove interferences from the matrix and to obtain a fraction of the sample or the final analyte extract in a solvent compatible with the analytical technique used, e.g. with the mobile phase in HPLC. Sometimes it is also necessary to preconcentrate the target analytes. The most commonly used sample preparation technique is solid phase extraction (SPE) due to its speed, simplicity of procedures and equipment, automatization and the small amount of solvents required compared to traditional extraction techniques, e.g. liquid-liquid and liquid-solid extraction. There are many of SPE sorbents but in most procedures only a few types are used (e.g. C18). Their selectivity can be sometimes low, especially in case of complex samples, and the target analyte can co-elute with the matrix interferences. A new type of sorbents with increased selectivity for target analytes are the molecularly imprinted polymers (MIP), synthetic tailor-made materials with predefined selectivity for the target analyte or structurally related compounds based on specific interactions between the analyte and the binding sites on MIP. In most cases, the application of MIPs in cosmetics' analysis is mainly focused on the extraction of active ingredients such as parabens, antimicrobials, UV filters (Figuierido et al., 2016; Vicario et al., 2018; Wang et al., 2018), but they are also applied for selective extraction of toxic compounds, e.g. bisphenol (Zhu et al., 2010). MIP based sorbents are also useful in the analysis natural resources and extracts, e.g. herbal plant extracts, used in natural cosmetics, both for isolation and enrichment, active compounds such as alpha-lipoic acid (Xu et al., 2020) and toxins such as pyrrolizidine alkaloids (Luo et al., 2019). Only a few papers have been published regarding the application of MIPs selective for coumarins. MIPs have been used as sorbents for offline MIP-SPE extraction of coumarins from traditional Chinese medicine herbs, such as esculin from *Ash bark*

(Hu et al., 2005) and esculin from *Cortex fraxini* (Wang et al., 2007). Coumarin, herniarin and umbelliferone were extracted from plants (lavender, archangel, camomile) macerates (Machyňáková and Hroboňová 2017a; Machyňáková and Hroboňová 2017b) and sesquiterpene coumarins from *Asafoetida* plant (Eidi et al., 2020).

In this study, extraction efficiency of simple coumarins obtained using different types of SPE sorbents were compared. The traditional sorbent of C18 type and selective polymer-based sorbents (laboratory synthesized and commercial) were tested. An offline extraction procedure and HPLC method were used for deodorant analysis.

## Material and Methods

### Chemicals and samples

Standards of coumarin (99 %), esculin (6,7-dihydroxycoumarin-6- $\beta$ -D-glucoside, 98 %), umbelliferone (7-hydroxycoumarin, 99 %), 4-methylumbelliferone (4-methyl-7-hydroxycoumarin, 98 %), scoparone (6,7-dimethoxycoumarin, 98 %), herniarin (7-methoxycoumarin, 98 %) were purchased from Sigma-Aldrich (St. Louis, USA). Methanol (HPLC gradient grade) and acetic acid (99 %) were purchased from Merck (Darmstadt, Germany). Deionized water (resistivity of 18.2 M $\Omega$ /cm) was obtained from a AquaMax ultra (series 370) water purification system.

Samples of deodorants (Sample 1 was deodorant with the aroma of green tea and agave containing alcohol; Sample 2 was deodorant for sensitive skin without alcohol; Sample 3 was natural cosmetic deodorant where the manufacturer guarantees conscious renunciation of disputed ingredients) were obtained from a local drugstore network. For all tested samples, the manufacturers do not list coumarin as an ingredient in the product. The samples were kept at room temperature.

### Preparation of standard solutions

Accurately weighed amounts of standards were dissolved in solvent (initial mobile phase – methanol/1 % acetic acid (20/80, v/v) to reach stock solutions with the concentration of 0.1 mg mL<sup>-1</sup>. Mixed working solutions were prepared by diluting the stock solutions to concentrations in the range of 0.5–100  $\mu$ g mL<sup>-1</sup> for coumarin and of 15–100 ng mL<sup>-1</sup> for other substances under study.

### Solid phase extraction procedure

SPE was performed with C18 Hydra (Chromabond, Macherey-Nagel, Germany; 100 mg of sorbent), MIP-phenolics (AFFINIMIP, Affinisep, France; 100 mg of sorbent), and MIP-coumarins (labora-

tory prepared under procedure by Machyňáková and Hroboňová, 2017a; 100 mg of sorbent). SPE cartridges were preconditioned with 2 mL of methanol and 2 mL of water. Then, 0.5 mL of sample or standard solution of coumarins was passed through the cartridge. The cartridge was washed with 1 mL of water and finally the analytes were eluted with 0.5 mL of methanol/acetic acid (9/1, v/v). This extract was filtered through a 0.45 µm nylon membrane filter and an aliquot of 20 µL was injected into the HPLC.

### **HPLC analysis**

HPLC separation was carried out on an Agilent Technologies, series 1260, Liquid chromatographic system equipped with a binary pump, injector valve (Rheodyne), column thermostat, diode array detector, and a fluorescence detector. A Kinetex C18 analytical column (100 mm × 4.6 mm I.D., 5 µm particle size) was employed. The chromatographic elution was performed with binary mobile phase gradient consisting of methanol/acetic acid (99/1, v/v) (A) and a 1 % aqueous solution of acetic acid (B) at the flow rate of 1.0 mL min<sup>-1</sup>. The gradient program was as follows: initial gradient conditions were set to 20 % A, then linear gradient was increased to 45 % A over 12 min. At 12 min, the gradient was programmed to 100 % A over 0.5 min and held for 2 min. At 14.5 min, the gradient was returned to initial conditions over 0.5 min and held for 4 min. Column temperature was maintained at 23 °C. Injection volume was 20 µL. DAD was operated in the wavelength range of 190–400 nm and for quantification of coumarin, detection at 280 nm was used (corresponding to the wavelength of absorption maximum of coumarin in appropriate mobile phase). Fluorescence detection of esculin, umbelliferone, 4-methylumbelliferone, scoparone, herniarin was operated at the wavelengths of 330 nm ( $\lambda_{ex}$ ) and 450 nm ( $\lambda_{em}$ ) (corresponding to the wavelengths of absorption/emission maximum of coumarins in appropriate mobile phase). Fluorescence spectra were scanned in the wavelength range of 340–500 nm.

### **Method validation**

Analytical evaluation of the HPLC method was investigated using standard solutions in concentration ranges from 0.5 to 100 µg mL<sup>-1</sup> for coumarin and from 15 to 100 ng mL<sup>-1</sup> for other substances under study (six concentration levels of each analyte, three replicate measurements for each solution). Calibration curve of the analyte was obtained by plotting a graph of mean peak area versus the corresponding analyte concentration. LODs of six analytes were estimated using 3  $s_a$  criteria and LOQs as 10  $s_a$  criteria ( $s_a$  is the standard deviation of

the intercept of the calibration curve). For recovery study, two aliquots of deodorant (sample 3) were spiked with coumarins stock solutions giving a concentrations of 2.0 µg mL<sup>-1</sup> and 20 µg mL<sup>-1</sup> of coumarin, 20 ng mL<sup>-1</sup> and 50 ng mL<sup>-1</sup> of esculin, umbelliferone, scoparone, 4-methylumbelliferone, herniarin. The spiked samples were vigorously vortexed for 1 min and subsequently treated by the SPE procedure with an MIP-coumarins sorbent. Recoveries were determined by comparing the peak areas obtained from sample spiked with analytes after the extraction with those from the reference solution. Precisions of the method was evaluated for six sample preparations within three days and was expressed as relative standard deviation (RSD %).

## **Results and Discussion**

### **Selection of SPE sorbent**

Commercial SPE sorbents, C18 Hydra, MIP-phenolics and laboratory prepared MIP-coumarins were tested for coumarins extraction from deodorant samples. The extraction procedure was the same for all tested sorbents and includes optimal conditions, methanol and water as conditioning solvents, water as washing solvent, methanol/acetic acid as eluting solvent. Octadecyl silica sorbent is most frequently used for the isolation of less polar compounds. The main retention mechanism is based on van der Waals forces. Modified C18 Hydra sorbent enables the extraction of more polar analytes from water matrices. MIP-phenolics sorbent is suitable for the extraction, clean up, and preconcentration of phenolic compounds (information of sorbent producers). Laboratory prepared MIP was synthesized by thermal bulk polymerization using umbelliferone as the template. Optimization of polymerization (ratios and types of polymerization constituents) allows preparing sorbents with good morphology (evaluated by scanning electron microscopy), high specific adsorption capacity (270 µg of umbelliferone per 1 g of polymer), and group selectivity for structurally related simple coumarins (Machyňáková and Hroboňová, 2017a). MIP sorbents, contrary to the traditional SPE materials (silica-based sorbents), are characterized by higher selectivity and specificity to the target analyte, which leads to effective elimination of interferences and matrix effects.

Extraction efficiencies of SPE sorbents were evaluated for standard solution of coumarin at the concentration level of 2.0 µg mL<sup>-1</sup> and esculin, umbelliferone, scoparone, 4-methylumbelliferone, herniarin at the concentration level of 20 ng mL<sup>-1</sup>. Results of the recovery study are shown in Fig. 2. C18 type and MIP-phenolic sorbents showed

nearly equal recovery for the investigated coumarins (87–97 %), except for esculin where the recovery reached values close to 60 %. Esculin is a molecule significantly different from other coumarins under study as it is a glucoside compound (Fig. 1). Thus, this more polar compound is weakly retained on the C18 sorbent which results in lower recovery. Comparing MIP based sorbents, the laboratory synthesized MIP-coumarins sorbent is suitable for the extraction of selected simple coumarins. Compared with other tested sorbents, higher recovery values (90–97 %, RSDs < 6 %) were obtained for five aglycone coumarins. Also, higher recovery was achieved for esculin (72 %, RSD = 5 %). Reduced recovery of esculin, compared to other analytes, on MIP-coumarins is related with the incompatibility of imprinted cavity with the shape and functionality of the analyte. MIP-phenolic, although they are more universal (imprinted cavity designed for phenolic compounds) are less selective for simple coumarins. Similar to MIP-coumarins, lower recovery for esculin was observed.

Average recovery of up to 74.7 % was achieved for extraction and enrichment of esculin from *Cortex fraxini* plant using MIP sorbent prepared with MAA as the functional monomer and esculin as the template (Wang et al., 2007). Comparable recovery values as in the presented work were obtained for selective MIP-SPE extraction of umbelliferone and herniarin from chicory macerate (81.2–98.7 %) (Machyňáková and Hroboňová, 2017a) as well as for extraction of coumarin, umbelliferone and herniarin from lavender, archangel and chamomile macerate (78.7–90.3 %, respectively) using MIP sorbent coated magnetite (Machyňáková and Hroboňová, 2017b).

A significant advantage of MIP based sorbents, in addition to selectivity for target analyte or analogues, is its reusability, which can be considered as green chemistry approach and it makes the

analysis cheaper (Mariusz, 2019; Machyňáková and Hroboňová, 2017a). In this work, the MIP sorbents were reused more than five times for sample treatment (without the change of effectiveness by 5 %), versus only once for C18 type. One of the problems of MIP based sorbents are template residues present in the polymer matrix even after exhaustive washing steps. Leakage of the template can affect the accuracy of analyte determination. To overcome this problem, dummy MIP synthetic approach can be used. Eidi et al. (2020) synthesized MIP sorbent using umbelliferone as the template and it was used in SPE of structural analogues, galbanic acid, 7-isopentenylcoumarin and auraptene from aqueous plant macerate. The recovery was in the range of 68.3–84.7 %. (Eidi et al., 2020)

### Selection of chromatographic conditions

HPLC conditions were selected after testing different columns and mobile phase compositions. The proportion of organic and aqueous phases as well as gradient profile were selected to provide efficient separation of esculin, umbelliferone, coumarin, scoparone, 4-methylumbelliferone and herniarin with a satisfactory run time, resolution higher than 1.5, good peak symmetry and minimal high equivalent theoretical plate. Optimization and evaluation of HPLC separation were performed using standard solution of coumarins. The core shell C18 type of stationary phase and the mobile phase consisting of methanol and water with an addition of 1 % acetic acid in gradient elution mode at the flow rate of 1.0 mL min<sup>-1</sup> were selected as the best chromatographic conditions. Figure 3a shows the chromatogram of a standard mixture and Table 1 documents relevant chromatographic characteristics obtained at the selected optimal conditions. The advantage of this type of column is the short total analysis time (about 15 min) compared to columns with traditional silica based stationary phase (about 30 min; Hroboňová et al.,

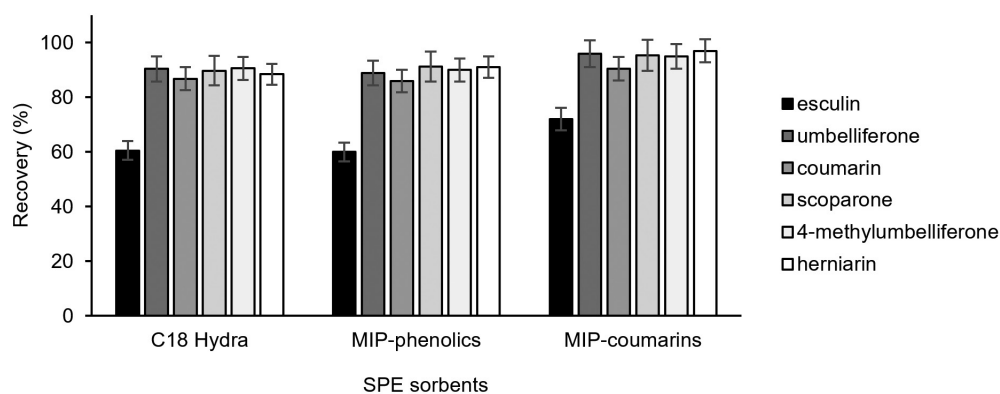


**Fig. 2.** Recovery of coumarins obtained for C18-Hydra, MIP-phenolics and MIP-coumarins SPE sorbents.

**Tab. 1.** Chromatographic characteristics (elution time ( $t_R$ ), resolution ( $R_s$ ), high equivalent to a theoretical plate ( $H$ )) and reproducibility of retention times and peak areas ( $A$ ) for HPLC separation of coumarins under optimal chromatographic conditions<sup>1</sup>.

Compound	$t_R$ (min)	$R_s$	$H$ ( $\mu\text{m}$ )	Reproducibility RSD (%)	
				$t_R$	$A$
Esculin	2.8	18.6	4.5	0.8	5.1
Umbelliferone	7.1	7.9	7.2	0.4	4.8
Coumarin	8.9	2.6	5.7	0.3	5.5
Scoparone	9.4	1.8	3.6	0.3	5.5
4-Methylumbelliferone	9.9	7.6	3.6	0.3	4.5
Herniarin	11.9		3.4	0.2	4.5

<sup>1</sup>esculin, umbelliferone, scoparone, 4-methylumbelliferone and herniarine – parameters for fluorescence detection ( $\lambda_{\text{ex}}/\lambda_{\text{em}}=330/450$  nm); coumarin – parameters for UV detection at ( $\lambda = 280$  nm).

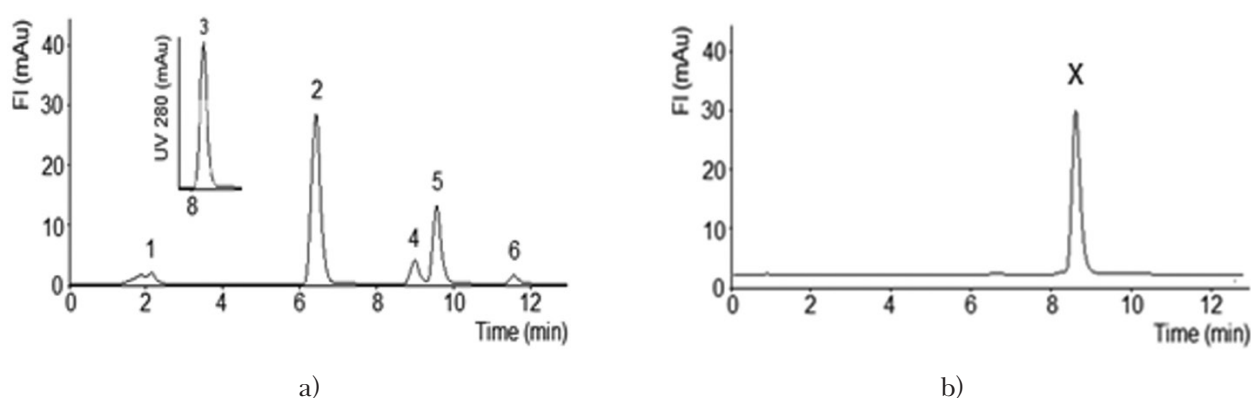


**Fig. 3.** Chromatograms of standard mixture (a) and sample 2 extract after MIP-coumarins SPE (b). Chromatographic conditions: Kinetex C18 (100 mm  $\times$  4.6 mm I.D., 5  $\mu\text{m}$ ) column, gradient elution with methanol–1 % acetic acid as mobile phase, flow rate of 1.0 mL  $\text{min}^{-1}$ , column temperature of 23  $^{\circ}\text{C}$ , UV detection at 280 nm, Fluorescence detection at 330 nm ( $\lambda_{\text{ex}}$ ) and 450 nm ( $\lambda_{\text{em}}$ ); legend: 1 – esculin, 2 – umbelliferonene, 3 – coumarin, 4 – scoparone, 5 – 4-methylumbelliferone, 6 – herniarin, X – unknown compound.

2013), which results from decreased core shell particles resistance to solute mass transfer into the porous structure of the stationary phase due to short diffusion distances (Hayes et al., 2014). For quantitative analysis, on-line coupled UV spectrophotometric and fluorescence detection were used. The UV detection wavelength was set to 280 nm for coumarin detection. The fluorescence excitation/emission wavelengths were set to 330/450 nm for the detection of other coumarins under study, as it provides higher selectivity and sensitivity and less interference potential compared to UV detection.

#### Method validation

The developed method was validated in terms of linearity, LOQs, recoveries, and intra-day precision showing good linearity in the calibration ranges of 0.5–100  $\mu\text{g mL}^{-1}$  for coumarin and of 15–100  $\text{ng mL}^{-1}$  for other coumarins; with correlation coefficients above 0.99. LODs and LOQs of the

six analytes are summarized in Table 2. The LOQs were found to be in the range of 1–12  $\text{ng mL}^{-1}$  for esculin, umbelliferone, scoparone, 4-methylumbelliferone and herniarin and 0.5  $\mu\text{g mL}^{-1}$  for coumarin. The European Cosmetics Regulation prescribes to declare coumarin content from the concentration of 0.001 % for leave-on and of 0.01 % for rinse-off products. Thus, with lower LOQs, the developed method is suitable for coumarin determination (for other derivatives, there are no limits) in deodorants and antiperspirants of all types including fragranced body sprays (Guidance for the use of IFRA standards, 2019; EU Council Directive No 76/768/EEC). LOQs of coumarins in this study was lower than those reported in literature (32–45  $\text{ng mL}^{-1}$  for simple coumarins by HPLC-DAD (Xiongfeng et al., 2016); 0.17  $\text{mg kg}^{-1}$  for 6-methylcoumarin by HPLC-DAD, 5.0  $\text{mg kg}^{-1}$  by GC-FID (Liu et al., 2018)), although the LOQs obtained by fluorescence detection are slightly higher

**Tab. 2.** Linearity, LOQs, recoveries, inter-day precision of six coumarins.

Compound	Linearity <sup>1</sup>	R <sup>2</sup>	LOD <sup>1</sup>	LOQ <sup>1</sup>	Recovery <sup>2</sup> (%)	RSD (%)
Esculin	10–100	0.987	3	10	70 / 72	4.2 / 5.4
Umbelliferone	1–100	0.998	0.3	1	93 / 95	4.5 / 5.0
Coumarin	0.5–100	0.995	0.2	0.5	89 / 90	5.4 / 5.9
Scoparone	10–100	0.998	3	10	93 / 95	4.1 / 5.2
4-Methylumbelliferone	3–100	0.997	1	3	92 / 95	4.9 / 5.4
Herniarin	12–100	0.998	4	12	95 / 97	6.4 / 6.4

<sup>1</sup>ng mL<sup>-1</sup> for esculin, umbelliferone, scoparone, 4-methylumbelliferone and herniarin; µg mL<sup>-1</sup> for coumarin;

<sup>2</sup>spiked concentrations: 2.0 µg mL<sup>-1</sup>/20 µg mL<sup>-1</sup> of coumarin, 20 ng mL<sup>-1</sup>/50 ng mL<sup>-1</sup> of esculin, umbelliferone, scoparone, 4-methylumbelliferone, herniarin.

than that obtained by the HPLC-MS/MS methods (0.5–2 ng mL<sup>-1</sup> for 22 coumarin derivatives (Ma et al., 2015)). The recovery values of 70–97 % were obtained (RSD % 4.1–6.4) for sample 3 spiked with two substances concentration levels, confirming the applicability and good precision of the presented method.

### Samples analysis

Practical applicability of the proposed method with MIP based SPE extraction was demonstrated on deodorant analysis. Sensitivity and selectivity of the developed method were found to be sufficient for the characterization of the six coumarins under study in samples. A representative chromatogram of the deodorant extract obtained by MIP-coumarins SPE is shown in Fig. 3b. No peaks were observed in the elution times of target coumarins, indicating that there were not interferences from other constituents of the sample. The results show that MIP sorbents are suitable for the extraction of substances from complex samples, mainly for cleaning and/or preconcentration of analytes. The sample preparation method in this study is efficient for the extraction of esculin, umbelliferone, coumarin, scoparone, 4-methylumbelliferone and herniarin from deodorants. For the tested samples, manufacturers do not specify the presence of synthetic coumarin, which does not exclude the presence of natural coumarins from plant extracts used in the preparation of the products. Based on HPLC analysis, coumarin nor its derivatives were detected at concentration levels over LOD in the tested deodorant samples.

### Conclusions

In this study, laboratory prepared polymeric sorbent based on molecularly imprinted polymer reached nearly equal recovery for investigated coumarins compared to the C18 type and MIP-phenolics SPE sorbents. The advantage of the applied

MIP sorbent was its reuse (more than five times for sample pretreatment; C18 type can be used only once). Higher recovery was achieved for esculin extraction, a less hydrophobic compound under study, compared to the C18 sorbent. The method based on SPE using MIP-coumarins as the selective adsorbent showed good recovery and precision. The HPLC method with UV spectrophotometric and fluorescence detection was found to be suitable for the separation and determination of coumarins in cosmetic products within a short time (sample preparation below 10 min, chromatography of 15 min). After some modification, this method can be extended for the analysis of various cosmetic or other complex samples.

### Acknowledgement

*This research was financially supported by the Scientific Grant Agency of the Ministry of Education of the Slovak Republic and the Slovak Academy of Sciences (grant No. VEGA 1/0159/20).*

### References

- Eidi S, Iranshahi M, Mohammadinejad A, Mohsenzadeh MS, Farhadi F, Mohajeri SA (2020) J. Chromatogr. B 1138: 121943.
- EU Council Directive of 27 July 1976 on the approximation of the laws of the Member States relating to cosmetic products (No 76/768/EEC) (OJ L 262, 27. 9. 1976, p. 169).
- Felter SP, Vassallo JD, Carlton BD, Daston GP (2006) Food Chem. Toxicol. 44: 462–475.
- Figuierido L, Erny GL, Santos L, Alves A (2016) Talanta 146: 754–765.
- Guidance for the use of IFRA standards, The International Fragrance Association, December 12, 2019.
- Hayes R, Ahmed A, Edge T, Zhang H (2014) J. Chromatogr. A 1357: 36–52.
- Hroboňová K, Lehotay J, Čižmárok J, Sádecká J (2013) J. Liq. Chromatogr. Rel. Technol. 36: 486–503.
- Hu SG, Li L, He XW (2005) J. Chromatogr. A 1062(1): 31–37.
- Liu H, Zhang J, Hu B, Wei L (2018) China Surfactant Detergent and Cosmetics 48: 419–422.

- Luo Z, Chen G, Li X, Wang L, Shu H, Cui X, Chang C, Zeng A, Fu Q (2019) *J. Sep. Sci.* 42(21): 3352–3362.
- Ma Q, Xi H, Ma H, Meng X, Wang Z, Bai H, Li W, Wang C (2015) *Chromatographia* 78: 241–249.
- Machyňáková A, Hroboňová K (2017a) *Chromatographia* 80(7): 1015–1024.
- Machyňáková A, Hroboňová K (2017b) *Anal. Methods* 9: 2168–2176.
- Mariusz M (2019) Mip Synthesis, Characteristics and Analytical Application, in *Comprehensive Analytical Chemistry*, vol 86. Elsevier, Amsterdam.
- Murray RDH (2002) The Naturally Occurring Coumarins. In: Herz W., Falk H., Kirby G.W., Moore R.E. (eds) *Fortschritte der Chemie organischer Naturstoffe / Progress in the Chemistry of Organic Natural Products*, vol 83. Springer, Vienna.
- Pan TL, Wang PW, Aljuffali IA, Leu YL, Hung YY, Fang JY (2014) *Toxicol. Lett.* 226: 173–181.
- Rahim AA, Saad B, Osman H, Yahya SA (2011) *Food Chem.* 126: 1412–1416.
- Regulation (EC) No 1223/2009 of the European Parliament and of the Council of 30 November 2009 on Cosmetic Products (OJ L 342, 22. 12. 2009, p. 59) Official Journal of the European Union.
- Srikrishna D, Godugu C, Dubey PK (2018) *Mini Reviews in Medicinal Chemistry* 18(2): 113–141.
- Vicario A, Solari M, Felici E, Aragón L, Bertolino F, Gomez MR (2018) *Microchem. J.* 142: 329–334.
- Waksmundzka-Hajnos M, Petruczynik A, Hajnos M, Tuzimski T, Hawryl A, Bogucka-Kocka A (2006) *J. Chrom. Sci.* 44: 510–517.
- Wang GS, Cao QE, Ding ZT, Wang YG, Yang MH (2007) *Helv. Chim. Acta* 90(6): 1179–1189.
- Wang F, Li X, Li J, Zhu C, Liu M, Wu Z, Liu L, Tan X, Lei F (2018) *J. Colloid Interf. Sci.* 527: 124–131.
- Xiongfeng H, Lvy L, Qun X, Rogrer J (2016) *Thermo Scientific Application Note* 1128: Determination of coumarins in cosmetics.
- Xu L, Zhao ZX, Huang YA, Zhu QJ (2020) *Molecules* 25(312): 1–15.
- Zhu R, Zhao W, Zhai M, Wei F, Cai Z, Sheng N, Hu Q (2010) *Anal. Chim. Acta* 658: 209–216.

# Antibiotic resistant bacteria in surface waters in Slovakia

Andrea Štefunková<sup>a</sup>, Klára Cverenkárová<sup>a</sup>, Monika Krahulcová<sup>a</sup>,  
Tomáš Mackulák<sup>b</sup>, Lucia Bírošová<sup>a</sup>

<sup>a</sup>Department of Nutrition and Food Quality Assessment, Faculty of Chemical and Food Technology, Slovak University of Technology in Bratislava, Radlinského 9, SK-812 37 Bratislava, Slovak Republic

<sup>b</sup>Department of Environmental Engineering, Faculty of Chemical and Food Technology, Slovak University of Technology in Bratislava, Radlinského 9, SK-812 37 Bratislava, Slovak Republic  
andrea.stefunkova@stuba.sk

**Abstract:** This work deals with the occurrence of selected antibiotic resistant bacteria in Slovak surface waters. Total and antibiotic resistant coliform bacteria, enterococci and coagulase positive staphylococci were determined in 34 samples of surface water from rivers and still waters (dams, natural lakes, thermal bath) some of them used for recreational swimming. Sampling was performed during summer season 2017 (July and August). The number of total coliforms ranged from 1.74 log CFU/10 mL to 3.69 log CFU/10 mL. Coliform bacteria were registered in each tested sample. The highest number was observed in the sample from river Hron. Majority of samples contained ampicillin and tetracycline resistant bacteria. Enterococci were determined in 70 % of samples ranging from 0.78 log CFU/10 mL to 3.81 log CFU/10 mL. The highest number of enterococci was observed in river Váh. Ampicillin and vancomycin resistance prevailed over ciprofloxacin and gentamicin resistance. Coagulase positive staphylococci were present in 91 % of samples in the range of 0.70–3.03 log CFU/10 mL. Antibiotic resistant coagulase positive staphylococci were observed only in 32 % of samples, predominantly from rivers. In these samples, chloramphenicol resistance predominated. In three samples of water used for recreational purposes, the limit value for enterococci and *E. coli* according to Slovak legislation (Decree no. 308/2012 Coll.) for the quality of water in natural swimming pools during bathing season was exceeded.

**Key words:** antibiotic resistance, coliforms, enterococci, surface water

## Introduction

Antibiotic resistance represents a huge problem, already killing hundreds of thousands of people around the world. Although this threat is lurking behind the current virus outbreak, it could already complicate the care of many COVID-19 patients. Emergence and spread of multidrug resistant bacteria are not connected only to healthcare institutions as these bacteria can persist in animals, humans and the environment (Aslam et al., 2018).

Many studies point out that wastewater treatment plants (WWTPs) represent a hotspot of such resistance (Berendonk et al., 2015; Ribeiro et al., 2015; Mackulák et al., 2019). Treated water contains different pharmaceuticals (including antibiotics in subinhibitory concentrations), susceptible and antibiotic resistant bacteria as well as antibiotic resistance genes. Such water gets to the recipient which can also be surface water (river, lake, etc.). Sub-inhibitory concentrations of antibiotics play an important role in bacterial communication as a regulatory compound and signalling molecules, which leads to biofilm formation or changes in the underlying bacterial metabolism. On the other hand, low antibiotic concentrations lead to the selection of antibiotic resistant population (Stiborová et al., 2018). One of

the greatest concerning the presence of these drugs in the environment is the emergence and spread of antibiotic resistant bacteria and genes encoding resistance. Subinhibitory concentrations of antibiotics can also contribute to horizontal transfer of such genes located on transposons, integrons or plasmids between bacteria of the same but also of different species (Huerta et al., 2013).

Biological contamination of surface water is predominantly caused by anthropogenic activity (O’Flaherty and Cummins, 2017). This contamination includes also antibiotic resistant bacteria and antibiotic resistance genes, which present a threat to human health, especially in surface waters intended for recreational swimming. In early 1980s, coliform bacteria of genus *Escherichia*, *Klebsiella*, *Citrobacter* and *Enterobacter* isolated from surface water samples were found to possess antibiotic resistance (Niemi et al., 1983). Stange et al. (2016) studied resistance genes in coliform bacteria isolated from river Rhine in Germany demonstrating that surface water is an important reservoir of genes encoding resistance to a wide spectrum of antibiotic classes, such as sulfonamides, tetracyclines and  $\beta$ -lactams. The majority of bacteria originating in seawater are resistant to more than one antibiotic (Baquero et al. 2008).

The object of our work was to monitor antibiotic resistant coliforms, enterococci and coagulase positive staphylococci prevalence in different Slovak surface waters.

## Material and methods

### Characterization of sampling sites

Samples of surface water were obtained from 12 rivers (Table 1), six lakes, two dams and one thermal

bath (Table 2) in the Slovak Republic and one sample was taken from a lake in Austria (Lake Neusiedl) (Table 2). Altogether 24 samples from rivers were tested; however, more sampling sites on the same river were taken on different dates in some cases (samples 1 and 5; samples 13 and 23). Sampling was realized in the summer season 2017 (July–August) and the samples were collected into sterile cold tubes and transferred in a fridge box to the laboratory for microbiological assessment.

**Tab. 1.** Sampling sites of surface water from rivers.

Sample	Sampling site	GPS	Sample	Sampling site	GPS
1	Rudno stream	48° 52' 55.5" N 18° 44' 51.2" E	14	Danube – Devín	48° 10' 13.8" N 16° 58' 56.6" E
2	Hron – near Kame- nica nad Hronom	47° 49' 38.0" N 18° 43' 18.0" E	21	Čierny Hron – Čierny Balog	48° 44' 04.9" N 19° 41' 16.5" E
3	Váh – behind WWTP Trenčín	48° 52' 46.6" N 18° 00' 16.9" E	22	Hron – Kremnička	48° 41' 51.9" N 19° 07' 40.8" E
5	Rudno stream	48° 53' 19.5" N 18° 44' 31.1" E	23	Nitra – Klačno	48° 55' 04.5" N 18° 39' 43.4" E
6	Nitra – Nováky	48° 26' 09.2" N 18° 19' 31.1" E	24	Bebrava – Krušovce	48° 35' 37.9" N 18° 13' 41.9" E
7	Confluence of Danube and Morava – Devín	48° 10' 23.1" N 16° 58' 36.3" E	25	Bebrava – Bánovce nad Bebravou	48° 43' 55.8" N 18° 15' 56.0" E
8	Nitra – Nedožery-Brezany	48° 49' 33.1" N 18° 38' 19.1" E	26	Bebrava – Šípkov	48° 51' 01.0" N 18° 17' 03.4" E
9	Danube – Štúrovo	47° 47' 26.5" N 18° 43' 27.0" E	28	Bočovka – Čierne Klačany	48° 20' 22.4" N 18° 25' 33.5" E
10	Morava – near the confluence of Morava and Thaya	48° 36' 56.9" N 16° 56' 22.2" E	29	Žitava – Vlkaš	48° 07' 34.6" N 18° 16' 13.2" E
11	Nitra – Nitrianske Pravno	48° 52' 25.9" N 18° 38' 29.6" E	30	Leveš – Topolčianky	48° 25' 10.4" N 18° 24' 45.2" E
12	Myjava – near the confluence of Myjava and Morava	48° 37' 42.5" N 16° 57' 29.5" E	31	Nitra – Chalmová	48° 39' 43.8" N 18° 28' 56.6" E
13	Nitra – Klačno	48° 54' 34.9" N 18° 39' 24.8" E	32	Nitrica – Valaská Belá	48° 53' 19.7" N 18° 24' 07.5" E

**Tab. 2.** Sampling sites of surface water from lakes, dams and thermal bath.

Sample	4	15	16	17	18
Sampling site	Orava dam	Zlaté piesky lake	Vajnory lakes	Kuchajda lake	Štrkovec lake
GPS	49° 25' 10.5" N 19° 30' 22.7" E	48° 11' 6.6" N 17° 11' 14.9" E	48° 11' 37.4" N 17° 12' 34.6" E	48° 10' 10.8" N 17° 8' 44.2" E	48° 9' 30.8" N 17° 8' 55.0" E
Sample	19	20	27	33	34
Sampling site	Veľký Draždiak lake	Lake Neusiedl	Nitrianske Rudno	Lake Virt	Thermal bath – Patince
GPS	48° 06' 21.8" N 17° 06' 27.1" E	47° 55' 42.9" N 16° 50' 4.2" E	48° 48' 52.4" N 18° 29' 01.2" E	47° 44' 56.3" N 18° 19' 15.6" E	47° 44' 50.0" N 18° 18' 28.5" E

**Tab. 3.** Final concentrations of applied antibiotics according to EUCAST (EUCAST, 2017).

ATB	Coliform bacteria	Enterococci	Coagulase positive staphylococci
	Resistant breakpoint [mg/L]		
Ampicillin	9	9	3
Ciprofloxacin	1	5	2
Chloramphenicol	9	-	9
Gentamicin	5	129	2
Tetracycline	16*	-	3
Vancomycin	-	5	3

\*tetracycline concentration according to CLSI resistant breakpoints in case of coliform bacteria (CLSI, 2017).

### Detection of antibiotic resistant bacteria

Samples of surface water (10 mL) were filtered through a GH Polypro membrane (0.2 µm, Pall Corporation, USA) placed on antibiotic and antibiotic free selective diagnostic agar plates. Counts of total coliforms were determined on chromogenic Chromocult coliform agar (Merck, Darmstadt, Germany), enterococci were determined on Slanetz-Bartley agar (Himedia, India) and coagulase positive staphylococci on Baird-Parker agar (Sigma Aldrich, St. Louis, USA). Antibiotic resistant strains were detected after cultivation on plates containing diagnostic media with different antibiotics. Before counting bacterial forming units, plates with coliform bacteria and coagulase positive staphylococci were incubated for 24 h at 37 °C and those with enterococci for 42 h at 40 °C. Each experiment was ran in triplicate and it was repeated twice. Applied antibiotics (ampicillin, ciprofloxacin, gentamicin, chloramphenicol, tetracycline, and vancomycin) were purchased from Sigma-Aldrich (Germany). Antibiotic resistance was detected according to European Committee on Antimicrobial Susceptibility Testing (EUCAST, 2017) resistance breakpoints summarized in Table 3. Microorganisms that can grow and multiply at this and higher concentrations of antibiotics are considered as resistant. However, EUCAST did not establish resistance breakpoints for tetracycline, which was applied in diagnostic media for resistance testing in concentration established by the Clinical Laboratory Standards Institute for United States (CLSI, 2017). Data were statistically evaluated by the Student's t test.

## Results and discussion

At present, various pollutants are introduced into the environment mainly by anthropogenic activity. Many of these substances end up in wastewater treated in WWTPs. However, many studies have pointed out that current treatment efficiency of WWTP is insufficient and micropollutants end up in surface waters. Moreover, sub-inhibitory concen-

trations of pharmaceuticals or metals contribute to the spread and development of antimicrobial resistance (Lépesová et al., 2019; Mackuľak et al., 2019; Břošová et al., 2020).

Based on the obvious importance of this issue, surface waters in Slovakia were analyzed focusing on the presence of selected antibiotic resistant bacteria. Surface water samples were taken from various rivers, lakes, dams and one thermal bath in Slovakia. One sample came from a lake in Austria. The samples were taken during the summer season to consider also the exposition of swimmers. Sampling time can greatly affect the detection results. Antibiotic levels in water fluctuate during the year due to increased prescriptions during flu season (February, August), which corresponds with the research of wastewater from WWTPs in Slovakia (Bratislava), when higher concentrations of ciprofloxacin, levofloxacin and norfloxacin were detected in wastewater in February (Birosova et al., 2014).

The number of total coliform bacteria in samples of surface water ranged from 1.74 to 3.69 log CFU/10 mL (Table 4). *Escherichia coli* was observed in 85 % of samples in lower counts (0.3 to 3.1 log CFU/10 mL). The highest number of coliform bacteria was observed in sample 2 from river Hron. The highest amount of *E. coli* was detected in river Hron (sample 22). Enterococci were registered only in 24 samples (70 %) in the range from 0.78 to 3.81 log CFU/10 mL, the highest number was recorded in river Váh behind WWTP Trenčín (sample 3). Coagulase positive staphylococci were present in 91 % of samples in the range of 0.70–3.03 log CFU/10 mL. Coagulase positive staphylococci were observed in 91 % of samples and ranged from 0.70 to 3.03 log CFU/10 mL (Table 4). However, some monitored lakes serve as natural swimming pools during recreational season and water should not exceed some microbial indicators of water quality. According to the Slovak Ministry of Health Decree no. 308/2012 Coll. on the requirements for water quality, water quality control and the requirements for operation, equipment of

**Tab. 4.** Number of total coliform bacteria (TCB), *E. coli* (TEC), enterococci (TE) and coagulase positive staphylococci (TCPS) in samples of surface water from rivers, lakes, dams and thermal bath.

Type of surface water	Sample	TCB	TEC	TE	TCPS	
		log CFU/10 mL				
RIVERS	1	2.98 ± 0.11	ND	2.96 ± 0.20	3.03 ± 0.19	
	2	3.69 ± 0.15	1.90 ± 0.07	3.00 ± 0.15	2.23 ± 0.15	
	3	3.25 ± 0.13	1.00 ± 0.10	3.81 ± 0.24	1.84 ± 0.15	
	5	2.76 ± 0.17	ND	1.71 ± 0.01	1.60 ± 0.08	
	6	3.41 ± 0.10	1.70 ± 0.18	2.65 ± 0.22	1.70 ± 0.11	
	7	3.54 ± 0.21	ND	2.77 ± 0.18	ND	
	8	2.01 ± 0.01	2.24 ± 0.10	2.18 ± 0.15	2.00 ± 0.10	
	9	2.87 ± 0.12	2.43 ± 0.06	2.68 ± 0.12	2.50 ± 0.18	
	10	2.73 ± 0.15	0.30 ± 0.02	2.08 ± 0.12	1.78 ± 0.12	
	11	2.84 ± 0.15	ND	2.86 ± 0.09	ND	
	12	3.52 ± 0.07	1.84 ± 0.11	2.88 ± 0.25	1.63 ± 0.11	
	13	1.74 ± 0.01	ND	2.25 ± 0.13	ND	
	14	2.88 ± 0.05	1.52 ± 0.19	2.13 ± 0.18	1.30 ± 0.07	
	21	3.16 ± 0.17	2.96 ± 0.24	2.00 ± 0.21	1.93 ± 0.10	
	22	3.23 ± 0.12	3.10 ± 0.23	2.43 ± 0.16	1.70 ± 0.15	
	23	2.24 ± 0.11	ND	ND	2.18 ± 0.19	
	24	2.83 ± 0.11	1.40 ± 0.17	ND	2.64 ± 0.10	
	25	2.57 ± 0.10	1.78 ± 0.06	ND	2.47 ± 0.12	
	26	2.18 ± 0.16	ND	ND	1.56 ± 0.18	
	28	2.72 ± 0.21	1.70 ± 0.08	1.00 ± 0.05	2.06 ± 0.24	
	29	2.44 ± 0.19	1.30 ± 0.10	ND	2.80 ± 0.20	
	30	2.60 ± 0.15	1.78 ± 0.05	0.78 ± 0.02	2.42 ± 0.17	
	31	2.72 ± 0.22	1.48 ± 0.03	ND	2.27 ± 0.21	
	32	2.62 ± 0.10	1.00 ± 0.11	ND	2.11 ± 0.26	
	LAKES AND DAMS	4	2.50 ± 0.28	0.60 ± 0.08	1.34 ± 0.12	1.00 ± 0.01
		15	2.34 ± 0.21	ND	1.36 ± 0.19	1.60 ± 0.05
		16	2.45 ± 0.13	1.30 ± 0.13	1.38 ± 0.21	1.70 ± 0.11
		17	2.74 ± 0.10	2.45 ± 0.22	2.52 ± 0.26	1.84 ± 0.15
		18	2.41 ± 0.19	1.54 ± 0.16	1.30 ± 0.19	1.64 ± 0.18
		19	2.70 ± 0.14	2.60 ± 0.11	2.24 ± 0.15	1.34 ± 0.09
		20	3.24 ± 0.29	2.18 ± 0.18	2.77 ± 0.11	2.29 ± 0.07
		27	2.43 ± 0.16	1.60 ± 0.05	ND	1.70 ± 0.17
33		2.97 ± 0.11	ND	ND	1.60 ± 0.10	
34		3.34 ± 0.10	2.00 ± 0.09	ND	0.70 ± 0.18	

ND – not detected

operating areas, premises and facilities at natural and artificial swimming pools, samples 17, 19 and 20 exceeded limits for *E. coli* and enterococci.

**Occurrence of antibiotic resistant coliform bacteria in surface water**

World Health Organization has established a list of antibiotic resistant priority pathogens for which new antibiotics are urgently needed. The group of critical priority includes also the family of

*Enterobacteriaceae* resistant to carbapenems, and/or producing extended spectrum  $\beta$ -lactamases (Taconelli et al., 2018). Thus, antibiotic resistant coliform bacteria from this family was investigated. Bírošová et al. (2014) and Mackuľak et al. (2019) stated that high prevalence of ampicillin resistant coliform bacteria is consistent with frequent prescription of  $\beta$ -lactams in Slovakia. Fig. 1 shows the comparison of monitored surface water samples. In all cases, ampicillin resistant bacteria were observed

in the range from 0.6 log CFU/10 mL in sample 1 (Rudno stream) to 3.01 log CFU/10 mL in sample 22 (Hron – Kremnička). This finding is not very surprising since, except for *E. coli*, most coliforms exhibit intrinsic resistance to this antibiotic. In 12 river samples and five lake samples, also tetracycline resistance was determined. Resistance to other tested antibiotics was registered at much lower rate. Seven rivers and one dam contained coliform bac-

teria resistant to all applied antibiotics. Antibiotic resistant *E. coli* was determined in 21 samples of surface water (Fig. 2). Ampicillin resistance predominated in all samples and ranged from 0.48 log CFU/10 mL in Orava dam to 2.62 log CFU/10 mL in river Hron (sample 22). Watkinson et al. (2007) determined high incidence of tetracycline resistant *E. coli* isolated from various sources of surface waters (including those directly affected by WWTP

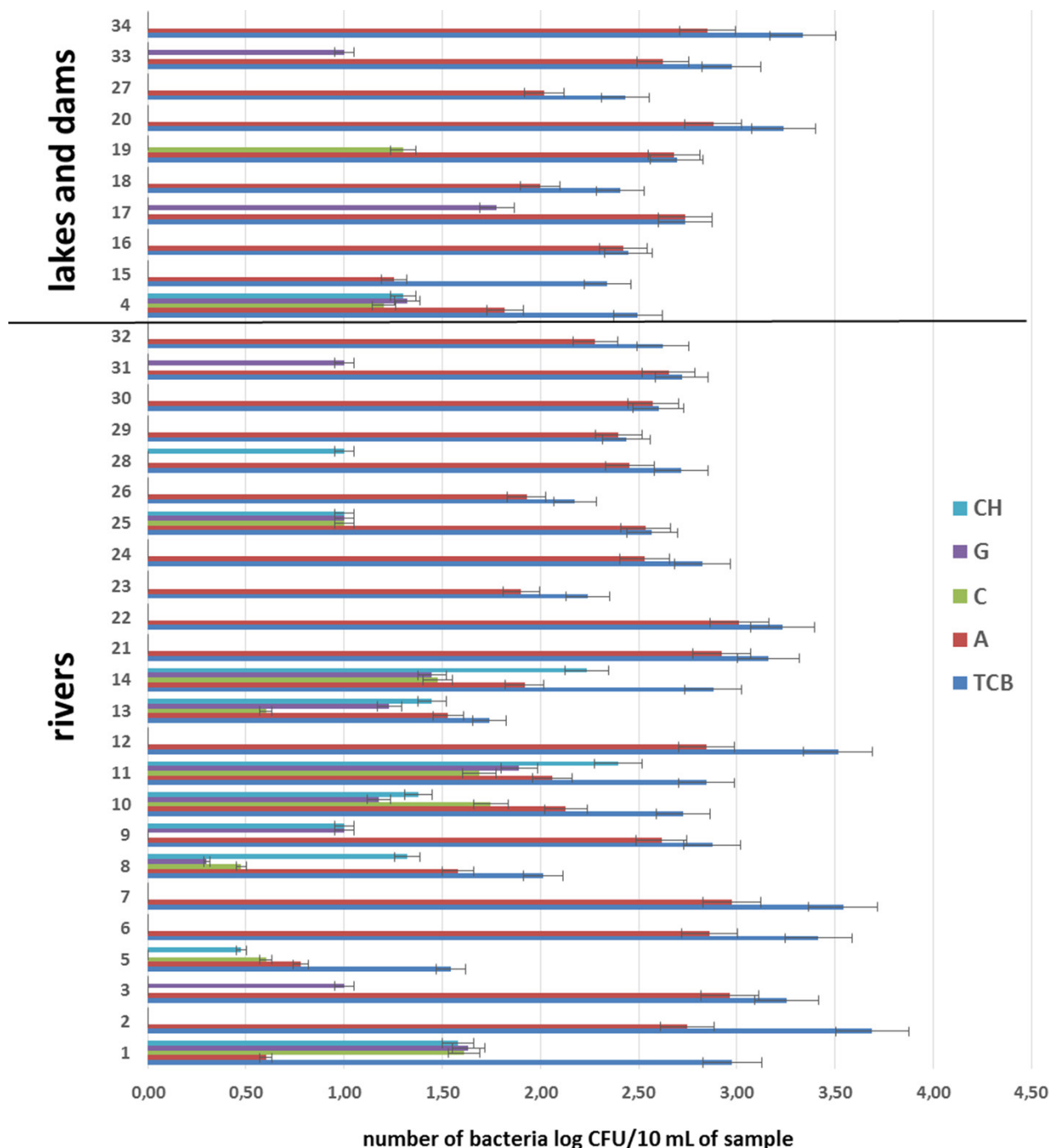


**Fig. 1.** Number of total and antibiotic resistant coliform bacteria in surface water samples from rivers, lakes, dams and thermal bath (TCB – total coliform bacteria, A – ampicillin resistant coliform bacteria, C – ciprofloxacin resistant coliform bacteria, G – gentamicin resistant coliform bacteria, CH – chloramphenicol resistant coliform bacteria).

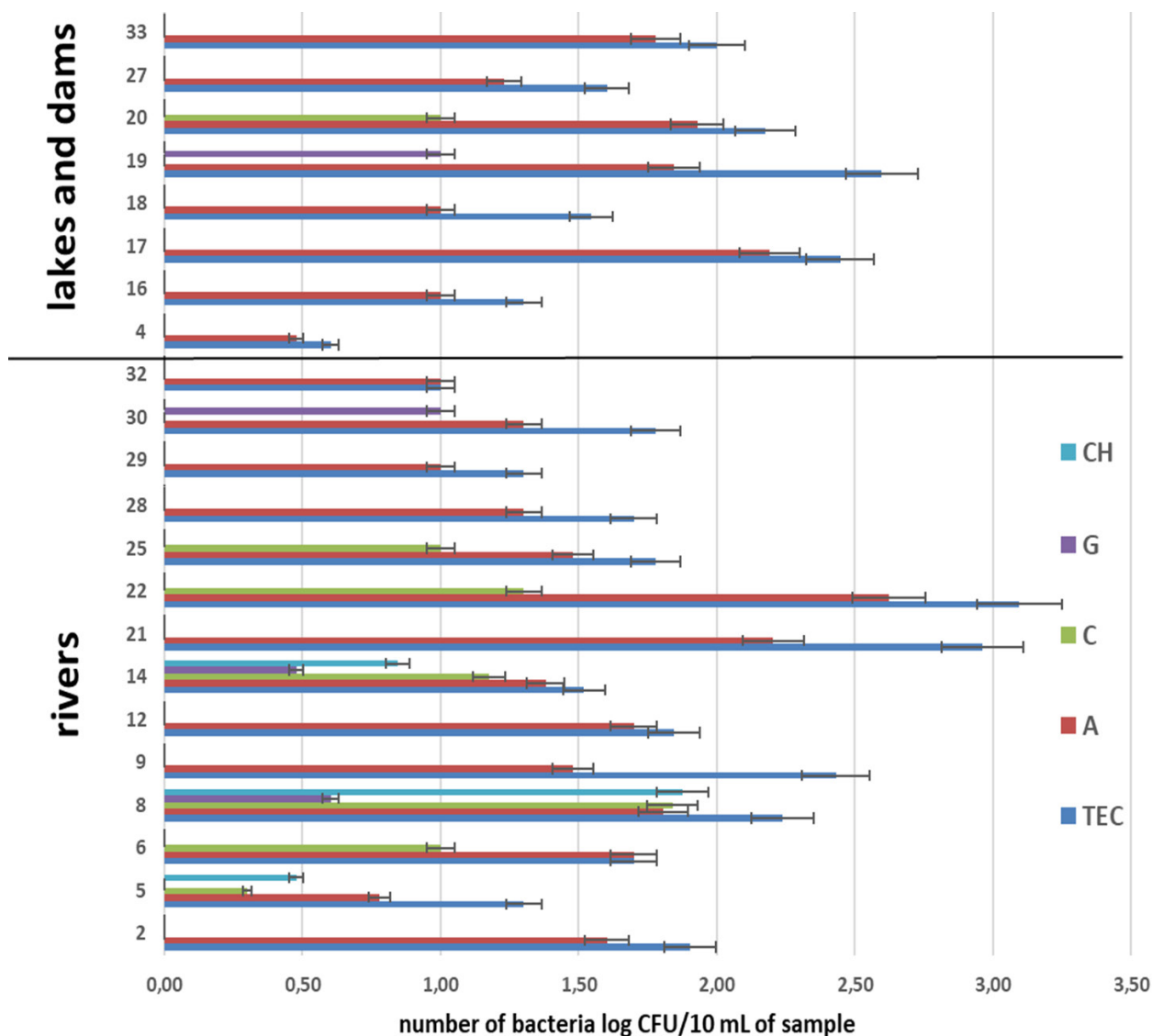


**Fig. 2.** Number of total and antibiotic resistant *E. coli* in surface water samples from rivers, lakes, dams and thermal bath (TEC – total *E. coli*, A – ampicillin resistant *E. coli*, C – ciprofloxacin resistant *E. coli*, G – gentamicin resistant *E. coli*, CH – chloramphenicol resistant *E. coli*).

discharges). This partially corresponds with our results; however, tetracycline resistance was also observed predominantly in river samples. River Nitra – Nedožery/Brezany and Danube – Devín, as well as Orava dam contained *E. coli* resistant to all studied antibiotics.

**Occurrence of antibiotic resistant enterococci in surface water**

In recent years, enterococci, belonging to another group of bacteria with significantly increased resistance, are the second most important nosocomial pathogen. This is probably due to the transfer of resistance genes from non-pathogenic enterococci (commonly found within gut microbiota) to pathogenic species. Enterococci, which were initially relatively multidrug resistant, also became vancomycin resistant. The greatest threat

is the transmission of vancomycin resistance from enterococci to staphylococci as both strains may occur simultaneously in one patient (Mokrý et al., 2013). Compared to coliform bacteria, much more samples contained enterococci resistant to all applied antibiotics (Fig. 3). In case of lakes (Zlaté piesky, Vajnory lakes, Štrkovec lake) and dam (Orava), this can be due to increased traffic and presence of wild animals (especially birds such doves) which are the source of contamination. All samples contained vancomycin resistant enterococci, which are of high priority in WHO priority pathogen list (Taconelli et al., 2018). This also copies the situation with the prevalence of vancomycin resistant enterococci in hospital effluents and wastewater which finally gets into rivers and environment (Schwartz et al., 2003; Novais et al., 2005; Mackufak et al., 2019).

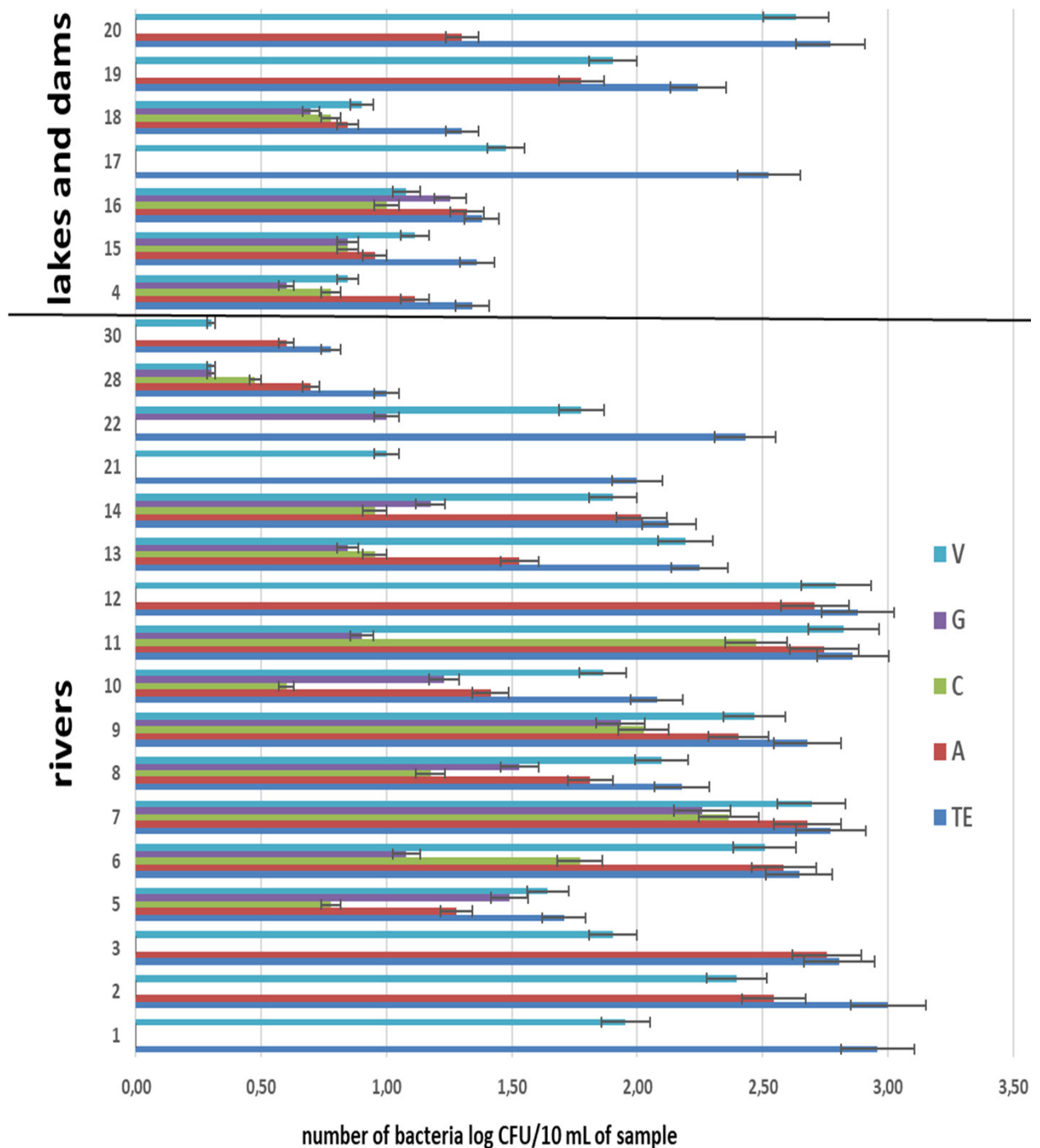


**Fig. 3.** Number of total and antibiotic resistant enterococci in surface water samples from rivers, lakes, dams and thermal bath (TE – total enterococci, A – ampicillin resistant enterococci, C – ciprofloxacin resistant enterococci, G – gentamicin resistant enterococci, V – vancomycin resistant enterococci).

***Occurrence of antibiotic resistant coagulase positive staphylococci in surface water***

Staphylococci belong to potential pathogens forming common skin microbiota of many people. On the other hand, current emergence of antibiotic resistant strains of staphylococci complicates their treatment. One of the most endangering problem is methicillin resistant *Staphylococcus aureus* which displays multi-drug resistance (Yamamoto et al., 2019). Antibiotic

resistant staphylococci were observed only in nine samples of surface water (four rivers and five lakes) (Fig. 4). No sample contained coagulase positive staphylococci resistant to all applied antibiotics. The majority of samples (5) contained chloramphenicol resistant strains. However, the use of this antibiotic in Slovakia is delimited and this phenomenon is probably caused by cross resistance. Surprisingly, no ciprofloxacin resistance was observed.

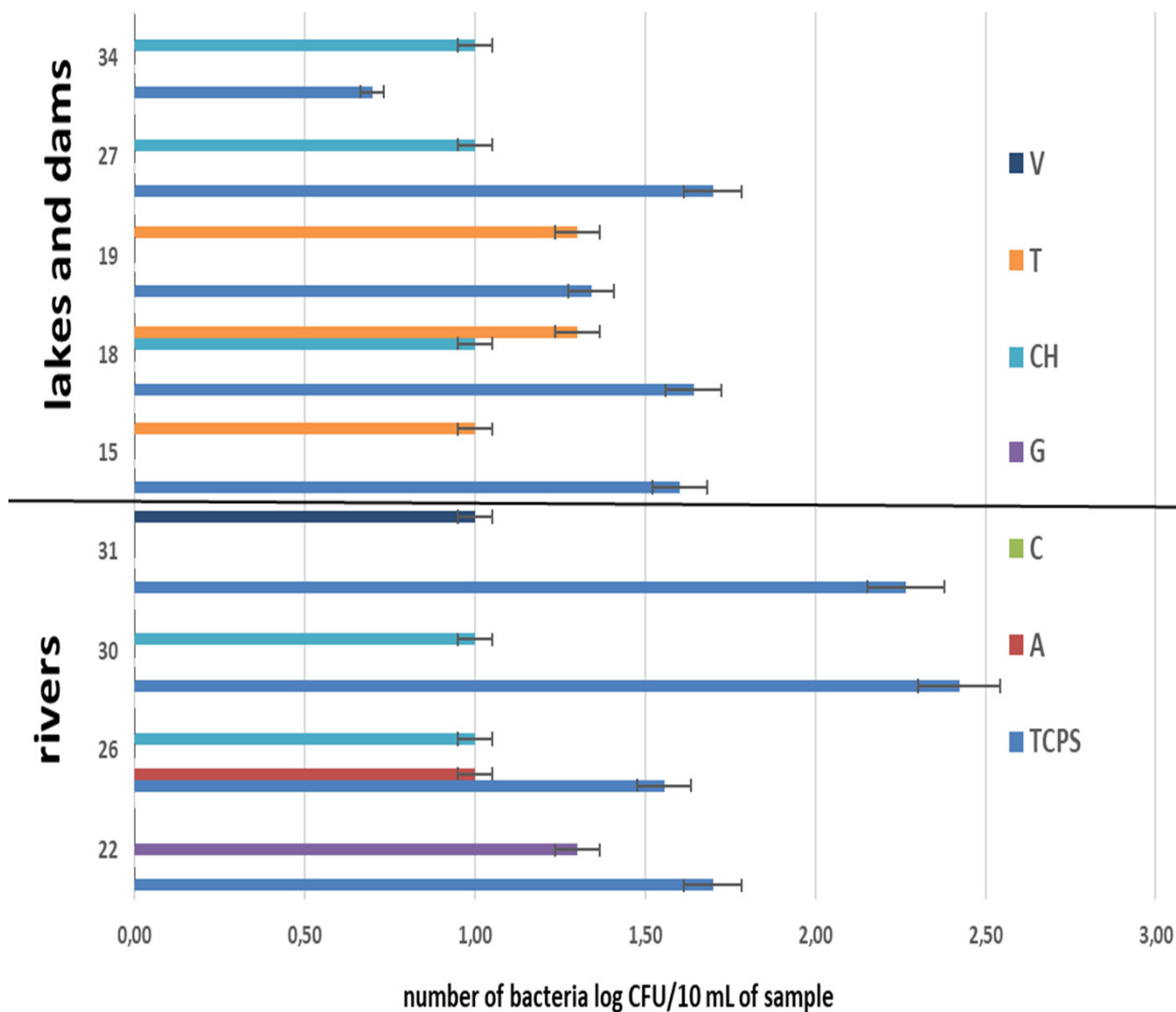


**Fig. 4.** Number of total and antibiotic resistant coagulase positive staphylococci in surface water samples from rivers, lakes, dams and thermal bath (TCPS – total coagulase positive staphylococci, A – ampicillin resistant coagulase positive staphylococci, C – ciprofloxacin resistant coagulase positive staphylococci, G – gentamicin resistant coagulase positive staphylococci, CH – chloramphenicol resistant coagulase positive staphylococci, T – tetracycline resistant coagulase positive staphylococci, V – vancomycin resistant coagulase positive staphylococci).

## Conclusion

Our data show that Slovak surface waters contain different antibiotic resistant bacteria, which can spread resistance genes to other present susceptible microbiota. Some parts of rivers are more microbiologically contaminated, especially near wastewater treatment plants. Our results also point out lakes serving as natural swimming pools during recreational season. In these surface waters, antibiotic resistant bacteria also occur but in lower extent compared to rivers. This contamination is due to higher anthropogenic activity as well as the presence of wild birds, which can contribute to microbiological contamination. During sampling season, three natural swimming pools did

not meet limits for water quality given by Decree 308/2012 Coll.

## Acknowledgments

This work was supported by the Slovak Research and Development Agency under the contract No. APVV-16-0171 and Research grant agency MŠVVaŠ SR and SAV VEGA grant 1/0096/17.

## References

- Aslam B, Wang W, Arshad MI, Khurshid M, Muzammil S, Rasol MH, Nisar MA, Alvi RF, Aslam MA, Qamar MU, Salamat MKF, Baloch Z (2018) Infection and Drug Resistance 11: 1645–1658.
- Baquero F, Martínez J-L, Cantón R (2008) Current Opinion in Biotechnology 19(3): 260–265.

- Berendonk U, Manaia CM, Merlin C, Fatta-Kassinos D, Cytryn E, Walsh F, Burgmann H, Sorum H, Norstrom M, Pons M-N, Kreuzinger N, Huovinen P, Stefani S, Schwartz T, Kisand V, Baquero F, Martinez JL (2015) *Nature Reviews Microbiology* 13 (5): 310–317.
- Birošová L, Mackuľak T, Bodík I, Ryba J, Škubák J, Grabic R (2014) *Science of the Total Environment* 490: 440–444.
- Birošová L, Lépesová K, Grabic R, Mackuľak T (2020) *Environmental Science and Pollution Research* (in press).
- Clinical Laboratory Standards Institute, CLSI (2017) <https://www.sciencedirect.com/science/article/abs/pii/S1473309917307533>
- European Committee on Antimicrobial Susceptibility Testing, EUCAST (2017) Breakpoint tables for interpretation of MICs and zone diameters; Version 7.0 valid from 2017.
- Huerta B, Marti E, Gros M, López P, Popeo M, Armengol J, Barceló D, Balcázar JL, Rodríguez-Mozaz S, Marcé R (2013) *Science of the Total Environment* 456–457: 161–170.
- Lépesová K, Olejníková P, Mackuľak T, Tichý J, Birošová L (2019) *Environmental Science and Pollution Research* 26(18): 18470–18483.
- Ribeiro AR, Nunes OC, Pereira MFR, Silva AMT (2015) *Environment International* 75: 33–51.
- Mackuľak T, Černanský S, Fehér M, Birošová L, Gál M (2019) *Current Opinion in Environmental Science and Health* 9: 40–48.
- Mokrý J, Povrazník I, Váňa J (2013) In: *Vybrané kapitoly z klinickej farmakológie, Antimikrobiálne látky I. – farmakológia*, (pp. 160) Martin: UK, ISBN 978-80-89544-48-6.
- Niemi M, Sibakov M, Niemela S (1983) *Applied and Environmental Microbiology* 45 (1): 79–83.
- Novais C, Coque TM, Ferreira H, Sousa JC, Peixe L (2005) *Applied and Environmental Microbiology* 71: 7 4162.
- O'Flaherty E, Cummins E (2017) *Human and Ecological Risk Assessment: An International Journal* 23(2), 299–322.
- Schwartz T, Kohnen W, Jansen B, Obst U (2003) *FEMS Microbiology Ecology* 43: 325–335.
- Stange C, Sidhu JPS, Tieh A, Toze S (2016) *International Journal of Hygiene and Environmental Health* 219(8), 823–831.
- Stiborová H, Bačáková A, Musilová L, Demnerová K (2018) *Chemické listy*. 2018, roč. 112: 833–839.
- Tacconelli E, Carrara E, Savoldi A, Harbarth S, Mendelson M, Monnet DL, Pulcini C, Kahlmeter G et al. (2018) *The Lancet Infectious Diseases* 18(3): 318–327.
- Watkinson AJ, Micalizzi GB, Graham GM, Bates JB, Costanzo SD (2007) *Applied and environmental microbiology* 73: 5667–5670.
- Yamamoto T, Wan TW, Khokhlova O, Hung WC, Lin YT, Peryanova O, Teng LJ (2019) *Medical University* 2(4).

# Apiin-induction of $\beta$ -apiosidase production by *Aspergillus* sp. strains

Klaudia Karkeszová<sup>a</sup>, Viera Illeová<sup>a</sup>, Peter Kis<sup>b</sup>,  
Vladimír Mastihuba<sup>b</sup>, Milan Polakovič<sup>a</sup>

<sup>a</sup>Department of Chemical and Biochemical Engineering, Institute of Chemical and Environmental Engineering,  
Faculty of Chemical and Food Technology, Slovak University of Technology,  
Radlinského 9, 812 37 Bratislava, Bratislava, Slovakia

<sup>b</sup>Institute of Chemistry, Slovak Academy of Sciences, Dúbravská cesta 9, 845 38 Bratislava, Slovakia  
milan.polakovic@stuba.sk

**Abstract:**  $\beta$ -Apiosidase is a rare glycosidase applied in winemaking for flavour enhancement. This enzyme is involved in the release of volatile terpenes by hydrolysis of their odourless glycosidic precursors. It is found as a minor component in commercial pectinase/cellulase preparations. Microbial production of  $\beta$ -apiosidase was confirmed only during the cultivation of *Aspergillus niger* CBS 554.65 but the high productivity value reported in the work of Dupin et al. (1992) J. Agric. Food Chem. 40(10): 1886–1891 could not be reproduced. The achieved productivity was by far not satisfactory considering the apiin cost. Commercial enzyme preparations with  $\beta$ -apiosidase side-activity thus remain a better alternative as the enzyme source for biocatalytic applications.

**Keywords:**  $\beta$ -apiosidase, *Aspergillus niger*, *Aspergillus aculeatus*, cultivation

## Introduction

The role of aroma compounds in wine has been in the centre of interest for many decades. It is well established that the glycoconjugates of monoterpenes are one of the most influential sources of wine aroma (Mateo and Jiménez, 2000; Maicas and Mateo, 2005; Ruiz et al., 2019). There has been a continuous research on the enhancement of wine quality and aroma by an addition of exogenous enzymes to improve the liberation of a volatile aglycone linked by a glycosidic bound to glucose or disaccharides comprising  $\beta$ -D-glucose at the reducing end (Günata et al., 1988; Williams et al., 1989; Günata et al., 1990; Cabaroglu et al., 2003; Palomo et al., 2005).

In case of disaccharides, the second monosaccharide attached to glucose can be arabinose, rhamnose or apiose. Hydrolysis of disaccharide-containing glycosides takes place in two steps. The mentioned monosaccharides are first released by the action of specific glycosidases. In the second step,  $\beta$ -glucosidase hydrolyses the resultant glucosidic linkage and releases the free aromatic compound (Günata et al., 1988; Günata et al., 1990).

$\beta$ -Apiosidase is a glycosidase involved in the cleavage of apiosylglycosides. Properties, production and purification of this enzyme were intensively studied for the first time in 1990's (Dupin et al., 1992). Depending on grape variety, the level of

apiosylglycosides can reach up to 50 % of the total glycoside content (Mateo and Jiménez, 2000). On the other hand,  $\beta$ -apiosidase is present in very low amounts in the enzymatic systems of grapes and yeast or it is even absent. Hydrolysis of grape glycosides can be therefore enhanced through enrichment of the enzymatic activity by exogenous glycosidases (Günata et al., 1990; Cabaroglu et al., 2003; Sarry and Günata, 2004; Castro Vázquez et al., 2002; Spagna et al., 2002).

Abundant levels of  $\beta$ -apiosidase side activities were identified in some fungi-derived enzyme preparations formulated for their pectinase or cellulase activities. Fungi-originated glycosidases were observed to be more stable in wine pH compared to those of plant origin (Cabaroglu et al., 2003; Sarry and Günata, 2004). Dupin et al. (1992) showed that the production of  $\beta$ -apiosidase by *Aspergillus niger* can be induced by an addition of apiin to the culture medium. Likewise, the presence of Tween 80 (0.15 % v/v) and peptone (2.0 % w/v) also enhanced the synthesis of this glycosidase. The enzyme was partially purified from the culture extract and some of its characteristics were determined. Günata et al. (1997) purified  $\beta$ -apiosidase from an *Aspergillus niger* enzyme preparation and characterised this glycosidase in detail. Guo et al. (1999) achieved tenfold  $\beta$ -apiosidase purification degree from the same preparation. Characteristics of the isolated and purified  $\beta$ -apiosidases are shown in Table 1.

**Table 1.** Properties of isolated  $\beta$ -apiosidases.

Product (Enzyme source)	Specific activity [nkat/mg]	Purification factor	Optimum pH	Optimum temperature [°C]	Ref.
Cultivation supernatant ( <i>A. niger</i> CBS 554.65)	6150	9.4	5.6	50	Dupin et al. (1992)
Klerzyme 200 ( <i>A. niger</i> )	216	27	6	50–60	Günata et al. (1997)
Klerzyme 200 ( <i>A. niger</i> )	1285	270	5	40	Guo et al. (1999)

A renewed interest in  $\beta$ -apiosidase has recently been observed with the aim of investigating its potential in biocatalytic synthesis of specialty chemicals. Kis et al. (2016) examined the occurrence of  $\beta$ -apiosidases in 45 samples of commercial enzyme preparations and in eight samples of plant materials. The enzyme was identified in 16 enzymatic preparations, from which the highest  $\beta$ -apiosidase activity was found in Rapidase AR 2000, Lallzyme BETA, Amano  $\alpha$ -galactosidase DS, Viscozyme L and Novozym 188. All preparations exhibiting  $\beta$ -apiosidase activity originated from *Aspergillus* sp. (Kis et al., 2016). Reaction mechanism of exo-acting  $\beta$ -apiosidase found in Viscozyme L, a product of *Aspergillus aculeatus*, has recently been studied in detail by Mastihuba et al. (2019). Results obtained from experiments using H NMR spectroscopy revealed the inverting mechanism of the enzyme, which is therefore unable to provide transglycosylation reactions. Exo- $\beta$ -apiosidase can anyway find applications not only in terpenyl glycosides hydrolysis but also in lignocellulosic biomass degradation. However, endo- $\beta$ -apiosidase cleaving  $\beta$ -apiosidase bonds in rhamnogalacturonan-II found in gut bacterium *Bacteroides thetaiotaomicron* can reportedly provide the retaining mechanism (Ndeh et al., 2017). Since there is no commercially available  $\beta$ -apiosidase and its activity in commercial pectinase/cellulase preparations is relatively low, the objective of this work was to investigate the potential of two *Aspergillus* strains, *Aspergillus niger* CBS 554.65 and *Aspergillus aculeatus* CBS 101.43, to produce  $\beta$ -apiosidase using plant-isolated apiin as the inducer.

## Materials and methods

### Materials

*Aspergillus niger* CBS 554.65 and *Aspergillus aculeatus* CBS 101.43 were purchased from Westerdijk Fungal Biodiversity Institute (Utrecht, The Netherlands). Enzyme preparation Viscozyme L (protein concentration of 85 g/l as given by the producer), a product of Novozymes (Bagsværd, Denmark), was purchased from Biotech (Trnava, Slovakia). A synthetic substrate, 4-nitrophenyl  $\beta$ -D-

apiosidase, for the detection of  $\beta$ -apiosidase activity was synthesised using the chemoenzymatic procedure described by Kis et al. (2016). Crude apiin (65 % according to HPLC) was prepared by extraction from parsley leaves using a proprietary in-house procedure based on the method of Hulyalkar et al. (1965). Oxoid bacteriological peptone was purchased from Thermo Fisher Scientific Inc. (Waltham, Massachusetts, USA). Tween 80 was obtained from Sigma Aldrich (Steinheim, Germany). Other culture medium and buffer components were of analytical grade and were purchased from Centralchem (Bratislava, Slovakia).

### Cultivation conditions

Purchased lyophilized fungal cultures *Aspergillus niger* CBS 554.65 and *Aspergillus aculeatus* CBS 101.43 were grown on agar plates containing potato dextrose agar at ambient temperature (25 °C). Based on the supplier's recommendations, spore inoculum was collected after three weeks of revitalisation. Suspension of spores was prepared by washing the agar plates by 5 ml of sterilised 0.1 % Tween 80 solution. Total concentration of the harvested spores was determined microscopically by counting them in a Bürker chamber. Composition of the cultivation medium for  $\beta$ -apiosidase production was adopted from Dupin et al. (1992). Experiments were conducted in 50 ml Erlenmeyer flasks containing 20 ml of liquid medium consisting of the following nutrients (% w/v):  $\text{MgCl}_2 \cdot 6\text{H}_2\text{O}$ , 0.1;  $\text{KH}_2\text{PO}_4$ , 0.1; apiin, 1.0; peptone, 2.04; and Tween 80, 0.15 (% v/v). After sterilisation in an autoclave, the flasks were inoculated with  $1 \times 10^6$  spores of fungi and incubated at 30 °C in a rotary shaker at 140 rpm for seven days. The culture broth was centrifuged at 5000 rpm and 5 °C for 15 minutes. Supernatant with the secreted enzyme was filtered through a 0.22  $\mu\text{m}$  polyethersulfone syringe filter. The clear filtrate was used as a source of extracellular enzyme for the assays.

### Enzyme activity assay

$\beta$ -Apiosidase activity in the culture filtrate and Viscozyme L preparation was determined using a

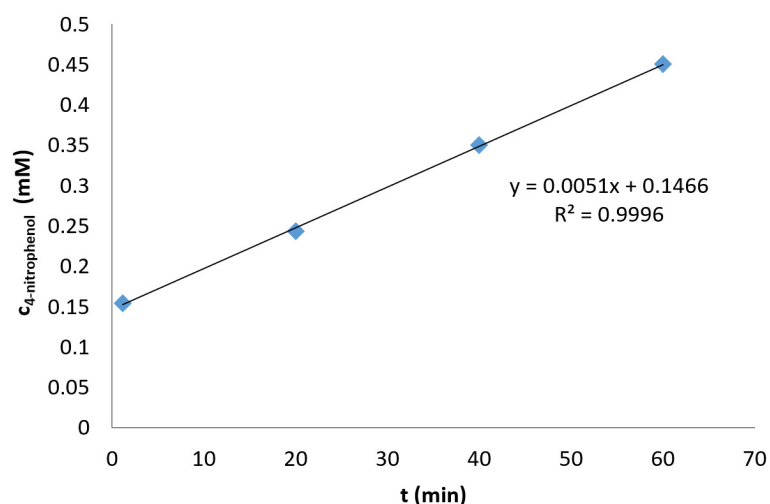


Fig. 1. Apiosidase activity measurement using the initial rate method.

slightly adapted method described by Dupin et al. (1992). The assay was conducted by incubating a properly diluted sample and 2.2 mM 4-nitrophenyl  $\beta$ -apiofuranoside in a 0.1 M acetate buffer (pH 4.4) at 40 °C. The reaction was initiated by adding the enzyme solution to the synthetic 4-nitrophenyl substrate in the volumetric ratio of 1:1.  $\beta$ -Apiosidase activity was determined using the initial reaction rate method (Fig. 1). Samples at different time intervals were withdrawn from the assayed mixture in 20-minute intervals and added to 0.1 M  $\text{Na}_2\text{CO}_3$  to stop the reaction. Concentrations of the released 4-nitrophenol were evaluated from the absorbance measured at 405 nm. The activity was expressed in nanokatals per volume of the enzyme sample.

#### Protein assay

Total protein concentration was estimated according to the bicinchoninic acid (BCA) assay. Suitably diluted aliquots of culture filtrate were used for the determination in microplates. Formation of a purple-coloured complex was measured at 562 nm after 30 minutes of incubation at 37 °C. Bovine serum albumin was used as a protein standard.

## Results and discussion

The main motivation for this work was the disparity between the  $\beta$ -apiosidase activity in nowadays enzyme preparations reported in the paper of Kis et al. (2016) and that reported in selected 1990's papers (Table 1). As it follows from Table 1, crude preparation of Klerzyme 200 had the activity of 5–8 nkat/mg. Table 2 shows that Viscozyme L, selected as the best enzyme source by Kis et al. (2016) considering its price and availability has the specific activity by one order of magnitude lower. It is difficult to interpret this difference by the former

preparation being obtained by *A. niger* cultivation whereas the latter one is a product of *A. aculeatus*. Kis et al. (2016) examined 13 commercial enzyme preparations of *Aspergillus* species and all but one *A. niger* preparation showed no  $\beta$ -apiosidase activity. However, the last one, Novozym 188, had the second highest activity after Viscozyme L. Variation of the  $\beta$ -apiosidase side-activity by two orders of magnitude in this kind of preparations is thus common.

Since these commercial preparations are rather crude protein concentrates, it can be expected that  $\beta$ -apiosidase specific activity was not significantly reduced during downstream processing. Specific activity in the corresponding cultivation broth could be very similar. From this point of view, the results of *A. niger* laboratory cultivation presented by Dupin et al. (1992) are striking. As shown in Table 1, they achieved a specific activity of more than 6,000 nkat/mg at a small purification degree. The corresponding  $\beta$ -apiosidase specific activity in the cultivation broth was about 650 nkat/mg. An interesting aspect of the work of Dupin et al. (1992) is that, without induction by apiin, no detectable  $\beta$ -apiosidase activity was observed for any of the four investigated *A. niger* strains. Moreover, they found that the enzyme yield increased 50-fold when the basal medium was supplemented with peptone as nitrogen source and surfactant improving the enzyme release from cells.

These results inspired the investigation of the option of preparing sufficient amount of  $\beta$ -apiosidase for the respective biocatalytic research. Two strains, *Aspergillus niger* CBS 554.65 and *Aspergillus aculeatus* CBS 101.43, were selected for this purpose. The former one was used by Dupin et al. (1992) and the latter one was probably used to produce Viscozyme L since this strain is typically found in patents filed

by Novozymes (Dörreich et al., 1993). Optimal conditions for induced  $\beta$ -apiosidase production were adopted from the work Dupin et al. (1992). A medium with the concentration of crude apiin of 1.0 % w/v was used.

Unfortunately, the cells of *A. aculeatus* CBS 101.43 were unable to grow in the chosen medium. Evidently, apiin is not a convenient carbon source for this strain. Consequently, the work focused on the cultivation of *A. niger* CBS 554.65. The cultivation was carried out for seven days. The cell biomass was subsequently removed from the culture broth by centrifugation and  $\beta$ -apiosidase activity in the supernatant was determined by the initial reaction rate. Table 2 shows that the final value of  $\beta$ -apiosidase activity was 0.79 nkat/ml, which is remarkably lower than the values of 200–300 nkat/ml declared by Dupin et al. (1992). It should however be emphasised that more typical values of  $\beta$ -apiosidase activity of about 3–4 nkat/ml were achieved due to the induction by apiin. The enormous increase of the mentioned values was achieved only by the change of the nitrogen source and surfactant permeabilisation of cell membrane. It is also interesting that substitution of the laboratory grade apiin with a very crude apiin source, parsley seeds, resulted in the activity decrease to several nanokatals per millilitre.

Thus, lower purity (about 65 %) of used apiin is a potential reason of lower levels of apiosidase activity in our experiments. On the other hand, apiin purification costs are very high. Several chemical suppliers currently offer 95–99 % apiin from 5 €/mg to 220 €/mg depending on the package size. The lowest unit price is for 100 mg package. Considering the optimal apiin concentration of 1 %, even the best price results in the apiin cost of 30,000 €/l of cultivation medium. Obviously, this cost is simply unaffordable. A cultivation experiment was made using 1.0 % glucose as the carbon source instead of apiin but it did not provide a positive result. As it was also observed by Dupin et al. (1992), *A. niger* CBS 554.65 cells cannot produce  $\beta$ -apiosidase when they grow on glucose.

**Tab. 2.**  $\beta$ -Apiosidase activity in examined enzyme preparations.

Enzyme preparation	Activity (nkat/ml)	Specific activity (nkat/mg)
<i>A. niger</i> CBS 554.65 cultivation broth	0.79	>0.2*
Viscozyme L	29	0.3

\*Due to the interference of residual peptone, the measured protein concentration can be overestimated.

As it follows from Table 2, cultivation using crude apiin resulted in  $\beta$ -apiosidase specific activity comparable to that of Viscozyme L but in a much less concentrated form. The idea of overproduction of this desired enzyme via apiin induction thus appears less advantageous. Viscozyme L produced by *Aspergillus aculeatus* represents an available and economical source of  $\beta$ -apiosidase. It can be a suitable source for further purification to obtain a biocatalyst free of undesired enzymatic activities.

## Conclusions

Induced production of  $\beta$ -apiosidase by two strains of filamentous fungi of the genus *Aspergillus* was examined. *Aspergillus aculeatus* CBS 101.43 was not able to grow in the cultivation medium optimised by Dupin et al. (1992) for the overproduction of  $\beta$ -apiosidase by a strain of *Aspergillus niger*. This fact is fully understandable since the composition of nutrients in the medium can be very specific for each strain. The second investigated strain, *Aspergillus niger* CBS 554.65, exhibited induction of  $\beta$ -apiosidase production by apiin but the level of apiosidase activity was not sufficiently high probably due to the use of crude apiin. On the other hand, very high cost of pure apiin makes this approach to the  $\beta$ -apiosidase production not feasible. Thus, the use of commercial enzyme preparations with  $\beta$ -apiosidase side activity identified in two dozens of enzyme preparations by Kis et al. (2016) is a better alternative.

## Acknowledgement

This work was supported by grants from the Agency of the Ministry of Education, Science, Research and Sport of the Slovak Republic for Structural Funds of EU (Grant number: ITMS 26240220071) and the Slovak Research and Development Agency (Grant numbers: APVV-16-0111 and APVV-18-0188).

## References

- Cabaroglu T, Selli S, Canbas A, Lepoutre JP, Günata Z (2003) Enzyme Microb. Technol.
- Dörreich K, Christensen FM, Schnell Y, Mischler M, Dalbøge H, Heldt-Hansen HP (1993) WO 93/20193.
- Dupin I, Günata Z, Sapis JC, Bayonove C, M'Bairaroua O, Tapiero C (1992) J. Agric. Food Chem. 40(10): 1886–1891.
- Günata Z, Bitteur S, Brillouet JM, Bayonove C, Cordonnier R (1988) Carbohydr. Res. 84: 139–149.
- Günata Z, Bayonove CL, Tapiero C, Cordonnier RE (1990) J. Agric. Food Chem. 38(5): 1232–1236.
- Günata Z, Dugelay I, Vallier MJ, Sapis JC, Bayonove C (1997) Enzyme Microb. Technol. 21(1): 39–44.
- Guo W, Salmon JM, Baumes R, Tapiero C, Günata Z (1999) J. Agric. Food Chem 47(7): 2589–2593.

- Hulyalkar RK, Jones JKN, Perry MB (1965) *Can. J. Chem.* 43: 2085–2091.
- Kis P, Potocká E, Mastihuba V, Mastihubová M (2016) *Carbohydr. Res.* 430: 48–53.
- Maicas S, Mateo JJ (2005) *Appl. Microbiol. Biotechnol.* 67: 322–335.
- Mastihuba V, Karnišová Potocká E, Uhliariková I, Kis P, Kozmon S, Mastihubová M (2019) *Food Chem.* 274: 543–546.
- Mateo JJ, Jiménez MJ (2000) *J. Chromatogr.* 881(1–2): 557–567.
- Ndeh D, Rogowski A, Cartmell A, Luis AS, Baslé A, Gray J, Venditto I, Briggs J, Zhang X, Labourel A, Terrapon N, Buffetto F, Nepogodiev S, Xiao Y, Field RA, Zhu Y, O’Neil MA, Urbanowicz BR, York WS, Davies GJ, Abbott DW, Ralet MC, Martens EC, Henrissat B, Gilbert HJ (2017) *Nature.* 544(7648): 65–70.
- Palomo ES, Hidalgo MDM, Gonzalez-Vinas MA, Pérez-Coello MS (2005) *Food Chem.* 92(4): 627–635.
- Ruiz J, Kiene F, Belda I, Fracassetti D, Marquina D, Navascués E, Calderón F, Benito A, Rauhut D, Santos A, Benito S (2019) *Appl. Microbiol. Biotechnol.* 103: 7425–7450.
- Sarry J, Günata Z (2004) *Food Chem.* 87(4): 509–521.
- Spagna G, Barbagallo RN, Greco E, Manenti I, Pifferi PG (2002) *Enzyme Microb. Technol.* 30(1): 80–89.
- Williams PJ, Sefton MA, Wilson B (1989) *ACS Sym. Ser.* 35–48.

# Carbon family nanomaterials – new applications and technologies

Petra Roupčová<sup>a</sup>, Karel Klouda<sup>a</sup>, Paula Brandeburová<sup>b</sup>, Rastislav Šipos<sup>c</sup>,  
Jan Hives<sup>d</sup>, Miroslav Gal<sup>d</sup>, Tomas Mackulak<sup>b</sup>, Michaela Skrizovská<sup>a</sup>, Lenka Kissiková<sup>a</sup>

<sup>a</sup>VSB – TU Ostrava, Faculty of Safety Engineering, Lumírova 13, 700 30 Ostrava – Vyskovice

<sup>b</sup>Department of Environmental Engineering, Faculty of Chemical and Food Technology,  
Slovak University of Technology, Radlinského 9, 812 37, Bratislava

<sup>c</sup>Department of Inorganic Chemistry, Faculty of Chemical and Food Technology,  
Slovak University of Technology, Radlinského 9, 812 37, Bratislava

<sup>d</sup>Department of Inorganic Technology, Faculty of Chemical and Food Technology,  
Slovak University of Technology, Radlinského 9, 812 37, Bratislava  
petra.roupcova@vsb.cz

**Abstract:** Research on carbon-based nanomaterials (CBNMs) and their development is one of the major scientific disciplines of the last century. This is mainly because of their unique properties which can lead to improvements in industrial technology or new medical applications. Therefore, it is necessary to examine their properties such as shape, size, chemical composition, density, toxicity, etc. This article focuses on the general characteristics of nanomaterials (NMs) and their behavior when entering the environment (water and soil). In addition, it presents individual members of the graphene family including porous ecological carbon (biochar). The article mainly deals with the new potential technologies of CBNMs considering their possible toxic and genotoxic effects. This review also highlights the latest developments in the application of self-propelled micromotors for green chemistry applications. Finally, it points to the potential biomedical applications of CBNMs.

**Keywords:** biochar, ecology, biosensors, graphene family, nanostructures, micromotors

## Introduction

With the intensive use of nanoparticles, it has been shown that many of them may have negative effect on human health and the environment. Manufactured nanoparticles are likely to be more damaging than particulate matter of the same materials but with conventional size as they, for

example, penetrate deeper into the lungs due to their ‘nano’ size (Liu et al., 2014). There is still a lack of information about the interactions of nanoparticles with biological systems; therefore, the research in this field is essential (Bakand et al., 2012).

NMs are an innovative science discipline that has grown steadily and has gained interest of the general

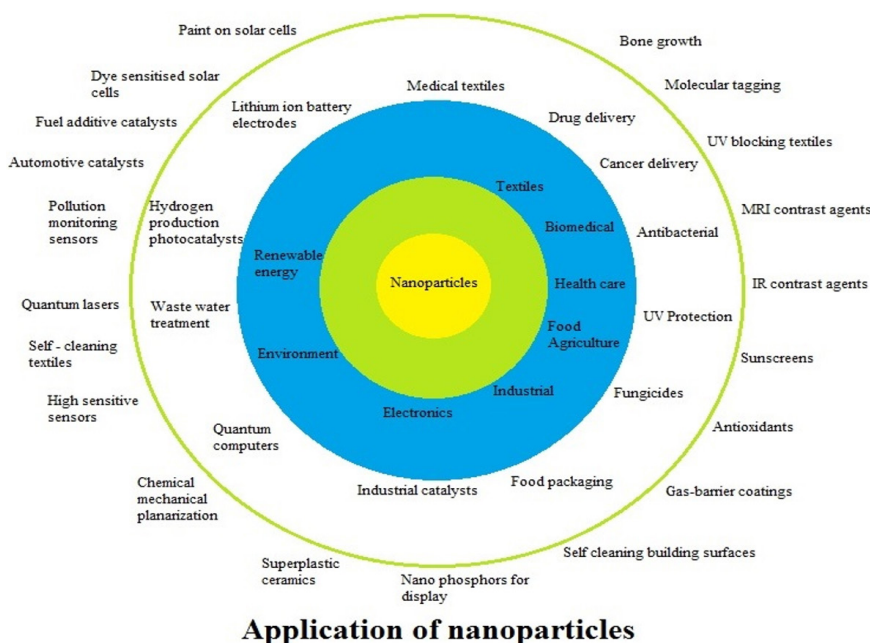


Fig. 1. Potential applications of carbon-based nanomaterials (Garcia, 2017).

public due to various reasons such as the high number of new materials produced by synthesis, improved techniques for their characterization and diverse applications across a wide range of disciplines (Fig. 1).

This article describes the members of the graphene family and provides their brief characteristics. It also deals with new potential applications of CBNMs, such as graphene oxide (GO), graphene, and their other hybrid modifications with other materials – biochar, composites/oxides of metals etc. The review highlights the last development in the application of self-propelled micromotors and the treatment of cancer considering toxicity and genotoxicity of graphene nanoparticles.

## Characteristics of NMs and CBNMs

### *Nanoparticles and their general characteristics*

**Each type of nanoparticle, in addition to its dimension within 1 to 100 nm, can be described by the following characteristics (Ju, 2018):**

- chemical composition,
- functional groups on the surface (hydrophilicity, lipophilicity),
- shape,
- distribution layout of particles,
- density,
- crystalline structure,
- zeta potential,
- ability of aggregation, agglomeration, and sedimentation (Terrones et al., 2012).

With these properties they enter the external environment (Loureiro et al., 2018). In air, the so-called abiotic impact factor takes effect; it may comprise

temperature, humidity, salinity, solar radiation, smog, pollutants of inorganic and organic origin etc. In an aqueous medium, physico-chemical characteristics of the aqueous phase have to be considered: ground water, surface water, river and sea water, temperature, pH, ionic strength, concentration ions, concentration of natural organic matter, and composition of the sediment (Terrones et al., 2012).

Surface water may be considered as one of the main points of entry, facilitating dispersion of NMs in the environment and establishing a link to other parts of environment such as soil, sediment, and biota. Factors influencing the fate of nanoparticles in an aqueous medium are (Baun et al., 2017; Freixa et al., 2018):

- surface hydrophilicity (water solubility),
- hydrolysis, redox reactions,
- adsorption (plays an important role in C-nanoparticles) (Kyzas et al., 2014),
- aggregation,
- hetero-aggregation,
- presence of aquatic organisms (bacteria, algae, protozoa, plankton, larvae, fish, etc.),
- sedimentation rate,
- composition of sediment and its reactivity (adsorption, reduction by phytoextracts and biological material, presence of soil organic matter, presence of polyaromatic hydrocarbons pollutants, hetero-aggregation, etc.) (Kyzas et al., 2014) see Figure 2.

Also in soil, the physico-chemical characteristics have to be taken into account. The solid phase contains minerals of different grains (considering the content of the 0.01 mm fraction) and organic soil

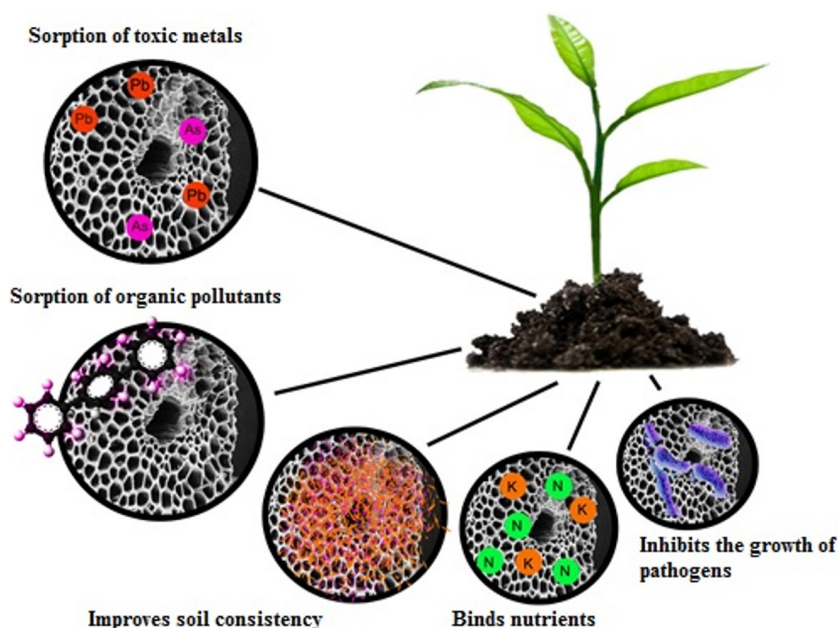


**Fig. 2.** Effect of biochar in soil.

components (Theng and Yuan, 2008). The basis of this matter are humic substances, i.e. mixtures of polydisperse compounds with high molecular weight and aromatic and aliphatic parts with functional groups —COOH, —OH, phenolic —OH, —NH<sub>2</sub>, N-heterocycles, etc. (Theng and Yuan, 2008). Basic partitioning of humic substances is according to solubility in relation to pH: fulvic acids are soluble in water, humic acids in alkaline environment, and humine is insoluble (Theng and Yuan, 2008). Soil water, also known as the soil solution, can contain fulminic acids, phytoextracts and substances with polyphenol structures, glycidic ions etc. Thanks to the soil solution, the influence caused by nanoparticles is similar as in case of an aqueous medium.

Main factors influencing the fate of nanoparticles in the soil environment are (Loureiro et al., 2018; Freixa et al., 2018):

- surface hydrophilicity and lipophilicity,
- hydrolysis,
- reduction (green reduction by substances from phytoextracts),
- hetero-aggregation (clay soils),
- presence of soil micro-organisms and animals (bacteria, larvae, earthworms, etc.),
- adsorption ( $\pi$ -binding interactions, hydrogen bonds, electrostatic interaction, acid-base interaction).

Environmental behavior and effects of CBNMs in natural aquatic systems are related to their ability to interact and aggregate, creating clusters exhibiting colloidal behavior. Despite the virtual water insolubility of individual CNM molecules, the formed aggregates are stable under certain environmental conditions. To put it simply, transport and fate of carbon nanoparticles can be divided into three main possible effects that can exist independently, intermingle or coexist in synergy (Freixa et al., 2018):

- modification of nanoparticles (adsorption plays the main role here),
- change in the composition of nanoparticles (mutual reaction of functional groups with organic or inorganic substances),
- degradation of nanoparticles (physical, chemical, or biological) (Zhao et al., 2014).

The question remains as to how the future fate, transport, and mainly toxicity of these nanoparticles changes after degradation or the change of functional groups on their modified surface. One of the least inert NMs to the environment seems to be graphene oxide (Zhao et al., 2014). Its strong adsorption capacity, propensity to biological reduction, reactivity of its functional groups on the carbon skeleton (Park and Yan, 2013; Shanmugaraj et

al., 2013), and lastly the ease of photochemical degradation (Shanmugaraj et al., 2013) have already been described. Interaction of GO and graphene with cell membrane can lead to indirect toxicity, i.e. blocking of ions and gases exchange. Their internalization into cells can cause oxidative stress, DNA damage as well as mitochondrial malfunction (Zhao et al., 2014).

### **Graphene based NMs**

Graphite is a natural laminated compound with sp<sup>2</sup> hybridization and the distance between the layers of 338 pm (Seabra et al., 2014; Lin et al., 2016). The plane graphite layer is formed by six-C-cycles; among other things, it is possible to prepare a series of compounds with carbon skeleton from this natural compound. Graphite can be intercalated, fluorinated, oxidized or exfoliated. Intercalation allows the formation of an inter-layer space, into which, e.g. alkali metals or volatile halogens can be intercalated. The interchange force is the exchange of electrons between the carbon layer and the intercalated substance (Lin et al., 2016). The so-called graphene family includes: fluorine graphite (CF), GO, reduced graphene oxide (rGO), graphene, multilayer graphene, single and multi-walled carbon nanotubes (SWCNT, MWCNT), fullerenes (ex. C<sub>60</sub>), carbon quantum dots (CQDs) and porous carbon (biochar). Graphite exfoliation (spherical grinding, sonication, dynamic fluid shear forces) results in the formation of graphene (one plane carbon layer) with a honeycomb structure: -C- hexagons in a plane (Zhao et al., 2014). Under certain conditions it can be doped, and therefore it is possible to partially replace carbon for N, S, B, or P (Hu and Sun, (2013).

GO is prepared by graphite oxidation by strong oxidizing reagents; it serves as a precursor for the chemical preparation of graphene (Zhang et al., 2011). Its carbon skeleton contains the main functional groups such as carboxyl-, carbonyl-, epoxide-, etheric- and hydroxy-groups. Using the functional groups, GO functionalization can be realized chemically e.g. by amidation, esterification, or substitution (Kyzas et al., 2014). GO can also be non-covalently functionalized e.g. with biomolecules, where  $\pi$ - $\pi$ , cation- $\pi$ , anion- $\pi$ , and hydrogen bridges interactions are formed. It also serves as a deposit for nanoparticles of metals and their oxides (Kyzas et al., 2014). It can be applied as a composite in a series of polymers. All of this affects its application options. Non-covalent interactions are used in the preparation of composite biopolymers (Yoo et al., 2014) using the adsorption and absorptive ability of GO (Kyzas et al. 2014; Chabot et al., 2014; Fakhri, 2017). Graphene oxide has unique characteristics

such as electronic, magnetic, optical, and thermal (Xu et al., 2013; Paulchamy et al., 2015), it is also an electrical insulation material, hygroscopic and dispersible (Paulchamy et al., 2015). By selecting a processing technology, various modifications of GO in suspension can be obtained, such as quantum dots (Chien et al., 2012) or films applied in biology (Paredes et al., 2013), electrical applications (Zhu et al., 2012) optics (Xu et al., 2013) and biomedicine (Fernandez-Merino et al., 2010; Sanchez et al., 2012); Zhang et al., 2016), as well as fibers (Shahil and Balandin, 2012). Graphene-based NMs also belong to the one of the most promising modifications of electrode surfaces resulting in impressive properties of advanced electrochemical sensors in biomedical application (Stanković et al., 2017; Svítková et al., 2016).

The publications concerning the oxidation of graphite with a view to obtain GO mostly state that a method was used bearing the names of particular authors: Hofmann ( $\text{HNO}_3$ ,  $\text{KClO}_3$ ), Tour ( $\text{P}_2\text{O}_5$ ,  $\text{KMnO}_4$ ), Hummers ( $\text{NaNO}_3$ ,  $\text{KMnO}_4$ ) (Seabra et al., 2014). In all these methods the reactive environment is concentrated sulphuric acid (Chng and Pumera, 2013).

After oxidation, GO has on its carbon skeleton the above mentioned oxygen functional groups that can be reduced by a number of agents (methods) affecting the C/O ratio and the diversity in reduced groups; e.g. hydrazine reduces preferably epoxy groups,  $\text{NaBH}_4$  reduces  $-\text{C}=\text{O}$  and  $-\text{COOH}$ . The most commonly used reducing agents are  $\text{NH}_2\text{NH}_2$  (Ramesha et al., 2011),  $\text{NaBH}_4$  (Chua and Pumera 2013), metal-acid (Agharkar et al. 2014), HI, polyphenols (chinons), polysaccharides, “green” reduction – plant extracts (Agharkar et al. 2014; Roupцова and Klouda, 2017), ascorbic acid (Paredes et al., 2013),  $\text{FeSO}_4$ , bacteria (Wang et al., 2011); the methods used include: thermal, hydrothermal and electrochemical reduction (Chua and Pumera, 2013). Partially reduced graphene oxide is marked rGO and is used in a variety of applications, mostly as the combination of GO/rGO. Total reduction of oxygen-containing groups provides graphene (Chng and Pumera, 2013).

Current publications include articles describing common oxidation of graphite with fullerene ( $\text{C}_{60}$ ), CF, or biochar to create a unique hybrid product with different weight ratios (Roupцова et al., 2017; Zhang et al., 2009). In addition, these syntheses have been enriched with the combined oxidation of graphite with MWCNT (Roupцова and Klouda, 2017).

Fullerenes are wide closed-cage carbon clusters with extraordinary properties (Notariani et al., 2016). They were discovered in 1985 and belong to

the group of carbon allotropes (3<sup>rd</sup>) after graphite (1<sup>st</sup>) and diamond (2<sup>nd</sup>). Fullerene  $\text{C}_{60}$  (so far the most stable form) named after Buchmister Fuller, who built buildings in the shape of domes resembling a soccer ball (bucky ball) (Sharma et al., 2015). Many techniques to synthesize fullerenes have been introduced: laser ablation of graphite + He; AC arc discharge of graphite + gas (He, Ar), combustion of benzene ( $\text{O}_2$ ), chemical synthesis and introduction of dopants inside the structure (Lee et al., 2002; Saunders et al., 1994).

Fullerenes possess excellent stability, large specific surface area, superior electrical conductivity, and individual three-dimensional structure. One of the major applications of fullerenes is photocatalysts (pollutants degradation, production of hydrogen, antibacterial, water disinfection) (Pan et al., 2020). From the biomedical applications, fullerenes are known as antioxidants, drug delivery and antiviral agents (against flu viruses, herpes simplex virus (HSV), human immunodeficiency virus (HIV) and cytomegalovirus (CMV)) (Pochkaeva et al., 2020).

The structure, shape and the emergence of carbon nanotubes (CNT) can be pictured as a graphene plane rolled in the direction of two possible vectors. This will arrange the tubes with mutual arrangements of six-member-C-circles into the structure of: chair, zigzag, or chiral. According to the number of layers, the carbon tubes can be divided into single-walled and multi-walled types (Lee et al., 2012). The basic preparation consists of the deposition of chemical vapor using the CVD method at high temperatures (500–900 °C), depending on the organic material and the catalysis by various metals (Lee et al., 2012). Rolling of the carbon plates can also be carried out under normal laboratory conditions from graphene oxide in a strongly acidic environment and in the presence of ferrocene aldehyde (Calvaresi et al., 2013). The surface of carbon nanotubes can be functionalized to form covalent bonds between the surface of the nanotubes and the substituent, non-covalent ones by modification with a macromolecule (hybrid, composite), or by physical adsorption of molecules on the surface of the nanotube (Calvaresi et al., 2013). Reactions that allow covalent bonding on the nanotube include:

- oxidation (in solution, gaseous phase, plasma),
- halogenation (iodination, bromination, chlorination, fluorination by reaction with  $\text{BrF}_5$ ,  $\text{XeF}_2$ ),
- reaction with diazonium salts ( $\text{ArN}^{2+}$ ) (Calvaresi et al., 2013).

Non-covalent modification of nanotubes is predominantly provided by  $\pi$ - $\pi$  interactions,  $\pi$ -stacking, electron transfer, hydrophobic interaction with pyrene derivatives, polymer composites, or

composites with biological molecules, DNA, proteins, etc. This type of reaction may include graphene rGO-MWCNT composites. Published preparations of these composites comprise mixing of graphene oxide and MWCNT in a certain weight ratio; sonication and subsequent reduction by hydrazine (Woo et al., 2012), ferrous sulfate (Kabiri et al., 2014), ascorbic acid (Chartarawayadee et al., 2013), or i-propanol under  $\gamma$ -radiation  $^{60}\text{Co}$  (Sun et al., 2014).

The thus-prepared composites, rGO-MWCNT, can be used in super-capacitors (Sun et al., 2014) or, after morphological treatment, as an ideal adsorbent for organic substances, especially oils (Kabiri et al., 2014). Modern applications of carbon nanotubes utilize their ability to behave as a unique nano-reactor. In such nano-reactor, i.e. within the carbon nanotubes, the concentration of chemical reactants increases thereby increasing the reaction rate; the charge transfer effects are reflected in the reduction of free activation energy, and the arrangement of the molecules allows the reaction to be directed in the desired direction (Miners et al., 2016). Electron transmission also affects catalytic activity. Metal nanoparticles of Ni, Fe, Pd, Pt, Ru, Co, and Cu (Miners et al., 2016; Wang et al., 2012) are often used as catalysts, adsorbed on the carbon surface (Miners et al., 2016). Several hydrogenation reactions, synthetic gas conversions, ammonia synthesis or decomposition, oxidation reaction, etc. (Miners et al., 2016) have been realized in this way.

GO, graphene, hybrid compounds, composites, and porous carbon (biochar) have the following applications:

- adsorption materials (absorbents) for metal ions, organic pollutants in waste water treatment plants (WWTP) (Gopalakrishnan et al., 2018; Wei et al., 2018),
- sensors (of gases, metals, biomolecules) (Ju, 2018),
- energy accumulation – electrode material for super-capacitors, Li-ion batteries, solar collectors,
- hybrid compounds and composites – magnetic composites, ternary composites,
- C-catalysts,
- C-M, C-MO<sub>x</sub>-catalysts,
- photochemical catalysts (C-TiO<sub>2</sub>),
- environmental applications (Oladipo and Ifebajo, 2018),
- construction, diagnostics (Roupcova, 2017).

CQDs belong to nanostructures consisting of C atoms and their size is below 10 nm (Molaei, 2019a, 2019b). They are functionalized with biomolecules or organic substances (Molaei, 2020) and they are characterized by (Lim et al., 2015; Zuo et al., 2016):

- fluorescence emission,
- solubility in water,
- preparation simplicity,
- low toxicity,
- biocompatibility,
- chemical inertness,
- functionalization.

CQDs have found many applications in various areas such as bioimaging (both in vivo/vitro) (Jamieson et al., 2007), drug and gene delivery, solar energy, sensors, solar energy conversion, photoelectrochemical (PEC) cells, solar cells, etc. They can be considered as a substituent for semiconductor quantum dots (QDTs) due to the characteristics mentioned above as in comparison to semiconductor quantum dots (QDs), they can be considered as alternatives in solar energy conversion applications (Molaei, 2020).

### **Biochar**

Biochar is also ranked among carbon NMs because it is a porous carbonaceous material. Biochar, or bio-charcoal, is the product of waste pyrolysis after biomass fermentation (Zhu et al., 2012; Weber and Quicker, 2018). Biomass or wastes, from which biochar is most often produced, can come from various sources, such as cow and pig manure, straw, fruit skins, rice, peanuts, maize, soy, wood waste, sludge from WWTP etc. (see Figure 3). After the biomass fermentation process, which aims to produce biogas, so called digestate remains, mostly containing a solid portion and a liquid portion, is left (Zhu et al., 2012; Weber and Quicker, 2018). The separated solid material can be treated by pyrolysis at 300–600 °C with restricted air access or without it. Decomposition temperature can be reduced by hydrothermal pyrolysis (wet pyrolysis), where the main ongoing reaction is hydrolysis of hemicellulose, cellulose and lignin and subsequent decarboxylation, dehydrogenation, aromatization and condensation (Zhu et al., 2012). Pyrolysis or hydrothermal pyrolysis yields a porous carbonaceous material with a compact hydrophobic core of a predominantly aromatic structure and a shell exhibiting hydrophilic and chemically active properties (surface groups —OH, —C=O, —C—O—C—, —COOH) (Wei et al., 2018). Surface of biochar can be reduced (ascorbic acid), oxidized (hydrogen peroxide) or further modified, and thereby its properties can be altered (Roupcova, 2017).

The Biochar Journal (Schmidt and Wilson, 2014) published 55 examples of biochar application with a precondition for commercialization. In addition to its specific use (Yao and Wu, 2015; Zhang et al., 2014), such as a heterogeneous catalyst with wide application and energy conversion/storage as a super-

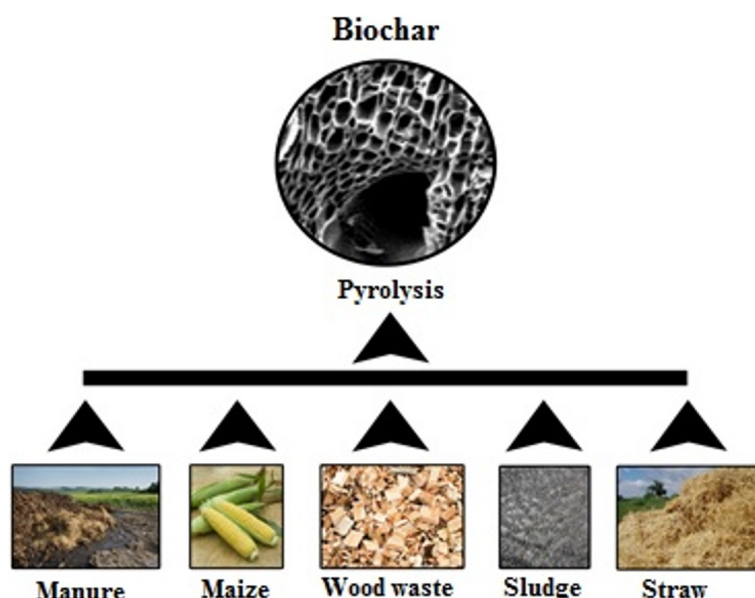


Fig. 3. Most common substrates for biochar production.

capacitor or Li-batteries, the main application of biochar is in soil engineering and as an adsorbent for various inorganic and organic pollutants, both in water and soil – see below. In relation to agriculture (soil), biochar provides the following benefits (Krishnakumar et al., 2014; Roupцова et al., 2017):

- increased water capacity of soil;
- increased biomass production;
- increased pH of soil;
- reduced toxicity of aluminium;
- reduces tensile strength of soil;
- changed (supported) microbial activity;
- reduced emissions of CO<sub>2</sub>, N<sub>2</sub>O, CH<sub>4</sub> from soil, absorbs organic and inorganic compounds (Krishnakumar et al., 2014; Roupцова et al., 2017).

Applications of biochar are very diverse, ranging from heat and power production, flue gas cleaning, metallurgical applications, agriculture and animal husbandry, building material, to medical use. In an attempt to reduce greenhouse gas emissions, it has gained increasing popularity in the last years as a replacement for fossil carbon carriers in several of these applications (Weber and Quicker, 2018) due to its ability to absorb both inorganic substances (ions of heavy metals) and organic contaminants in an aqueous medium and in soil preventing or reducing the entry of undesirable substances in the plants (Krishnakumar et al., 2014).

#### NMs toxicity and genotoxicity

The science which deals with toxicity and effects of artificially created nano-structures and mechanisms to living organisms is called nano-toxicology (Durnev and Lapitskaya, 2013). Toxicity of nanoparticles is affected by several factors such as the

quantity and size of particles, their concentration, specific surface, charge, shape, structure, reactivity, or solubility; therefore, their physical and chemical properties should be considered in the analysis of nanoparticles (Freixa et al., 2018; Borm et al., 2006). It is rather complicated to examine the toxicity of NMs because they behave differently in various environments and change their structure and composition. Therefore, to determine their toxicity, various studies have to be conducted to examine their contact with organisms (dermal, oral, or other means), and their effects (Freixa et al., 2018). To examine the toxicity, various analytical techniques are needed; it is not possible to analyze it only by one single analytical technique.

Various methods are used to determine the toxicity of NMs: cell toxicity (Tabei et al., 2019), genotoxicity (Martínez-Paz et al., 2019), toxicity of microorganisms (Chen et al., 2019), test on larvae (Moon et al., 2019). Standardized methods of NMs ecotoxicity include tests on:

- higher green plants – e.g. *Sinapis Alba* L. (white mustard) (OECD 208/1984) Terrestrial plants, growth test, methodical instruction of the Department of Waste of the Ministry of the Environment of the Czech Republic to determine the ecotoxicity of waste,
- invertebrates – e.g. *Daphnia magna* (pearl mussel) (Gao et al., 2018),
- vertebrates – e.g. *Brachydanio rerio* (Striped Danio) (Jia et al., 2019),
- autotrophic unicellular green algae – e.g. *Desmodesmus subspicatus* (Nam et al., 2018).

Another reason why their toxicity is relatively unexplored is that most of the analytical methods are destructive, and so it is not possible to re-use the

samples (Brandeburova et al., 2017; Mackulak et al., 2016; Tiede et al., 2008). Particles are made of the same material but their toxicity varies with different sizes. The material in form of nanoparticles is more toxic than the larger particles that can still be breathed in. Nanoparticles can be moved from the place of accumulation via nasal vessels up to the brain and gain access to blood and other organs; phagocytosis is not able to stop them. Nanoparticles of very small dimensions, smaller than some molecules, can bind to larger molecules and then modify the protein structures (Donaldson et al., 2004; Ghika et al., 2018). In addition to the size of nanoparticles and their surface, an important factor in their toxicity is also oxidative stress causing inflammation and genotoxicity (Ghika et al., 2018; Hussain et al., 2009).

#### ***Ecotoxicity of NMs of the graphene family***

A whole series of specialized studies has been devoted to the toxic effects of NMs from the graphene group. Detailed research studies (Seabra et al., 2014; Guo and Mei, 2014; Jastrebska et al., 2012) summarize the contemporary findings concerning the toxic effects and possible mechanisms of toxicity. While their conclusions agree that graphene, graphene oxide, and reduced graphene oxide have toxic effects both in the *in vitro* and in the *in vivo* tests (Roupcova, 2017), the interpreted toxicity results vary and depend on many factors, such as the physical form of the tested substance, method of its preparation (contamination during chemical preparation or during reduction), environment where the toxicity test was carried out, or biological system the tests were performed on (bacteria, green algae, nematodes, crustaceans, mammalian cells, etc.) (Roupcova, 2017). For example, the following data have been published concerning GO toxicity in an aqueous medium (Roupcova et al., 2016):

- toxicity to crustaceans *Amphibalanus Amphitrite* (Mesaric et al., 2013),
- toxicity to microbiological community in effluents (Ahmed and Rodrigues, 2013),
- non-toxicity against bacterium *Shewanella oneidensis* (Wang et al., 2011),
- slight toxicity to embryos of Zebra Danio (*Danio rerio*) (Chen et al., 2012),
- non-toxicity to embryos of Zebra Danio (*Danio rerio*) (Zhou et al., 2012),
- either toxic or non-toxic to field bean seeds (*Vicia faba*) (Anjum et al., 2014).

From this summary, the disunity of results can be seen. The interaction with live systems is influenced by both the concentration of the test substance and the functional groups on its surface, particle size, exposure time, type of exposed cells (Seabra et al.,

2014), and, in our opinion, also purity of the test substance. All these variables affect the results of the toxicity tests.

For example, phytotoxicity of graphene and GO was analyzed by tests carried out with seeds and germination plants of tomato, headed cabbage, red spinach and lettuce (Roupcova et al., 2016; Begum et al., 2011). Concentrations of 0, 500 mg/l, 1000 mg/l, and 2000 mg/l were tested and the exposure time was 20 days. Results of the tests showed significant reduction of growth and the number and size of leaves at the highest concentration in almost all products, with the exception of lettuce; at the same time, there increase in the production of reactive oxygen species (ROS) and of the necrotic symptoms was observed (Roupcova et al., 2016; Begum et al., 2011).

Similar tests were conducted by Anjum et al. with field bean seeds (*Vicia faba*). The seeds were exposed to different concentrations of GO suspension (suspension contained particles of 0.5–5 µm created from a simple GO bi-layer) in the concentration range of 0–1600 mg/l. The study revealed both positive and negative impact on the growth parameters (Anjum et al., 2014). Positive impact has been determined with GO concentrations of 400 and 800 mg/l. For other concentrations, either lower or higher, the impact on the bean growth parameters was negative. The negative effect was indicated by the drop of growth parameters, increased activity of enzymes decomposing hydrogen peroxide, increased level of electrolyte leak (damaged stability of cell membranes), and finally by increased levels of hydrogen peroxide and lipids and proteins oxidation. These results demonstrate the complexity of phytotoxicity results interpretation. A question remains why the specified GO concentrations optimized the physiological process of germination and growth (Hussain et al., 2009; Lanwani et al., 2016).

## **Applications of NMs**

### ***Environmental applications of CBNMs***

Many hazardous pollutants from industry enter the environment every year. To help protect the environment and humans, adequate safety management is required employing chemical, biological or physical treatment (Jurado-Sanchez and Wang, 2018; Tratnyek and Johnson, 2006).

Micromotors present a brand new paradigm for actual time environmental monitoring with huge promise for detection of sudden changes and possible threats or for monitoring remediation processes or hardly accessible environments. One effective strategy depends on the changes in the floating behavior of catalytic self-propelled micromotors

when hazardous chemicals are present (Jurado-Sanchez and Wang, 2018; Sen et al., 2009).

### **Use of micromotors for adsorption**

Adhesion of atoms, molecules or ions from a liquid, dissolved solid or gas to a surface is called adsorption. Concerning micromotors and the environment, research has been directed towards the proposal of micromotors functionalized with proper (bio)-ligands or composed of activated carbon or graphene. A great part of attention has been paid to dynamic oil removal using micromotors as an effective way to encounter petroleum drops (Jurado-Sanchez and Wang, 2018). For example, hydrophobic graphene/Pt tubular micromotors, made by rolling together with wax-printed sheets, were successfully tested for collecting lubricants from water samples. The high surface-to-volume ratio combined with graphene along with self-propelled micromotor motion offers friendly conditions to collect lubricant droplets occurring in water through its hydrophobic interactions (Baptista-Pires et al., 2018).

Graphene is the most used allotrope of carbon for adsorptive removal of pollutants. For example, reduced graphene oxide coated silica/Pt Janus magnetic self-propelled micromotors show enhanced removal of persistent organic pollutants (triclosan and polybrominated diphenyl ethers) from water. Micromotors can be repeatedly used in four cycles in sequence without any difference in their adsorption characteristics (Orozco et al., 2016).

### **Pollutant degradation micromotors**

Progressive oxidation processes play an important role in the chemical treatment removing organic and inorganic pollutants in water by oxidation through chemical reactions with ozone (O<sub>3</sub>), hydrogen peroxide (H<sub>2</sub>O<sub>2</sub>), hydroxyl radicals ( $\cdot$ OH) or UV light. Peroxide driven self-propelled micromotors provide a new dimension to progres-

sive pollutant removal because peroxide behaves as a strong oxidizing agent broadly used by environmental communities for the degradation of dangerous organic substances. The micromotor motion enables faster contact of the pollutants and active reactants, developing in more dynamic degradation processes that can be compared to static opposites (Jurado-Sanchez and Wang, 2018). A short overview of CBNMs used as self-propelled micromotors is given in Table 1.

### **CBNMs and their applications in medicine**

The development of different NMs for diagnosis and therapy caused NMs to become an interesting and important area of biomedical research. Due to the high toxicity and side effects of the use of traditional chemotherapy in cancer, scientists are working on the development of alternative therapeutic technologies (Roacho Perez et al., 2018). The above mentioned NMs can assist in the monitoring of disease progress and treatment efficacy, recognize blood type of the patient, or the type of tissue at transplantation (Li et al., 2018). One of the main advantages of these substances is their non-invasive use as a diagnostic tool. Another new and exciting feature is the multi-modal use of one sensor formed from NMs. This allows for a better and more accurate understanding of the *in vivo* action (Wang et al., 2017). Moreover, the connection of diagnosis and treatment in one system provides new possibilities in the treatment of diseases such as cancer. This type of treatment is called teranostics. When applying a modified nanomaterial in various imaging techniques and treatment possibilities, higher therapeutic efficacy can be achieved (Barreto et al., 2011).

### **NMs characteristics in cancer treatment**

The prerequisite of successful use of NMs *in vivo* as well as *in vitro* is their correct synthesis. A particle that has the right size, surface, or polarity has to

**Tab. 1.** Summary of carbon based micromotors for potential environmental applications.

Motor	Pollutant	Reference
<i>Removal of pollutants by adsorption</i>		
<b>Activated carbon/Pt Janus micromotors</b>	Heavy metals, explosives, nerve agents, azo dyes	(Jurado-Sanchez et al., 2015)
<b>Zr/rGO/Ni/Pt tubular micromotors</b>	Chemical warfare agents	(Singh et al., 2015)
<b>rGO/Ni/Pt tubular micromotors</b>	Heavy metals	(Vilela et al., 2016)
<b>rGO/Pt Janus micromotors</b>	Persistent organic pollutants	(Orozco et al. 2016)
<b>GO/Pt nanoparticles (NPs) rolled – up micromotors</b>	Oil droplets	(Baptista-Pires et al., 2018)
<i>Degradation of pollutants</i>		
Advanced oxidation		
<b>rGO/Prussian blue hydrogel micromotor</b>	Azo dyes	(Hao et al., 2015)

be created. Toxicity of nanoparticles and their biocompatibility have also to be considered (Ghika et al., 2018).

The reticulo-endothelial system (RES) is a part of the immune system composed of phagocytic cells. Macrophages and monocytes are located in spleen and in lymph nodes, while Kupffer cells are located in liver. The main role of this system is to eliminate old or foreign cells and create new cells for immune and inflammatory response. Tumor cells induce the infiltration of other cell types and instruct them (fibroblasts, endothelial cells and immune cells) in cell-contact dependent (paracrine, receptor-mediated) and contact independent manner (endocrine, cytokines and other signaling molecules) to establish a self-promoting and mutually self-reinforcing tumor microenvironment (TME) that promotes tumor progression (Conde et al., 2016). This system is active mainly in the elimination of larger nanoparticles. The smaller the particle, the longer time is needed to eliminate the particles from blood circulation. It was found that particles smaller than 200 nm are the ideal size for cancer treatment (Song et al., 2017). The lower limit of the size is derived from the ability to filter particles in the kidneys. Glomerular barrier transmits particles smaller than 6 nm, while those larger than 8 nm will not pass through. Also, a healthy endothelium has an effective pore size of about 5 nm; therefore, NMs smaller than this size will pass through into the extra-vassal spaces. The entry of foreign particles into a cell is blocked by three stage mechanism. Using opsonization, macrophages recognize foreign particles and absorb them via endocytosis, and the digestive enzymes try to break them down. If the particle is not biodegradable, it is removed by kidneys or stored in the reticulo-endothelial system (Barreto et al., 2011).

Degradation of NMs through RES is also linked to the polarity and charge of particles. This process is faster if the particles are more hydrophobic, which allows for better adsorption of blood proteins on their surface. Also surface charge affects the elimination of NMs; neutral particles or particles with low charge are removed immediately. Positively charged particles are not specifically linked to the cells, whereas the negative charge attracts phagocytes in liver. It has been proved that zeta potential of a particle higher than  $\pm 30$  mV prevents its agglomeration in a model suspension (Barreto et al., 2011).

## Conclusions

The article briefly summarizes the general characteristics of NMs, especially their properties with which they penetrate into the environment (water,

soil). Furthermore, individual members of the graphene family, including porous carbon (biochar), are described. The main characteristics, preparation, and the new eco-friendly applications of carbon based NMs as self-propelled micromotors are introduced. NMs have become an important part of medical research combining diagnosis and therapy into one system, which provides new possibilities in treatment of diseases such as cancer.

## Acknowledgements

*This work was supported by the grant scheme for supporting young researchers at STU in Bratislava: "Nanomateriály – inovatívny postup odstraňovania mikropolutantov" and the grant scheme for supporting excellent teams of young researchers at STU in Bratislava: "Mikropolutanty a rezistentné kmene baktérií ich monitoring a možnosti použitia inovatívnych postupov na ich odstránenie – nanomateriály a železany". The publication was written within the Student grant competition "Preparation of New Carbon – based Nano – materials and their Modifications on Nano – metal Composites Using New Ways and Monitoring of Nano – material Relation to the Natural Environment" – project number SP2017/95. This work was also supported by VEGA 1/0343/19.*

## References

- Agharkar M, Kochrekar S, Hidouri S, Azeez MA (2014) Mater Res Bull 59: 323.
- Ahmed F, Rodrigues DF (2013) J Hazard Mater 256–257: 33.
- Anjum NA, Singh N, Singh MK, Sayeed I, Duarte AC, Pereira E, Ahmad I (2014) Sci Total Environ 472: 834.
- Bakand S, Hayes A, Dechsakulthorn F (2012) Inhalation Toxicol 24: 125.
- Baptista-Pires L, Orozco J, Guardia P, Merkoci A (2018) Small (Weinheim an der Bergstrasse, Germany) 14.
- Barreto JA, O'Malley W, Kubeil M, Graham B, Stephan H, Spiccia L (2011) Adv Mater 23: H18.
- Baun A, Sayre P, Steinhäuser KG, Rose J (2017) NanoImpact 8: 1.
- Begum P, Ikhtiar R, Fugetsu B (2011) Carbon 49: 3907.
- Borm PJ, Robbins D, Haubold S, Kuhlbusch T, Fissan H, Donaldson K, Schins R, Stone V, Kreyling W, Lademann J, Krutmann J, Warheit D, Oberdorster E (2006) Part Fibre Toxicol 3: 11.
- Brandeburová P, Bírošová L, Vojs M, Kromka A, Gál M, Tichý J, Híveš J, Mackulák T (2017) Monatsh Chem – Chemical Monthly 148: 525.
- Calvaresi M, Quintana M, Rudolf P, Zerbetto F, Prato M (2013) Chem Phys Chem 14: 3447.
- Chabot V, Higgins D, Yu A, Xiao X, Chen Z, Zhang J (2014) E Environ Sci 7: 1564.
- Chartarrayawadee W, Moulton SE, Too CO, Kim BC, Yepuri R, Romeo T, Wallace GG (2013) J Appl Electrochem 43: 865.
- Chen L, Hu P, Zhang L, Huang S, Luo L, Huang C (2012) Sci China Chem 55: 2209.

- Chen M, Sun Y, Liang J, Guangming Z, Li Z, Tang L, Zhu Y, Jiang D, Song B (2019) *Environ Int* 126: 690–698.
- Chien CT, Li SS, Lai WJ, Yeh YC, Chen HA, Chen IS, Chen LC, Chen KH, Nemoto T, Isoda S, Chen M, Paredes JI, Fernández-Merino MJ, Villar-Rodil S, Solís-Fernández P, Guardia L, García R, Martínez-Alonso A, Tascón JMD (2013) Preparation of graphene and graphene-metal nanoparticle hybrids with enhanced catalytic activity by reduction of graphite oxide with efficient natural bioreductants Paper presented at the Imagine Nano, Bilbao Spain.
- Chng ELK, Pumera M (2013) *Chemi – A Europ J* 19: 8227.
- Chua CK, Pumera M (2013) *Chem Soc Rev* 42: 3222.
- Chung C, Kim YK, Shin D, Ryoo SR, Hong BH, Min DH (2013) *Acc Chem Res* 46: 2211.
- Conde J, Arnold CE, Tian F, Artzi N (2016) *Mater Today* 19: 29.
- Donaldson K, Stone V, Tran CL, Kreyling W, Borm PJA (2004) *Occupational Environ Med* 61: 727.
- Duarte, Armando C. In: Cachada A, Rocha-Santos T (eds) *Soil Pollution*. Academic Press, pp 161. doi: 10.1016/B978-0-12-849873-6.00007-8.
- Durnev AD, Lapitskaya AS (2013) *Russ J Genet: Applied Research* 3: 388.
- Fakhri A (2017) *J Saudi Chem Soc* 21: S52.
- Fernández-Merino MJ, Guardia L, Paredes JI, Villar-Rodil S, Solís-Fernández P, Martínez-Alonso A, Tascón JMD (2010) *J Phys Chem C* 114: 6426.
- Freixa A, Acuña V, Sanchís J, Farré M, Barceló D, Sabater S (2018) *Sci Total Environ* 619–620: 328.
- Fujita T, Eda G, Yamaguchi H, Chhowalla M, Chen CW (2012) *Angew Chem Int Ed Engl* 51: 6662.
- Gao M, Zhang Z, Lv M, Song W, Lv Yu (2018) *Ecotoxicol and Environ Saf* 148: 261–268.
- Garcia IL (2017) Antimicrobial activity of graphene and its viability. Degree final project. University of Barcelona pp 34.
- Gkika DA, Magafas L, Cool P, Braet J (2018) *Toxicology* 393: 83.
- Gopalakrishnan I, Sugaraj Samuel R, Sridharan K (2018) Nanomaterials-Based Adsorbents for Water and Wastewater Treatments. In: Sridharan K (ed) *Emerging Trends of Nanotechnology in Environment and Sustainability: A Review-Based Approach*. Springer International Publishing, Cham, pp 89. doi: 10.1007/978-3-319-71327-4\_11.
- Guo X, Mei N (2014) *J Food and Drug Anal* 22: 105.
- Hao J, Yang W, Zhang Z, Tang J (2015) *Nanoscale* 7: 10498.
- Hu Y, Sun X (2013) Chemically Functionalized Graphene and Their Applications in Electrochemical Energy Conversion and Storage. In: Aliofkhaezei M (ed) *Ad Graphene Sci. InTech*, Rijeka, p Ch. 07. doi: 10.5772/55666.
- Hussain S, Boland S, Baeza-Squiban A, Hamel R, Thomassen LC, Martens JA, Billon-Galland MA, Fleury-Feith J, Moisan F, Pairon JC, Marano F (2009) *Toxicology* 260: 142.
- Jamieson T, Bakhshi R, Petrova D, Roccock R, Imani M, Seifalian AM (2007) *Biomaterials* 28: 31, 4717–4732.
- Jastrzebska AM, Kurtycz P, Olszyna AR (2012) *J Nanopart Res* 14: 1320.
- Jia H-R, Zhu Y-X, Duan Q-Y, Chen Z, Wu F-G (2019) *J of Control Rel* 311–312, 301–318.
- Ju H (2018) *Appl Mater Today* 10: 51.
- Jurado-Sanchez B, Sattayasamitsathit S, Gao W, Santos L, Fedorak Y, Singh VV, Orozco J, Galarnyk M, Ramesha GK, Vijaya Kumara A, Muralidhara HB, Sampath S (2011) *J Colloid Interface Sci* 361: 270.
- Jurado-Sánchez B, Wang J (2018) *Environ Sci: Nano* 5: 1530.
- Kabiri S, Tran DN, Altalhi T, Losic D (2014) *Carbon* 80: 523.
- Krishnakumar S, Rajalakshmi AG, Balaganesh B, Manikandan P, Vinoth C, Rajendran V (2014) *Int J Ad Res* 2: 933
- Kyzas GZ, Deliyanni EA, Matis KA (2014) *J Chem Technol Biotechnol* 89: 196.
- Lalwani G, D'Agati M, Khan AM, Sitharaman B (2016) *Adv Drug Delivery Rev* 105: 109.
- Lee J, Lee B, Shin D, Kwak SS, Bahk JD, Lim CO, Yun DJ (2002) *Mol Cells* 13(3): 407–412.
- Lee JW, Hall AS, Kim J-D, Mallouk TE (2012) *Chem Mater* 24: 1158.
- Li J, Rao J, Pu K (2018) *Biomaterials* 155: 217.
- Lim SY, Shen W, Gao Z (2015) Carbon quantum dots and their applications. *Chem. Soc. Rev.* 44 (1), 362–381.
- Lin J, Chen X, Huang P (2016) *Adv Drug Delivery Rev* 105: 242.
- Liu Y, Tourbin M, Lachaize S, Guiraud P (2014) *Powder Technol* 255: 149.
- Loureiro S, Tourinho PS, Cornelis G, Van Den Brink NW, Díez-Ortiz M, Vázquez-Campos S, Pomar-Portillo V, Svendsen C, Van Gestel CAM (2018) Chapter 7 – Nanomaterials as Soil Pollutants A2.
- Mackulak T, Vojs M, Grabic R, Golovko O, Staňová AV, Birošová L, Medvedčová A, Híveš J, Gál M, Kromka A, Hanusová A (2016) *Monatsh Chem – Chemical Monthly* 147: 97.
- Martínéz-Paz P, Negri V, Esteban-Arranz A, Martínez-Guitarte JL, Ballesteros P, Morales M (2019) *Aquat Toxicol* 209: 42–48.
- Molaei MJ (2019b) A review on nanostructured carbon quantum dots and their applications in biotechnology, sensors, and chemiluminescence. *Talanta* 196, 456–478.
- Molaei MJ (2019a) Carbon quantum dots and their biomedical and therapeutic applications: a review. *RSC Adv.* 9 (12), 6460–6481.
- Molaei MJ (2020) The optical properties and solar energy conversion applications of carbon quantum dots: A review. *Sol. Energy* 196, 549–566.
- Mesarić T, Sepčić K, Piazza V, Gambardella C, Garaventa F, Drobne D, Faimali M (2013) *Chem Ecol* 29: 643
- Miners SA, Rance GA, Khlobystov AN (2016) *Chem Soc Rev* 45: 4727.
- Moon J, Kwak JI, An Y-J (2019) *Chemosphere* 215: 50–56.
- Nam S-H, An Y-J (2019) *Ecotoxicol and Environ Saf* 168: 388–393.
- Notarianni M, Jinzhang L, Vernon K, Motta N (2016) *Beilstein J of Nanotechnol* 7, 149–196.
- Oladipo AA, Ifebajo AO (2018) *J Environ Manage* 209: 9.
- Orozco J, Mercante LA, Pol R, Merkoçi A (2016) *J Mater Chem A* 4: 3371.
- Pan Y, Liu X, Zhang W, Liu Z, Zeng G, Shao B, Liang Q, He Q, Yuan X, Huang D, Chen M (2020) *Appl. Cat. B: Environ* 265: 118579.
- Park J, Yan M (2013) *Acc Chem Res* 46: 181.

- Paulchamy B, Arthi G, Lignesh B (2015) *J Nanomed Nanotechnol* 6: 1.
- Pochkaeva EI, Podolsky NE, Zakusilo DN, Petrov AV, Charykov NA, Vlasov TD, Penkova AV, Vasina LV, Murin IV, Sharoyko VV, Semenov KN (2020) *Prog Solid State Chem* 57: 100255.
- Roacho Perez JA, Gallardo Blanco HL, Sanchez Dominguez M, Garcia Casillas PE, Chapa Gonzalez C, Sanchez Dominguez CN (2018) *Mol Med Rep* 17: 1413.
- Roupcová P (2017) Monitorování ekotoxicity u nanočástic na bázi uhlíku. Thesis for dissertation work, Technical University of Ostrava, Ostrava.
- Roupcová P, Friedrichová R, Klouda K, Weisheitelová M, Perdochová M (2017) Biochar Modification, Thermal Stability and Toxicity of Products Modification. TRANSACTIONS of the VŠB – Technical University of Ostrava, Safety Engineering Series, vol 12. doi: 10.1515/tvsbses-2017-0012.
- Roupcová P, Klouda K (2017) Hybrid Compounds based on Graphene Oxide and their Compounds with Metals. Paper presented at the Nanocon 2017, Brno, Czech Republic.
- Roupcová P, Klouda K, Pavlovský J, Weisheitelová M (2017) DEStech Transactions on Engineering and Technology Research.
- Roupcová P, Kubátová H, Klouda K, Lepík P (2016) Phytotoxicological Tests – Applications of Foils Based on Graphene (Graphene Oxide). TRANSACTIONS of the VŠB – Technical University of Ostrava, Safety Engineering Series, vol 11. doi: 10.1515/tvsbses-2016-0011.
- Sanchez VC, Jachak A, Hurt RH, Kane AB (2012) *Chem Res Toxicol* 25: 15.
- Saunders DS, Gillanders SW, Lewis RD (1994) *J Insect Physiol* 40(11): 957–968.
- Sen A, Ibele M, Hong Y, Velegol D (2009) *Faraday Discuss* 143: 15.
- Seabra AB, Paula AJ, de Lima R, Alves OL, Duran N (2014) *Chem Res Toxicol* 27: 159.
- Schmidt H, Wilson K (2014) *the Biochar J*.
- Shahil KM, Balandin AA (2012) *Solid State Commun* 152: 1331.
- Shanmugharaj AM, Yoon JH, Yang WJ, Ryu SH (2013) *J Colloid Interface Sci* 401: 148.
- Sharma A, Anghore D, Awasthi R, Kosey S, Jindal S, Gupta N, Raj D, Sood R (2015) *World J of Pharm and Pharm Sci* 4, 1088–1113.
- Singh VV, Martin A, Kaufmann K, DS de Oliveira S, Wang J (2015) *Chem Mater* 27: 8162.
- Song W, Musetti SN, Huang L (2017) *Biomaterials* 148: 16.
- Stanković DM, Ognjanović M, Fabian M, Švorc E, Mariano JFML, Antić B (2017) *Anal Biochem* 539: 104.
- Svítková J, Ignat T, Švorc E, Labuda J, Barek J (2016) *Crit Rev Anal Chem* 46: 248.
- Sun M, Wang G, Li X, Li C (2014) *J Power Sources* 245: 436.
- Tabei Y, Fukui H, Nishioka A, Hagiwara Y, Sato K, Yoneda T, Koynama T, Horie M (2019) *Sci Rep* 9: 2224.
- Terrones H, Lv R, Terrones M, Dresselhaus MS (2012) *Rep Prog Phys* 75: 062501.
- Theng BK, Yuan G (2008) *Elements* 4: 395.
- Tiede K, Boxall ABA, Tear SP, Lewis J, David H, Hassellöv M (2008) *Food Addit Contam: Part A* 25: 795.
- Tratnyek PG, Johnson RL (2006) *Nano Today* 1: 44.
- Vilela D, Parmar J, Zeng Y, Zhao Y, Sánchez S (2016) *Nano Lett* 16: 2860.
- Wang D, Yang G, Ma Q, Wu M, Tan Y, Yoneyama Y, Tsubaki N (2012) *ACS Catal* 2: 1958.
- Wang G, Qian F, Saltikov CW, Jiao Y, Li Y (2011) *Nano Res* 4: 563.
- Wang J (2015) *Small (Weinheim an der Bergstrasse, Germany)* 11: 499.
- Wang L, Xiong Q, Xiao F, Duan H (2017) *Biosens Bioelectron* 89: 136.
- Weber K, Quicker P (2018) *Fuel* 217: 240.
- Wei D, Li B, Huang H, Luo L, Zhang J, Yang Y, Guo J, Tang L, Zeng G, Zhou Y (2018) *Chemosphere*.
- Woo S, Kim Y-R, Chung TD, Piao Y, Kim H (2012) *Electrochim Acta* 59: 509.
- Xu Z, Sun H, Zhao X, Gao C (2013) *Adv Mater* 25: 188.
- Yao Y, Wu F (2015) *Nano E* 17: 91.
- Yoo BM, Shin HJ, Yoon HW, Park HB (2014) *J Appl Polym Sci* 131: n/a.
- Zhang L, Jiang J, Holm N, Chen F (2014) *J Appl Electrochem* 44: 1145.
- Zhang W, Li X, Yang Z, Tang X, Ma Y, Li M, Hu N, Wei H, Zhang Y (2016) *Nanotechnology* 27: 265703.
- Zhang X, Huang Y, Wang Y, Ma Y, Liu Z, Chen Y (2009) *Carbon* 47: 334.
- Zhang Y, Ren L, Wang S, Marathe A, Chaudhuri J, Li G (2011) *J Mater Chem* 21: 5386.
- Zhao J, Wang Z, White JC, Xing B (2014) *Environ Sci Technol* 48: 9995.
- Zhou X, Laroche F, Lamers GEM, Torracca V, Voskamp P, Lu T, Chu F, Spaink HP, Abrahams JP, Liu Z (2012) *Nano Res* 5: 703.
- Zhu S, Tang S, Zhang J, Yang B (2012) *Chem Commun (Camb)* 48: 4527.
- Zuo P et al. (2016) A review on syntheses, properties, characterization and bioanalytical applications of fluorescent carbon dots. *Microchim. Acta* 183 (2), 519–542.

# Inclination to self-ignition and analysis of gaseous products of wood chips heating

Michaela Skrizovska, Hana Veznikova, Petra Roupцова

VSB – TU Ostrava, Faculty of Safety Engineering, Lumirova 13, 700 30 Ostrava – Vyskovice  
*michaela.skrizovska@usb.cz*

**Abstract:** This paper focuses on the assessment of the inclination to self-ignition of various types of wood chips according to the methodology of European standard EN 15188. The study also assesses the effect of heating temperatures on the composition and quantity of gaseous products of heating. Gases were analysed using an infrared spectrometer with Fourier transformation. From the measured results it was found that the inclination to self-ignition differs for various samples of wood chips. The paper discusses certain parameters assumed to affect the inclination of biomass to self-ignite. When assessing the effect of temperature on the composition of gaseous products, a sample of forest wood chips heated at temperatures from 50 to 150 °C resulted in the following gaseous products: carbon dioxide, carbon monoxide, water and aliphatic hydrocarbons; their concentrations increase with the increasing temperature. Carbon oxides have been proposed as indicators of the state of stored materials self-heating. Observations presented in this paper can be used as data for elaborating safety instructions for storage of fuels based on solid biomass.

**Keywords:** gaseous products, induction time, spontaneous combustion, self-heating temperature, wood chips.

## Introduction

One of the possible alternatives to fossil fuels is the use of solid biofuels whose combustion causes less damage to the environment. In the Czech Republic, the most common alternative used for energy-production purposes is wood chips. Wood chips are defined as chipped wood biomass typically 5 mm to 50 mm in size, produced by mechanical cutting of wood using sharp tools, e.g. blades (CSN EN ISO 17225-4, 2015).

No heating or drying is used during their production and most of the original wood humidity is retained. The production process of other types of solid biofuels, such as pellets or briquettes, involves heating and therefore their biological activity is reduced (Alakoski et al., 2016). For this reason, wood chips have higher tendency to spontaneous self-heating than other types of biofuels.

Self-ignition occurs mainly if chips are stored in large quantities and over long periods of time. Safe storage time is determined not only by the size of the stored pile, but also by the type of biomass, storage, material humidity and homogeneity as well as by other parameters.

Conditions for safe storage of solid biofuels are mainly determined based on the results of laboratory tests (Veznikova, 2016). A number of methods are used for this purpose, with both empirical and theoretical foundations. Methods currently used to assess the risk of spontaneous combustion evaluate the solids behaviour under adiabatic, isoperibolic or isothermal conditions (Babrauskas, 2003).

For example, the isoperibolic method according to European standard EN 15188 sets procedures for determining the volume dependence of self-ignition temperature of combustible dusts or granular materials. After determining this dependence in laboratory conditions, an extrapolation is performed for the expected conditions during storage of the evaluated material. The standard method is often used to assess the risk of spontaneous combustion of biomass and to determine safe storage conditions (Ramirez et al., 2010; Jones et al., 2015).

One of the methods used to control the development of material self-ignition in warehouses is to monitor changes in the concentration of gases produced during the self-heating process. Dominant gases emitted during heating by wood include carbon dioxide, carbon monoxide and methane (Alakoski et al., 2016). The method indicating the state of self-heating based on the analysis of gaseous products from heating has been used for many years, especially for coal materials. As the study of Derychova et al. (2016) shows, majority of gaseous products from coal and biomass are qualitatively identical. Therefore, analysis of gaseous products can also be used in the indication of the temperature of stored biomass. However, the composition and quantity of these products is affected, just like the self-ignition temperature, by the material properties and storage conditions. Therefore, besides the evaluation of the inclination of various wood chips to self-ignition, this study also evaluates the impact of temperature on the composition and quantity of carbon monoxide, carbon dioxide and methane for one type of biomass.

**Tab. 1.** Overview of studies on self-ignition.

Resolved issues	Source
Self-ignition in general	(Balog, 1999; Kalousek, 1999; Adamus et al, 2007, Věžníková & Adamus, 2007)
Self-ignition of plant materials	(Balog, 1999)
Effect of composition on self-ignition temperature	(Ekoporadna, 2010)
Effect of temperature on self-ignition temperature	(Balog, 1999)
Effect of grain size on self-ignition temperature	(Jirjis, 1995)
Effect of humidity on self-ignition temperature	(Lohrer et al, 2005)
Effect of volume of accumulated material on self-ignition temperature	(Jirjis, 2005)
Methods for determining inclination to self-ignition	(Adamus, 2004; Bowes, 1984)
Issue of gaseous products released during wood material self-heating	(Kuang et al, 2009; Yazdanpanah et al, 2014; Kuang et al, 2008; Jäppinen et al, 2014; He et al, 2014; Oren et al, 1987)
Effect of temperature on the quantity of gaseous products released during wood material self-heating	(Oren et al, 1987; Perdochova, 2014)
Effect of concentration of oxygen on the composition of gaseous products produced during wood sawdust self-heating	(Perdochova et al., 2015)

Numerous experimental studies have focused on the issue of self-ignition. An overview of the most important studies in this field is provided in Tab. 1. The cited papers focus primarily on the issue of self-ignition in general, self-ignition of plant material, evaluation of various phenomena on self-ignition temperature and on the effect of temperature on the composition of products of wood material self-heating.

The effect of wood material variability on the self-ignition process has not been deeply studied, most probably because biomass has been combusted on an industrial scale for a relatively short time. The variability of wood material composition is greater than in case of other fuels (Vassilev et al., 2015) and it affects the properties and behaviour of the material during its combustion and storage. The effect of chemical composition and physical properties (granulometry and ash content) on flammability, explosibility and inclination to self-ignition has only recently been addressed (Torrent et al., 2016). Numerous other papers deal with the comparison of economic parameters of combusting coal or fuel oil and wood material (Esteban et al., 2016).

In this study, the inclination to self-ignition was evaluated for four various types of wood chips and the effect of temperature on the composition of gaseous products of heating forest wood chips was also studied. The aim of the paper was to determine the effect of the biomass type on the self-ignition process and on the change of the gaseous products composition with temperature for forest wood chips. Based on the results, suitable measures were proposed to prevent self-ignition as unified instructions for safe storage of wood material.

## Material and Methods

### Tested materials

The following samples were subjected to testing (Fig. 1):

- **Sample No. 1 – wood chips from deciduous trees** – wood chips and crushed wood fuel, water M45, ash A5.0 according to ČSN EN ISO 17225-1 (CSN EN ISO 17225-1, 2015).
- **Sample No. 2 – wood-working (white) wood chips** – wood chips and crushed wood fuel, water M45, ash A5.0 according to ČSN EN ISO 17225-1 (CSN EN ISO 17225-1, 2015).
- **Sample No. 3 – forest wood chips** – wood chips and crushed wood fuel, water M50, ash A10.0+ according to ČSN EN ISO 17225-1 (CSN EN ISO 17225-1, 2015).
- **Sample No. 4 – wood chips from poplars** – sorted wood chips class B1 according to ČSN EN ISO 17225-4 (CSN EN ISO 17225-4, 2015).



**Fig. 1.** Tested materials (Perdochova, 2015).

**Tab. 2.** Proximate and ultimate analyses of samples.

Properties/Tested material	Deciduous wood chips	Wood-working wood chips	Forest wood chips	Deciduous wood chips – poplar
<i>Proximate analysis (wt %)</i>				
Ash A <sup>d</sup>	4.66	3.95	11.90	2.86
Volatile combustible matter V <sup>daf</sup>	82.93	83.38	81.10	85.07
Fixed carbon C <sup>daf</sup> <sub>f</sub>	17.07	16.62	18.90	14.93
<i>Ultimate analysis (wt %)</i>				
Carbon total C <sup>d</sup> <sub>t</sub>	49.34	49.54	46.89	49.44
Hydrogen total H <sup>d</sup> <sub>t</sub>	5.46	5.55	5.14	5.54
Nitrogen N <sup>d</sup>	0.18	0.09	0.34	0.16
Sulphur S <sup>d</sup> <sub>t</sub>	0.04	0.03	0.04	0.03
Oxygen O <sup>d</sup> <sub>d</sub> (by calculation)	44.98	44.79	47.59	44.83

Note: meaning of symbols

Ash	A <sup>d</sup>	Ash in dry matter
Volatile combustible matter	V <sup>daf</sup>	Volatile combustible matter in dry ash-free basis
Fixed carbon	C <sup>daf</sup> <sub>f</sub>	Fixed carbon (f) in dry ash-free basis
Carbon total	C <sup>d</sup> <sub>t</sub>	Carbon total in dry ash-free basis
Hydrogen total	H <sup>d</sup> <sub>t</sub>	Hydrogen total in dry matter
Nitrogen	N <sup>d</sup>	Nitrogen in dry matter
Sulphur	S <sup>d</sup> <sub>t</sub>	Sulphur in dry matter
Oxygen (by calculation)	O <sup>d</sup>	Oxygen (by calculation) in dry matter

**Tab. 3.** Summary of physical parameters of respective samples – moisture, apparent density, screen analysis (Perdochova, 2015).

Physical property	Deciduous wood chips	Wood-working wood chips	Forest wood chips	Deciduous wood chips – poplar
Moisture (%)	43.35	41.02	47.74	44.23
Apparent density (kg · m <sup>-3</sup> )	330	280	320	300
Mean grain size (mm)	8.88	13.23	8.75	9.40

The aforementioned materials were sampled from a power company in the Czech Republic, which is one of the most significant consumers utilising renewable sources in large quantities.

Proximate and ultimate analyses were performed for all the tested samples – Tab. 2.

Tab. 3 shows measured values of the physical properties for the respective tested samples.

### **Experimental methods**

Sampling was done according to standard ČSN EN 14778 – Solid biofuels – Sampling (CSN EN 14778, 2011). A total of four varieties of wood chips were sampled (four combined samples). According to standard ČSN EN 14780 – Solid biofuels – Methods for sample preparation (CSN EN 14780, 2011), subsamples were taken from the samples, for which the moisture content was determined immediately using a METTLER TOLEDO HS 153 halogen moisture analyser.

Furthermore, the subsamples were subject to proximate and ultimate analyses, apparent den-

sity according to standard ČSN EN 15103 – Solid biofuels – Determining apparent density (CSN EN 15103, 2010) and screen analysis according to standard ČSN EN 933-1 – Testing of geometric properties of aggregates – Part 1: Determining granularity – Screen analysis (CSN EN 933-1, 2012).

Inclination to self-ignition, the so-called basket test, was determined for all combined samples using the method according to standard ČSN EN 15188 – Determination of the spontaneous ignition behaviour of dust accumulations (CSN EN 15188, 2008). This method is used to determine self-ignition temperature in relation to quantity based on piling in a furnace at a constant temperature. In addition, the induction period, defined by the standard as the period between reaching the storage temperature and ignition, was monitored.

The self-ignition temperatures were measured in a furnace for solid materials self-heating CLASIC CZ KK5006 (Czech Republic) with the volume of

54 dm<sup>3</sup>. A special device for hanging a cubic basket with a sample and three thermocouples is installed in the test furnace. The furnace temperature is measured by two thermocouples placed in the middle of the distance between the furnace wall and the basket. The temperature of the sample is measured in the centre of the cubic basket with another thermocouple. The measurement takes place in the isoperibolic mode.

The first furnace test temperature was chosen according to the experience with the evaluated material. Once the selected temperature was reached, the sample basket with the sample was placed in the oven. The thermocouple located in the centre of the sample was used to indicate whether self-ignition has occurred at the constant furnace temperature. Temperature for the next test is governed by the result of the previous test. The self-ignition temperature ( $T_{SI}$ ) was calculated as the temperature average of the two thermocouples that measure the temperature in the furnace.

Furthermore, in case of forest wood chips, gases were analysed in relation to temperature. The analysis of gaseous products was done using a NICOLET iS10 infrared spectrometer with Fourier transformation (USA).

After the measurements, the measured data of the respective samples were compared and evaluated in terms of fire due to self-ignition. Besides determining the self-ignition temperature, critical sample dimensions were also calculated, which characterise the degree of self-ignition risk at an ambient temperature and also the time in which self-ignition can occur at the given temperature and size. Based on the gas analysis, the effect of temperature on the composition and quantity of the gases produced during forest wood chips self-heating was evaluated.

#### *Analysis of gaseous products from forest wood chips*

The apparatus used for the analysis of gaseous products of the forest wood chips self-heating was built from the following parts: furnace for solid materials self-heating with selectable atmosphere CLASIC CZ KK5006 (CR), NICOLET iS10 infrared spectrometer with Fourier transformation (FTIR spectrometer- USA) equipped with a gaseous cuvette of the optical length of 10 m, a pump and a computer. Samples of forest wood chips were heated at 50 °C, 100 °C and 150 °C in a cubic wire basket with the side dimensions of 7 cm for 1 hour. The gaseous products were identified using the OMNIC 8 software, and quantitative determination of carbon oxides and methane was done using the TQ Analyst spectroscopic software.

## Results and discussion

### *Determination of self-ignition temperature*

According to standard ČSN EN 15188 (CSN EN 15188, 2008), the measured temperature-time relation is used to determine the self-ignition temperature,  $T_{SI}$  for each basket volume. Cube-shaped baskets are used for the measurement. Furthermore, the measured results can be used to determine the induction burning period for various volumes. Table 4 shows results of the basket test of the tested samples; the given values are averages from two measurements. From the results it follows that with the increasing material volume, the self-ignition temperature decreases and the induction period is extended.

**Tab. 4.** Results of the basket test (Perdochova, 2015).

Tested sample	Basket volume (cm <sup>3</sup> )	$T_{SI}$ (°C)	ID (hour)
<b>Deciduous wood chips</b>	343	204	2.17
	1000	183	3.20
	3375	160	4.90
<b>Wood-working wood chips</b>	343	211	1.23
	1000	205	1.50
	3375	195	1.90
<b>Forest wood chips</b>	343	193	1.33
	1000	177	2.83
	3375	160	6.23
<b>Deciduous wood chips – poplar</b>	343	207	0.93
	1000	187	2.29
	3375	167	6.54

Evaluation of the test results of self-ignition temperature determination was performed using the dependence of the logarithm of volume to surface ratio for the respective shape and site of the basket used ( $\log [V/A]$ ) and the inverted reciprocal value of the self-ignition temperature ( $1/T_{SI}$  [K<sup>-1</sup>]), known as the pseudo-Arrhenius graph of self-ignition temperature.

Equation (1) was used for the extrapolation of data outside the zone of measured temperatures and dimensions is as follows (CSN EN 15188, 2008):

$$\log (V/A) = a + b \times (1/T_{SI}) \quad (1)$$

where  $V$  – volume of precisely defined body (m<sup>3</sup>),  $A$  – surface of precisely defined body (m<sup>2</sup>),  $T_{SI}$  – self-ignition temperature (K).

The results obtained from Equation (1), i.e. logarithm of volume to surface ratio, are shown in Fig. 2. This Figure shows self-ignition temperatures (upper side of the graph) for different volumes of the material depending on ( $\log (V/A)$  to  $1/T$ ).

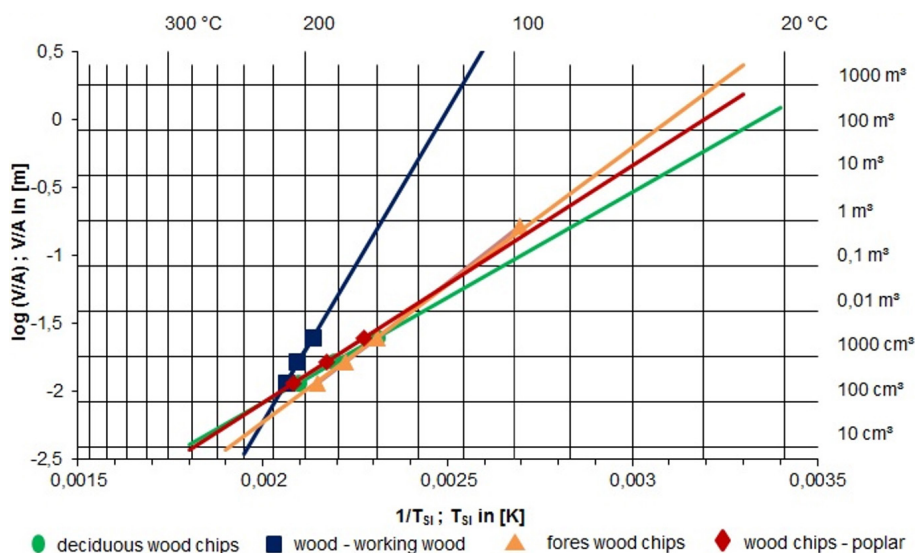


**Fig. 2.** Pseudo-Arrhenius graph of self-ignition temperature for tested samples (Perdochova, 2015).

From the graph above it is evident that samples of deciduous, forest wood chips and poplar have a similar course, whereas the dependence for wood-working wood chips is different. In case of wood-working wood chips, the intensity of oxidation is more strongly dependent on temperature than in case of the other samples, which can be due to different ingredients and structure. Based on this graph, self-ignition temperature  $T_{si}$  of wood-working wood chips is less dependent on the change of volume than in other materials. Wood-working wood chips are less prone to self-ignition than other types because of their higher self-ignition temperatures compared to other samples.

In addition, the logarithmic dependence of wood-working wood chips does not describe the course of the measured data as accurately as for other materials. Therefore, other types of mathematical expressions were tested and a third-degree polynomial was found applicable for wood-working wood chips. However, confirmation of the correctness using other experiments is necessary, at least for the 2000 cm<sup>3</sup> basket volume.

The different dependence for wood-working wood chips may be due to the different properties of this material as wood working wood chips are made from wood free of bark, leaves or needles and therefore have lower nitrogen content (see Table 2) than the other samples. Nitrogen content is related to the presence of needles and leaves in the biomass (Blomqvist & Persson, 2003) and can affect the course of self-heating, as these materials have lower ignition temperature (270–350 °C) than wood (410–450 °C) (Babrauskas, 2003).

Another possible cause of the different behaviour of wood-working wood chips is the grain size, which

is different than in the other samples. In case of wood-working wood chips, the mean grain size was about 13 mm, whereas in the other samples it was around 9 mm. According to literature (Jirjis, 1995), the increased size of particles means a decreasing risk of self-ignition, which has been confirmed by the self-ignition temperature measurement (wood-working wood chips have the lowest inclination to self-ignition).

The graph in Fig. 3 shows that the dependence of the volume to surface ratio logarithm on temperature also differs for different samples (other than wood-working wood chips). For small sample volumes, forest wood chips are most easily self-ignited, whereas the lowest inclination to self-ignition is demonstrated by wood-working wood chips. However, during extrapolation to larger volumes, deciduous wood chips, which contained bark just like forest wood chips, were shown to be more inclined to self-ignition.

Also, induction time of combustion for various volumes as a dependence of the induction time logarithm ( $t_i$ ) to the volume to surface ratio logarithm ( $\log [V/A]$ ) can be determined from the measured results (Fig. 3). The induction time is designed by the standard ČSN EN 15188 (CSN EN 15188, 2008) as a period between reaching storage temperature and ignition. The determined dependence is described by Equation (2):

$$\log(t_i) = a \times \log(V/A) - b \quad (2)$$

where  $t_i$  – induction time (h),  $V$  – volume of precisely defined body (m<sup>3</sup>),  $A$  – surface of precisely defined body (m<sup>2</sup>).

Graph 3 shows the induction time,  $t_i$ , required to reach the self-ignition temperature,  $T_{si}$ , under opti-

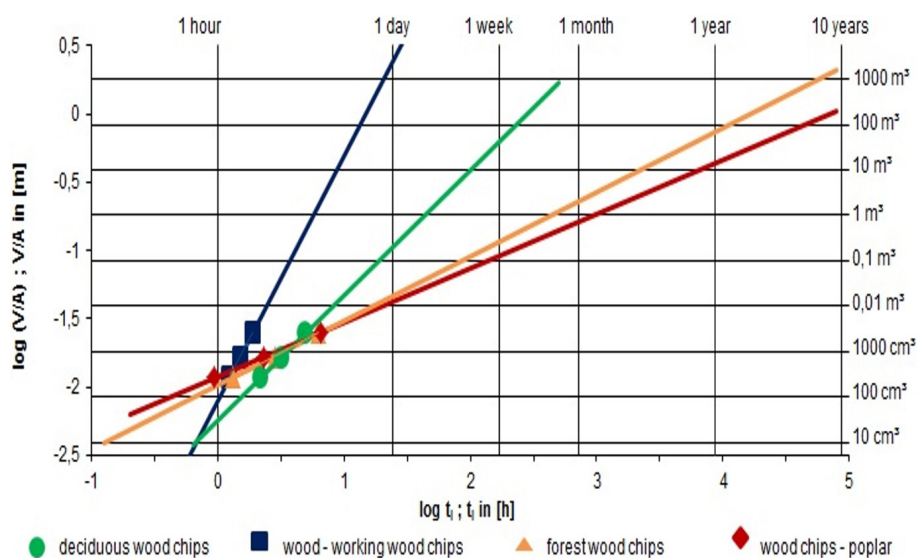


**Fig. 3.** Dependence of induction time on the volume to surface ratio of the tested samples (Perdochova, 2015).

mal condition for the advancement of self-heating at a given volume to surface ratio,  $V/A$ .

The dependence of induction time on the self-ignition temperature has an approximately linear character. This dependence is described by Equation (3):

$$t_i = -0.0961 T_{SI} + 20.932 \quad (3)$$

Its coefficient of determination  $R^2 = 0.8161$  indicates strong dependence of the induction time on temperature. Therefore, samples of materials (deciduous wood chips – green line, wood-working wood chips – blue line) with higher self-ignition temperature behave differently.

From the above graphs (Figs. 2 and 3), self-ignition temperatures and times necessary for the self-ignition of samples for volumes approximating the realistic storage of the tested materials, i.e. for larger volumes, can be estimated. For example, wood-working wood chips with the cubic volume of  $1 \text{ m}^3$  self-ignite above  $98 \text{ }^\circ\text{C}$  (Fig. 2). If this sample is stored at this constant temperature, a fire would start after 15.4 days (Fig. 3).

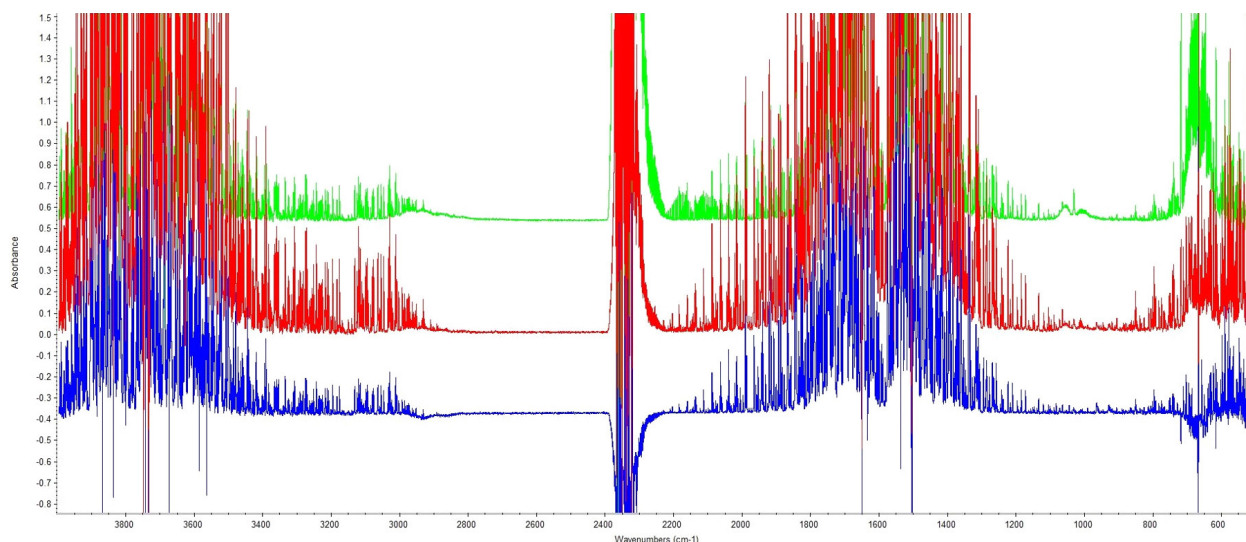
After modification, the extrapolated dependence also provided critical dimensions of stored dust for the respective samples, which presents a risk of self-ignition at the given ambient temperature, and also the time after which self-ignition can occur at the respective temperature and dimensions; characteristic dimensions, i.e. the cube's side, which are limiting for the self-ignition. These dependencies can also be used to evaluate the danger of layers of deposited dust at higher temperatures. According to the calculated values, a deciduous wood chips pile of about 5.17 m would self-ignite after being stored for about 9.78 days at  $30 \text{ }^\circ\text{C}$ . From this evaluation it follows that under normal conditions it is highly probable

that storage of deciduous wood chips can lead to self-ignition. If this stored material is heated to an even higher temperature, the risk of fire increases. Therefore, to prevent self-ignition, the stored material must be protected against sources of heat and by increasing its surface area. Self-ignition is also probable in case of poplar and forest wood chips because they can self-ignite at  $30 \text{ }^\circ\text{C}$  and dimensions of 9.31 m (poplar) and 15.07 m (forest wood chips). Compared to that, wood-working wood chips under normal conditions are improbable to self-ignite during storage because the calculated layer height at which self-ignition could occur at around  $30 \text{ }^\circ\text{C}$  exceeds realistic storage conditions.

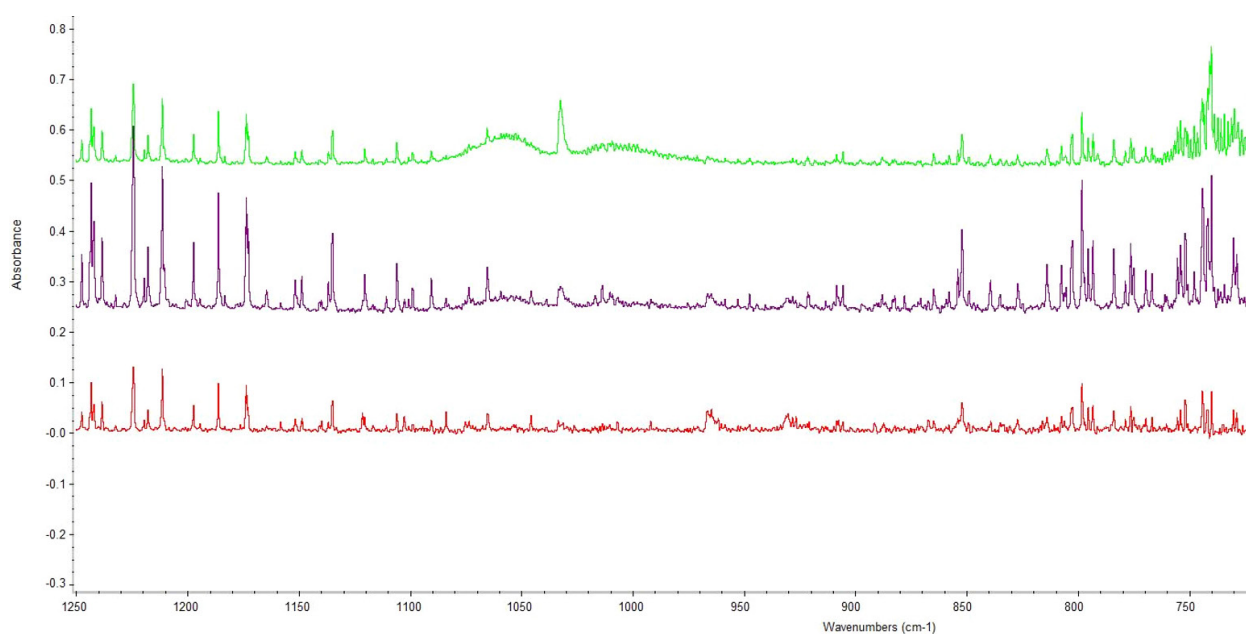
#### ***Effect of temperature on the composition of gaseous products of forest wood chips***

Fig. 4 shows an example of infrared spectra of gaseous product composition for forest wood chips at 50, 100 and  $150 \text{ }^\circ\text{C}$  in the 60<sup>th</sup> minute from the measurement start.

Spectral analysis has shown that at temperatures of 50, 100 and  $150 \text{ }^\circ\text{C}$ , carbon oxides, water and aliphatic hydrocarbons are produced. In all cases, water demonstrated the highest intensity in the  $4000\text{--}3500 \text{ cm}^{-1}$  and  $1700\text{--}1300 \text{ cm}^{-1}$  zones, followed by carbon dioxide in the  $2350 \text{ cm}^{-1}$  and  $670 \text{ cm}^{-1}$  zones. Carbon monoxide, which is found immediately next to carbon dioxide, lies in the  $2240\text{--}2040 \text{ cm}^{-1}$  zone. In case of the sample tested at  $150 \text{ }^\circ\text{C}$ , the presence of carbon monoxide was evident, whereas for samples heated at lower temperatures, only its traces are shown in the spectrum throughout the entire sample heating time. During wood chips heating, a clear band appeared in the  $3000\text{--}2800 \text{ cm}^{-1}$  zone indicating the presence of



**Fig. 4.** Infrared spectrum of gaseous products produced by decomposition of forest wood chips at 50 (blue spectrum), 100 (red spectrum) and 150 °C (green spectrum) in the 60<sup>th</sup> minute.



**Fig. 5.** Band of methanol in the spectrum of gaseous products of forest wood chips decomposition at 150 (green spectrum), 100 (purple spectrum) and 50 °C (red spectrum).

aliphatic hydrocarbons. Aliphatic hydrocarbons also have a band in the 1450–1300  $\text{cm}^{-1}$  zone, which however also includes a water absorption band; therefore, their presence could not be confirmed. When heating forest wood chips to 150 °C, methanol was detected in the gaseous products, with a band in the 1100–960  $\text{cm}^{-1}$  zone which has a significant peak at 1030  $\text{cm}^{-1}$  (see green spectrum in Fig. 5) and a band around 3100  $\text{cm}^{-1}$ . Here, it is necessary to emphasize that methanol, just like carbon monoxide, is a toxic substance.

As it is evident from the spectra above, heating temperature affects the composition of gaseous products. At higher temperatures, more harmful

substances are released and it is therefore necessary to monitor the temperature of the stored material to prevent self-ignition and the occurrence of hazardous substances.

#### ***Effect of temperature on $\text{CO}_2$ , $\text{CO}$ and $\text{CH}_4$ concentrations in forest wood chips***

The effect of heating temperature on the concentration of  $\text{CO}_2$ ,  $\text{CO}$  and  $\text{CH}_4$  was evaluated and the changes in the concentrations of these gases at 50–150 °C for forest wood chips are shown in Tab. 5.

From Table 5 it is evident that the heating temperature affects the quantity of the produced gases. For

**Tab. 5.** Time-dependent concentrations of CO<sub>2</sub>, CO and CH<sub>4</sub> in forest wood chips at different temperatures.

Time (min)	CO <sub>2</sub> concentration (ppm)			CO concentration (ppm)			CH <sub>4</sub> concentration (ppm)		
	50 °C	100 °C	150 °C	50 °C	100 °C	150 °C	50 °C	100 °C	150 °C
0	19.74	2117.08	19567.00	3.32	8.79	139.86	19.31	39.03	82.31
10	24.28	1610.67	11300.74	2.88	10.51	124.60	16.79	43.35	78.83
20	23.65	944.44	4711.99	3.81	10.10	119.00	11.59	42.48	64.74
30	21.16	490.87	3666.46	4.29	8.62	110.88	8.70	38.85	75.41
40	19.48	186.66	3064.21	3.31	8.99	98.05	10.82	42.99	62.95
50	18.05	53.00	2767.79	3.50	11.27	85.14	9.42	42.64	56.49
60	12.00	28.00	2772.60	3.01	8.15	87.7	9.13	45.53	56.49
<b>Average</b>	<b>19.77</b>	<b>775.82</b>	<b>6835.83</b>	<b>3.45</b>	<b>9.49</b>	<b>109.32</b>	<b>12.25</b>	<b>42.12</b>	<b>68.17</b>

all tested gases applies that increasing temperatures increases the gas concentration. At 150 °C, the increase of gas concentration is very sharp for carbon oxides, whereas in case of methane, the increase already occurs at 100 °C and a further increase in temperature does not lead to such a sharp increase in the concentration as in case of carbon oxides. Therefore, it can be concluded that the reaction mechanism of carbon oxide production is different to that of methane.

During wood chips heating, the highest volume of released gases was found for carbon dioxide even though the volume of methane at 50 °C was comparable.

Thus, the heating temperature affects the quantity of gases produced by wood material decomposition and the carbon dioxide and methane concentration can be used as indicators of self-ignition development. It is generally known that these gases are used for the indication of self-ignition in coal. Nevertheless, based on the difference of gases concentrations at various temperatures, it is necessary to consider which gas is most suitable as the indicator of self-ignition state.

Also, the CO/CO<sub>2</sub> ratio (Adamus et al, 2007) is often used as an indicator of the stored material temperature. Nonetheless, Derychová et al. (2016) stated that the use of the CO/CO<sub>2</sub> concentration ratio to estimate the temperature of wood material, especially saw dust, is not possible. In addition, in case of forest wood chips evaluated in this study, the CO/CO<sub>2</sub> ratio cannot be used to indicate the temperature increase.

With respect to the safety of workers, carbon monoxide should be used as the indicator of self-ignition due to its toxicity. However, because the differences in concentrations at various temperatures are more distinct for carbon dioxide, its production has also to be monitored in addition

to carbon monoxide, using it to more accurately monitor the early stages of self-ignition.

An intervention upon the increase of the measured gases concentration can serve as a measure against the initiation of fire due to the self-ignition of stored wood material.

The measurements and evaluated data lead to the following conclusions:

- The lowest inclination to self-ignition is demonstrated by wood-working wood chips. It was found that at small volumes, forest wood chips are most inclined to self-ignition, but after extrapolation to larger volumes, deciduous wood chips have proved to be more prone to self-ignition.
- In case of wood-working wood chips, a different trend of dependence was observed than for the remaining tested samples, which is probably due to the absence of bark, leaves or needles in the sample as well as different particle size.
- Qualitative analysis of gaseous products of forest wood chips showed that carbon oxides, water and aliphatic hydrocarbons are produced at 50, 100, 150 °C. When heating forest wood chips to 150 °C, methanol was also detected in the gaseous products.
- Concentrations of carbon dioxide, carbon monoxide and methane increase with the increasing temperature.
- Carbon oxides and methane can be considered as characteristic gases for the indication of wood chips self-heating.

## Conclusion

This study focuses on the evaluation of the inclination to self-ignition and the effect of heating temperature on gaseous products for various types of wood chips with the aim to compare their behaviour at increased temperatures, and thereby to obtain

objective data for the proposal of suitable measures to prevent self-ignition.

Measurement results showed that the inclination to self-ignition is not the same for all types of wood chips. Besides the self-ignition temperature for the respective volumes, which were different for each sample, the character of the dependence between the self-ignition temperature and biomass volume also differed.

Three of the evaluated samples demonstrated a strong inclination to self-ignition. The sample of wood-working wood chips showed differences compared to the other samples. This wood chip type demonstrated the lowest inclination to self-ignition, so its self-ignition is very improbable. Its low inclination to self-ignition is probably due to the low content of bark, leaves and needles in the sample, which was also demonstrated by the low nitrogen content.

Furthermore, it was found that the heating temperature affects the gases released from the forest wood chips. Gaseous products of heating are comprised mainly of water vapour, carbon oxides and aliphatic hydrocarbons. At the highest heating temperature, methanol was also released. The heating temperature also affects the amount of monitored gases. Higher concentrations were measured with increasing temperature.

The performed measurements showed that self-heating of biomass based on wood material stored in large quantities can lead to a fire. During self-heating, production of toxic gases occurs compromising safety at the worksite in case of storage in closed areas.

From the above it follows that for safe storage of wood material, no universal instructions can be drawn. Each company should elaborate its own instructions for the specific type of biomass and situation regarding the storage of biomass in terms of self-ignition.

For each type of biomass, the instructions should include the maximum storage height of loosely dumped piles and the maximum time of storage. These safety parameters can be determined experimentally. Verification of the course of self-ignition can be done by analysing the carbon dioxide and carbon monoxide released from the stored wood chips.

#### *Acknowledgement*

*This article was written in the framework of the project "Innovation of the Subject Transport of Hazardous Substances and Waste". Project number: RPP2020/131 funded by the University Development Fund (FRVŠ) of the Ministry of Education, Youth and Sports of the Czech Republic.*

## References

- Adamus A (2004) Collection of scientific works of Vysoká škola báňská – Technical University of Ostrava, Mining–geological series 50.
- Adamus A, Věžníková H, Šancer J (2007) Coal, ore, geological survey: 31–37.
- Alakoski E, Jämsén M, Agar D, Tampio E, Wihersaari M (2016) Renewable and Sustainable Energy Reviews 54: 376–383.
- Babrauskas V (2003) Ignition Handbook: Principles and applications to fire safety engineering, fire investigation, risk management and forensic science. Fire Science Publishers, USA.
- Balog K (1999) Self-ignition. SPBI, Ostrava.
- Blomqvist P, Persoon B (2003) Spontaneous Ignition of Biofuels – A Literature Survey of Theoretical and Experimental Methods. Boras: SP Swedish National Testing and Forsknings institut Research Institute.
- Bowes P (1984) Self-heating: evaluating and controlling the hazards. Dept. of the Environment, Building Research Establishment, Elsevier, Amsterdam.
- CSN EN ISO 17225-1 (2015) Solid biofuels – Fuel specifications and classes – Part 1: General requirements. Czech Office for Standards, Metrology and Testing, Prague.
- CSN EN ISO 17225-4 (2015) Solid biofuels – Fuel specifications and classes – Part 4: Graded wood chips. Czech Office for Standards, Metrology and Testing, Prague.
- CSN EN 15188 (2008) Determination of the spontaneous ignition behaviour of dust accumulations. Czech Normalization Institute, Prague.
- CSN EN 14778 (2011) Solid biofuels – Sampling. Czech Office for Standards, Metrology and Testing, Prague.
- CSN EN 14780 (2011) Solid biofuels – Sample preparation. Czech Office for Standards, Metrology and Testing, Prague.
- CSN EN 15103 (2010) Solid biofuels – Determination of bulk density. Czech Office for Standards, Metrology and Testing, Prague.
- CSN EN 933-1 (2012) Tests for geometrical properties of aggregates – Part 1: Determination of particle size distribution – Sieving method. Czech Office for Standards, Metrology and Testing, Prague.
- Derychova K, Perdochova M, Veznikova H, Bernatik A (2016) Journal of Loss Prevention in the Process Industries 43: 203–211.
- Ekoporadna (2010) Why use biomass for heating? Available at: [http://www.ekoporadna.cz/wiki/doku.php?id=energie:proc\\_topit\\_biomasaou](http://www.ekoporadna.cz/wiki/doku.php?id=energie:proc_topit_biomasaou).
- Esteban B, Riba JR, Baquero G, Rius A (2015) Renewable Energy 74: 568–575.
- He X, Lau AK, Sokhansanj S, Lim CJ, Bi XT, Melin S (2014) Fuel 134: 159–165.
- Jäppinen E, Korpinen OJ, Laitila J, Ranta T (2014) Renewable and Sustainable Energy Reviews 29: 369–382.
- Jirjis R (1995) Biomass and Bioenergy 9: 181–190.
- Jirjis R (2005) Biomass and Bioenergy 28: 193–201.
- Kalousek J (1999) Basics of physical chemistry of combustion, explosion and extinguishing. SPBI, Ostrava.

- Kuang X, Shankar TJ, Bi XT, Sokhansanj S, Lim CJ, Melin S (2008) *Annals of Occupational Hygiene* 52: 675–683.
- Kuang X, Shankar TJ, Bi XT, Lim CJ, Melin S (2009) *Annals of Occupational Hygiene* 53: 789–796.
- Lohrer CH, Krause U, Steinbach J (2005) *Process Safety and Environmental Protection* 83: 145–150.
- Oren MJ, Karunakaran KP, Pegg MJ, Mackay MD (1987) *Fuel* 66: 9–12.
- Perdochova M (2014) Safety, reliability and risks 2014: XI. International Conference for Young Scientists. Liberec: Technical University of Liberec.
- Perdochova M (2015) Post-graduate thesis, VŠB – Technical University of Ostrava, Faculty of Safety Engineering.
- Perdochova M, Derychova K, Veznikova H, Bernatik A, Pitt M (2015) *Process Safety and Environmental Protection* 94: 463–470.
- Stuart BH (2004) *Infrared Spectroscopy: Fundamentals and Applications*. Chichester, UK: John Wiley & Sons, Ltd.
- Torrent JG, Gómez ÁR, Anez, NF, Pejic LM, Tascón A (2016) *Fuel* 184: 503–511.
- Yazdanpanah F, Sokhansanj S, Lim CJ, Lau A, Bi X, Melin S (2014) *Biomass and Bioenergy* 71: 1–11.
- Vassilev SV, Vassileva CHG, Vassilev VS (2015) *Fuel* 158: 330–350.
- Věžníková H, Adamus A (2007) *Coal – Ores – Geological survey* 14: 32–36.
- Veznikova H (2016) The self-heating of organic materials. SPBI, Ostrava.
- Ramirez A, Garcia-Torrent J, Tascón A (2010) *Journal of Hazardous Materials* 175: 920–927.
- Jones JM, Saddawi A, Dooley B, Mitchell EJS, Werner J, Waldron DJ, Weatherstone S, Williams A (2015) *Fuel Processing Technology* 134: 372–377.

# Dechloromethylation of the berberine to berberrubine – tricks to obtain pure product

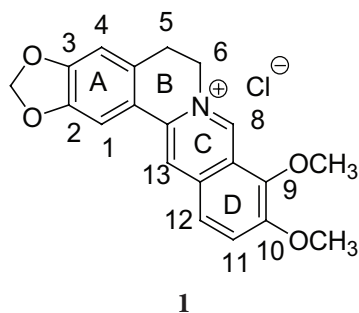
Viktor Milata, Eva Holúbková

Department of Organic Chemistry, Institute of Organic Chemistry, Catalysis and Petrochemistry,  
Faculty of Chemical and Food Technology, Slovak University of Technology,  
812 37 Bratislava, Radlinského 9, Slovakia  
viktor.milata@stuba.sk

**Abstract:** Berberine (**1**), as a compound with interesting biological activities, can be modified at various positions to obtain more potent substances. Modifications at position 9 are based on demethylation with simultaneous dechlorination resulting in berberrubine. The most frequent process is thermal dechloromethylation and this work describes this method with detailed tricks to obtain almost pure product in high yield.

## Introduction

Berberine (**1**) (Scheme 1) is an isoquinoline alkaloid belonging to protoberberine alkaloids (Nechepurenko 2010). About thousand structurally similar alkaloids with planar isoquinoline skeleton are currently known (Huang 2011).



Scheme 1. Berberine.

Berberine can be found in many plants such as *Hydrastis canadensis*, *Coptis chinensis*, *Berberis aquifolium*, *Berberis vulgaris* or *Berberis aristata* mostly in crust of their roots, roots or rootstocks obtained by extraction with ethanol and isolated like chloride or hydrogen sulfate, respectively. Berberine shows antibacterial activity against various bacteria, fungi, protozoa, chlamydia or viruses, and it also shows other pharmacological effects (Birdsall, 1997). Very important applications are in the treatment of Alzheimer's disease (Ling, 2012), schizophrenia (Sun, 2013) and HIV (Bodiwala, 2011) due to the inhibition of AChE or topoisomerase I resulting in antiproliferative (antineoplastic, anticancer) (Yang-Biao, 2013; Lo, 2013; Su, 2013; Xiao, 2012; Zhang, 2012), antimicrobial (Shao-Lin, 2013; Zhan, 2013a), antihyperlipidemic (Peng, 2008) or hypoglycemic activity (Yan-Xiang, 2012).

Most frequent reactions run at positions 2, 3, 9, 10 or on the immonium fragment, e.g. nucleophilic addi-

tion (Man, 2001). Reactivity of berberine has been thoroughly summarized by Nechepurenko (2010).

## Experimental

Spectrometer INOVA 300 (300 MHz, Varian Inc., Palo Alto, CA, USA) was used to measure  $^1\text{H}$  NMR spectra at RT frequencies. Chemical shifts in ( $\delta$ )-[ppm] (parts per million) were referenced to the residual signal of the solvent. Coupling constants ( $J$ ) are given in [Hz] with multiplicity: s (singlet), d (doublet), dd (doublet of the doublet), t (triplet), q (quartet), q (quintet) and m (multiplet). Tetramethylsilane was used to calculate  $^1\text{H}$  chemical shift scales and it was correctly referenced using the (residual) solvent signals (2.50 and 39.52 ppm for DMSO).

All reagents (incl. berberine chloride) and solvents were purchased from Sigma-Aldrich® (Darmstadt, Germany), Alfa-Aesar® (Ward Hill, MA, USA), Fluka® (Buchs, Switzerland) and Mikrochem® (Pezinok, Slovakia). Solvents were purified and/or dried using standard laboratory methods and stored over molecular sieves (4 Å). Column chromatography was performed using silica gel Nomasil-40-63 m (VWR®, Randor, PA, USA) and a suitable eluent according to TLC. Reaction progress was monitored by thin layer chromatography on Silufol or Alufol plates (Merck®, Darmstadt, Germany) with a UV indicator at  $\lambda = 254$  nm.

Melting points (m. p.) of the prepared compounds were determined on a Boetius micro hot stage using a digital thermometer TD 121 (VWR®, Randor, PA, USA) and are uncorrected.

### 5,6-Dihydro-9-hydroxy-10-methoxybenzo[g]-1,3-benzodioxolo[5,6-a]quinolinium (berberrubine)

A sample of 2.0 g (2.3 mmol) of berberine (**1**) was heated without any solvent under vacuum and magnetic stirring to 200 °C for 40 minutes. During heat-

ing, yellow berberine powder slowly turned to deep red-brown-black matter of the crude product. Yield was around 1.54 g of raw berberrubine. Recrystallization from methanol – ethanol 1:1 mixture gave almost analytically pure product.

**<sup>1</sup>H NMR:** (CD<sub>3</sub>OD) δ 9.28 (s, 1H, H-8), 8.70 (s, 1H, H-13), 7.54 (t, 1H, <sup>3</sup>J<sub>HH</sub> = 8.04 Hz, H-12), 7.49 (s, 1H, H-1), 6.91 (d, 1H, <sup>3</sup>J<sub>HH</sub> = 7.60, H-11), 6.85 (s, 1H, H-4), 6.04 (s, 2H, H-2'), 4.60 (t, 2H, <sup>3</sup>J<sub>HH</sub> = 5.32, H-6), 3.89 (s, 3H, H-10'), 3.12 (t, 2H, <sup>3</sup>J<sub>HH</sub> = 5.46, H-5)

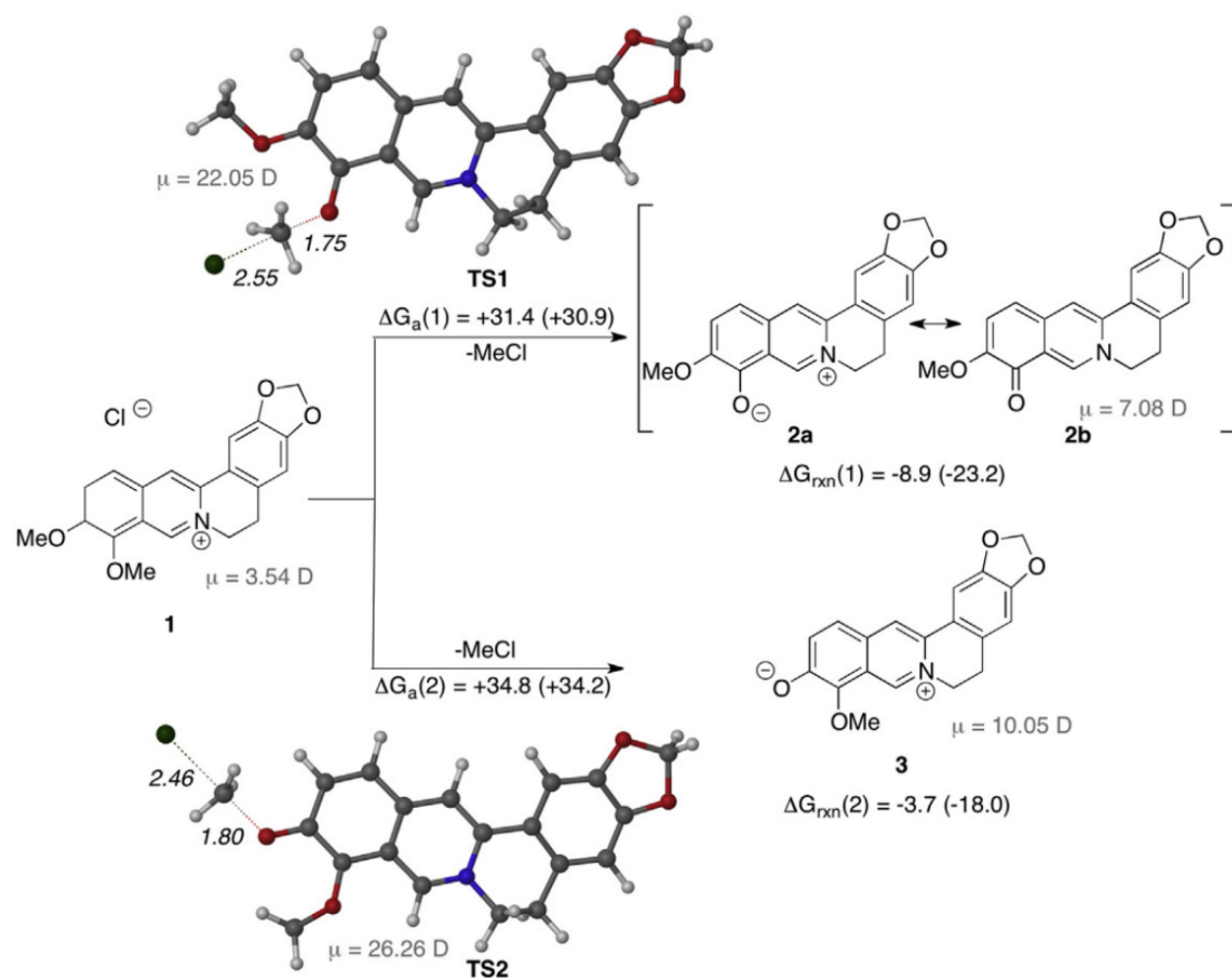
**<sup>13</sup>C NMR:** (CD<sub>3</sub>OD) δ 149.5 (C-13'), 149.4 (C-9), 148.0 (C-10), 145.9 (C-8), 134.2 (C-2), 132.2 (C-3), 129.2 (C-12'), 122.6 (C-8'), 121.4 (C-4'), 120.1 (C-13''), 118.3 (C-12), 107.7 (C-11), 107.1 (C-13), 104.4 (C-4), 101.8 (C-1), 56.9 (C-2'), 55.2 (C-10'), 54.1 (C-6), 27.5 (C-5)

## Results and Discussion

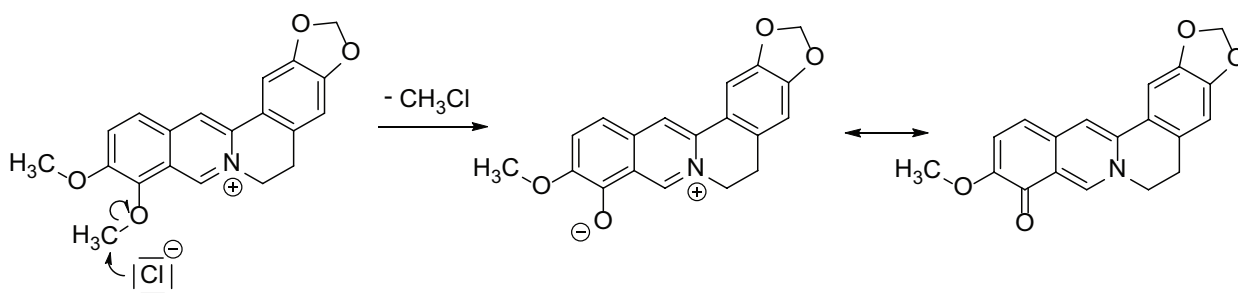
Berberrubine alone has interesting properties. It behaves as a fluorescent chemosensor of alkanes with an almost constant response regardless of the alkane

chain length (Delgado-Camón, 2015). Because many biological activities are related to structural modifications (Xiao, 2017) at position 9 (Liu, 2017, Xiao 2018), some 9-substituted derivatives were prepared (Milata, 2019). Dechloromethylation of the starting berberine (1) selectively occurring at position 9 is the key step leading to derivatization of this position. Therefore, a number of berberrubine preparations are known (Iwasa, 1996; Lo, 2013; Basu, 2012; Zhan, 2013a, 2013b), including microwave one (Liu, 2014; Delgado-Camón, 2015; Das, 2002), but these procedures are not recommended to be used with larger batches (more than 1 g). Due to the volatility of methylchloride, most of these reactions proceed under vacuum. In 2015, quantum chemical calculations have been published (Delgado-Camón, 2015, Scheme 2).

DFT calculations explain that the observed selectivity depends on the electron delocalization capability and the selectively demethylated species **2a/2b** are in oxo-enol tautomeric equilibria. Thus, a simple mechanism of berberine (1) dechloromethylation to berberrubine (2) was proposed (Scheme 3).



**Scheme 2.** DFT calculations of the dechloromethylation of **1**. Reproduced from Delgado-Camón 2015 with permission of Elsevier Ltd.



**Scheme 3.** Proposed mechanism of berberine (**1**) dechloromethylation to berberrubine (**2**).

The crucial step was optimized also under microwave irradiation in an open vessel, closed vessel and in a closed vessel under vacuum (1.6 kPa) but the obtained yields were not higher than 80 % and, according to our experience, yields close to the quantitative one are not real (Delgado-Camón, 2015). Classical procedures have proved to be the most efficient, economical and simple. The best results were obtained in a round bottomed flask for a 2 g batch with the volume of 100 ml (Fig. 1a). An Apolon (pear-shaped) flask might be better but one with an NZ 29 ground was not at disposal. A tear drop-shaped flask is not as advantageous and the last one, which can be used under vacuum – heart-shaped flask, is totally unsuitable considering the following mechanical stirring.

The starting deep yellow berberine (**1**) is a voluminous, mobile, lightweight powder and 2 g of it is the optimum quantity for each run: the flask is connected to vacuum (1.6 kPa). Higher vacuum gives does not result in better yields or faster reaction; on the contrary, when the flask is closed and vacuum is applied, the dust outlet at 1.6 kPa is low (estimated approx. 2–3 % – see Fig. 1a), at higher vacuum, the dust outlet is much higher (perhaps it is influenced by sublimation).

The flask with berberine (**1**) was placed in an oil bath preheated to 205 °C, the temperature then drops down to 195–200 °C (sometimes isolation with aluminium foil is required). At this particular time, a powerful crosshead or cross-like stirrer (suitable for solid substances, Fig. 1b) and flexible fitted apparatus are necessary to help stirring the reaction mixture by balancing the whole apparatus. After a few minutes, berberine started to change its color to brown, strating from the wall (Fig. 1c), and the powder became heavier and turned to deep red/brown color, mainly at the wall of the flask.

Then, the apparatus was removed from the bath, vacuum was stopped and the content of the flask was thoroughly stirred to remove burned parts from the wall (Fig. 1d); after that, it was quickly returned into the heated bath (under vacuum). The use of a heating mantle is not recommended due to burned residues on the wall and more difficult heat control with scorch production. As the reaction proceeded, the color became darker and mechanical stirring was repeated approximately 7–9 times. After about 35 min, heating was switched off and the reaction mixture was left under vacuum to cool. Using this procedure, between 1.45–1.62 g (75.3–84.2 %) of raw berberrubine (**2**) can be obtained.

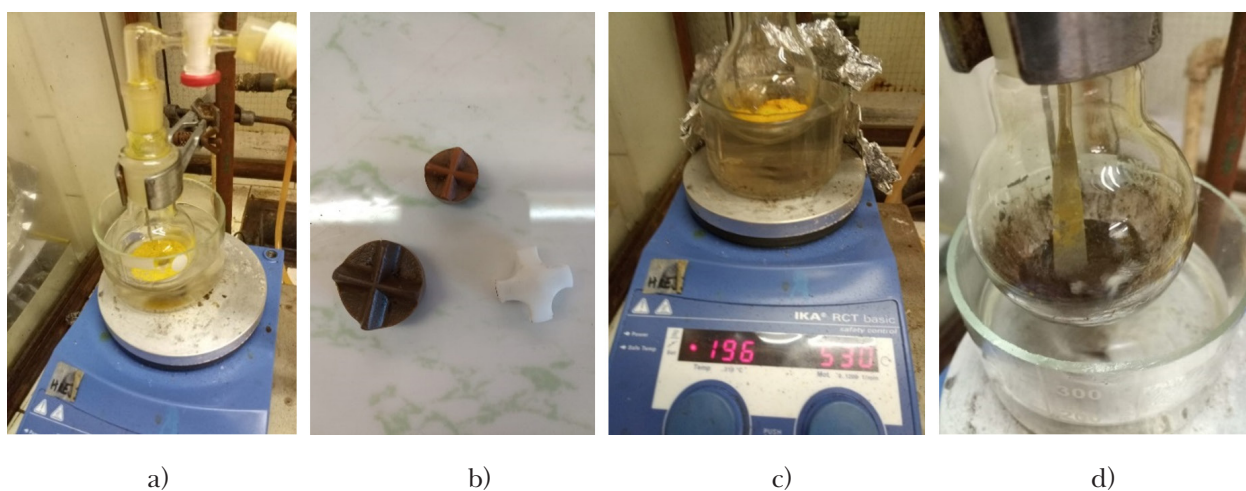


**Fig. 1.** a) Apparatus for effective preparation of **1**, b) Mag. stirrers, c) First step of heating of **1**, d) Final product.

Recrystallization was carried out from a mixture of ethanol:methanol (1:1); 1.57 g of raw 1 was refluxed in a sufficient amount of solvent (about 18 ml). After cooling, the separated ruby-red colored crystals were filtered off and washed with cold ethanol (berberrubine is insoluble in ethanol, contrary to methanol). After vacuum drying (1.6 kPa, 40 °C, 1 h), an analytical sample of berberrubine (**2**) (usually 1.25 g, 62.5 %) with m.p. 275–279 °C was obtained.

#### Acknowledgement

*This work was financially supported by the Science and Technology Assistance Agency under the contract No. APVV-17-0513.*

## References

- Basu A, Jaisankar P, Kumar SG (2012) *Bioorg. Med. Chem.* 20: 2498–2505.
- Birdasall TC, Kelly GS (1997) *Alt. Med. Rev.* 2: 94–103.
- Bodiwala HS, Sabde S, Mitra D, Bhutani KK, Sigh IP (2011) *Eur. J. Med. Chem.* 46: 1045–1049.
- Das B, Srinivas KVNS (2002) *Synth. Commun.* 32: 3027–3029.
- Delgado-Camón A, Jarne C, Cebolla VL, Larrañaga O, de Cózar A, Cossio FP, Vara Y, Domínguez A, Membrado L, Galbán J, Garriga R (2015) *Tetrahedron* 71: 6148–6154.
- Huang Z, Zeng Y, Lan P, Sun PH, Chen WM (2011) *Mini. Rev. Med. Chem.* 11(13): 1122–1129.
- Iwasa K, Kamiguchi K, Ueki M, Taniguchi M (1996) *Eur. J. Med. Chem.* 31: 469–478.
- Ling H, Tao S, Wenjun S, Zhonghua L, Yang S, Feng H, Xinshu L (2012) *Bioorg. Med. Chem.* 20: 3038–3048.
- Liu L-X, Yuan X, Gao Y, Zhou D-B, Li W-M, Tianran Chanwu Yanjiu Yu Kaifa (2014) 26(3): 427–430.
- Lo Ch-Y, Hsu L-Ch, Chen M-S, Lin Y-J, Chen L-G, Kuo Ch-D, Wu J-Y (2013) *Bioorg. Med. Chem. Lett.* 23: 305–309.
- Man S, Potáček M, Nečas M, Žák Z, Dostál J (2001) *Molecules* 6: 433–441.
- Milata V, Švédová A, Barbieriková Z, Holúbková E, Čipáková I, Cholujová D, Pánik M, Jantová S, Brezová V, Čipák I (2019) *Int. J. Mol. Sci.* 20(9): 2169–2187.
- Nechepurenko IV, Salakhutdinov NF, Tolstikov GA (2010) *Chem. Sust. Devel.* 18: 1–23.
- Peng Y, Dan-Qing S, Ying-Hong L, Wei-Jia K, Yan-Xiang W, Li-Mei G, Shu-Yu L, Rui-Qiang C, Jian-Dong J (2008) *Bioorg. Med. Chem. Lett.* 18: 4675–4677.
- Shao-Lin Z, Juan-Juan C, Guri LVD, Bo F, Xiang-Dong Z, Rong-Xia G, Cheng-He Z (2013) *Bioorg. Med. Chem. Lett.* 23: 1008–1012.
- Su T, Xie S, Yan J, Huang L, Li X (2013) *Bioorg. Med. Chem.* 21: 5830–5840.
- Sun H, Zhu L, Yang H, Qian W, Guo L, Zhou S, Gao B, Li Z, Zhou Y, Jiang H, Chen K, Zhen X, Liu H (2013) *Bioorg. Med. Chem.* 21: 856–868.
- Xiao D, Liu Z, Zhang S, Zhou M, He F, Zou M, Peng J, Xie X, Liu Y, Peng D (2017) *Mini-Reviews Med. Chem.* 17: 1424–1441.
- Xiao N, Chen S, Ma Y, Qiu J, Tan J-H, Ou T-M, Gu Z-S, Li D (2012) *Biochem. Biophys. Res. Commun.* 419: 567–572.
- Yan-Xiang W, Wei-Jia K, Ying-Hong L, Sheng T, Zheng L, Yang-Biao L, Yong-Qiang S, Chong-Wen B, Jian-Dong J, Dan-Qing S (2012) *Bioorg. Med. Chem.* 6552–6558.
- Yang-Biao L, Wu-Li Z, Yan-Xing W, Cai-Xia Z, Jian-Dong J, Chong-Wen B, Sheng T, Ru-Xian C, Rong-Guang S, Dan-Qing S (2013) *Eur. J. Med. Chem.* 68: 463–472.
- Zhan L, Chang J-J, Damu GLV, Fang B, Zhou X-D, Geng R-X, Zhou C-H (2013a) *Bioorg. Med. Chem. Lett.* 23: 1008–1012.
- Zhan L, Chang J-J, Zhang S-L, Damu GLV, Geng R-X, Zhou Ch-H (2013b) *Bioorg. Med. Chem.* 21: 4158–4169.
- Zhang L, Li J, Ma F, Yao S, Li N, Wang J, Wang Y, Wang X, Yao Q (2012) *Molecules* 17: 11294–11302.

# Determination of phosphate in water by flow coulometry

A. Manová<sup>a</sup>, E. Beinrohr<sup>b</sup>

<sup>a</sup>*Slovak University of Technology, Faculty of Chemical and Food Technology Institute of Analytical Chemistry, Radlinského 9, 812 37 Bratislava, Slovakia*

<sup>b</sup>*Department of Chemistry, Faculty of Natural Sciences, University of SS. Cyril and Methodius in Trnava  
alena.manova@stuba.sk*

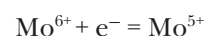
**Abstract:** In this work, the possibility of flow coulometry application as coulometric titration was studied. The method was used to analyze phosphates in wastewater samples. The principle of the determination consisted in the formation of molybdophosphate and its subsequent one-electron electrolytic reduction. The present method is applicable under optimal conditions in the concentration range of  $1.5 \times 10^{-6}$  to  $5.5 \times 10^{-5}$  mol/dm<sup>3</sup>. Detection limit of the method is  $3.42 \times 10^{-7}$  mol/dm<sup>3</sup>. Mineralization step has been proved a problem in total phosphate content determination. If mineralization was not carried out, only inorganic soluble phosphates were determined. It is a new method characterized by its simplicity of instrumentation and handling, which is a prerequisite for its further use in the field of trace analysis.

**Keywords:** coulometry, coulometric titration, phosphates, wastewater samples, porous electrode

## Introduction

Coulometry is based on the measurement of the electrical charge required to affect the electrochemical conversion of a studied substance. Faraday's law expresses the relationship between the amount of the substance and the charge. Coulometric measurements are very often used for quantitative analysis. With complete electrolytic conversion of the studied substance while maintaining the current efficiency of 100 %, this method can be used for direct or indirect determination of the substance without any reference materials in the coulometric analysis. The coulometric measurement can be performed for electrolysis at controlled current or potential. For coulometric titration of the sample solution in the porous electrode volume, no separate indicator system is required. If the pore size is approximately equal to the thickness of the diffusion layer, concentration of the analyte during electrolysis is practically the same throughout the electrode volume. In accordance with the Nernst equation, a change in the analyte concentration in the electrode volume is reflected by the change in the electrode potential. When the substance titration is complete, the electrode potential changes abruptly, indicating an equivalent point. In this way, substances which can be electrochemically oxidized or reduced in the aqueous solution or converted into an electrochemically active form can be titrated. Such substances also include phosphates and they, form a complex compound when reacted with ammonium molybdate with the P:Mo ratio of 1:12 (Heslop and Jones, 1985). Thus bound hexavalent molybdenum is electrochemically

reduced to pentavalent at different potential than molybdenum not bound to a heteropolyacid salt. Thus, an electrochemical reaction takes place on the electrode:



Phosphate content can be determined by the amount of molybdenum reduced. The high molybdenum-phosphorus binding rate ranks this method among very sensitive methods of quantitative analysis of phosphates in water. Phosphorus is mainly present in water in form of various phosphates: inorganic phosphates, polyphosphates, and organically bound phosphorus. Methods available in a conventional laboratory do not enable, the determination of individual groups of compounds as exact distribution cannot be achieved. All groups of phosphorus compounds are determined by their conversion to soluble inorganic orthophosphates which are then determined by absorption spectrophotometry (Nollet and De Gelder, 2000).

The Handbook of Water Analysis provides 29 references to phosphate determination in literature.

The review by Zaporozhets et al. (2019) covers the advantages of phosphorus determination in environmental objects such as saline and fresh water, soil, human serum and urine, food and fertilizers for the period of 2000–2018. Spectrophotometry as well as spectrophotometry combined with liquid or solid-phase extraction, flow-analysis system, electrochemical, luminescent and visual test-system have been considered. Spectrophotometry remains the most multipurpose method (applicable for the analysis of different objects), cost-effective despite

the rapid progress of electrochemical sensors. Flow-analysis systems are successfully implemented for surface and groundwater analysis as well as for saline water. Complex multicomponent luminescent and voltamperometric systems are used for phosphorus determination in biological matrices, e.g. serum and blood plasma, urine, etc. Test-systems can provide simple and prompt reactive phosphate monitoring without using complex devices. However, the limitation of columns with color band formation include the short range of phosphate concentrations and UV radiation effect on some components of paper-based test-systems.

Snigur et al. (2020) reported fast room temperature cloud point procedure for spectrophotometric determination of phosphate in water samples with linear calibration graph in the phosphate concentrations range of 1.58–63 µg/L.

This topic has also been studied by Afkhami and Norooz-Asl (2009) in the work 'Cloud point extraction for the spectrophotometric determination of phosphorus(V) in water samples'. Linearity was obeyed in the range of 1.0–125 ng/mL of P and the detection limit of the method was 0.5 ng/mL of P.

Najafi and Hashemi (2020) introduced a new supra-molecular solvent from a non-ionic nonylphenol ethoxylate surfactant, and its potential was evaluated for microextraction of orthophosphate before molybdenum blue spectrophotometric determination. Under the optimized conditions, orthophosphate can be determined in the linear range of 0.5–28.0 µg/L ( $R^2 = 0.9933$ ) with the detection limit of 0.1 µg/L and preconcentration factor of 50.

Katsaounos et al. (2003), in an effort to monitor orthophosphate in natural waters and wastewater in the Ipirou region (Greece), proposed an analytical interference-free determination method for low mg/L levels, preparing a derivative which conveniently solubilized in the micelles of a non-ionic surfactant under mild conditions, and using spectrophotometrical measurements at 370 nm after its uptake with a sulfuric acid-methanol solution. Preconcentration of 10 mL of the sample volume provided the detection limit of 2.6 µM.

In the work by Kiso et al. (2002), an alternative phosphate spot test is introduced, where phosphate concentration is measured by the color band length of phosphoantimonymolybdenum blue formed in a detection tube similar to a gas detection tube. This method has been successfully used for the determination of phosphate concentrations in actual wastewaters, indicating the quantification range of 3–18 mg/L  $\text{PO}_4^{3-}$  without dilution prior to the analysis.

The determination of phosphates as dissolved anions using ionic liquid chromatography was

studied by Xie et al. (2019). The determination range was 1–500 mg/L and the detection limit was in the range of 0.17–0.54 mg/L.

Special attention has been paid to preconcentration methods and the chromatographic determination of heteropoly acids in phosphorus determination (Dubovik et al., 2003, Tikhomirova et al., 2002). Detection limit for phosphorus is  $(6.7 \times 1.2) \times 10^{-3}$  µg/mL. Calibration curve for phosphorus is linear in the concentration range of 0.02–0.15 µg/mL.

Different electrochemical sensing strategies adopted for the determination of phosphate using selective ionophores are discussed in the review 'Determination of inorganic phosphate by electro-analytical methods' (Berchmans et al., 2012). The sensing strategies are classified based on the electrochemical detection techniques used viz. potentiometry, voltammetry, amperometry, unconventional electrochemical methods, etc. Enzymatic sensing of phosphate coupled with electrochemical detection is also included. Various electroanalytical methods available in literature were assessed for their advantages in terms of selectivity, simplicity, miniaturization, adaptability, and suitability for field measurements.

Berchmans et al. (2011) reported an amperometric method for phosphate analysis based on the use of a surface modified glassy carbon electrode. The linear range of detection for phosphate is between 19 and 100 pM with the first electrode configuration. The limit of determination can be extended to a lower range, 0.79–32 µM, using the second electrode configuration.

In the paper 'Novel reagentless paper-based screen-printed electrochemical sensor to detect phosphate' (Cinti et al., 2016), a novel reagent-less paper-based electrochemical phosphate sensor was prepared using a simple and inexpensive approach. This novel and highly sustainable configuration readily enables the determination of phosphate ions with high reproducibility and long storage stability, achieving the detection limit of 4 µM over a wide linear range of up to 300 mM.

Initial steps in the development of an autonomous in situ electrochemical sensor for orthophosphate determination in seawater were presented by Jonca et al. (2011). The molybdophosphate complex is detectable by amperometry with an average precision of 2.2 % for the concentration range found in the open ocean and the detection limit of 0.12 µM.

Kahveci et al. (2017) described the development of a novel fluorescent biosensor based on the inhibition of alkaline phosphatase.

On basis of the composite, a novel ratiometric fluorescence probe with good sensitivity and selectivity

for the detection of phosphate in aqueous solutions was developed (Dai et al., 2015). The limit of detection is 0.06  $\mu\text{M}$  and the relative standard deviation for ten replicate detections of 10  $\mu\text{M}$  phosphate was 0.6 %. Recovery of spiked phosphate in water, human urine, and serum samples ranged from 94.1 % to 103.4 %.

Knochen (2020) specified continuous flow analysis (CFA) methods for the determination of orthophosphate indicating the mass concentration range from 0.01 mg/L to 1.00 mg/L P, and total phosphorus in the mass concentration range from 0.10 mg/L to 10.0 mg/L P.

A novel and automated sequential injection procedure for spectrophotometric determination of orthophosphate without unstable chemical reducing species used in the classical molybdenum blue method was proposed by Mas-Torres et al. (2004). The proposed method is linear up to 20 mg/L P and the proposed analyzer features an extremely wide dynamic range of 0.3–800 mg/L as well as improved tolerance to silicate interference.

A sequential injection system with dual analytical line was developed and applied by Mesquita et al. (2011), who compared two different detection systems: a conventional spectrophotometer with a commercial flow cell, and a multi-reflective flow cell coupled with a photometric detector under the same experimental conditions. The achieved detection limit of 0.007  $\mu\text{M}$   $\text{PO}_4^{3-}$  is consistent with the requirement of the target water samples; a wide quantification range of 0.024–9.5  $\mu\text{M}$  was achieved using both detection systems.

Automation of the molybdenum blue method by sequential injection (SIA) for on-line monitoring of phosphate in natural waters was presented by van Staden and Taljaard (1998). The proposed SIA analyzer is able to monitor phosphate in the range of 0–70 mg/L with a standard deviation of 0.9 %. The detection limit is 0.5 mg/L  $\text{PO}_4^{3-}$ .

The aim of the paper 'Determination of phosphorus in natural waters: A historical review' (Worsfold et al., 2016) introduced a virtual special issue reviewing the development of analytical approaches to the determination of phosphorus species in natural waters.

Environmentally friendly, simple and sensitive isotachophoretic method for the identification and quantification of orthophosphates, pyrophosphates, tripolyphosphates in various samples was developed (Jastrzebska, 2011). This system is characterized by its linearity ( $R^2 = 0.999$  for all ions), accuracy (recoveries ranging from 97 to 98 % for pyroP and 95 to 97 % for tripolyP), detection: 0.64 (pyroP) and 0.27 mg/L P (tripolyP) and quantification: 2.12 (pyroP) and 0.91 mg/L P

(tripolyP) limits, as well as by intra-assay of relative step height RSH (1.27–10.73 %) and inter-assay of RSH (3.95–11.17 %).

## Experimental

Chemicals of defined purity and deionized water, purified with a NANOpure instrument, boiled and cooled before the measurement, were used throughout the analyses. For calibration, a 0.1 mol/dm<sup>3</sup> HCl solution was used as the electrolyte. A solution of 0.0001 mol/dm<sup>3</sup> of  $\text{K}_4[\text{Fe}(\text{CN})_6] \cdot 3\text{H}_2\text{O}$  in 0.1 mol/dm<sup>3</sup> of HCl was used to calibrate the electrode. Electrolyte for the measurement of phosphates with the following composition: 0.00284 mol/dm<sup>3</sup> of Mo and 0.1 mol/dm<sup>3</sup> of  $\text{H}_2\text{SO}_4 \cdot \text{NaH}_2\text{PO}_4 \cdot 2\text{H}_2\text{O}$  dried at 105 °C for two hours, was used to prepare  $1.0 \times 10^{-5}$  mol/dm<sup>3</sup> of phosphate in electrolyte solution for model samples. Interferences of substances such as humic acid and other inorganic ions were monitored. An ECA<sup>flow</sup> model GLP 150 (Istran, Ltd., Bratislava, Slovakia; internet address: www.istran.sk) flow analyzer for calibration-less analysis of trace concentrations of the analyte was used. An integrated three-electrode electrochemical cell was coupled with an easily replaceable powdered glass working electrode showing the most advantageous properties in terms of use. The procedure consisted of flow analyzer preparation for the measurement, replacement of the working electrode if necessary, removal of air bubbles, and determination of the flow rate. The measurement procedure consisted of setting the working parameters, determination of the effective electrode volume, measurement, and final integration of the dissolution peak to obtain the measured analyte concentration in the sample. Some matrices such as: high solids samples, dissolved gases, samples containing strong oxidizing agents, sulfur compounds, and organic substances affect the yield, which results in a systematic error, when these possible interfering disturbances have to be removed. Samples were taken in three wastewater treatment plants in the district of Dunajska Streda by employees of Zapadoslovenska vodarenska spolocnost a.s. Dunajska Streda into PE containers and subsequently treated.

## Results and Discussion

### Electrode calibration

Several substances were used to calibrate the effective electrode volume, of which  $\text{K}_4[\text{Fe}(\text{CN})_6] \cdot 3\text{H}_2\text{O}$  was the most successful. The effective electrode

volume depends on the electrode dimensions but mainly on the oxidation current. As the oxidation current increases, the effective electrode volume decreases due to uneven loss of analyte in the electrode. At the electrode surface, electrolysis proceeds faster than in the center of the electrode, where unoxidized analyte remains at higher oxidation current. The peak height decreased, and the peak position shifted to higher values. The effective electrode volume was about  $20 \times 10^{-6} \text{ dm}^3$ .

#### **Optimization of measurement parameters**

Working parameters of the measurement were used to optimize the reduction current, filling potential, sample volume and electrolyte composition. The effect of temperature on phosphate determination was also studied using currents ranging from  $-0.1 \text{ mA}$  to  $-0.8 \text{ mA}$  to reduce the model sample of phosphate with the concentration of  $1 \times 10^{-5} \text{ mol/dm}^3$ . Reducing current of  $-0.2 \text{ mA}$  was chosen as optimal because at this current the measured concentration corresponded to the actual value. Therefore, when replacing the electrode, effective electrode volume was calibrated at the oxidation current of  $0.2 \text{ mA}$ . As the absolute current increased, the signal height decreased, and the peak maximum position shifted to more negative values. At the optimum filling potential, the electrode should be completely filled with the sample solution and no electrode reactions should occur. The measurement was performed with a model sample ranging from  $-300 \text{ mV}$  to  $800 \text{ mV}$ . The measured phosphate concentration approached the true value at the filling potential of  $0 \text{ mV}$ .

The sample volume was optimized based on the assumption that analyte adsorption to the electrode also occurs during electrode loading. This as-

sumption can be confirmed by the increase of the measured concentration with the increasing sample volume. However, the measurement results did not confirm this assumption.

Electrolyte optimization was done by varying the concentrations of  $\text{H}_2\text{SO}_4$  and molybdenum, thus changing the ratio of hexavalent molybdenum to phosphate anions. The measured value corresponded to the actual molybdenum/phosphate ratio of 284:1, which corresponds to the of  $\text{H}_2\text{SO}_4$  concentration of  $0.1 \text{ mol/dm}^3$ .

Chronopotentiometric recording of phosphate measurements is presented in Fig 1.

#### **Interference effects**

Interferences were observed in a model phosphate sample solution with given additions of interfering inorganic ions and humic acid.  $\text{Fe}^{2+}$  ions caused positive measurement error,  $\text{Ca}^{2+}$  and  $\text{NO}_3^-$  ions influenced the determination to a minor extent,  $\text{Cl}^-$ ,  $\text{Na}^+$ ,  $\text{Mn}^{2+}$ ,  $\text{Mg}^{2+}$  ions, and especially  $\text{Fe}^{3+}$  ions at higher concentrations caused negative error of determination. Measurements of humic acid interference showed that phosphates concentrations above  $5.0 \times 10^{-3} \text{ g/dm}^3$  cannot be determined.

#### **Metrological parameters**

Metrological parameters such as results accuracy, measurement repeatability, detection limit and working range were monitored. Results accuracy for concentrations below  $1.0 \times 10^{-6} \text{ mol/dm}^3$  was 13 % and more, from  $1.5 \times 10^{-6} \text{ mol/dm}^3$  to  $5.5 \times 10^{-5} \text{ mol/dm}^3$  it was 2 % and from  $5.5 \times 10^{-5} \text{ mol/dm}^3$  to  $8.0 \times 10^{-5} \text{ mol/dm}^3$  it was from 7 % to 20 %. When investigating measurement repeatability, the average measured concentration of phosphate in the model sample over ten

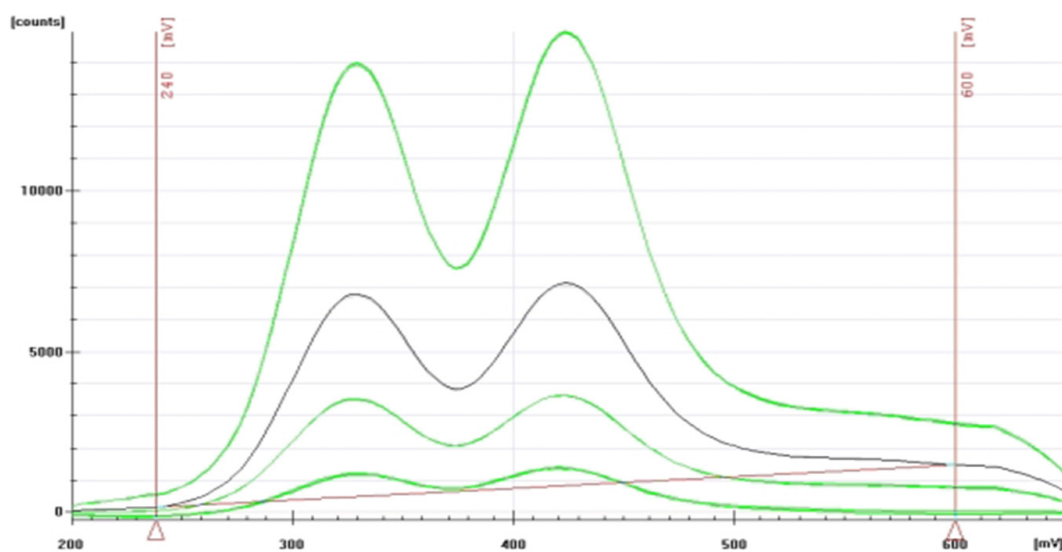


**Fig. 1.** Chronopotentiometric recording of phosphate.

days was  $1.003 \times 10^{-5}$  mol/dm<sup>3</sup> with a relative standard deviation of 0.60 %. The detection limit of the method is  $3.42 \times 10^{-7}$  mol/dm<sup>3</sup>. The presented method is applicable under optimal conditions in the concentration range of  $1.5 \times 10^{-6}$  to  $5.5 \times 10^{-5}$  mol/dm<sup>3</sup> (Slana, 2001).

### Analysis of real samples

Wastewater samples were taken before and after the treatment in Slovak cities Kutý, Samorín and Gabčíkovo as 8-hour cast samples. Activated charcoal was added to the collected fractions to remove colloids and other interferents. The samples were then filtered through filter paper and preserved by the addition of CHCl<sub>3</sub> to prevent biological processes. The measured phosphate concentrations in real wastewater samples from given sites before (1) and after (2) the treatment in a wastewater treatment plant are given in Table 1 which provides the confidence interval of phosphate concentrations determined without and with the standard addition by the flow coulometric method and the phosphate concentrations determined spectrophotometrically after mineralization according to the standard norm (STN EN ISO 6878 (757465)).

Phosphate concentrations measurements by flow coulometry (Methodological guidelines 1982) were performed with non-mineralized samples and therefore only the content of dissolved inorganic phosphates is probably obtained. For the mineralized sample from location Kutý taken prior to purification, a poorly integrated high peak with the maximum shifted by about 40 mV to more positive values was obtained. At the indicated integration, the phosphate concentration was 4.60 mg/dm<sup>3</sup> and no peak in the potential range typical for reduction of molybdophosphate was observed. This indicates a likely disturbance of the mineralization background and therefore, mineralization of the

blank was performed. The result of this measurement showed a peak similar to that of the sample, of course, approximately ten times smaller. After adding the standard addition to the blank mineralization experiment, a peak similar to that of a real sample, with a significantly shifted the maximum and high signal, was obtained. Another standard addition caused that the peak height increased only to a small and apparently inadequate extent. Nonconformity of the results measured by flow coulometry and spectrophotometry and the procedure of wastewater samples mineralization will be the subject of further study.

### Conclusion

The aim of the presented work was to study the application of flow coulometry as coulometric titration. The method was used to analyze phosphates in wastewater samples. The determination principle consisted in the formation of molybdophosphate and its subsequent one-electron reduction. The presented method is applicable under optimal conditions in the concentration range of  $1.5 \times 10^{-6}$  to  $5.5 \times 10^{-5}$  mol/dm<sup>3</sup>. The detection limit of the method is  $3.42 \times 10^{-7}$  mol/dm<sup>3</sup>. The mineralization step in total phosphate content determination was problematic. If the mineralization was not carried out, only inorganic soluble phosphates were determined. It is a new method characterized by its simplicity of instrumentation and handling, which is a precondition of its further use in trace analysis. As this is an absolute method it ranks among reliable and independent methods.

### Acknowledgement

This work was supported by the Slovak Grant Agency (VEGA No 1/0489/16).

**Tab. 1.** Measured concentrations of phosphate in real samples.

Location	Concentration*	Concentration**	Concentration***
	without standard addition [mg/dm <sup>3</sup> ]	with standard addition [mg/dm <sup>3</sup> ]	[mg/dm <sup>3</sup> ]
Kutý 1	1.64 ± 0.04	2.91 ± 0.12	2.67
Kutý 2	0.53 ± 0.02	1.74 ± 0.03	1.69
Samorín 1	1.88 ± 0.09	3.06 ± 0.11	5.11
Samorín 2	0.53 ± 0.02	1.77 ± 0.02	4.54
Gabčíkovo 1	1,91 ± 0,07	3,15 ± 0,18	5,86
Gabčíkovo 2	1,43 ± 0,05	2,59 ± 0,08	5,48

\*measured by flow coulometry

\*\*measured by flow coulometry with standard addition of 1.24 mg/dm<sup>3</sup>

\*\*\*measured spectrophotometrically

## References

- Afkhami A, Norooz-Asl R (2009) *Journal of Hazardous Materials* 167: 752–755.
- Berchmans S, Issa TB, Singh P (2012) *Analytica Chimica Acta* 729: 7–20.
- Berchmans S, Karthikeyan R, Gupta S, Poinern GEJ, Issa TB, Singh P (2011) *Sensors and Actuators B-Chemical* 160: 1224–1231.
- Cinti S, Talarico D, Palleschi G, Moscone D, Arduini F (2016) *Analytica Chimica Acta* 919: 78–84.
- Determination of trace elements by flow coulometry (1982) *Methodological guidelines compiled according to ISO 78/2*. ISTRAN, Ltd., Bratislava.
- Dai C, Yang CX, Yan XP (2015) *Analytical Chemistry* 87: 11455–11459.
- Dubovik DB, Tikhomirova TI, Ivanov AV, Nesterenko PN, Shpigun OA (2003) *Journal of Analytical Chemistry* 58: 802–819.
- Heslop RB, Jones K (1985) *Inorganic Chemistry*. SNTL, Prague.
- Chemical and physical analysis of wastewater (2004) *STN EN ISO 6878 (757465)*.
- Jastrzebska A (2011) *Journal of Food Composition and Analysis* 24: 1049–1056.
- Jonca J, Fernandez VL, Thouron D, Paulmier A, Graco M, Garcon V (2011) *Talanta* 87: 161–167.
- Kahveci Z, Martinez-Tome MJ, Mallavia R, Mateo, CR (2017) *ACS Applied Materials & Interfaces* 9: 136–144.
- Katsaounos CZ, Giokas DL, Vlessidis AG, Paleologos EK, Karayannis MI (2003) *Science of the Total Environment* 305: 157–167.
- Kiso Y, Kuzawa K, Saito Y, Yamada T, Nagai M, Jung YJ, Min KS (2002) *Analytical and Bioanalytical Chemistry* 374: 1212–1217.
- Knochen M, Carlos Rodriguez-Silva J, Silva-Silva J (2020) *Talanta* 209.
- Mas-Torres F, Estela JM, Miro M, Cladera A, Cerda V (2004) *Analytica Chimica Acta* 510: 61–68.
- Mesquita RBR, Ferreira MTSOB, Toth IV, Bordalo AA, McKelvie ID, Rangel AOSS (2011) *Analytica Chimica Acta* 701: 15–22.
- Najafi A, Hashemi M (2020) *Journal of Molecular Liquids* 297.
- Nollet LML, De Gelder LSP (2000) *Handbook of Water Analysis*. CRC press, New York.
- Slana I (2001) *Diploma Thesis, Faculty of Chemical and Food Technology Slovak University of Technology in Bratislava*.
- Snigur D, Chebotarev A, Duboviy V, Bulat K (2020) *Analytical Biochemistry* 597.
- van Staden JF, Taljaard RE (1998) *Microchimica Acta* 128: 223–228.
- Tikhomirova TI, Krokhin OV, Dubovik DB, Ivanov AV, Shpigun OA (2002) *Journal of Analytical Chemistry* 57: 18–23.
- Worsfold P, McKelvie I, Monbet P (2016) *Analytica Chimica Acta* 918: 8–20.
- Xie WJ, Wang XL, Li YS, Xu DH, Zhong YJ, Yang JX (2019) *Chromatografia* 82: 1687–1695.
- Zaporozhets OA, Zinko LS, Sumarokova GS (2019) *Methods and Objects of Chemical Analysis* 14: 175–191.

# *Pichia pastoris* – recombinant enzyme producent for environment treatment – review

Tamara Kyzeková, Vladimír Krasňan, Martin Rebroš

*Institute of Biotechnology, Slovak University of Technology,  
Radlinského 9, 812 37 Bratislava, Slovakia  
martin.rebros@stuba.sk*

**Abstract:** Since environmental pollution is increasing, scientists try to find a sustainable way for its clean up and for environment protection. Due to increasing knowledge of genetics and recombinant technologies, recombinant enzymes have been increasingly applied for these purposes. This article deals with the possibilities of environmental treatment with different types of enzymes produced by *P. pastoris*. Environment is polluted mostly with pesticides, wastewaters, phenol compounds, plastics, toxic compounds, wastes from medical treatment, etc. All these compounds have to be eliminated considering the deteriorating biodiversity, human health, and condition of plants. Enzymes are an environmentally friendly way of such treatment.

**Keywords:** *Pichia pastoris*, recombinant enzymes, environment, pollution

## Introduction

In the last century, a massive expansion of oil industry and different industries have negatively affected our environment. The situation got serious a long time ago and that is why scientists already devised some ways to stop damaging and even partially restore environment. First significant effort was the concept of chemical catalysis which dealt with catalytical reduction of contaminants derived from petroleum. The idea started in the 1960s and was in its heyday in the 1990s due to widespread application of chemical catalysis in industry (Alcade et al., 2006). Nowadays, long-term use of chemical catalysis is questioned mostly because of its health risks, and waste and toxic compounds production. Even though chemical catalysis has advantages in reducing chemicals footprint, a “cleaner technique”, biocatalysis, had to be introduced. Its concept was introduced in the 1990s and it is still interesting as an environmentally friendly technique. Basically, it is an application of microorganisms, or their enzymes, in the production of renewable and clean products replacing chemical catalysts mainly due to their negative environmental impact or energy and raw material requirements. Biocatalysis requires mild reaction conditions and it offers high activity products and chemo-, regio- and stereoselectivity (Sheldon & van Rantwijk, 2004). The same enzymes and microorganisms can also be used for the remediation of toxic wastes. Biocatalysis is very closely connected with recombinant techniques (Alcade et al., 2006). Combined with remediation efforts, microorganisms producing recombinant enzymes for environment remediation. Also, bio-industry wastes are studied as carbon source for

some microorganisms. Attention, especially these days, is focused on crude glycerol.

## *Pichia pastoris*

One of the most widely used microorganism in recombinant technologies is *Pichia pastoris*. This methylotrophic yeast belongs to the family of *Saccharomycetaceae* (Satyanarayana & Kunze, 2009) and its genome was sequenced in 2009, which opened the door to further research (Schutter et al., 2009). Previously, in the 1970s, *P. pastoris* was used as “single cell protein” (SCP) producer for animal feeding. At that time, there was an effort to produce SCP from cheap carbon sources, e.g. methanol. *P. pastoris* later became the most cited methylotrophic yeast, but due to oil crisis, this interest decreased. Ten years later, the company which started to use *P. pastoris* for SCP – Philips Petroleum – together with the Salk Institute of Biotechnology prepared a strain for heterologous expression for academic and industrial purposes (Cos et al., 2006). Since the production of a functional heterologous protein expression is closely related to the metabolism of the production microorganism, *P. pastoris* offers several advantages in this respect. It is suitable for the expression of milligrams up to grams of protein per liter of fermentation broth – for basic laboratory research but also for industrial production. The advantages include its easy production in fermenters, where it is possible to regulate parameters affecting protein productivity, such as pH, aeration, the amount of carbon source supplied and induction of protein production. Compared to other producers, *P. pastoris* does not need complex growth media and the culture conditions are easily ensured. Yeasts are easily manipulated on the genetic level and their protein synthesis is similar to

that of higher organisms. Therefore, some proteins that cannot be efficiently expressed in bacteria, *Saccharomyces cerevisiae* or baculoviruses are often produced in functionally active forms in *P. pastoris*. These yeasts are beneficial for several reasons: easy genetic manipulation, functional complementation cloning, high-frequency DNA transformation, high intra- and extracellular protein production, and post-translational modifications of proteins. The yeast's post-translation modifications include disulfide bridge formation, glycosylation, and phosphorylation. During the cultivation, high cell densities are achieved using minimal media, which means production of proteins can reach high yields. Also, vectors with recombinant genes are integrated into the yeast chromosome which makes them genetically stable even in continuous and large-scale fermentation processes. At the same time, recombinant *P. pastoris* produces low levels of native proteins facilitating the purification of recombinant proteins. Powerful and available genetic techniques, together with the overall economics of the process, make *P. pastoris* a suitable expression system for the production of homologous proteins (Macauley-Patrick et al., 2005).

Cultivation of *P. pastoris* consists of two steps. The first is the growth of *P. pastoris* on glycerol to reach high cell density. Then, after glycerol depletion, methanol is added to the medium and protein production begins (Markošová et al., 2015).

The beginning of the methanol pathway (Fig. 1) in *P. pastoris* is in special organelles – peroxisomes and continues in cytoplasm. First step, where formaldehyde and hydrogen peroxide are formed, is catalyzed by alcoholoxidase (AOX). For methanol utilization, dihydroxyacetone synthase is necessary for formaldehyde assimilation in peroxisomes. A part of formaldehyde leaves the peroxisomes and is further oxidized by cytoplasmic dehydrogenases

to formate and carbon dioxide. These reactions are an important source of energy for the cell growth (Cereghino & Cregg, 2000). Genetically modified *P. pastoris* has, under AOX promoter control, located the gene encoding the homologous protein of interest. This promoter is induced only by methanol, which means methanol is the carbon source as well as the inducer. Since formaldehyde is formed during its utilization, methanol has to be added carefully due to its toxic effect (Markošová et al., 2015).

As mentioned above, *P. pastoris* initial substrate is usually glycerol, which is mainly used as pure compound. However, several publications show that *P. pastoris* is also able to grow on industrial crude glycerol (Anastácio et al., 2014). It is a by-product of biodiesel production and in the last decades started to be an environmental burden (Bartocci et al., 2018). The possibility of utilizing crude glycerol is only one way in which *P. pastoris* can participate in the reduction of environmental pollution. It has also great potential in the production of proteins, which can help the environment directly. Genetic engineering tools and commercial *P. pastoris* strains availability are also important advantages of this yeast application in research and industry (Fisher & Glieder, 2019).

## Recombinant products of *Pichia pastoris* and their use in the environment

### Antimicrobial peptides

Currently, the massive use of pesticides in the agro-sector causes significant pollution. Pesticides have been used worldwide and for many years to prevent pathogen diseases of plants. On the other hand, pesticide residues accumulate in soil and from there they can reach drinking water supplies. In the 1990s, a study by U.S. Geological Survey

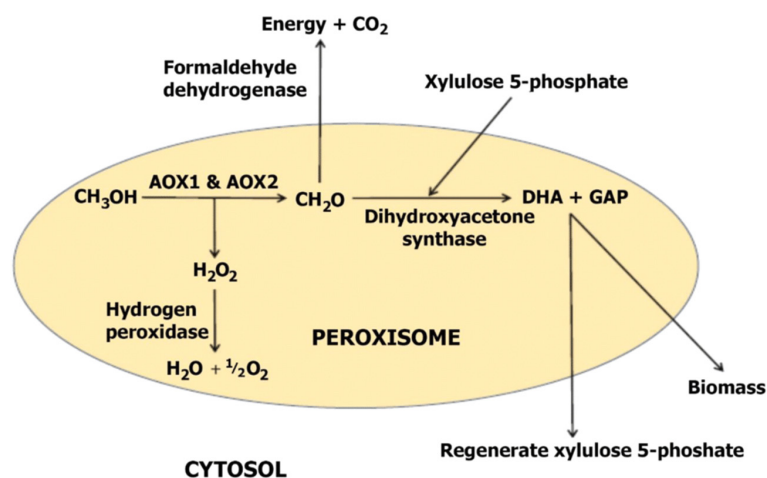


Fig. 1. Methanol pathway of *P. pastoris* (Ali et al., 2020).

(USGS) stated that 90 % of fish samples and water from all streams were contaminated by one or several pesticides. According to USGS, pesticides from every major chemical class were found in ground water and its pollution is a worldwide problem (Aktar et al., 2009). From water, pesticides can easily enter any organism. There is evidence that they cause cancer, respiratory problems, neurologic deficiency, birth defects, miscarriages or dermatologic difficulties (Bassil et al., 2007) (McCauley et al., 2006). Moreover, biodiversity is damaged since many animals are endangered by them (Mahmood et al., 2006). Pathogens have become resistant to pesticides, and new and more environmentally safe agents are needed.

One of the antimicrobial peptides is pexiganan, which has lethal effect on many types of undesirable microorganisms. It attacks the bacterial membrane resulting in pores on their surface and thus causing their death (Lazarev & Govorun, 2010). This peptide is recombinantly produced by *P. pastoris* because it has low sensitivity to almost no antimicrobial effect in eukaryotic cells. Thanks to that, large quantities can be produced without damaging the host microorganism. For example, production of recombinant peptide via *E. coli* reached 30 mg/L (Sun et al., 2018) while via *P. pastoris* it was 52 mg/L. Furthermore, to avoid *E. coli* inhibition, inactivation sequence is added to the peptide gene which has to be cleaved using thermal, enzymatic or chemical methods leading to higher production costs and partial loss of produced peptide. Recombinant peptide produced in *P. pastoris* was tested on eight plant pathogens causing significant economic losses in agriculture industry and on two human pathogens (Tab. 1). Pexiganan showed 500 times stronger antimicrobial activity than copper oxychloride

which is a common chemical pesticide against plant pathogens. Peptide has high long-term stability and temperature resistance. According to calculations, production of 52 mg of recombinant peptide costs about 10 \$, while synthetic production of crude pexiganan is 20–30 times more expensive and in case of 98 % purity, it is even 120 times more expensive (Neshani et al., 2019), ([www.entonbio.com](http://www.entonbio.com); [www.synpeptide.com](http://www.synpeptide.com)).

Pathogens elimination can also be done using killer toxin produced by the yeast *Tetrapisispora phaffii*. Killer toxin, known as Kptk, has  $\beta$ -1,3glucanase and killer activity which induces ultrastructural modifications to the cell wall of the yeast of genera *Kloeckera/Hanseniaspora* and *Zygosaccharomyces* causing spoilage of grapes and losses in wine and sweet beverage production. Recombinant killer toxin was produced by *P. pastoris* and reached final concentration of 23 mg/L which is significantly more than the amount produced by native *Tetrapisispora phaffii*. Moreover, compared to native Kpkt, recombinant Kpkt shows a wider spectrum of activities, e.g. toxic effect on *Dekkera bruxellensis*, spoilage yeast in wine making and biofuel industry (Chessa et al., 2017).

### Pesticides

Enzymes are also applied for pesticides monitoring and their degradation. One of them is organophosphorus hydrolase from *Pseudomonas pseudoalcaligenes* (Shen et al., 2016) which can be used for biodegradation of residues from organophosphorus pesticides or their detection (Mulchandani et al., 1998). These pesticides are synthetic esters, amides, or thiol derivatives of phosphonic, phosphoric or phosphonothioic acid. They are widely used in agriculture and domestic cultivation. Organophosphorus pesticides were

**Tab. 1.** Minimum inhibitory concentration of recombinant pexiganan and copper oxychloride needed for lethal effect on pathogen (Neshani et al., 2019).

		Minimum inhibitory concentration (µg/ml)	
		Pexiganan-based biopesticide solution	Cooper oxychloride 35 % WP
<b>Plant pathogens</b>	<i>Pseudomonas syringae</i> pv. <i>syringae</i>	0.81	625
	<i>Ralstonia solanacearum</i>	0.4	1250
	<i>Pantoea stewartii</i>	0.4	312.5
	<i>Xanthomonas arboricola</i> pv. <i>pruni</i>	0.81	625
	<i>Erwinia amylovora</i>	0.4	2500
	<i>Pectobacterium carotovorum</i>	0.4	625
	<i>Agrobacterium tumefaciens</i>	0.4	1250
	<i>Brenneria nigrifluens</i>	0.4	312.5
<b>Human pathogens</b>	<i>Staphylococcus aureus</i> ATCC 25923	8	-
	<i>Escherichia coli</i> ATCC 25922	16	-

detected in soil and drinking water long after their application and they belong to the most toxic pesticides causing long-term damage to human health since they inhibit the enzyme acetylcholinesterase which is essential for the function of central nervous system (Songa & Okonkwo, 2016). Decontamination methods for these pesticides are often toxic, corrosive, allergic and not environmentally friendly and thus it is essential to hydrolyze them, preferably with enzymes (Farnoosh & Latifi, 2014). Organophosphorus hydrolase was produced on purified glycerol with later methanol induction by *P. pastoris*. Recombinant organophosphorus hydrolase had good biodegradation properties and expression reached high level (7.8 g/L of protein); this production can provide an effective way of dealing with organophosphorus pesticides. Activity of this enzyme was measured by hydrolysis of substrate methyl parathion, a popular organophosphorus pesticide widely used for crop protection, its activity reached 21.6  $\mu\text{mol/h/mg}$  of wet weight (Shen et al., 2016). To compare, organophosphorus hydrolase produced in *Moraxella sp.* Hydrolysing reached the activity of only 0.6  $\mu\text{mol/h/mg}$  of dry weight using the same substrate (Shimazu et al., 2001).

#### **Wastewater, phenol compounds and lignin treatment**

Historically, the most well-known enzymes used for bioremediation of wastewater and soils are wood-destroying fungal enzymes involved in lignin degradation (laccase, lignin peroxidase, manganese peroxidase). Water and soils are widely polluted with chemical compounds like phenol, aromatic amines, synthetic dyes, antibiotics, hydrocarbons, chlorine etc., which have negative effect on the biodiversity or plant and human health. Since industry is very developed and these pollutants are still used, there is no other option than to eliminate them. The use of oxidative enzymes for their biodegradation is environmentally friendly, low cost and more effective compared to physical and chemical methods which have many disadvantages such as hazardous by-products or limited degradation activity (Alcade et al., 2006). Besides biodegradation, the mentioned enzymes can also be used in other industrial sectors. First and the most studied enzyme is laccase, which can be found in bacteria, fungi, higher plants and even insects. Laccase finds its application in the following industries: food, paper, pulp, textile, cosmetics, and it is used for bioremediation, removal of endocrine disruptors and biodegradation of phenolic pollutants. Laccases are also able to oxidize non-phenolic lignin-related compounds. An important environment application of laccase is decolorization of dyes (Shraddha et al., 2011). More than 100,000 dyes are commercially available, most

of which are very difficult to eliminate from water due to their complicated structure and synthetic origin. They are specially designed to resist fading after exposure to light, water and oxidizing agents. Due to their high stability, wastewater treatment techniques to decompose them include electrochemical destruction, membrane filtration, electroflotation, ozonation, ion exchange or adsorption (Nigam et al., 2000). The use of enzymes is a more simple, clean, and effective technique leaving less waste. One of the examples of enzymatic treatment is detoxification and reduction of color and aromatic compounds of black liquor – wastewater from pulp production. Detoxification was performed with *Trametes versicolor* producing laccase. This microorganism was also used for complete decolorization of Amaranth, Congo Red, Reactive Black 5, Tropaeolin O, and Reactive Blue 15 colors (Ramsay & Nguyen, 2002). In bioremediation, laccase also achieves excellent results; laccase from *T. villosa* removed 100 % of 2,4-dichlorophenol from soil (Ahn et al., 2002). Recently laccases have been applied in nanobiotechnology, since they are able to catalyze electron transfer reactions with no additional cofactors (Shraddha et al., 2011). Laccase and other ligninolytic enzymes are produced during the secondary metabolism of fungi under nitrogen or other nutrient limited conditions when they are secreted in the medium extracellularly. Most widely known species for laccase production are *Basidiomycetes* and *Saprotrophic* fungi and the production usually proceeds via solid-state or submerged fermentation, which have some disadvantages like broth viscosity, oxygen and mass transfer problems (Moreira et al., 2003). Laccase production via solid-state and submerged fermentation does not reach the maximum yield and it is not possible to produce large volumes of highly active enzyme at affordable cost (Shraddha et al., 2011).

Although enzymes are widely used, due to the slow growth of fungi and the mentioned disadvantages, their recombinant production by *Pichia* is a more effective way of production (Xu et al., 2017). As an example, recombinant laccases from *Pleurotus ostreatus* produced by *P. pastoris* were capable of efficient removal of nitrophenols, chlorophenols and sulfonamide antibiotics (Fig. 2), dangerous agents with high toxicity and carcinogenic effect. Their residues were found mainly in wastewater. The best degradation effect was achieved in case of sulfonamide antibiotics (sulfadiazine: 98.1 %, sulfamethazine: 97.5 % and sulfamethoxazole: 97.8 %). Degradation of nitrophenols was also successful (2-nitrophenol: 59.21 %, 3-nitrophenol: 47.91 % and 4-nitrophenol: 60.24 %). The worst results were obtained for chlorophenols (4-chloro-

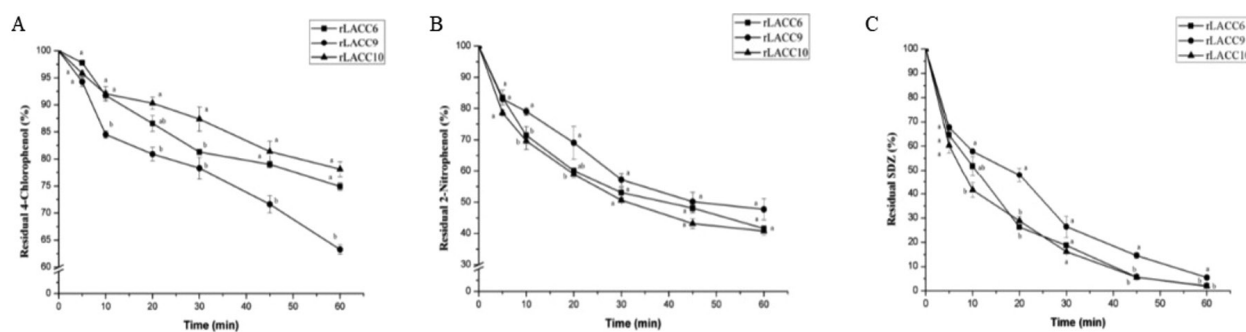


**Fig. 2.** Degradation of 4-chlorophenol (A), 2-nitrophenol (B) and sulfadiazine (C) by three recombinant laccases produced by *P. pastoris* (Zhou et al., 2018).

phenol: 47.9 %, 2,4-dichlorophenol: 28.9 % and 2,6-dichlorophenol: 35.1 %) (Zhou, et al., 2018).

In comparison, laccase from *T. versicolor* provided 97 % degradation of 4-nitrophenol (Levil et al., 2016) and laccase from *T. pubescens* ensured 41.1 % degradation of 2,4-dichlorophenol (Gaitan, et al., 2011). However, this result may be affected by the cooperation of multiple enzymes in fungi. Also the reaction mixture for laccase from *T. pubescens* and *T. versicolor* contained 15 mg/L and 139 mg/L of the pollutant while recombinant laccase showed the concentration of 100 mg/L. Degradation ability of recombinant laccase was observed only for 1 hour and in case of native laccase from *T. pubescens* and *T. versicolor*, a 4 and 72 hour experiments were done, respectively. Based on these results, it can be concluded that recombinant laccase has better degradation ability the native one (Zhou et al., 2018).

Different types of laccase from the wood-destroying fungi *T. troglia* was also successfully expressed in *P. pastoris* (Colao et al., 2006). The recombinant enzyme exhibited similar specific activity (232 U/mg) and the same properties as the native one. Its decolorizing ability was tested on synthetic dyes including azo dyes, triarylmethane, indigo carmine and the anthraquinonic dye alizarin red S. Relative decolorization (almost 100 %) was the highest in case of blue indigo and since this is the most important dye in blue jeans manufacturing, it is an important advantage of recombinant laccase. Moreover, production of recombinant laccase achieved concentrations (129,6 mg/L) which, according to the authors, exceeds that obtained from *T. troglia* cultures, which also produce a number of laccase isoforms and are difficult to separate since they have similar chemico-physical properties. This does not happen in case of *P. pastoris* production (Colao et al., 2003).

Another ligninolytic enzyme is manganese peroxidase catalyzing the depolymerization of plant lignin. Manganese peroxidase is one of the most common lignin degradation enzymes and has great

potential in agriculture for its ability to degrade cellulose, hemicelluloses, and lignin. It was first isolated in 1985 from the wood-destroying fungus *Phanerochaete chrysosporium* (Paszczynski et al., 1985). It is the most abundant lignolytic enzyme in nature. Currently, it has been isolated and characterized from several fungi and its properties are the subject of extensive research. Many studies suggest manganese peroxidase to effectively degrade azo dyes. In the field of environmental protection, it is also used for the degradation of organic and toxic substances such as polycyclic aromatic hydrocarbons, chlorophenols, industrial dyes and nitroaromatics (Xu et al., 2017). Polycyclic aromatic hydrocarbons are derived from industrial activities causing health risks due to their carcinogenic and mutagenic potential. Manganese peroxidase from *Bjerkandera* sp. degraded them (specifically anthracene, dibenzothiophene and pyrene) to a large extent and in a short period of time, 7 hours for anthracene, and 24 hours for dibenzothiophene and pyrene (Eibes et al., 2006). Manganese peroxidase from *Pleurotus ostreatus* detoxicated aflatoxin, which is a mycotoxin with carcinogenic, mutagenic, hepatogenic and immunosuppressive properties (Yehia, 2014). Enzyme from *Phanerochaete chrysosporium* was successful in removing tetracyclines and oxytetracyclines. The results show that manganese peroxidase degraded 72.5 % of tetracyclines and 84,3 % of oxytetracyclines (Wen et al., 2010). Manganese peroxidase crude enzyme extract of *Nematoloma frowardii* and *Stropharia rugosoannulata* proved to convert several aminonitrotoluenes such as 2-amino-4,6-dinitrotoluene, 4-amino-2,6-dinitrotoluene and 2,6-diamino-4-nitrotoluene (Scheibner & Hofrichter, 1998). All mentioned application showed great potential in the removal of impurities from the environment. However, natural production of this enzyme is disadvantageous due to the slow growth of fungi, accumulation of extracellular polysaccharides, or production of compounds with similar chromatographic properties. Therefore, recom-

binant microorganisms have been studied for its production (Xu et al., 2017).

Manganese peroxidase from *Ganoderma lucidum* produced by *P. pastoris* was tested for phenol and synthetic azo dyes degradation (Xu et al., 2017). It was proved that during photocatalytic degradation of azo dyes, several aromatic intermediates are produced (Fig. 3). They are harmful to the nature and human health (Tanaka et al., 2000).

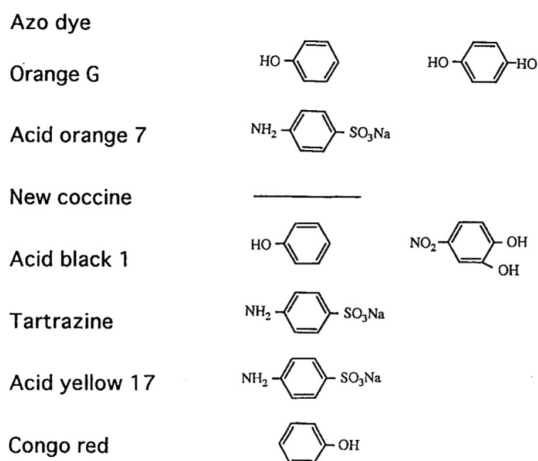


**Fig. 3.** Intermediates (phenolic compounds, aromatic amines) in photocatalytic degradation of azo dyes (Tanaka et al., 2000).

It is an advantage that manganese peroxidase can degrade both phenol and synthetic dyes. There are several studies confirming that manganese peroxidase decolorizes wastewaters from factories. However, expression on high level has to be considered before commercial use. In many isolates it is usually too low for industrial application but *P. pastoris* could meet these requirements. Compared with the natural host, *P. pastoris* increases expression levels by 10-, 100- or even 1000-fold. Recombinant enzyme from *P. pastoris* was produced with specific activity of 524,61 U/L and final yield of 126 mg/L. Activity of manganese peroxidase was confirmed through its ability to degrade phenol which was monitored chromatographically. In case of the tested synthetic dyes, the results are easily visualized (Fig. 4). In Figure (c) are dyes before degradation and Figure (d) shows dyes after applying crude protein extract of recombinant *P. pastoris* containing manganese peroxidase. Decolorization of all dyes reached 70 % (Xu et al., 2017).

Manganese peroxidase is also important in pulp and paper industry. Pulp mills discharge a wide range of chlorinated and non-chlorinated organic compounds because they use molecular chlorine for bleaching. Chlorinated compounds include chlorinated phenolic derivatives and chlorinated

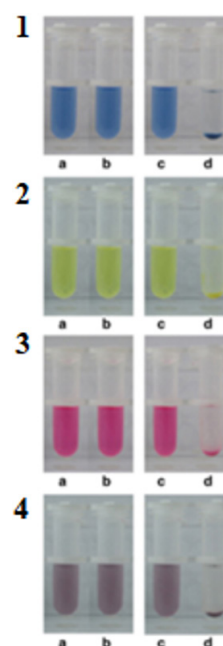


**Fig. 4.** Visual representation of dyes degradation: Drimamer Blue CL-BR (1), Yellow X-8GN (2), Drimaren Red K-4BI (3) a Disperse Navy Blue HGL (4). On the left side: crude protein extract of non-recombinant *P. pastoris* used as a control at the beginning (a) and the end of dye degradation (b). On the right side: (c, d) is crude protein extract of recombinant *P. pastoris* containing manganese peroxidase at the beginning (c) and the end of dye degradation (d) (Xu et al., 2017).

dioxins and furans, and they are known to accumulate in the tissue of fish (Owens et al., 1994). Public has forced pulp and paper mills to reduce chlorine-based chemicals and use more environmentally friendly bleaching techniques based on enzymes like manganese peroxidase. Results from *P. pastoris* manganese peroxidase fermentation showed that recombinant enzyme can degrade lignin and it is very effective when combined with alkaline extraction in delignification and brightening. Kappa number of the resulting pulp was reduced by 61 %, to 8.6 (ideal value should be below 6.5 (Viikari et al., 1968)) and brightness increased by 26 points (Xu et al., 2010).

Another enzyme involved in lignin degradation is lignin peroxidase, which oxidizes non-phenolic substrates. Lignin is an aromatic polymer which protects plants from microbial attacks. Lignin degradation in nature is interesting because it is an essential part of the carbon cycle and it is unusually biochemically stable (Hammel et al., 1993). Lignin as a waste is generated as a by-product from pulping or ethanol production. Due to its complex structure, it is an environmental burden and its degradation is essential (Li & Takkellapati, 2018).

Lignin peroxidase was expressed in various hosts. One of them was *Escherichia coli*. Even though the enzyme production was fast and provided high yields, it was limited by the low yield of subsequent *in vitro* refolding. This was necessary due to the lack of haem incorporation inside the cells and formation of inclusion bodies. Lignin peroxidase was also expressed in baculovirus with low yield of active peroxidase and high production cost. The yield in *Aspergillus niger* was also comparatively low. On the other hand, production of recombinant lignin peroxidase in *P. pastoris* was successful and it proved that multi-copy transformation of plasmid increases the final yield. Activity of the enzyme reached 15 U/L after a 12 hours induction (Wei & Xianghua, 2009).

From peroxidases, horseradish peroxidase is another interesting enzyme to be used for the treatment of the following pollutants and wastes: aromatic amines, bromophenols, chloromethylphenols, methoxyphenols, chlorophenols, methylphenols, phenol, bleach plant effluent, cotton mill effluent and coal conversion wastewater (Aitken, 1993). Nowadays, great progress has been made using directed evolution inside *P. pastoris*. The enzyme showed a 2.3-fold higher specific activity towards the pollutant guaiacol and a 5.4-fold higher activity towards ABTS [2,2'-azinobis(3-ethylbenzthiazoline-6-sulfonic acid)]. ABTS is a chemical compound used to determine the enzyme kinetics or enzyme-linked immunosorbent assay. It is used as a substrate for horseradish peroxidase to identify its kinetics. Production of horseradish peroxidase was also realized in *S. cerevisiae*, but the enzyme from *P. pastoris* had a 5.6-fold higher total activity and a three-fold higher cell density (Morawski et al., 2000).

Acrylonitrile and acrylamide are widely used in petroleum industry and are the main pollutants in generated wastewaters. Their high toxicity and carcinogenicity are very dangerous, but nitrile hydratase showed bioconversion activity for these compounds. It was expressed in *P. pastoris* but, unfortunately, it was unstable and low activity was achieved. To solve this problem and enhance the activity of the enzyme, directed evolution can be used combined with another *P. pastoris* strain (Shi et al., 2004).

#### **Pulp bleaching and conversion of agrowaste**

In addition to manganese peroxidase, xylanase also provided excellent bleaching results. Moreover, xylanase is commercially important due to its ability to convert lignocellulosic material and agrowaste enabling the production of high value products such as furfural, xylitol, biofuels, and artificial low-calorie sweeteners. Xylanolytic en-

zymes find their application in animal feed as they improve their digestibility by breaking down arabinoxylans and reduce the raw material viscosity. As it has already been stated, xylanase is also an effective enzyme for wood pulp bleaching and structure modification of pulp fibers (Barnoud et al., 1986). Together with manganese, peroxidase increased pulp delignification (Xu et al., 2010). Xylanase treatment is important for baking, where it breaks down hemicelluloses in wheat flour and water insoluble hemicellulose is converted to soluble forms, leaving the dough softer and easier to knead. Fruit juices are also treated with xylanase to reduce their viscosity and improve organoleptic characteristics. Natural sources of xylanases are bacteria and fungi, while those from fungi have higher activity. On the other hand, fungi also secrete cellulase, which is undesirable for some industrial applications, especially during paper pulping and bleaching. Xylanases are produced using submerged or solid-state processes. Solid-state fermentation suffers due to some limitations such as lower process control or low capacity (Malhotra & Chapadgaonkar, 2018). Since xylanase is a very interesting enzyme with wide use, its recombinant production has been studied. Xylanase was expressed in *P. pastoris* reaching very high yields (1.2 g/L). The final yield of the enzyme is important for its further application in industry, which makes *P. pastoris* suitable for industrial production of high quantities of enzymes (Mellitzer et al., 2012). *P. pastoris* is not only suitable due to its high enzyme yields but also due to post-translation modifications like glycosylation enzyme which show better properties. Higher thermostability of glycosylated enzyme from *P. pastoris* compared to those from *E. coli* were confirmed (Fonseca-Maldonado et al., 2013). Recombinant xylanase was produced in *P. pastoris* by directed evolution which yielded a strain with 1,3-fold higher xylanase production compared with the parent strain (Ma et al., 2019). This result excellently demonstrates how directed evolution can improve the produced enzyme quality.

#### **Degradation of bioplastics waste**

The problem with plastic waste is probably the most widespread and well-known. That is why biodegradable plastics produced from renewable agricultural sources are a promising alternative. Polyhydroxyalkanoates have commercial potential as biodegradable thermoplastics; their biodegradation and mineralization are attributed to polyhydroxyalkanoate depolymerase from *Thermobifida* sp. The enzyme was expressed in *P. pastoris* and it catalyzed the degradation of poly-[(R)-3-hydroxy-

butyrate] (PHB) films, which was accelerated in (R)-3-hydroxyvalerate copolymers with the maximum degradation rate of  $882 \text{ ng} \cdot \text{cm}^{-2} \cdot \text{h}^{-1}$ . Such prepared enzymes can be used in standard processing of bioplastics waste (Phithakrotchanakoon et al., 2009).

#### ***Pichia recombinant products for alternative medical treatment***

Overuse of drugs is also an environmental problem because their residues are found in water or animals. It means that replacement of pathogens' control methods with e.g. enzymes or antigens has to be prioritized. Strains of *P. pastoris* were used to produce AHL-lactonase which can be used as a cure of *Aeromonas hydrophila* infection in fish. This serious pathogen causes hemorrhagic septicemia which is controlled by antibiotics and chemicals. Excessive use of chemicals for the treatment of this disease leads to their accumulation in the food chain and thus they can enter human body. In addition, frequent use of antibiotics results in "superbugs" (strains resistant to antibiotics). Recombinant production was successful and the results indicate the possibility of mass low-cost production of AHL-lactonase (Chen et al., 2010). Another veterinary problem is caused by *Boophilus microplus* which is a cattle tick causing problems with their reproduction. Control methods of this ectoparasite include the use of chemicals which are costly and cause environmental and residual problems. Vaccination is a way of protection against tick infestations. Vaccine Gavac™ (Heber Biotec S.A., Cuba), a recombinant Bm86 protein, is produced in *P. pastoris* and used in Latin America. Unlike other expression system (baculovirus, *Aspergillus niger*, *E. coli*) recombinant antigen expressed in *P. pastoris* is acquired in a highly immunogenic, glycosylated, and particulate form (Canales et al., 1997).

#### ***Bioremediation of toxic compounds***

Cyanide is a very toxic and well-known compound. In plants such as almond, cassava, sorghum or flaxseed, cyanogenic products are widely distributed. Due to  $\beta$ -glucosidase in the intestines of mammals, acutely toxic hydrocyanic acid is produced and therefore detoxification is important for safe feeding of animals with these plants. Popular detoxification method is boiling, roasting, autoclaving, microwaving and extrusion. Also,  $\beta$ -glucosidase can be used to hydrolyze these compounds which releases hydrocyanic acid into air. This problem can be solved by cyanide hydratase which catalyzes the hydrolysis of cyanide to formamide. It is used for bioremediation of cyanide-containing wastes and to absorb hydrocyanic acid formed from the cyanogenic glycosides hydrolysis. Recombinant cyanide

hydratase was produced in *P. pastoris* together with  $\beta$ -glucosidase to develop a novel co-enzymatic method with high degradation activity of cyanogenic glycosides. Enzyme preparation produced by recombinant *P. pastoris* completely decomposes cyanogenic glycosides and catalyzes the hydrolysis of more than 80 % of cyanide (Wu et al., 2012).

*P. pastoris* recombinant proteins are not used only for pollutant degradation but also for their detection. One of the commercial *P. pastoris* product is Superior Stock produced by Nitrate Elimination Co. from Michigan (USA). It is a recombinant nitrate reductase used in kits to test nitrates in water, soil, and animal feed. Normally, nitrate is tested through its reduction to nitrite via a copper-cadmium reagent, which is quite a toxic method (Campbell et al., 1997). Thus, an enzymatic analysis has been verified for accuracy, sensitivity and reliability showing minimum impact on people and providing reliable data ([www.nitrate.com](http://www.nitrate.com)).

#### ***Production on crude glycerol***

All mentioned enzymes were produced on purified glycerol in *P. pastoris*. However, there are many studies where crude glycerol was used for enzymes production, e.g. phytase, a very important industrial enzyme used as animal feed additive for swine, poultry, and fish (Xie et al., 2020). Production of recombinant phytase on crude glycerol was upscaled up to a 7.5 l bioreactor. Enzyme activity and biomass concentration reached 137.8 U/ml, and 146 g/L, respectively. Maximum specific growth rate was higher when using crude glycerol than glucose ( $0.266 \text{ h}^{-1}$  vs.  $0.203 \text{ h}^{-1}$ ) as the carbon source; final enzyme activity obtained with glucose achieved 121.6 U/ml (Tang et al., 2009). This proves that crude glycerol does not negatively affect *P. pastoris* growth or recombinant protein expression, which is its advantage over other microorganisms.

#### **Conclusion**

High-level expression, growth to high cell densities and post-translation modifications prove that *P. pastoris* is a suitable microorganism for recombinant enzyme production. Given all available data of successfully produced enzymes, *P. pastoris* has also great potential in the environmental sector. Products of *P. pastoris* were able to degrade pesticides or replace them with more environmentally friendly variants, degrade phenol compounds, synthetic dyes, hydrocarbons, antibiotic residues, lignin, nitroaromatics, toluene, bioplastics, and toxic compounds like cyanide. Its products were used also for kraft pulp bleaching, detection of pollutants and as alternative medical treatment

**Tab. 2.** Summary of enzymes produced by *P. pastoris* with positive effect on environment.

Product	Environmental treatment	Reference
Pexiganan	replacement of pesticides	Neshani et al., 2019
Organophosphorus hydrolase	biodegradation of organophosphorus pesticides	Shen et al., 2016
Kpkt	$\beta$ -1,3glucanase and killer activity against spoilage yeast in wine and sweet beverage industry	Chessa et al., 2017
Laccase	degradation of synthetic dyes, lignin, nitrophenol, antibiotics and phenolic pollutants	Zhou et al, 2018; Colao et al., 2006
Manganese peroxidase	degradation of lignin, cellulose, hemicellulose, polycyclic aromatic hydrocarbons, chlorophenols, synthetic dyes, nitroaromatics, tetracyclines, oxytetracyclines, bleaching of pulp	Xu et al., 2017; Xu et al., 2010
Lignin peroxidase	degradation of lignin	Wei & Xianghua, 2009
Xylanase	conversion of lignocellulosic material and agrowaste to high-value products, paper pulping and bleaching	Ma et al., 2019
Phytase	helps to digest phytate which prevent phosphorus pollution	Tang et al., 2009
Nitrate reductase	test nitrates in water	www.nitrate.com
Cyanid hydratase	detoxification of cyanogenic glycosides, hydrolysis of cyanide	Wu et al., 2012
Horseradish peroxidase	degradation of aromatic amines, phenolic compounds, coal conversion wastewater, bleach plant effluent	Morawski et al., 2000
Polyhydroxyalkanoat depolymerase	biodegradation of polyhydroxyalkonotes	Phithakrotchanakoon et al., 2009
Bm86 antigen	vaccine against <i>Boophilus microplus</i>	Canales et al., 1997
Keratinase	improvement of nutritional value of feather meal and alleviate the environmental impact associated with its processing or disposal	Porres et al., 2002
AHL-lactonase	control of <i>Aeromonas Hydrophila</i>	Chen et al., 2010
Nitril hydratase	conversion of acrylonitrile and acrylamide	Shi et al., 2004
Azoreductase*	degradation of azo dyes	so far not produced by <i>P. pastoris</i>
Cyanidase*	treatment of cyanide	so far not produced by <i>P. pastoris</i>
Lactoperoxidase*	degradation of chlorophenols	so far not produced by <i>P. pastoris</i>
Polyphenol oxidase*	degradation of phenol compounds	so far not produced by <i>P. pastoris</i>

(Tab. 2). Due to many advantages of recombinant enzyme production, genetically engineered *P. pastoris* could completely replace the native sources of these enzymes. In addition, to enhance its positive environmental impact even more, combination of *P. pastoris* cultivation on crude glycerol, a biodiesel side product, with production of enzymes for environment treatment can be employed.

All these successful attempts point to the potential of *P. pastoris* production of other enzymes suitable for environmental treatment (Tab. 2\*).

#### Acknowledgement

This work was supported by the Slovak Research and Development Agency under the Contract no. APVV-18-0254. This publication is the result of the project implementation: Comenius University in Bratislava Science Park supported by the Research and Development Operational Programme funded by ERDF. Grant number: ITMS 26240220086. This publication was co-funded by project "ACCORD" (ITMS project code: 313021X329) supported by the Operational Programme Research and Development funded by ERDF.

## References

- Ahn MY, Dec J, Kim JE, Bollag JM (2002) *Journal of Environmental Quality* 31(5): 1509–1515.
- Aitken MD (1993) *Chemical Engineering Journal* 52: 49–58.
- Aktar MW, Sengupta S, Chowdhury A (2009) *Interdisciplinary toxicology* 2(1): 1–12.
- Alcade M, Ferrer M, Plou FJ, Ballesteros A (2006) *Trends in Biotechnology* 24(6): 281–287.
- Ali N, Zhang Q, Liu Z-Y, Li F-L (2020) *Applied Microbiology and Biotechnology* 104 (5): 1–19.
- Anastácio G, Santos K, Suarez P, Torres F, De Marco J, Parachin N (2014) *Bioresource Technology* 152: 505–510.
- Barnoud F, Comtat J, Joseleau J, Mora F, Ruel K (1986) *Biotechnology in the Pulp and Paper Industry*: 69–73. Conference in Stockholm.
- Bartocci P, Bidini G, Asdrubai F, Beatrice C, Frusteri F, Fantozzi F (2018) *Renewable Energy* 124: 172–179.
- Bassil KL, Sanborn VM, Cole DC, Kraur JS, Kerr KJ (2007) *Canadian Family Physician* 10(53): 1704–1711.
- Campbell ER, Corrigan JS, Campbell WH (1997) Field determination of nitrate using nitrate reductase: 851–860. Conference in Pittsburg.
- Canales M, Enríquez A, Ramos E, Cabrera D, Dandie H, Soto A, ... de la Fuente R (1997) *Vaccine* 15(4): 414–422.
- Cereghino JL, Cregg JM (2000) *FEMS Microbiology Reviews* 24: 45–66.
- Colao MC, Lupino S, Garzillo AM, Buonocore V, Ruzzi M (2006) *Microbial cell factories* 5(31): 1–11.
- Colao MC, Garzillo AM, Buonocore V, Schiesser A, Ruzzi M (2003) *Appl Microbiol Biotechnol* 63 (2): 153–158.
- Cos O, Ramón R, Montesinos JL, Valero F (2006) *Microbial Cell factories*, 5(17).
- Eibes G, Cajthaml T, Moreira MT, Feijoo G, Lema JM (2006) *Chemosphere* 64: 408–414.
- Eton Bioscience (2003–2019). Standard peptide synthesis. Retrieved from [www.entobio.com](http://www.entobio.com).
- Farnoosh G, Latifi AM (2014) *Journal of Applied Biotechnology Reports* 1(1): 1–10.
- Fischer JE, Glieder A (2019) *Current Opinion in Biotechnology* 59: 175–181.
- Fonseca-Maldonado R, Vieira DS, Alponi JS, Bonneil E, Thibault P, Ward RJ (2013) *Journal of biological chemistry* 288: 25522–25534.
- Gaitan IJ, Medina SC, González JC, Rodríguez A, Espejo AJ, Osma JF, ... Sánchez OF (2011) *Bioresource Technology* 102: 3632–3635.
- Hammel KE, Jensen KA, Mozuch MD, Landucci LL, Tien M, Pease A (1993) *The Journal of biological chemistry* 268(17): 12274–12281.
- Chen R, Zhou Z, Cao Y, Bai Y, Yoa B (2010) *Microbial Cell Factories* 9(39).
- Chessa R, Landolfo S, Ciani M, Budroni M, Zara S, Ustun M, ... Mannazzu I (2017) *Appl Microbiol Biotechnol* 101(7): 2931–2942.
- Lazarev VN, Govorun VM (2010) *Applied Biochemistry and Microbiology* 46: 803–814.
- Levil L, Carabajal M, Hofrichter M, Ulrich R (2016) *Int Biodeter Biodegr* 107: 174–179.
- Li T, Takkellapati S (2018) *Biofuels, Bioproducts and Biorefining* 12(5): 756–787.
- Ma C, Tan ZL, Lin Y, Han S, Xing X, Zhang C (2019) *Journal of Bioscience and Bioengineering* 6(128): 662–668.
- Maccauley-Patrick S, Fazenda ML, McNeil B, Harvey LM (2005) *Yeast* 22: 249–270.
- Mahmood I, Imadi SR, Shazadi K, Gul A, Hakeem KR (2016) *Plant, Soil and Microbes*: 253–269.
- Malhotra G, Chapadgaonkar SS (2018) *BioTechnologia, Journal of Biotechnology, Computational Biology and Bionanotechnology* 99(1): 59–72.
- Markošová K, Weignerová L, Rosenbegr M, Křen V, Rebroš M (2015) *Frontiers in Microbiology* 6(1140).
- McCauley LA, Anger WK, Keifer M, Langley R, Robson MG, Rohlman D (2006) *Environmental Health Perspectives* 114(6): 953–960.
- Mellitzer A, Weis R, Glieder A, Flicker K (2012) *Microbial Cell Factories* 11(61).
- Morawski B, Lin Z, Cirino P, Joo H, Bandara G, Arnold FH (2000) *Protein Engineering* 13(5): 377–384.
- Moreira MT, Feijoo G, Lema JM (2003) *Reviews in environmental science and Bio Technology* 2: 247–259.
- Mulchandani A, Mulchandani P, Kaneva I, Chen W (1998) *Analytical chemistry* 70(19): 4140–4145.
- Neshani A, Tanhaeian A, Zare H, Eidgahi RM, Ghazvini K (2019) *Gene Reports* 17.
- Nigam P, Armour G, Banat I, Singh D, Marchant R (2000) *Bioresource Technology* 72: 219–226.
- Owens JW, Swanson SM, Birkholz DA (1994) *Chemosphere* 29(1): 89–109.
- Paszczyński A, Huynh V-B, Crawford R (1985) *FEMS Microbiology Letters* 29(1–2): 37–41.
- Phithakrotchanakoon C, Daduang R, Thamchaipenet A, Wangkam T, Champreda V (2009) *Appl Microbiol Biotechnol* 82(131): 131–140.
- Ramsay JA, Nguyen T (2002) *Biotechnology Letters* 24: 1757–1761.
- Satyanarayana T, Kunze G (2009) *Yeast Biotechnology: Diversity and Applications*. Springer, Dordrecht.
- Sheldon RA, van Rantwijk F (2004) *Australian Journal of Chemistry* 57: 281–289.
- Shen W, Ma L, Shu M, Ni H, Yan H (2016) *Protein expression and purification* 119: 110–116.
- Shi Y, Yu H, Sun X, Tian Z, Shen Z (2004) *Enzyme and microbial technology* 35: 557–562.
- Shimazu M, Mulchandani A, Chen W (2001) *Biotechnology and Bioengineering* 4(76): 318–324.
- Shraddha Shekher R, Sehgal S, Kamthania M, Kumar A (2011) *Enzyme Research* 2011: 1–11.
- Scheibner K, Hofrichter M (1998) *J. Basic Microbiol.* 38(1): 51–59.
- Schutter KD, Lin Y-C, Tiels P, Hecke AV, Glinka S, Weber-Lehmann J, ... Callewaert N (2009) *Nature Biotechnology* (27): 561–566.
- Songa EA, Okonkwo JO (2016) *Talanta* (155): 289–304.
- Sun B, Wibowo D, Middelberg AP, Zhao C-X (2018) *AMB Express* 8(6).
- Syn High Quality Peptide (2010–2015). Peptide synthesis price list. [www.synpeptide.com](http://www.synpeptide.com).
- Tanaka K, Padermpole K, Hisanaga T (2000) *Water research* 1(34): 327–333.
- Tang S, Boehme L, Lam H, Zhang Z (2009) *Biochemical Engineering Journal* 43: 157–162.

- Viikari L, Ranua M, Kantelinen A, Sundquist J, Linko M (1968) Bleaching with enzymes: 67–69 Conference in Stockholm.
- Wei W, Xianghua W (2009) Journal of environmental science 21, 218–222.
- Wen X, Jia Y, Li J (2010) Journal of Hazardous Materials 177, 924–928.
- Wu C-F, Feng A-J, Xu X-M, Huang S-H, Deng M-C, Zheng X-N, ... Wang J-H (2012) African Journal of Biotechnology 11(19): 4424–4433.
- Xie Z, Fong W-P, Tsang PW-K (2020) Enzyme and microbial technology 137.
- Xu H, Guo M-Y, Gao Z-H, Bai X-H, Zhou X-W (2017) BMC Biotechnology 17(19): 1–12.
- Xu H, Scott GM, Jiang F, Kelly C (2010) Holzforschung 64(2): 137–143.
- Yehia RS (2014) Brazilian Journal of Microbiology 45(1): 127–133.
- Zhou R, Yu H, Yuan P, Fan J, Chen L, Li Y, ... Zhang X (2018) Journal of Hazardous Materials 344: 499–510.